STRATIGRAPHY AND SEDIMENTOLOGY OF CONGLOMERATES IN THE KIDNAPPERS GROUP, HAWKE'S BAY.

A thesis

submitted in partial fulfilment of the requirements for the Degree of

Master of Science in Earth Sciences

at the

University of Waikato

by

PETRUS JOHANNES JOZEF KAMP

1978

FRONTISPIECE: *Part of the coastal section of the Pleistocene Kidnappers Group, southern Hawke Bay. This view, 3 km west of Black Reef, shows the conformable nature of the westward dipping lithologically diverse strata, mildly deformed into fault blocks. The cliffs are up to 100 m high. (Photo by courtesy of M.J. Selby)*

ABSTRACT

The Middle to Late Pleistocene Kidnappers Group comprises 400 m of diverse lithologies deposited in fluvial, marginal marine and shallow marine environments. The stratigraphy and sedimentology of the greywacke conglomerates, the dominant lithology in the group, is investigated, in part using three new computer programmes.

Five environmentally sensitive lithologies are recognised: Lithotype 1 - Imbricated, inverse to normally graded conglomerate; Lithotype 2 - Planar cross-stratified conglomerate; Lithotype 3 - Thin, massive to stratified conglomerate; Lithotype 4 - Planar cross-stratified, shelly, sandy conglomerate; Lithotype 5 - Thin, massive to low-angle cross-stratified, shelly conglomerate.

On the basis of cross-stratification types, fossil content and the shapes, orientation fabrics and grain-size analyses of clasts, Lithotypes 1, 2 and 3 have a braided fluvial origin and Lithotypes 4 and 5 a shallow marine origin. Differences between Lithotypes 1, 2 and 3 identify a proximal-distal sequence within the braided fluvial environment.

Lithotype 1 is interpreted as proximal channel and longitudinal bar facies, Lithotype 2 as mid-reach transverse and longitudinal/diagonal bar facies, and Lithotype 3 as channel and topstratum overbank deposits in the distal reaches of a braided river system.

From the vertical succession of conglomeratic facies and marine fossiliferous units, a chronology of submergence

and emergence events in the Kidnappers Group has been established. This succession is dominantly controlled by glacio-eustatic fluctuations in sea level which agree in frequency and period with sea level fluctuations derived from deep sea core data from 0.5 to 0.1 m.y.B.P. Tectonism has also influenced the supply of sediment to the group and reinforced the magnitude of the submergence and emergence events.

ACKNOWLEDGEMENTS

I wish to acknowledge the assistance of my supervisor Dr Campbell S. Nelson. Also, Dr R.M. Briggs, Professor H.S. Gibbs and Dr M.J. Selby for helpful discussion on aspects of this study. I am indebted to Professor J.D. McCraw for his consideration in the organisation of my teaching commitments during 1977.

I would like to thank the farmers of the Kidnappers area for access to the inland sections, and Dr D.M. Ryan for writing Function PRPLOT(Z) of the Texture programme. Further, Messrs K. Stewart and R.R. Julian for assistance with some draughting and photography.

I am very appreciative of the support and assistance of my fellow students, especially David Lowe, David Burns and Ken Murray, with whom I have had many challenging discussions on the Kidnappers Group.

I am also grateful for the many forms of assistance during this study, and especially the moral support given by Christine Ryan, Norman Jager and Stewart McDowell.

I am indebted to Elaine Norton for her willingness and unfailing help in producing an excellent typescript.

Finally, completion of this degree, in large part, stems from the encouragement and understanding of my mother, Tine Kamp.

TABLE OF CONTENTS

LIST OF FIGURES, TABLES AND APPENDICES

Page

Figures:

Figures:

Page

Figures:

Page

Figures:

Page

Figures:

Page

Tables:

Appendices:

Appendix I	-	Computer Programmes.
I i	-	Calculate and plot clast shape.
I ii	-	Analyse orientation data.
I iii	-	Calculate and present the textural distribution of Earth Materials.
I iv	-	Identify the mineralogy of samples analysed by X-ray diffraction.
Appendix II	-	Clast orientation data Sites 1 to 6.
II i	-	Site 1: field measurements and values corrected for tectonic tilt.
II ii	-	Site 1: clast dimensions, sphericity and elongation index values.
II iii	-	Site 6: field measurements and values corrected for tectonic tilt.
II iv	-	Site 6: clast dimensions, sphericity and elongation index values.
II v	-	Site 2: field measurements and values corrected for tectonic tilt.
II vi	-	Site 3: field measurements and values corrected for tectonic tilt.
II vii	-	Site 4: field measurements and values corrected for tectonic tilt.
II viii	-	Site 5: field measurements and values corrected for tectonic tilt.
Appendix III	-	Current direction data from the Mt. Gordon Beds, 110 ft. Conglomerate, Rabbit Gully Beds, Trig. N Beds and Clifton Conglomerate.
Appendix IV i	-	Values for selected <u>ab</u> plane pole positions rotated about the normal to the trend of the <u>a</u>-axes maxima to remove the effects of <u>a</u>-axis plunge.
IV ii	-	All <u>ab</u> plane pole positions rotated about the normal to the trend of <u>a</u>-axes
Appendix V	-	Computer analysis of the <u>a</u>-axes and <u>ab</u> plane poles of clasts at Site 1 to establish the origin of clast orientation.
Appendix VI i	-	Heavy mineralogy of samples 039 and 040.
VI ii	-	Ferromagnesian mineralogy of tephric units A to I_2
Log I	-	Stratigraphic columns of the coastal and inland sections (pocket).

CHAPTER 1: INTRODUCTION

The Pleistocene Kidnappers Group (Kingma 1971) comprises 400 m of diverse lithologies dominated by greywacke conglomerates. Exposures provide a continuous stratigraphic sequence of sediments deposited in fluvial, marginal marine and shallow marine environments. This, together with the high rates of basin subsidence and sediment accumulation, good tephrostratigraphic and chronologic control, and only mild post-depositional deformation, offer a complete record of the Middle to Late Pleistocene history of Hawke's Bay.

1-1 THE STUDY AREA

The Kidnappers Group outcrops immediately south of Hawke Bay where it covers about 40 km^2 (Fig. 1-1.). The group intersects the coast between Clifton and Black Reef where the strata form cliffs over 100 m high. The Maraetotara River cuts through the middle of the group at right angles to the coast and flows into Hawke Bay just north of Clifton (Fig. 1-1.). This study has concentrated on those strata exposed along the coastal section and inland up the Maraetotara River.

The Kidnappers Group is incorporated in the Te Aute Subdivision (Kingma 1971) of central Hawke's Bay and is covered by Sheet N135 (Kingma 1970a).

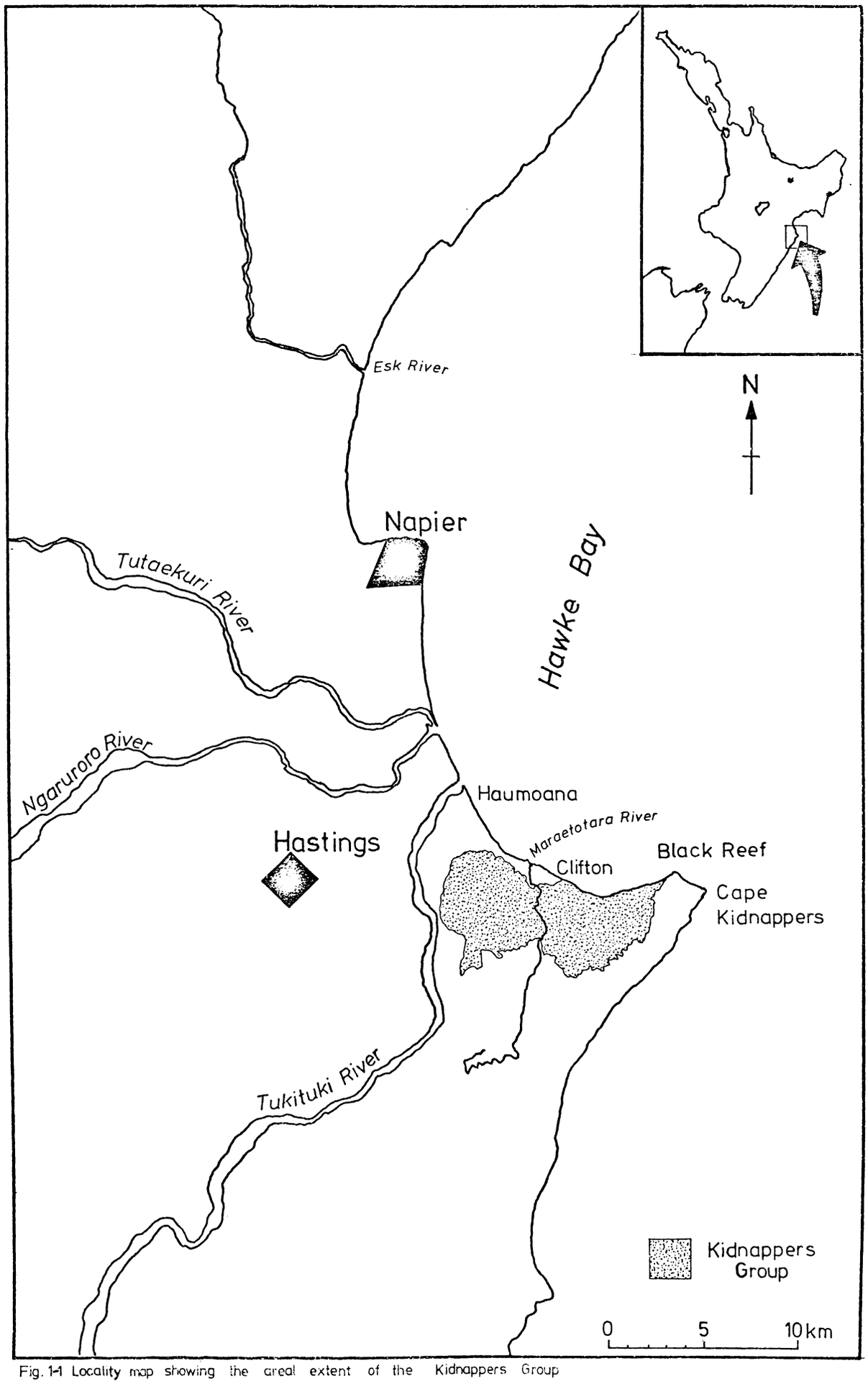

Fig. 1-1 Locality map showing the areal extent of the Kidnappers Group

1-2 THE SCOPE OF RESEARCH

Originally a stratigraphic and sedimentologic investigation of the entire Kidnappers Group was initiated with the aim of establishing and interpreting the depositional history of the group. However, during the early phases of this research it became increasingly apparent that interpretation of facies successions and alternating terrestrial/marine environments is largely reflected by the presence or absence of conglomerates. In turn the conglomerates reflected the external controls on sedimentation. Therefore, to interpret fully the depositional history of the group, it is necessary to have a thorough understanding of the conglomeratic lithofacies and their depositional environments. Hence, the emphasis in research shifted more towards a detailed investigation of the conglomerates.

Although considerable textural, compositional and paleoenvironmental information of finer-grained lithologies in the group have been established, these data are not presented here but form the basis of work in preparation. Within this context the scope of the thesis has narrowed so that the aims now include the following:

(i) To establish the vertical and lateral stratigraphic relationships of the conglomerates in the group.

(ii) To develop methods of data analysis applicable to the conglomerates.

(iii) To study in detail the sedimentology of the conglomerates and to establish their depositional paleoenvironments.

(iv) To interpret from the conglomerate paleoenvironments the depositional history of the group.

In view of the marked lithologic diversity of the group, the usual forms of lithostratigraphic correlation are of limited value. Hence, in order to fulfil the first objective, the heavy mineralogy of tephras in the group were investigated to establish, if possible, marker beds which would assist in correlation of the coastal and inland exposures.

Generally in conglomerates, sediment structures and other facies characteristics are sparse in comparison with sandstones. In order then to fulfil the third objective, clast shape and especially orientation fabric were studied. More particularly, clast orientation was investigated to determine paleocurrent directions, to distinguish marine from fluvial paleoenvironments, and to establish, if possible, the paleohydrologic regime of some conglomerates.

There have been very few detailed sedimentologic studies of Quaternary conglomerates in New Zealand, surprising in view of their wide areal extent (see Milne 1971). It is hoped this study will add to this knowledge and especially to the understanding of the Pleistocene history of Hawke's Bay.

1-3 GENERAL GEOLOGY OF HAWKE'S BAY

Pre-Cretaceous Basement

Triassic and Jurassic rocks belonging to the Torlesse Supergroup form the pre-Cretaceous basement and the main axial ranges in the west (Fig. 1-2.). Largely unfossiliferous, indurated, and consisting of alternating sandstone and argillite (Kingma 1957b), they are now exposed as highly deformed strata that are overturned to the north-west (Spörli & Bell 1976). These rocks are commonly called, and will be referred to hereafter, as greywackes.

Associated with the sandstones and argillites are basic volcanics, cherts and red argillites. The detrital suite is predominantly quartzofeldspathic with abundant lithic fragments of volcanic and sedimentary origin. A regional north-east trending schist belt has been mapped in the Kaimanawa Range (Grindly 1960), both the schistose and non-schistose rocks belonging to the higher grade prehnite-pumpellyite metagreywacke facies (Spörli & Barter 1973). The greywackes in the Ruahine Range are interpreted as having been deposited in a continental terrace/abyssal plain paleoenvironment (Spörli & Bell 1976).

To the east of the axial ranges the greywacke basement has been folded into a broad, NNE striking synclinal structure which has been infilled by a thick sequence of mainly marine Cretaceous and Cenozoic sediments (Kingma 1971).

Cretaceous Sedimentation

The subsurface Cretaceo-Jurassic boundary in Hawke's Bay is believed to be conformable (Kingma 1957a). Within the Te Aute Subdivision the Cretaceous and Tertiary sediments

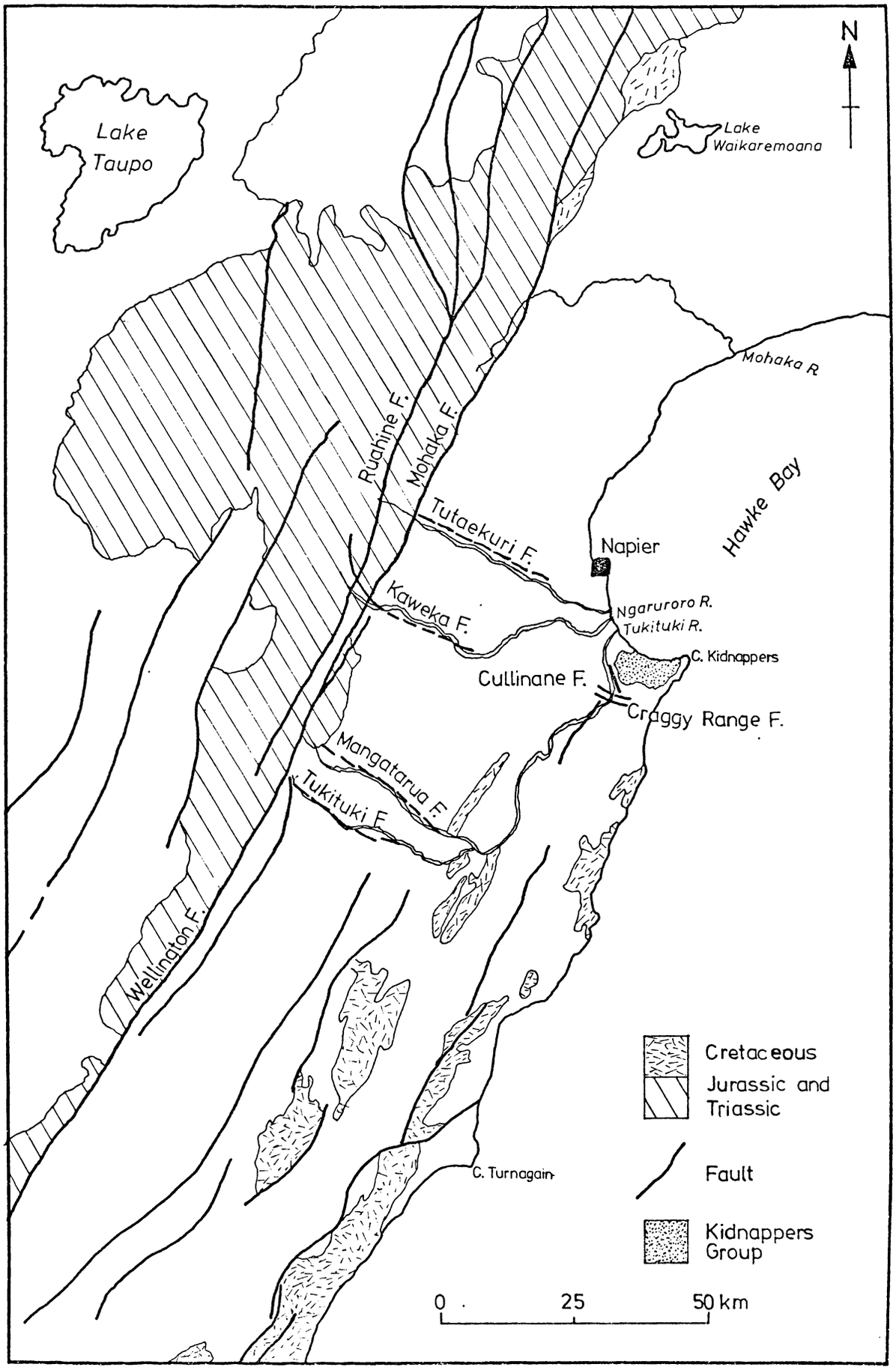

Fig 1-2. Generalised geologic map showing major fault trends and outcrops of Mesozoic rocks (after Suggate 1972; Clark 1976)

have been assigned to one or other of 29 stages (Table 1-1). The thickness and general lithologies for each stage are summarised by Kingma (1971, Table 3).

From the outcrop pattern of Cretaceous rocks in the extreme east of Hawke's Bay (Fig. 1-2.),together with their lateral facies changes, Kingma (1960a) envisaged a landmass immediately east of New Zealand as the source area for Cretaceous sediments. By the end of the Cretaceous this landmass, reduced to one of low relief, was no longer a significant source of sediment.

Tertiary Sedimentation

In the Lower Tertiary the greywacke basement began to rise in what is presently the main axial ranges. Between this feature and the rapidly subsiding Cretaceous landmass in the east, slow Tertiary sedimentation continued. Fine-grained Cretaceous rocks, weathered and eroded off the rising axial ranges, furnished the supply of sediments for the Dannevirke and Arnold Series. During Upper Landon times shelf conditions prevailed, indicating that the basin was largely infilled. The gradual coarsening of sediments suggests that the axial ranges had increased in elevation, although throughout the Tertiary they were never high enough to supply gravel except locally during the Mangapanian.

The culmination of intense tectonism in the Upper Oligocene is exemplified by a sequence of complexly folded and faulted Upper Cretaceous to Oligocene strata near Waimarama (Fig. 1-3.). This interpretation is supported by the existence of a regional unconformity throughout south-eastern Hawke's Bay and the absence of Pareora Series (J. Pettinga, pers. comm.).

Series	Stage	Age
RECENT		Holocene
HAWERA	High terraces 2 High terraces 1	Upper Pleistocene
WANGANUI	Castlecliffian Nukumaruan Mangapanian Waipipian Opoitian	Middle Pleistocene Lower Pleistocene Upper Pliocene Middle Pliocene Lower Pliocene
TARANAKI	Kapitean Tongaporutuan	Upper Miocene
SOUTHLAND	Waiauan Lillburnian Clifdenian	Middle Miocene Lower Miocene
PAREORA	Altonian Otaian	Lower Miocene
LANDON	Waitakian Duntroonian Whaingaroan	Upper Oligocene Middle Oligocene Lower Oligocene
ARNOLD	Runangan and Kaiatan Bortonian	Upper Eocene
DANNEVIRKE	Porangan Heretaungan Mangaorapan Waipawan Teurian - Upper - Lower	Middle Eocene Lower Eocene Paleocene Danian
MATA	Haumurian - Upper - Lower Piripauan	Maestrichtian Campanian
RAUKUMARA	Teratan Mangaotanean Arowhanan	Santonian Coniacian Turonian
CLARENCE	Ngaterian Motuan	Cenomanian Upper Albian

Table 1-1. Stratigraphic Classification adopted. (Modified after Kingma 1971, Table 3).

Southern and eastern Hawke's Bay became resubmerged during Southland times and shelf deposition recommenced. Major lateral movements along transcurrent fault zones during the Miocene initiated the formation of basinal conditions and the deposition of a thick sequence of Upper Miocene flysch. The presence of localised unconformities indicate that contemporaneous erosion of highs occurred with deposition in adjacent basins (Kingma 1958).

Regional uplift, corresponding to initiation of the Kaikoura Orogeny in the area, is expressed as an angular unconformity developed in Middle Pliocene to Lower Pliocene sequences. In the south of the Ruataniwha Basin (Fig. 1-3.), a Plio-Pleistocene sequence directly overlies greywacke basement. Further north in the same basin a Plio-Pleistocene sequence overlies dipping Middle Miocene and Eocene-Paleocene sediments (Clark 1976). Katz (1973) recorded the same unconformity north-west of Napier, and suggested that it developed during late Miocene to Mangapanian times. In the Waimarama District this angular unconformity developed during Uppermost Miocene times (J. Pettinga, pers. comm.). Hence major tectonism occurred in the Late Miocene, paralleled in the west by Lower Pliocene development of the Ruahine-Rimutaka Horst (Kingma 1957c).

The major Upper Miocene epeirogeny continued into the Opoitian, but was short-lived in the vicinity of Cape Kidnappers as Opoitian mudstone is separated from underlying Tongaporutuan beds by an angular unconformity of only 1-2° (Kingma 1971). In the period following Upper Miocene tectonism the Ruataniwha-Petane Trough (Fig. 1-3.) was formed by down-faulting along major NNE trending faults (Fig. 1-2; Clark 1976).

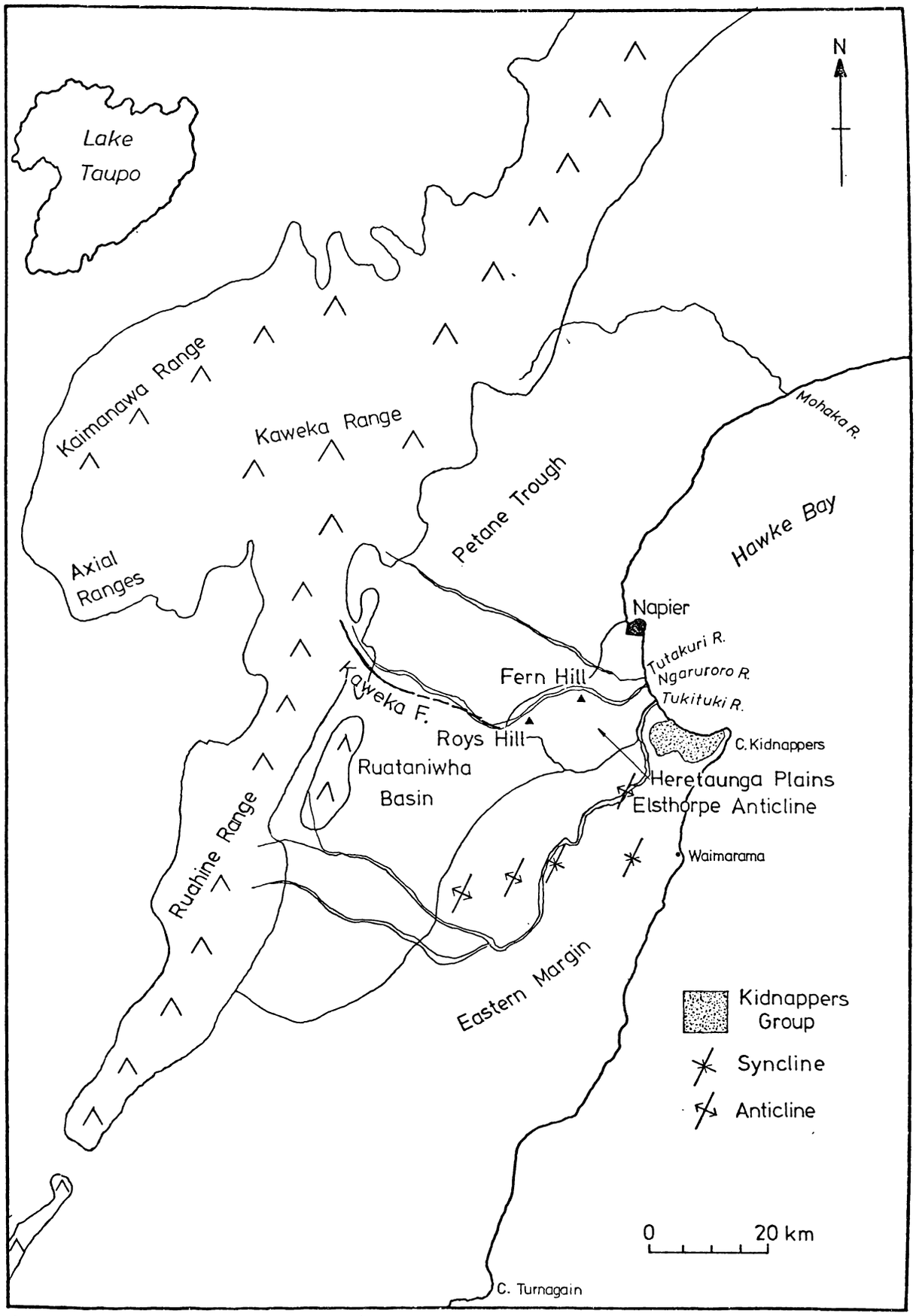

Fig 1-3 Main physiographic features in Hawke's Bay

Immediately following deposition of Waipipian sandstones and siltstones in the Ruataniwha Basin, the whole of the Hawke's Bay region became submerged and the widespread Te Aute Limestone, of Mangapanian age, was deposited. The limestone extended across the area now occupied by the Ruahine Range (Fig. 1-3.) and predates major uplift of the range. The size of terrigeneous pebbles in the limestone increases towards the north, suggesting that during the Mangapanian the Kaweka and Kaimanawa Ranges were emerging (Kingma 1957a).

Quaternary Sedimentation

During the Nukumaruan a thick sedimentary sequence accumulated with continuous tilting and subsidence in fault-angle depressions and grabens of the Ruataniwha Basin (Clark 1976). A thick succession of Nukumaruan sediments also accumulated in the Petane Trough in northern Hawke's Bay (Kingma 1959). Sediment supply was from both uplifted horsts along the eastern margin (Fig. 1-3.) and from the axial ranges, which supplied increasing quantities of greywacke gravels. Pumice derived from the central North Island also became a component of the sediment.

Terrestrial conditions became widespread at the end of the Nukumaruan in response to regional uplift. Most Castlecliffian strata rest unconformably on a variety of rocks ranging in age from Cretaceous to Pliocene. Hence, following the Mangapanian, extensive erosion, particularly of eastern and southern Hawke's Bay, preceded Castlecliffian deposition (Kingma 1971). In two restricted areas, the Kidnappers area and the eastern Ruataniwha Basin,

alternating marine and terrestrial sediments indicate continued periodic subsidence in parts of Hawke's Bay. Fluvial deposition occurred in the western Ruataniwha Basin and lacustrine sedimentation in the south (Fig. 2-3.). Greywacke gravels are the predominant lithology in Castlecliffian and Hawera sediments with locally thick units of volcanogenic material.

Sedimentation in the Heretaunga Plains (Fig. 1-3.) has continued through to the present day. Coastal and inland terraces of fluvial greywacke gravels record Hawera and Recent phases of uplift.

1-4 GEOLOGIC STRUCTURE OF CENTRAL HAWKE'S BAY

Periodic tectonism is largely responsible for the sedimentation patterns and the exposure of Cretaceo-Cenozoic rocks in Hawke's Bay. The regional structural trend is NE/SW (Figs. 1-2 to 1-4.). In the west Kingma (1962) describes a number of major faults (Fig. 1-2.) which delineate a series of well developed horsts and grabens trending NE/SW. In the east of Hawke's Bay, Kingma (1970b) mapped numerous faults, synclines and anticlines parallel to the regional trend (Fig. 1-4.). East-west cross-sections by Kingma (1962) and Clarke (1976), in southern and central Hawke's Bay respectively, depict a much faulted Tertiary sequence with greywacke basement progressively downthrown to the west.

Fault and Fold Systems

The major faults and folds are shown in Figs. 1-2 and 1-4. Two main fault systems occur - a dominant NE/SW system and a less pronounced NW/SE one.

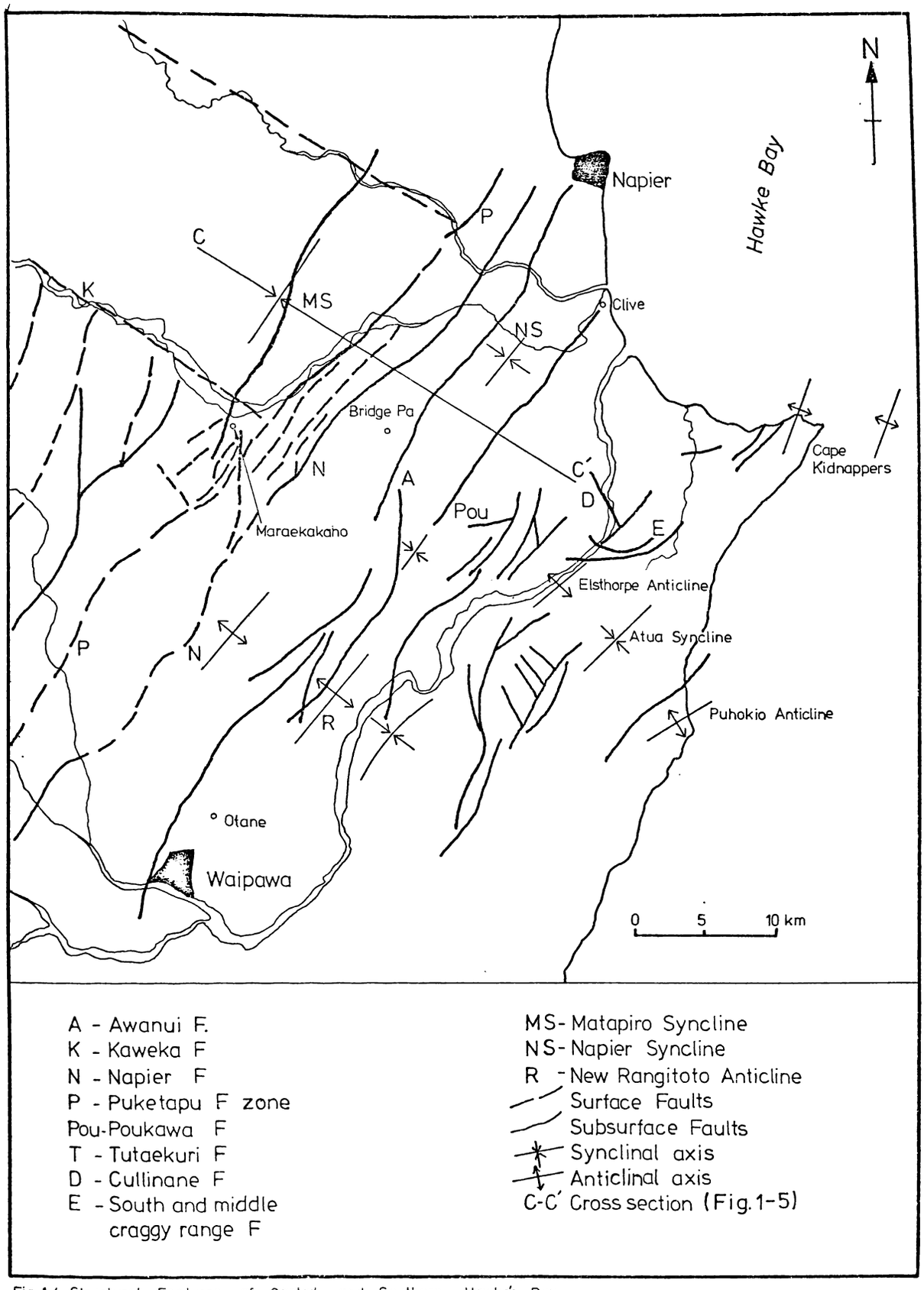

Fig 1-4 Structural Features of Central and Southern Hawke's Bay (after Kingma 1970a, 1970b; Lewis 1971; Clark 1970)

NE/SW Fault and Fold System:

The NE/SW fault system is a continuation of the regional trend throughout the East Coast of the North Island and probably continues into Hawke Bay (Clark 1976). In the Elsthorpe Anticline (Fig. 1-4.) numerous NE/SW trending faults occur. In anticlines and synclines further to the south and west the same structural trend is maintained (Fig. 1-4.).

Structure of the Heretaunga Plains:

Within the Heretaunga region, a number of important NE/SW trending faults occur: the Napier and Awanui Faults downthrown to the east, and the Puketapu Fault Zone with downthrows to the west (Fig. 1-4.). A simplified cross-section (Fig. 1-5.) illustrates that these faults bound the Matapiro Syncline in the west, the Napier Syncline in the east, and two up-domed structures, the Puketapu and Bridge Pa structures. The fold axes of the Matapiro and Napier Synclines are parallel and follow the regional NE/SW trend. It has been postulated (Clark 1976) that deformation resulting from transcurrent movement along the Napier and Awanui Faults caused up-doming of the Bridge Pa and Puketapu structures and the formation of the asymmetrical synclines in either side. The western limb of the Matapiro Syncline results from regional compression associated with uplift of the axial ranges.

NW/SE Fault System:

The present courses of the major rivers follow in part, and accentuate, the NW/SE fault lineations (Fig. 1-2.). In the south the Tukituki and Waipawa Rivers follow

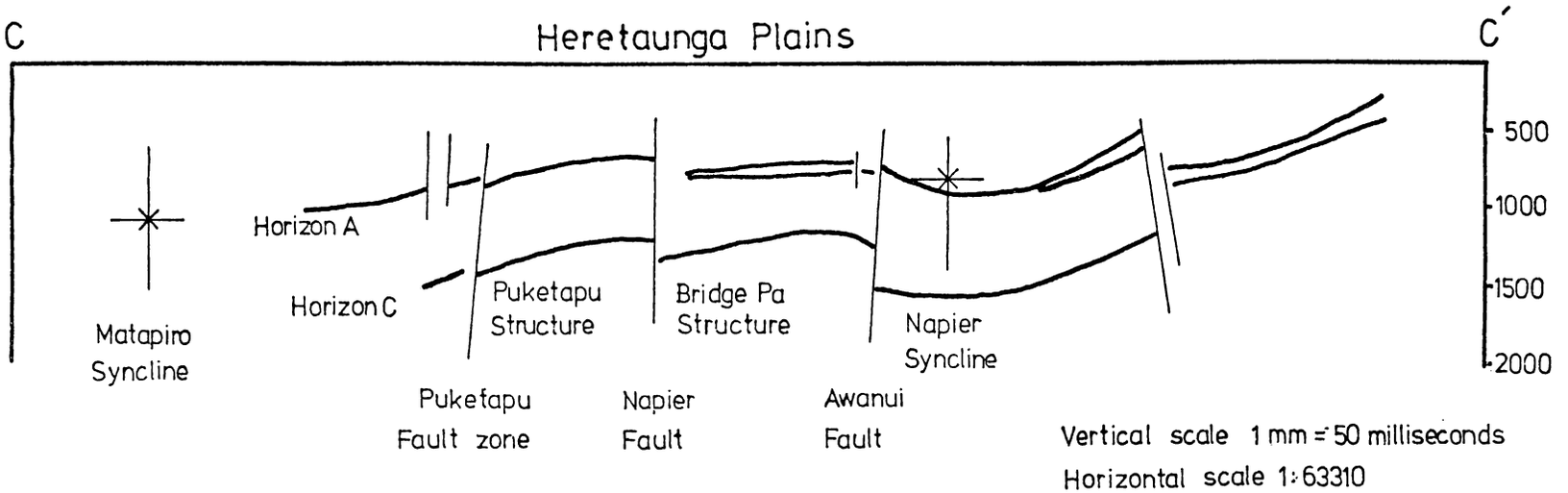

Fig. 1-5 Seismic cross-section across Heretaunga Plains (After Clark 1976)

respectively the Tukituki and Mangatarua Faults south-east from the axial ranges. Further north the Kaweka Fault, downthrown to the north, has been mapped (Kingma 1960b) as a NW/SE arc from the foot of the Kaweka Range to Marae-kakaho (Fig. 1-4.) and then eastwards to the Heretaunga Plains. The Ngaruroro River follows this fault to Marae-kakaho where it is directed north-east by the Puketapu Fault Zone (Fig. 1-4.). The Tutaekuri River follows the NE/SW Tutaekuri Fault (Kingma 1957b).

In the Kidnappers area the Cullinane Fault, which is downthrown to the north, cuts obliquely NW/SE across the Tukituki River and the northern part of the Elsthorpe Anticline (Fig. 1-4.). Most NE/SW faults within the anti-cline terminate against this fault but a few by-pass it to the east and disappear within the Kidnappers Group. In the same region the South and Middle Craggy Range Faults are moderately arcuate in a predominantly east-west direction (Fig. 1-4.).

Age of Folding and Faulting

A marked angular unconformity between Tongaporutuan siltstones and the Te Aute Limestone, together with a recognisable thinning of the limestone over the anticline, indicates Lower Pliocene initiation of anticlinal folding (Kingma 1971). Most uplift, and possibly up to 100 km of dextral transcurrent movement, has occurred along the faults bordering the axial ranges since the Pliocene (Dr A.G. Beu, pers. comm.).

Pre-Pliocene fault development and continuous movement through to the present for faults in the Ruataniwha Basin is

envisaged by Clark (1976). Eastward thinning of Nukumaruan sediments suggests that up-doming of the Bridge Pa structure was initiated in the Nukumaruan. The absence of extensive gravels in Nukumaruan sediments south of the Kaweka Fault indicates that this fault was active during the Nukumaruan, and prevented southward movement of gravels eroded from the Kaweka and Kaimanawa Ranges (Clark 1976).

Since the Upper Nukumaruan, compression associated with transcurrent movement has resulted in further up-doming of the Bridge Pa and Puketapu structures. Faulting has been continuous through to the present day as exemplified by the Napier earthquake of 1931.

Fault Control of River Systems

Fault control of river directions is important in view of the possible source and directions of transport of the greywacke clasts in the widespread conglomerates in the Kidnappers Group. The present river systems were thought, by Kingma (1971),to have developed in the Lower Castlecliffian.

The Tukituki River and its tributary , the Waipawa, originally flowed south-east to reach the coast below Kairakau (Beu & Grant-Taylor 1975). Diversion north was caused partly by elevation of the western limb of the New Rangitoto Anticline (Kingma 1971) and uplift along traces of the Puketapu and Napier Faults (Fig. 1-4; Clark 1976). Significant flow of the Tukituki River into Hawke Bay probably did not occur until the Mid-Castlecliffian at earliest. The occurrence of Castlecliffian deposits of fluvial origin near Otane and of lacustrine origin at

Patangata (Fig. 2-3.) indicate ponding of the river before breaking through the western limb of the Elsthorpe Anticline.

The Ngaruroro River, due west of the Kidnappers Group, has always followed the Kaweka Fault trace to Maraekakaho (Fig. 1-4.). During the greater part of the Castlecliffian the Ngaruroro River supplied greywacke gravel to the non-marine Salisbury terraces in the west and the marine Ruataniwha Basin further east (Fig. 2-3.). In Upper Castlecliffian or Hawera times the rise of the eastern flank of the Puketapu Fault restricted south-eastward flow. Ponding behind the barrier at Maraekakaho followed by successive down-cutting formed the Waharoa Terraces (Kingma 1971). Subsequently this river followed an eastwards course south of Roys Hill into the Kidnappers area. Renewed uplift along the Puketapu Fault then directed the river north-east to discharge between Roys Hill and Fernhill (Fig. 1-3.).

1-5 STRUCTURAL SETTING OF THE KIDNAPPERS GROUP

Pre-Castlecliffian Structure

Within the Kidnappers area the Elsthorpe-Atua-Puhokio fold system (Fig. 1-4.) continues north with a reduction of dip and a change of strike. The Puhokio Anticline intersects the coast south of Waimarama where the western limb dips gently north-west towards Cape Kidnappers and consequently Opoitian mudstones there, dip NNW (Figs. 1-4 and 1-7.). The weakly folded Atua Syncline in this area swings from north-east on the Maraetotara Plateau to almost east in the Maraetuna area (Fig. 1-7.). Similarly an eastward realignment is apparent in the western limb of the Elsthorpe Anti-

cline, the Kaokaoroa Range and the Raukawa Range (Kingma 1970a, Sheet N134).

A small but noticeable difference in dip and strike occurs between the Kidnappers Group and underlying sediments near Cape Kidnappers (Fig. 1-7.). Stereographic removal of dip on the Kidnappers Group rotates the strike of Pre-Castlecliffian strata at Black Reef and the Cape from 57° to 74°. Hence, prior to uplift associated with the group, the underlying strata at Cape Kidnappers were also aligned in a more easterly direction.

This evidence, together with that of NW/SE and east-west faults in the same area, suggests that a regional realignment in an east-west direction occurred immediately south of the Kidnappers Group before the Castlecliffian.

In the Heretaunga Plains the regional NE/SW structural trend continues, the most eastern fault passing in a line through Clive (Fig. 1-4.). In northern Hawke Bay the regional NE/SW trend continues as a series of well developed horsts and grabens progressively more downthrown towards the west (Clark 1976). Hence, the immediate Pre-Castlecliffian structure in the Kidnappers area was a depression that was fold and fault bounded in the south and fault bounded in the north-west (Fig. 1-6.).

Castlecliffian - Recent Structure

From offshore seismic profiles Lewis (1971) recognised a NE/SW trending anticline (Kidnappers Anticline 1) with an axis 5-10 km east of Cape Kidnappers (Fig. 1-6.). It is thought to involve Pliocene-Middle Pleistocene strata. Also, from a study of wave-planed surfaces offshore and

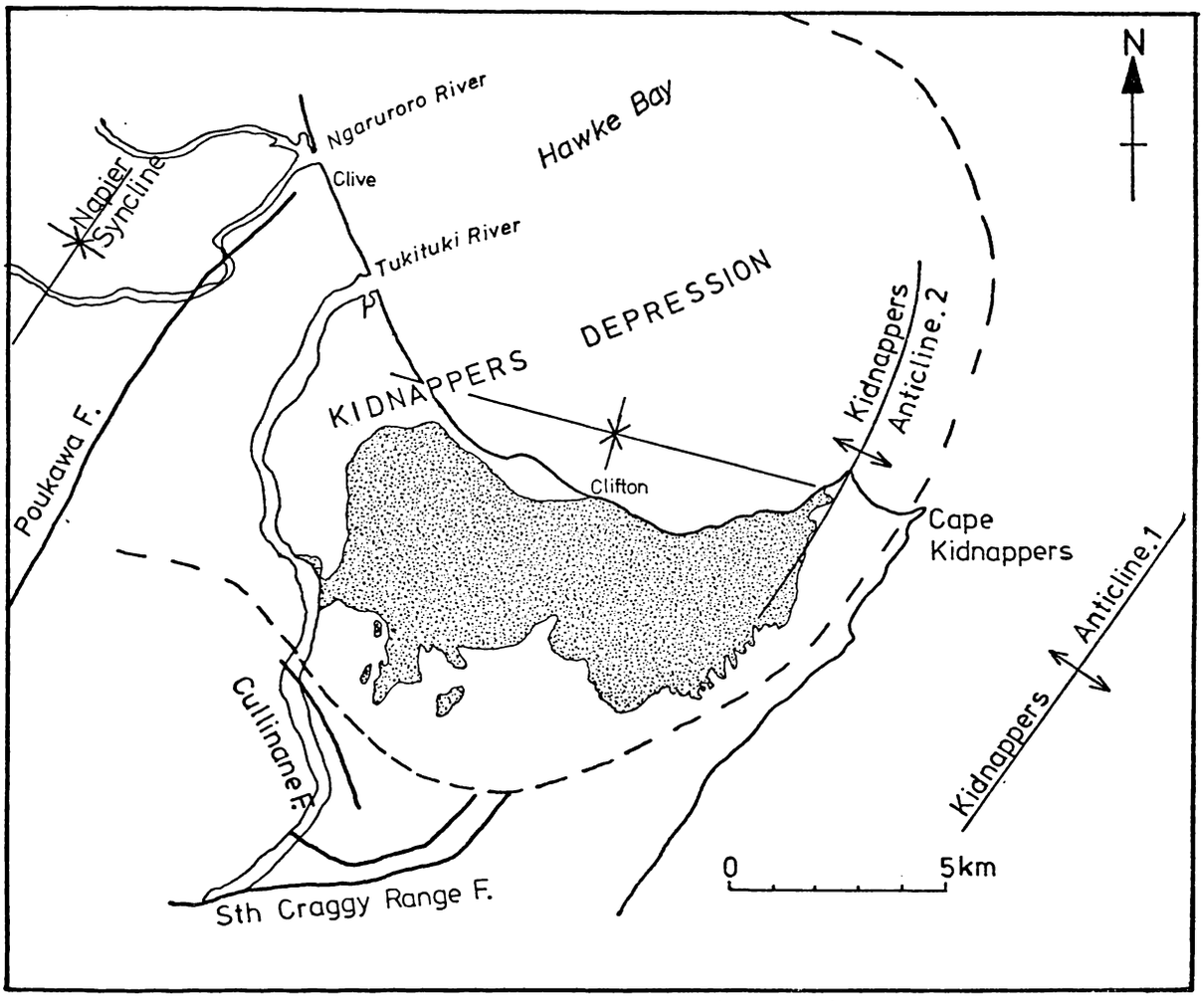

Fig. 1-6 Structural features of the Kidnappers District indicating possible extent of the Kidnappers Depression.

of interglacial raised beaches near Cape Kidnappers, Lewis (1971, 1973) suggested that the Kidnappers Group is folded about a growing anticline (Kidnappers Anticline 2) located on the western flank of Kidnappers Anticline 1 (Fig. 1-6.). The oldest wave-planed surface and offshore formation associated with this anticline are approximately 0.32 m.y. old (Lewis 1973).

Four NE/SW seismic profiles of the nearshore zone in the vicinity of Clifton (Carter & Lewis 1976) revealed a thin Holocene cover overlying Middle Pleistocene strata dipping landward and seaward at apparent angles of up to 4° and 3° respectively. The angles decrease towards the axis of a feature interpreted as a westward plunging syncline which intersects the western flank of Kidnappers Anticline 2 (Fig. 1-6.).

In addition to faults mapped by Kingma (1971) along the coastal section from Clifton to Black Reef, numerous other faults have been recognised by the writer both in the coastal section (represented as dotted lines in Fig. 2-1.) and inland (Fig. 1-7.). The faults are consistently normal (e.g. Fig. 2-10.) with downthrow to the east. Over most of the coastal section the vertical displacement is distributed amongst several splinter faults within a fracture zone, indicating east-west extension. The width of the fracture zone varies from 1 to 5 m and they consistently become wider towards the top of the cliff.

The major fault lineations and their postulated extensions are mapped in Fig. 1-7, and a stereonet plot of poles to fault planes is shown in Fig. 1-8. The most

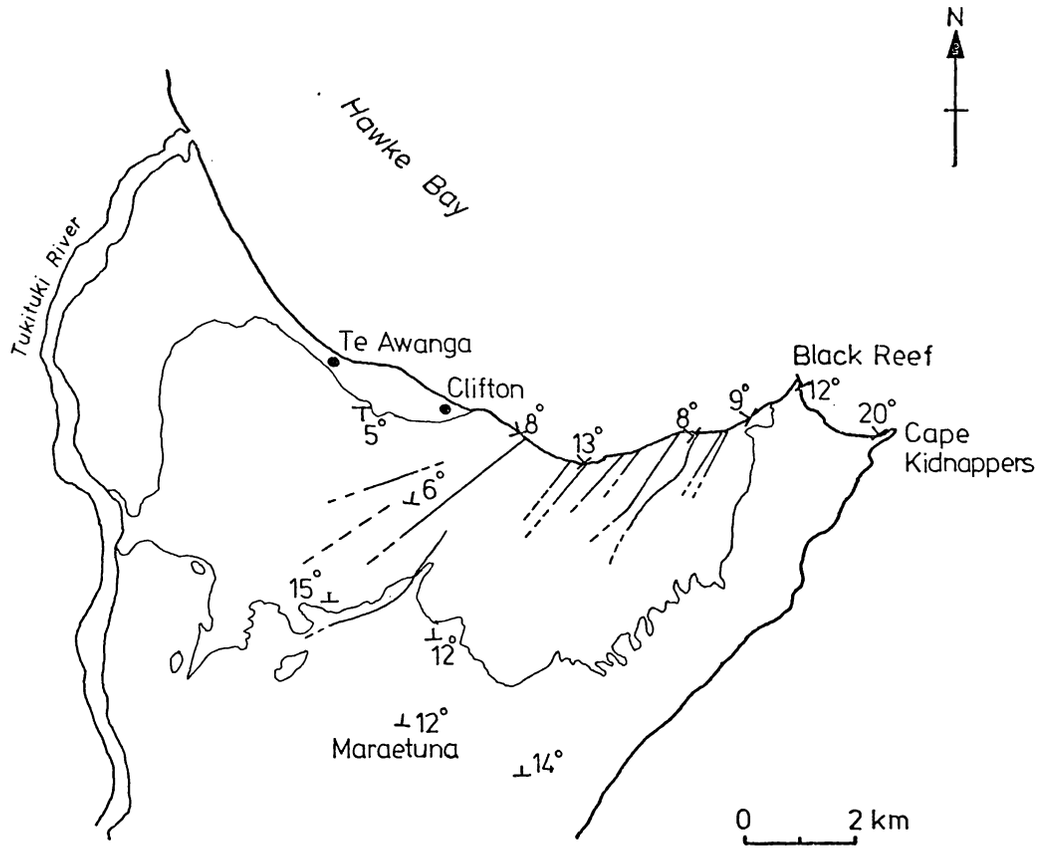

Fig 1-7. Surface faults and dip of strata in the Kidnappers Group

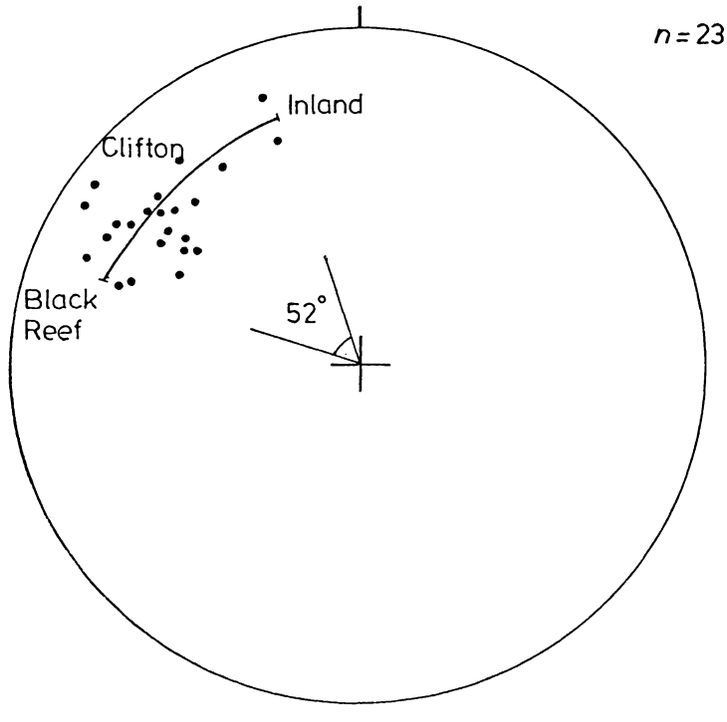

Fig 1-8. Plot of poles to fault planes in the Kidnappers Group

apparent feature is the general NE/SW trend. Close inspection shows the fault lineations change from NNE immediately west of Black Reef to ENE south-west of Clifton. In Fig. 1-8 this trend is recognised as a migration over 52° in the position of fault plane poles. The trend is also paralleled by a change in the dip of strata (Fig. 1-7.). The north-westerly dip direction at Black Reef changes to a NNE direction 2 km south-west of Clifton. An apparently anomalous south-west dip in strata was recorded immediately south of Te Awanga (Fig. 1-7.).

Hence structural features of the Kidnappers Group support the existence of an offshore westward plunging syncline. In particular the change in fault trends and dip of strata from a direction parallel to Kidnappers Anticline 2 to one approximating the synclinal axis is evidence of this. The block of strata dipping anomalously south-west is further onshore evidence for an offshore westerly plunging syncline, with the northern limb dipping south.

Kidnappers Depression

The existence of an east-west Pre-Castlecliffian structural realignment south of the group, together with the presence of a Recent syncline immediately offshore, tends to suggest that the Kidnappers Group was deposited in an east-west structural depression (Fig. 1-6.). Movement of Kidnappers Anticline 1 occurred prior to Castlecliffian times and is responsible for the angular unconformity between the group and underlying Mangapanian and Opoitian sediments. This anticline may have formed the eastern boundary of the depression.

Kidnappers Anticline 2 is a more recent feature as the oldest offshore wave planed surface and formation associated with it are 0.32 m.y. old (Lewis 1973). About 120 m of uplift of the last interglacial wave planed surface (Lewis 1971) indicates most movement may post-date 0.12 m.y. B.P. The Napier Syncline further west may have formed in response to rapid uplift of Kidnappers Anticline 2. The obliquity of the Kidnappers Depression to the regional NE/SW structural trend is similar to that described by Lewis (1971, 1973) for modern synclines and anticlines in Hawke Bay.

1-6 PREVIOUS WORK ON THE KIDNAPPERS GROUP

Most pre-1960 work is concerned with the age and correlation of beds exposed along the coastal section and has been adequately reviewed by Kingma (1971). On the basis of this earlier work Kingma felt justified in establishing a "Kidnappers Group" (1971, p83) to include all beds overlying the unconformity at Black Reef.

Deposition of the Group, which is fossiliferous in part, was considered by Kingma to be "typically paralic" (1960b, p9), meaning that terrestrial and estuarine/shallow marine conditions alternated in the basin. The sediment was envisaged as having been transported by the Tukituki, Tutaekuri and Ngaruroro Rivers. Kingma (1960b) also speculated on the tectonic setting of the group and proposed the development of a great rift due to trans-current faulting in response to southward movement of Hawke Bay.

Gibbs (1969) recognised paleosols in the group, and Seward (1975) established the ages of four tephras in the group by fission track dating. Beu and Grant-Taylor (1975) briefly discussed the paleontology and some other aspects of the group, and in particular noted the presence of ignimbrite pebbles in the coastal section stratigraphically below pebbles of Whangai argillite. On this basis they suggested a major rearrangement of Hawke's Bay's drainage patterns occurred approximately 0.25 m.y. ago. From off-shore seismic profiles Lewis (1971, 1973) and Carter & Lewis (1976) have contributed to the understanding of Upper Quaternary deposition on a tectonically active continental

shelf and (Lewis 1971) in particular, determined the growth rate of anticlinal and synclinal folds in offshore Hawke's Bay.

CHAPTER 2: STRATIGRAPHY

2-1 LITHOSTRATIGRAPHIC NOMENCLATURE

The Castlecliffian sediments exposed in the coastal section from Clifton to Black Reef (Fig. 2-1) were named the Kidnappers Group by Kingma (1971), who also nominated the section as standard for the Castlecliffian Stage in the Te Aute Subdivision. The formational nomenclature adopted at that time is presented in Fig. 2-2.

In this study Kingma's stratigraphic nomenclature is retained with one exception, namely that the Upper Clifton Sand be abandoned as a formation and become the Upper Clifton Sand Member of the Te Awanga Beds. Kingma recorded a thickness of 44 m for the formation in the coastal section (1971, Fig. 31.), when, in fact, a maximum thickness of only 10 m exists. While this discrepancy may be due to a draughting error, the justification for formational rank of the Upper Clifton Sand in relation to some of the other formations in the group is questioned. This situation highlights the difficulty of creating lithostratigraphic formations within the Kidnappers Group.

The unifying lithologic feature of the group is paradoxically its extreme lithologic diversity. Accordingly the group could be subdivided into numerous, lithologically homogeneous formations or, alternatively less numerous thicker formations displaying equivalent intraformational and interformational lithologic diversity. In the latter case any one unit within a formation is not as geologically significant as the lithologic diversity which characterises

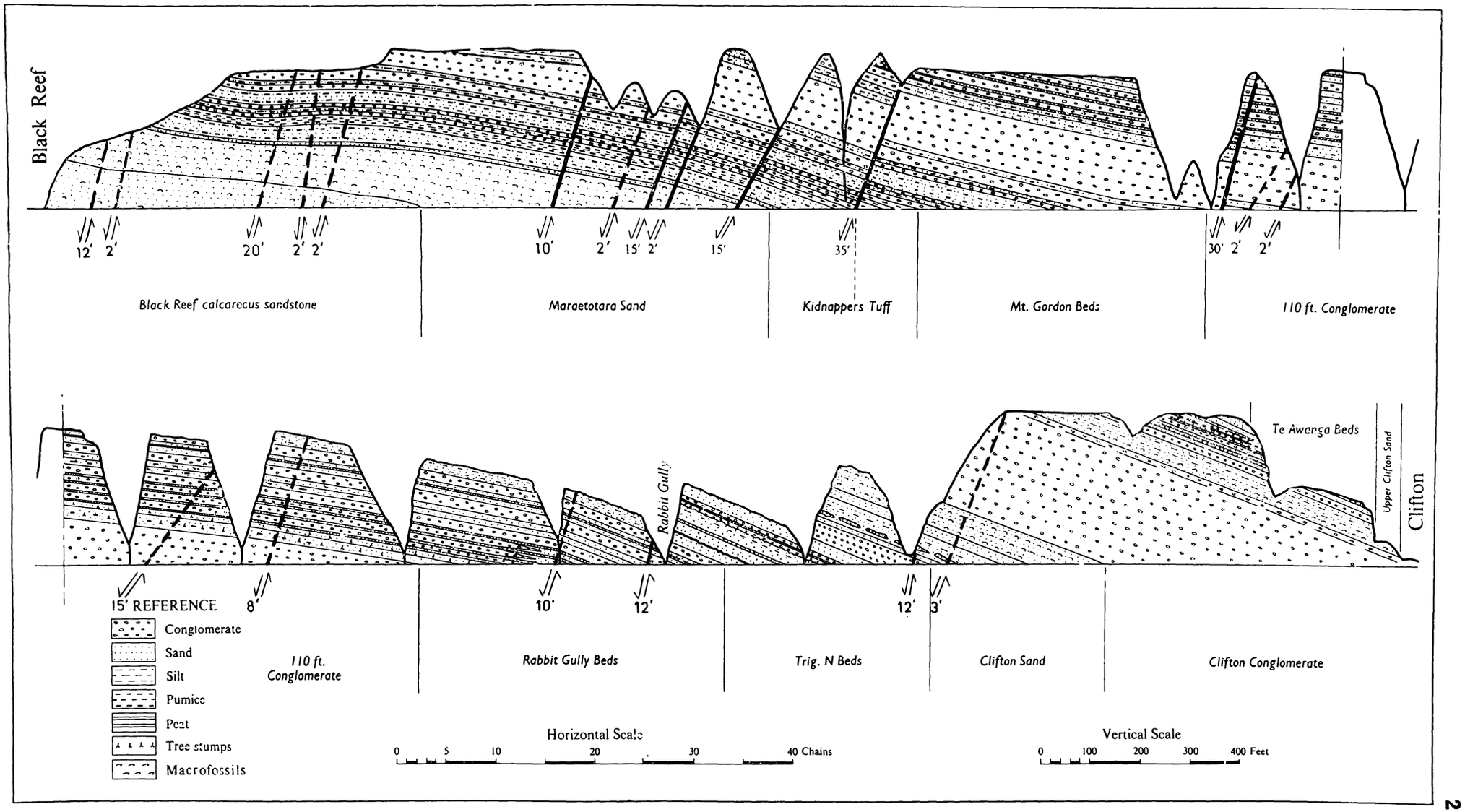

Fig. 2–1 Clifton - Black Reef Section (N135), Kidnappers Group.
(modified after Kingma (1971))

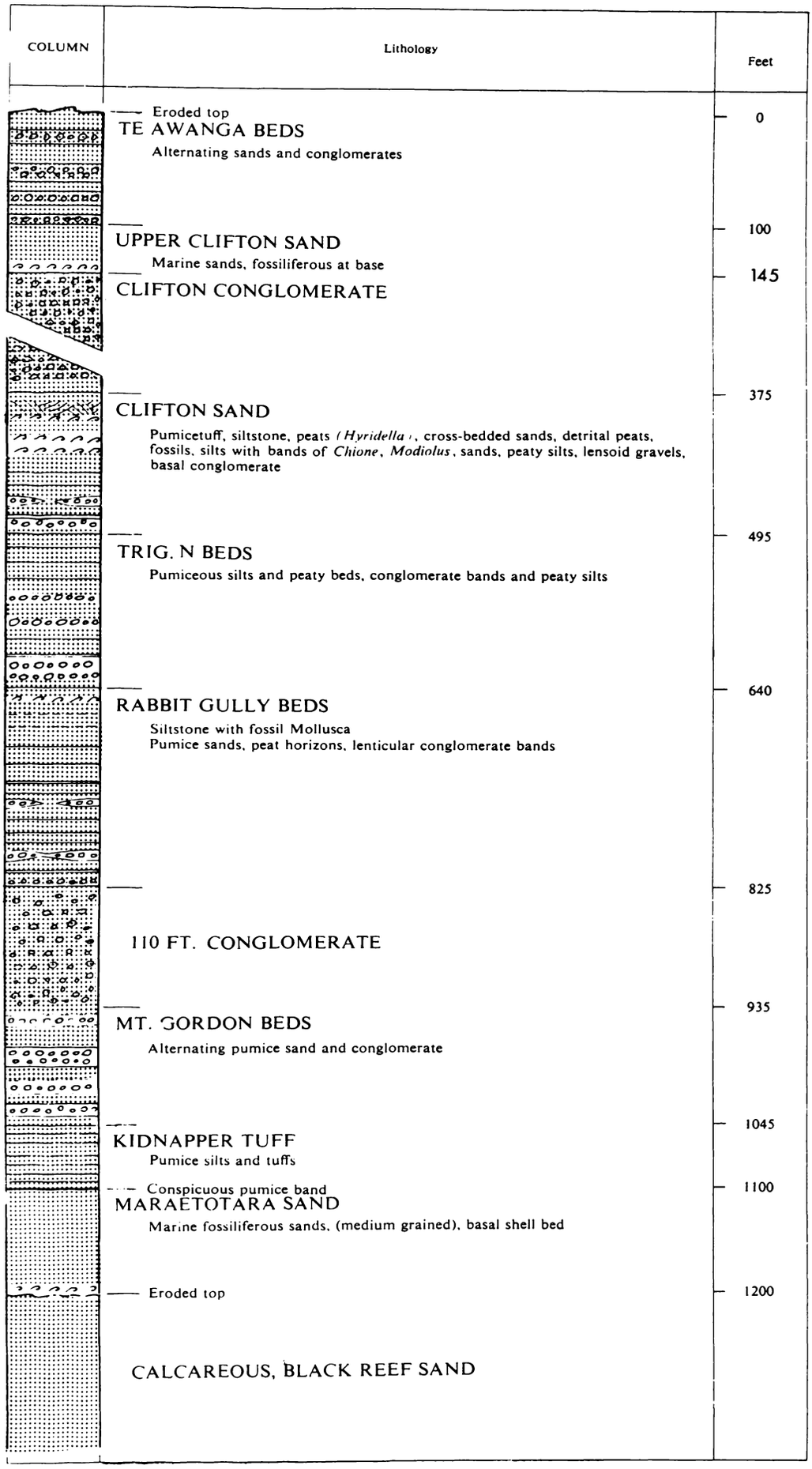

Fig. 2-2 Column through Clifton - Black Reef Section, showing lithologies
(After Kingma 1971)

that formation. Hence, for formational nomenclature to be meaningful, it is preferable that individual units be grouped into one formation until some geologically significant, lithologically unifying property is identified. In the view of the writer this case applies to the Upper Clifton Sand.

Within the Kidnappers Group three formations display equivalent intraformational and interformational diversity, namely the Rabbit Gully Beds, Trig. N Beds and Te Awanga Beds. The Upper Clifton Sand is equivalent to but one of the many lithologically homogeneous units contained within these formations. On the basis of thickness it is certainly no more extensive than any other unit, and its lithologic character rapidly changes laterally to the point where it is no longer distinguishable from any of the other sandy conglomeratic units in the Te Awanga Beds. Hence, on the basis of lithology, the Upper Clifton Sand has no special geologic significance which warrants formational distinction from the Te Awanga Beds and, at best, warrants only member status.

2-2 DISTRIBUTION AND THICKNESS OF THE KIDNAPPERS GROUP

The distribution of the group in relation to other Castlecliffian deposits and to other lithologies is shown in Figs. 2-3 and 2-4 respectively. The group was originally far more extensive, stretching in the south to the vicinity of the Cullinane and Craggy Range Faults (Figs. 2-5.). The postulated (Kamp, in prep.) shoreline position at the commencement of deposition of the group is indicated in Fig. 2.5. The scattering of "large scaren stones" (Kingma

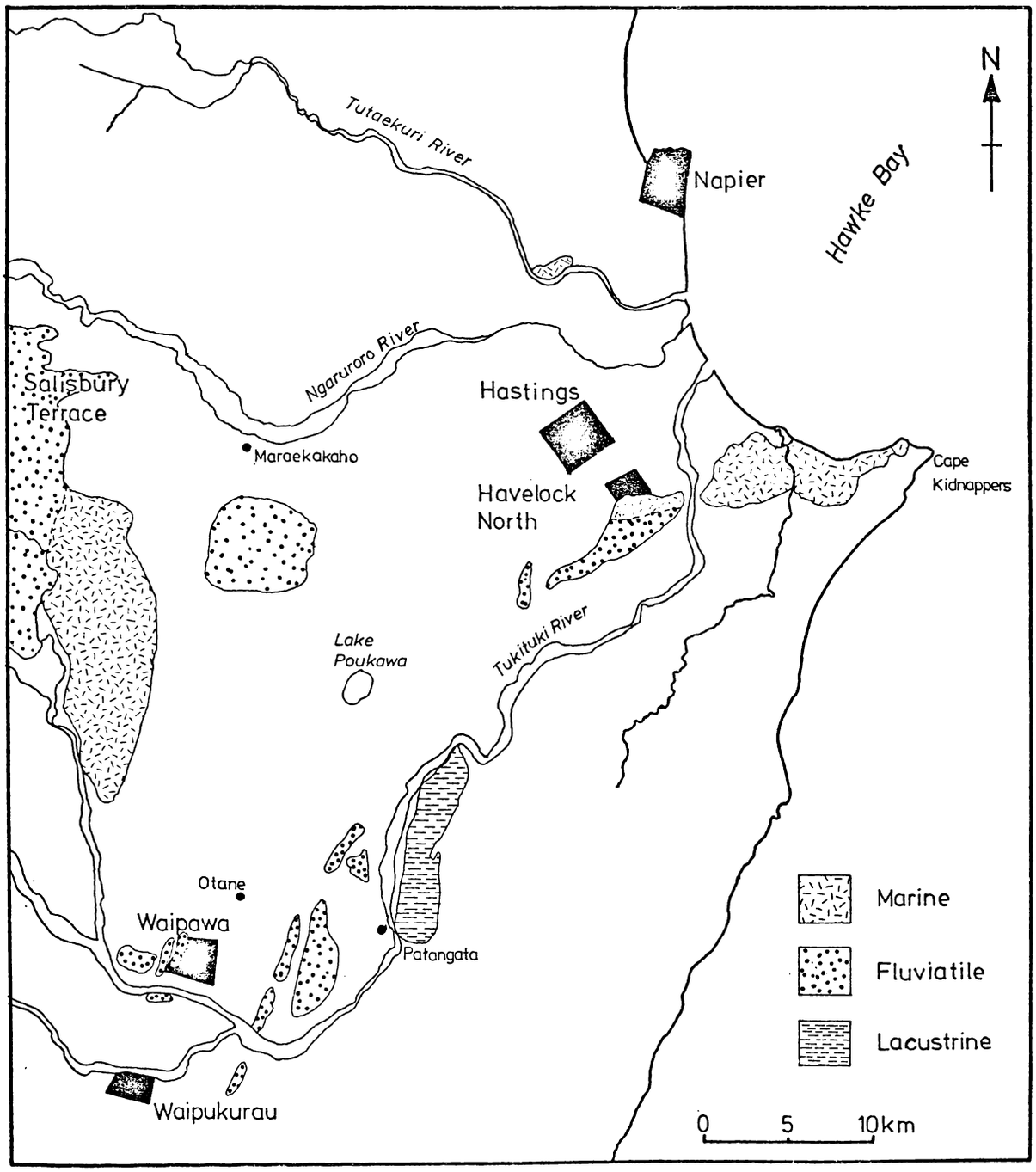

Fig 2-3. Distribution of facies in the Castlecliffian Stage After Kingma (1971)

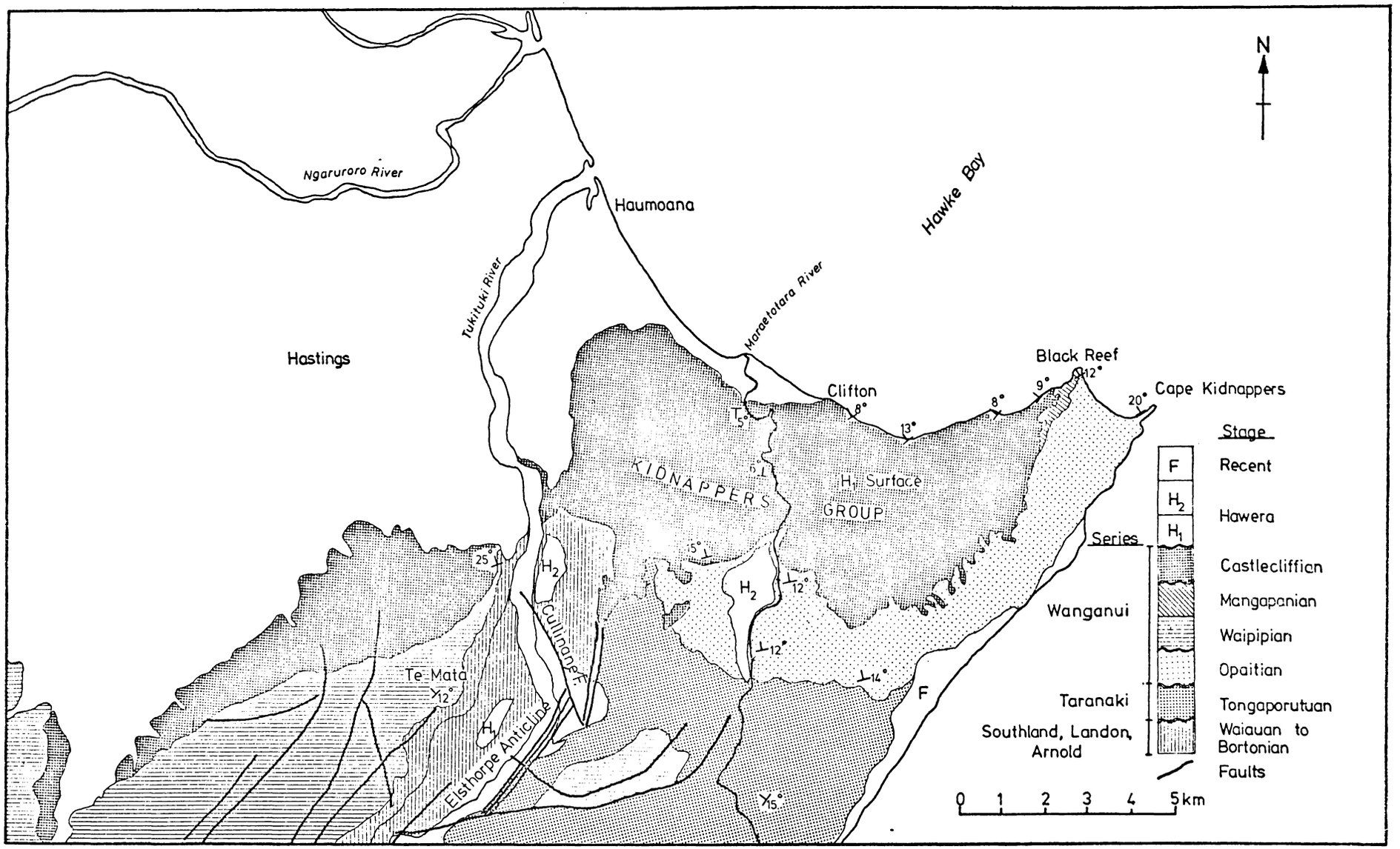

Fig. 2-4 Generalised geologic map of the Kidnappers District. After Kingma (1971)

1971, p136) over an area immediately north-east of the Cullinane Fault, further indicates a wider distribution of the group at one time.

Immediately offshore from Clifton and Rabbit Gully, reefs of conglomerate may be correlated with exposures in the coastal section (Fig. 2-5.). Also, from seismic profiles, Carter & Lewis (1976) suggested that Mid-Pleistocene deposits extend offshore from Clifton for 3 km. Thus the Kidnappers Group once extended further north than at present.

The total stratigraphic thickness of the group in the coastal section is 400 m, in the Maraetotara River valley to the south some 240 m, and in a more westerly section (z - z', Fig. 2-6.) about 200 m, indicating that the group thins south and west from Clifton. Sporadic inland exposures south-east and east of the coastal section show the group also thins in these directions.

From the above it is estimated that the Kidnappers Group had a former extent about twice that at present (Fig. 2-5.), a figure which compares well with that derived from structural evidence (Fig. 1-6.).

The decrease in altitude and dip of strata to the north-west means that only the Te Awanga Beds outcrop in the subdued relief north-west of the Maraetotara River.

2-3 RELATION TO UNDERLYING LITHOLOGIES

The Kidnappers Group rests unconformably on a number of lithologies ranging in age from Lower Miocene to Upper Pliocene (Fig. 2-4.). Over most of the region the under-

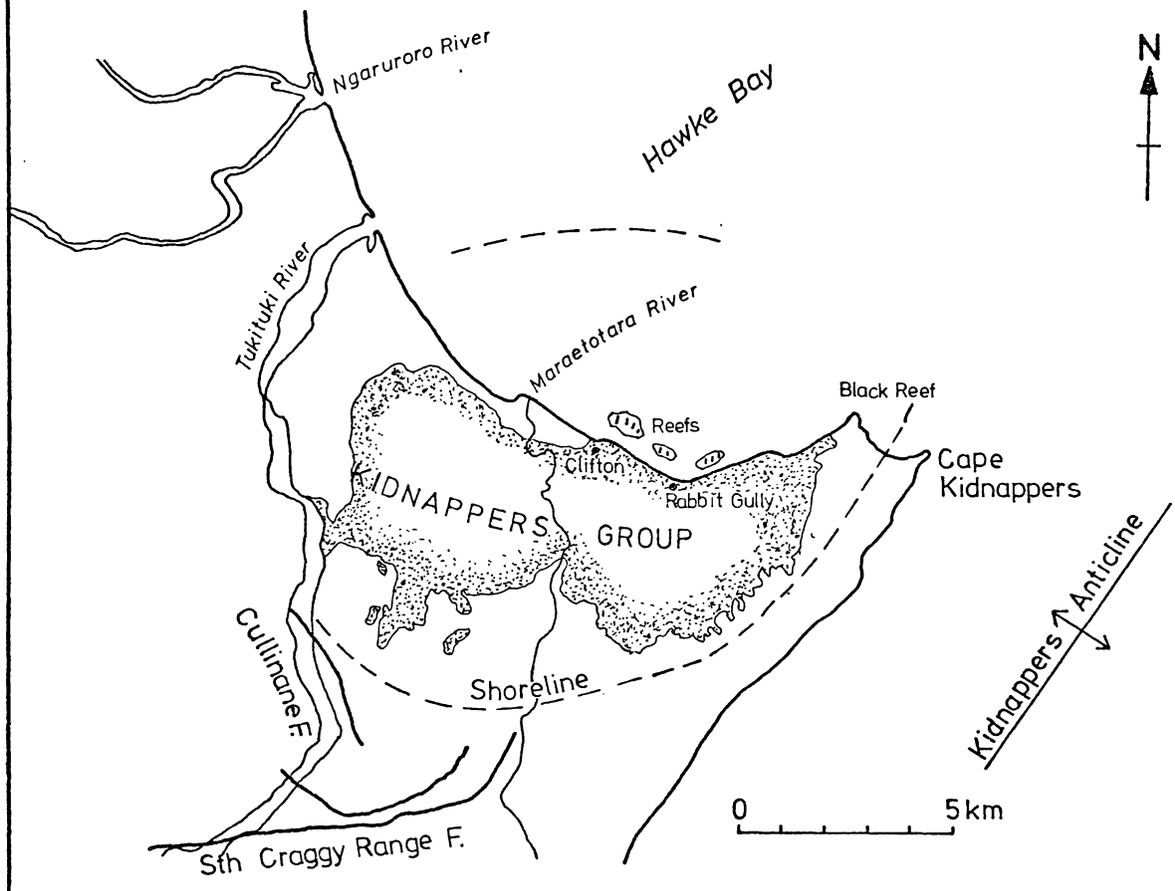

Fig. 2-5 Suggested former extent of the Kidnappers Group

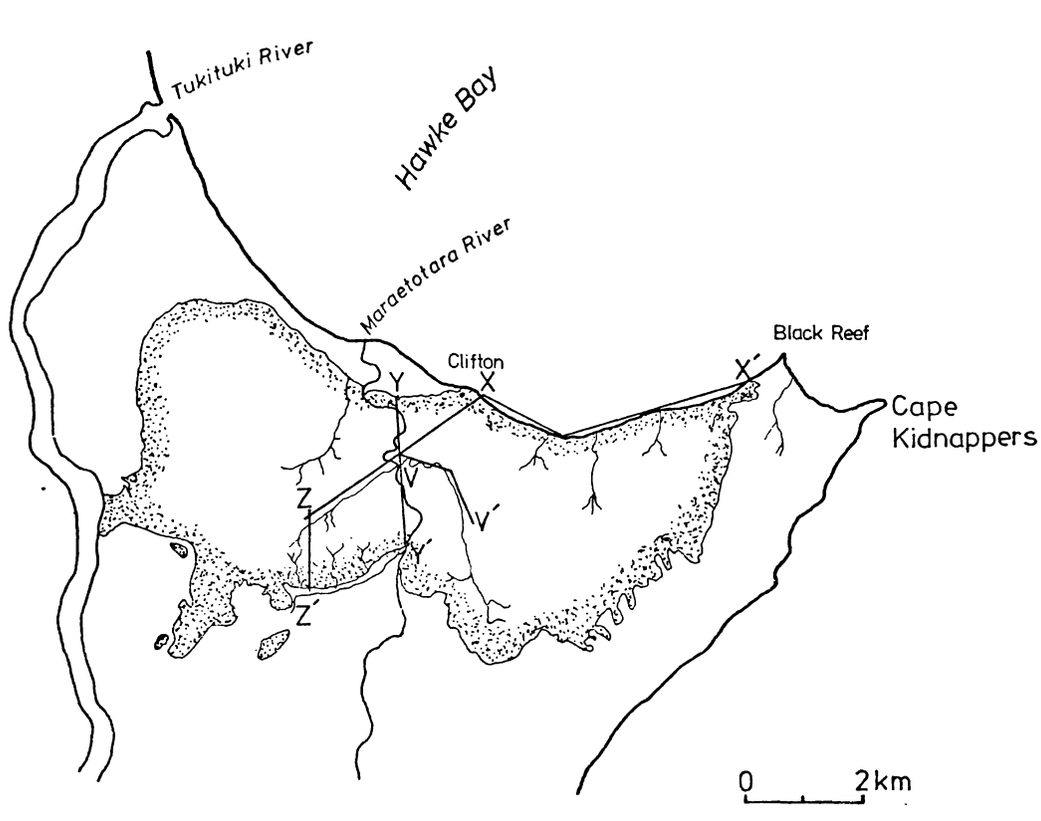

Fig. 2-6 Location of stratigraphic column sections

lying rocks are Opoitian Lower Pliocene mudstones, especially in the south and east (Fig. 2-4.) where the angular unconformity is only 2 - 3° with no detectable regional change in strike of the beds above and below. In the west (N135/360170)* the group lies on Altonian to Waiauan Lower to Mid-Miocene muddy siltstones. This unconformity is important in that it indicates the existence of any eroded Elsthorpe Anticline before Castlecliffian times. In a small area to the south (N135/370160), the group rests unconformably on Tongaporutuan Upper Miocene siltstones. In the extreme east the group rests on the Calcareous Black Reef Sand of Mangapanian age (Figs. 2-2 and 2-4.). Here the angular unconformity is 4°, with a noticeable difference in strike of 20° in beds above and below the unconformity (see Section 1-5). The contact is marked by a 30 cm thick, basal shell bed although elsewhere fossiliferous sands and silts more typically form the base of the Maraetotara Sand.

The Kidnappers Group is not overlain by other formations, although in the west it descends gently beneath the Heretaunga Plains where it probably shows angular discordance with the thick Recent gravels.

2-4 TEPHRAS, PALEOSOLS, AND LIGNITES

Tephrostratigraphy

Tephrostratigraphy forms a valuable means of correlation. Through detailed field-work (e.g. Vucetich & Pullar 1969)

---

* Grid reference based on the national thousand-yard grid of the 1 : 63 360 topographical map series (NZMS 1).

and laboratory analysis (e.g. Howarth & Rankin 1975; Hodder & Wilson 1976) tephrostratigraphy in New Zealand has reached an advanced stage especially in Late Quaternary sequences. In the main the tephras have been used in geomorphic studies as a tool for dating Late Pleistocene and Holocene events (e.g. Pullar 1967; Pullar & Selby 1971; Milne 1973). The use of tephra marker beds in earlier Quaternary sediments as a means of intrabasinal and interbasinal correlation is limited to the work of Seward (1974[a], 1976), Ninkovich (1968) and Watkins & Huang (1977).

Tephras are especially useful as marker beds because of their synchronous deposition and their widespread distribution. The base of a tephric horizon represents an instantaneous time-plane so that the marker bed is not time transgressive. These qualities become important in a sedimentary setting where there are rapid lateral facies changes.

The potential of tephrostratigraphic correlation in sediments is limited by two factors:

(1) Difficulties in the regional identification of a tephra because of textural and compositional changes with increasing distance from source, and because of differential weathering within the area covered by the tephra.

(2) Modification of the original composition of the tephra by sedimentary processes.

The first of these factors is not important in correlation within the Kidnappers Group as the distance of correlation is minimal in comparison with the distance

from source. Moreover, rapid burial with only recent exposure of outcrops has ensured a minimum of subaerial weathering. However, modification by sedimentary processes has been more important. In some cases in the group the tephras* overlie paleosols or paleodunes which indicates the deposits are of primary airfall origin. More frequently, however, the tephras are interbedded with lignites so that an airfall origin is not always certain (Fig. 2-8.). The tephras are sometimes interbedded with silty and sandy lithofacies. Nevertheless, provided little water sorting has occurred, the relative abundance of the major ferromagnesian minerals in these different situations does not appear to change markedly (see Section 6-3).

Distribution and Correlation of Tephras

In the coastal section 9 tephric units (A to I) have been recognised. These occur over 5 formations from the Kidnapper Tuff to the Trig. N Beds excluding the 110 ft. conglomerate (Fig. 2-9.). Fewer tephras have been found in the inland sections.

In the Kidnappers Group the correlation of tephras has been established on the basis of field characteristics and ferromagnesian mineral assemblages (see Section 6-3). The correlations are presented in Fig. 2-9.

---

* The nomenclature of Seward (1976) is adopted, where the term *Tephra* is used here for any bed that is composed of virtually 100% volcanic detritus.

Paleosols

Paleosols are soils developed on a terrestrial surface in a past environment. They have been formed by either burial (buried soils) or a change in the soil environment (relict soils) (Gibbs 1971). Buried soils were first recognised in the Kidnappers Group by Gibbs (1969) who briefly described one in the Mt. Gordon Beds and reported its chemical analysis. Elsewhere in New Zealand the study of paleosols, or paleopedology, has been carried out in association with tephras in Late Quaternary cover beds (e.g. Pullar *et al.* 1973) and loess deposits (e.g. Raeside 1964).

The potential of paleopedology in stratigraphic correlation and environmental interpretation has been discussed by Buurman (1975) and demonstrated by Meyer (1976) in Cretaceous sediments of the Paris Basin. Most importantly paleosols are unequivocal evidence of a terrestrial paleoenvironment.

Three well developed paleosols, or paleosol-like materials, displaying generally similar profile characteristics occur in the coastal section (Fig. 2-9.). The lower one is illustrated in Fig. 2-7 with a full profile description. The main features of the paleosols are the preservation of the dark *uA* horizon, their well developed structure, and their highly indurated nature. Indeed, the persistence of such well defined colour and structure is truly surprising for soils so old and deeply buried.

The occurrence of pumice fragments in the *uC* horizon,

Fig. 2-7. The lowest Paleosol in the Mt. Gordon Beds (N135/458205). The geological hammer rests on the upper boundary of the paleosol. Also evident in this illustration is tephric unit B overlying the paleosol. Faint shower-bedding is evident in the tephra especially to the left of the hammer.

Paleosol profile description

Horizon	*Description*
*uA**	*0-15 cm, humus stained, brown (7.5YR4/3) sandy loam*. Highly indurated, very coarse columnar to prismatic structure. Sharp upper and lower horizon boundaries.*
uB	*15-70 cm, greyish yellow (2.5Y7/2) sandy loam. Highly indurated, massive structure with a subgammate pattern. Occasional jarasite nodules and sulphur staining. Indistinct lower boundary.*
uBg	*70-100 cm, bright yellowish brown (2.5Y7/6) sandy loam. Indurated, massive structure with subgammate pattern and a horizontal system of cracks. Jarasite and sulphur staining. Grades diffusely into underlying occasionally bioturbated blue/grey sandy siltstone with abundant rootlets.*

** Horizon nomenclature and soil-texture classes after Taylor & Pohlen (1970).*

Fig. 2-8. Tephric unit F (Fig. 2-9, behind the geological hammer) interbedded with Type 1 lignite in the Trig. N Beds. Note the many thin lignite layers.

and the abundance of other fine-grained pumiceous units in the Mt. Gordon Beds, points to a volcanogenic soil parent material. In the Mt. Gordon Beds tephras commonly overlie the paleosols (e.g. Fig. 2-7.). Hence, a long period of soil formation was interrupted by a volcanic event, with the tephra protecting the *uA* horizon from subsequent erosion. The paleoenvironment of these soils is considered more fully in Chapter 7.

Lignites

Thin lignites 5 cm thick, and occasionally up to 15 cm, are a persistent feature in some formations of the group (Fig. 2-1 and Log I). The lignites often have a laminated appearance and consist of leafy vegetation, which gives them a degree of fissility. Jarasite nodules and associated sulphur staining are commonly found with the lignites, especially where they are interstratified with volcaniclastic sediments. Most often, multiple lignites occur interbedded with mudstone (e.g. Fig. 2-8.).

Two types of lignites are recognised in the group:

Type 1 Lignites are well developed and occur as multiple lignite layers up to 1 m thick (Fig. 2-8.). Type 1 lignites are found in the more extensive mudstone units, where abundant rootlets in the underlying mudstone, together with the presence of tree stumps, are evidence of *in situ* growth and accumulation of vegetation.

Type 2 Lignites, by comparison, are poorly developed with the total thickness of multiple layers never exceeding 30 cm. These lignites show little evidence of *in situ*

growth and are commonly found in thin mudstones overlying conglomerate.

There have been distinctive episodes of lignite formation in the group where they are extensive in the Rabbit Gully Beds, the Trig. N Beds, the lower parts of the Clifton Sand and the upper parts of the Te Awanga Beds (Log I). In the coastal section Type 2 lignites occur most frequently in the Rabbit Gully Beds while Type 1 lignites characterise the other formations. By comparison the inland sections are impoverished in lignites but where they occur they are generally of Type 2.

Many of the tephras in the Rabbit Gully and Trig. N Beds are interbedded with lignites (e.g. Fig. 2-8.). No evidence of charred lignite has been found and therefore the vegetation was probably not transported into the basin following the volcanic eruptions (c.f. Seward 1974a). Rather, the association of tephra with lignites is thought to represent accumulation and preservation of the former in a non-erosional environment. The abundance of rootlets through tephric unit F (Fig. 2-8.) indicates destruction of *in situ* vegetation with subsequent recovery.

2-5 CORRELATION OF FORMATIONS, CONTENT AND DISTRIBUTION OF CONGLOMERATE

Maraetotara Sand

The Maraetotara Sand differs from all other formations in the group in that it is abundantly fossiliferous, has a predominantly sandy texture, and lacks any volcanic

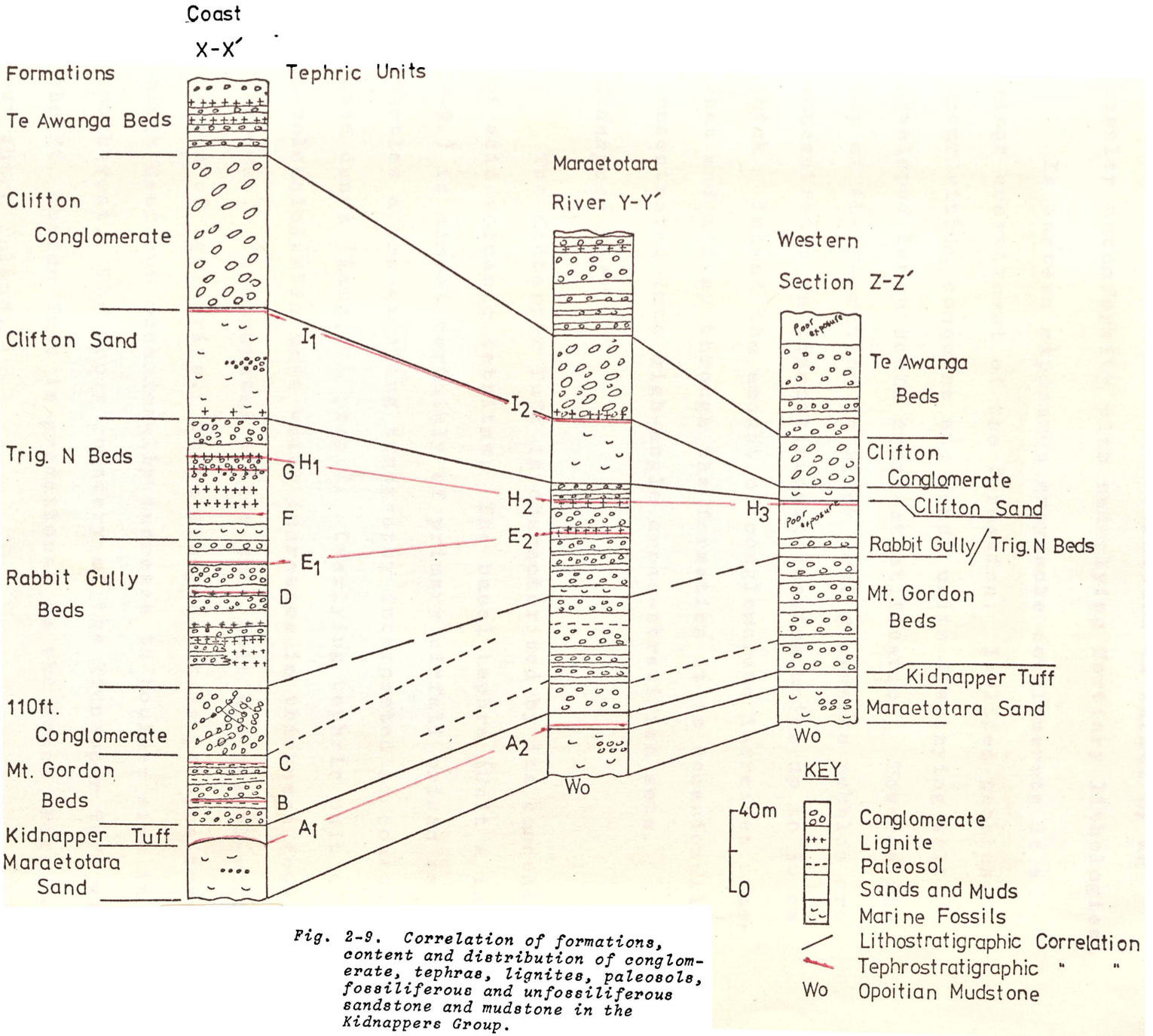

Fig. 2-9. Correlation of formations, content and distribution of conglomerate, tephras, lignites, paleosols, fossiliferous and unfossiliferous sandstone and mudstone in the Kidnappers Group.

detritus. The base of the formation is marked by an angular unconformity with underlying Tertiary lithologies.

In eastern exposures greywacke conglomerate is a minor constituent of the formation. Isolated pebbles occur within conquina and sandy units displaying well developed large-scale cross-stratification. Towards the top of the formation at Black Reef greywacke pebbles are concentrated in discontinuous, lensing units up to 30 cm thick. Inland the amount of conglomerate increases somewhat and midway through the formation it is occasionally concentrated into high-angle cross-stratified sets.

Kidnapper Tuff

The Kidnapper Tuff is characterised by its concentration of acid volcanic detritus. The basal tephra (Unit A in Fig. 2-9.) is almost certainly of primary airfall origin as it mantles a pre-existing topography interpreted as coastal sand dunes (Kamp, in prep.). Overlying tephric unit A is a volcaniclastic unit which increases in thickness towards the west. Incorporated within this unit are gravel-sized clasts of ignimbrite. These are present as pebbles near Black Reef but occasionally increase to boulder size in the south-west. The upper boundary of the Kidnapper Tuff with the Mt. Gordon Beds is gradational on the coast (Fig. 2-1.) but sharp inland.

Mt. Gordon Beds

The Mt. Gordon Beds are characterised by interbedded units of dark, weathered, greywacke conglomerate and light yellow, fine-grained volcaniclastic sediments (Fig. 2-10.).

Fig. 2-10. A typical exposure of the Mt. Gordon Beds displaying interbedded units of conglomerate and volcaniclastic sediments of Lithotype 3A (see Section 2-6). The off-set of a normal fault is highlighted by the fine-grained, light-yellow pumiceous beds. The thick conglomerate at the top of the photograph is the base of the 110 ft. Conglomerate. The vertical height in view is approximately 40 m. Locality: N135/468205.

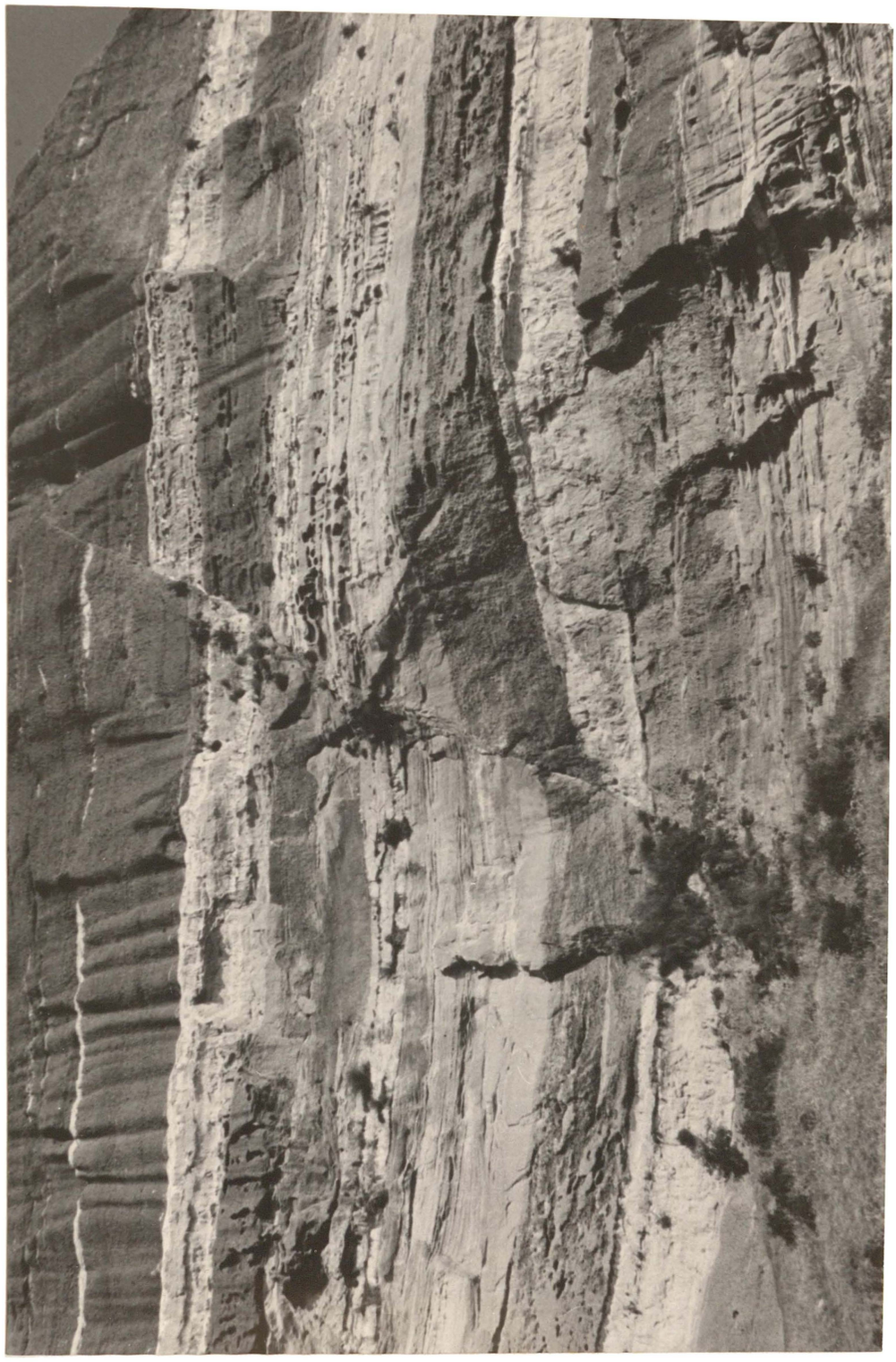

The conglomerate units are generally of similar thickness (10 - 15 m) and individual units can be traced for large distances (Fig. 2-1 and 2-9.). Tephrostratigraphy is of limited value in the Mt. Gordon Beds as tephric units B and C (Figs. 2-7.) have similar mineral assemblages (see Section 6-3.) and the tephric units inland have undergone some water reworking. Nevertheless, a paleosol towards the top of the Mt. Gordon Beds in the Maraetotara River section (N 135/407178) probably correlates with an upper paleosol in the coastal section (Fig. 2-9.). If this is correct the upper formational boundary inland lies above this paleosol.

110 ft. Conglomerate

The 110 ft. Conglomerate is well represented in the coastal section as a thick, profusely cross-stratified, gravel unit (Fig. 2-11.). However, the formation thins rapidly towards the south-west where it cannot be distinguished from the Mt. Gordon Beds. Correlation of the upper formational boundary was made on the basis of an overlying distinctive siltstone unit (Fig. 2-12.) present on the coast and inland. In the coastal exposure this unit is bioturbated and inland it is characterised by the abundant presence of macrofossils. As it seems highly unlikely that no deposition occurred inland while the 110 ft. Conglomerate was being deposited, the units between the paleosol and the siltstone unit are most probably the correlatives of the 110 ft. Conglomerate (Fig. 2-9.). A noticeable formational thinning, from about 33 m to 20 m, also occurs along the coastal section towards Black Reef (Fig. 2-1.).

Fig. 2-11. A view of the profusely planar cross-stratified sets of Lithotype 2 (see Section 2-6) in the 110 ft. Conglomerate. The scale (pack at lower left) is 15 m from the base of the formation. The current directions indicated by the dip direction of foreset beds are up to 130° apart. Locality: N135/450200.

Rabbit Gully Beds

In the coastal exposure of the Rabbit Gully Beds, conglomerates make up about half of the vertical thickness, where they are associated with mudstones, bioturbated sandstones with occasional tree stumps, Type 2 lignites and tephras. In the formation two of the conglomerate units, each 9 m thick, grade westwards into wavy, cross-stratified, sandy units (Fig. 2-1 and Log 1).

Tephric units D and E occur in the formation (Fig. 2-9.). The former is thin (20 cm) and included in mudstone. The major tephra occurs 20 m below the top of the formation and is tentatively correlated with a tephric unit in the inland section.

In the Maraetotara River section conglomerate forms 80% of the formational thickness and is associated with thin mudstones, sandstones and Type 2 lignites.

Trig. N Beds

The lower boundary of the Trig. N Beds on the coast is marked by a conglomerate overlain by a fossiliferous sandy siltstone (Fig. 2-13.); this contact cannot be placed accurately inland. Conglomerates in the Trig. N Beds have a similar thickness (5 - 10 m) to those in the Rabbit Gully Beds. It is evident for both formations that the rapid vertical change in lithology is reflected in an equivalent change laterally. Moreover there is a marked thinning of both formations inland, so that 3 km from the coast they are reduced to half their thickness (Fig. 2-9.).

Three tephras are recognised within the Trig. N Beds,

Fig. 2-12. The 12 m siltstone unit exposed in the coastal section (NB5/436197) at the base of the Rabbit Gully Beds. The lithology is predominantly horizontally-laminated silt with interbedded, bioturbated, sandy lenses. Type 1 lignite is well developed at the top of the unit, which is overlain here by conglomerate, but 50 m to the right (west) by wavy, cross-stratified and bioturbated sandy units.

namely tephric units F, G and H. Unit H, interbedded with lignites both on the coast and in the river section, is confidently correlated across the whole basin. No evidence was found in the river section of units G and F.

In view of their similarity in lithologic diversity, and in conglomerate thickness and the association with lignites and finer-grained sediments, the Rabbit Gully and Trig. N Beds are better considered as one formation, in the light of the discussion in Section 2-1. Further, the disparity in thickness of both formations between the coastal and inland sections (Fig. 2-9.) suggests that the intraformational lithologic diversity is geologically significant. Hence an apparently arbitary boundary between the formations is not meaningful in this context. However, the original nomenclature is retained until further evidence of similarity in lithologic diversity (Kamp, in prep.) is presented.

Clifton Sand

The Clifton Sand is distinguished by the absence of significant quantities of conglomerate (Figs. 2-9 and 2-14.). The entire formation is composed of abundantly fossiliferous sands and silts with only occasional, laterally discontinuous, conglomerates.

Tephrostratigraphy provides excellent control on the wedging-out of the Clifton Sand in a south-west direction (Fig. 2-9 and 2-15.). Although tephric unit H does not occur at the lower boundary of the formation, it is sufficiently close to confirm the trend shown by this contact. Tephric unit I delineates the upper boundary where it is

Fig. 2-13. The coastal exposure of the lower two-thirds of the Trig. N Beds (N135/430199). The lower boundary is marked by a wave-planed conglomerate overlain with a 5 m fossiliferous and bioturbated siltstone unit. Upwards are developed numerous mudstones, Type 1 lignites, conglomerates and interbedded tephras. Note pack for scale.

Fig. 2-14. The Clifton Sand exposed on the coast as 45 m of fossiliferous sands and silts (N135/427201). The formation extends here from sea level, upwards to the base of the conglomerate in view at top right of the photograph. The important features to note are the thick siltstone unit (centre of the photograph) underlain and overlain by thin horizontally-bedded, alternating sands and silts, and the paucity of conglomerate. Two conglomerates, both thickening towards the right (west), are visible as dark bands below the siltstone unit and to the left of the debris slopes.

mappable from the coast to the Maraetotara River and part way towards the Western section (Fig. 2-15.). This boundary is marked by a major lithologic discontinuity with the overlying Clifton Conglomerate.

Clifton Conglomerate

This formation is composed almost entirely of gravel with very few interbedded finer-grained units (Fig. 2-16.). There is an overall increase in the size of the largest clasts through the formation from about 9 cm (b-axis) at the base to 18 cm at the top. The top of the Clifton Conglomerate is clearly delineated by a remarkably sharp contact accentuated by the upper 2 m of the formation being limonite cemented. The contact lacks any undulations and may be traced as a uniform surface in outcrops from sections Z to V to V' (Fig. 2-6.) and beyond.

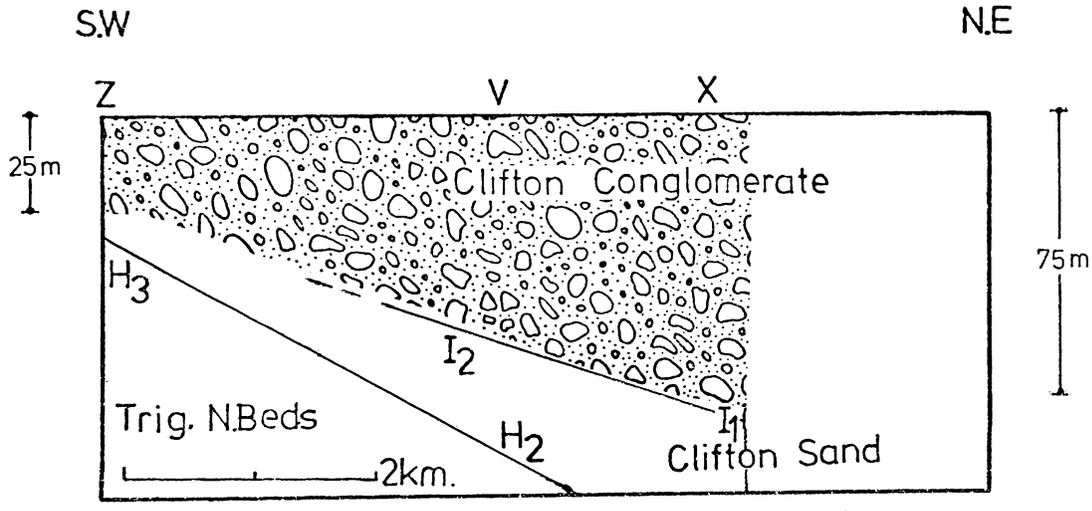

Fig.2-15 Cross section Z-V-X (Fig.2-6) showing marked decrease in the thickness to the south-west of the Clifton Conglomerate and Clifton Sand.

Fig. 2-16. The Clifton Conglomerate as exposed here on the coast (N135/422204) is a thick (75 m) conglomerate extending from the top of the prominent sandy siltstone (lower centre of photograph, Clifton Sand) to the saddle in the top right.

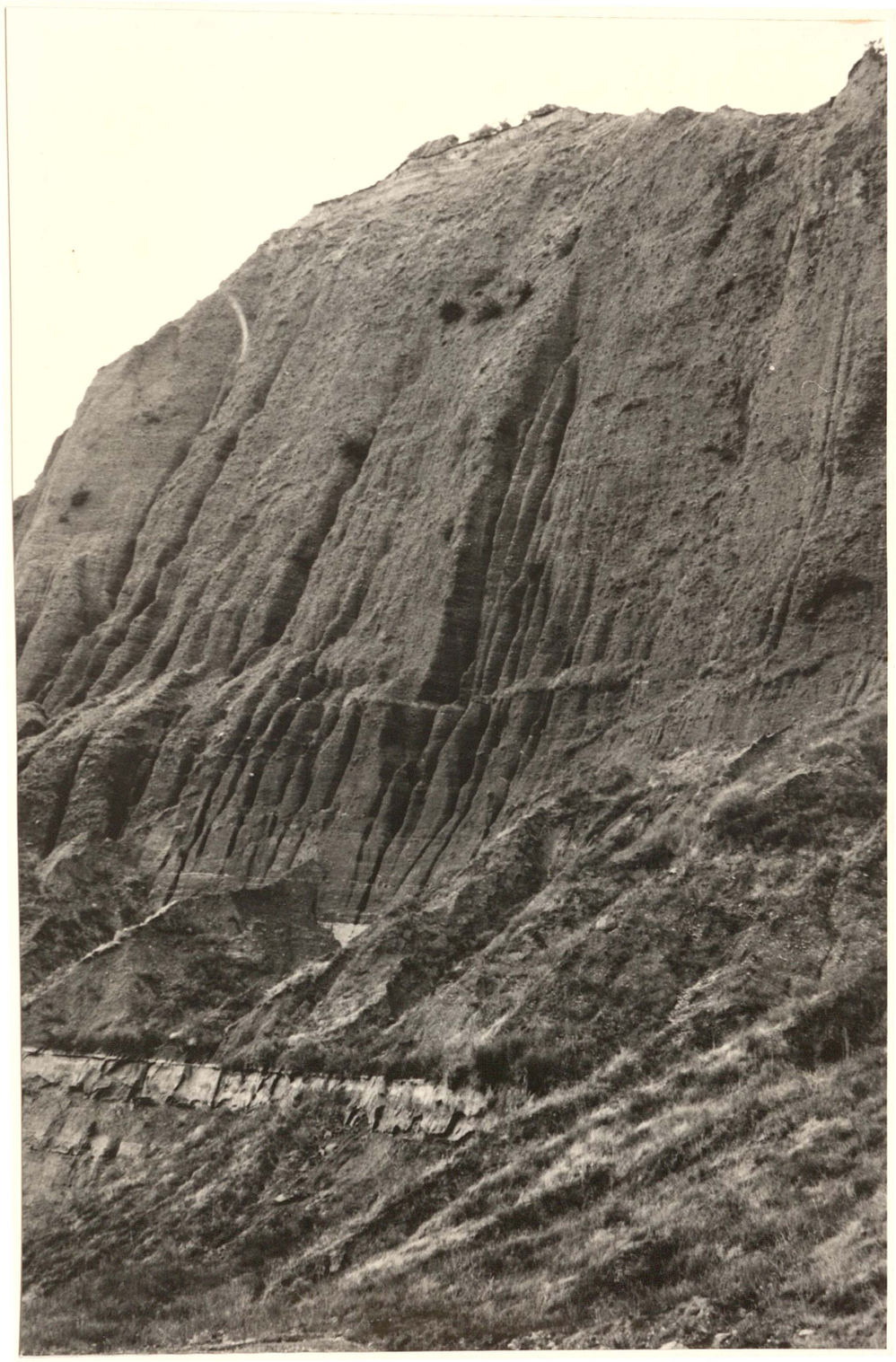

At various intervals along the linear section Z-V-X (Fig. 2-6.) the formational thickness was established with a Paulin altimeter. The readings were corrected for temperature variations and are reckoned accurate to within 0.5 m. From 6 readings a cross-section has been constructed (Fig. 2-15.) which shows a rapid thinning of the formation in a south-west direction. In only 4.5 km the formational thickness has diminished by two-thirds.

Te Awanga Beds

Over half of the Te Awanga Beds is made up of conglomerate units, individually some 5 - 10 m thick. The remainder of the formation is composed of fossiliferous sandy units with mudstone and Type 1 lignites. A similar stratigraphic sequence is recorded at each section, although a noticeable decrease in formational thickness and conglomerate content occurs towards the east.

Formational Associations of Conglomerates

On the basis of the content and the lateral and vertical distribution of conglomerates, together with their association with finer-grained lithologies, five stratigraphic classes are recognised:

Class 1 - Maraetotara Sand and Clifton Sand

Class 2 - Mt. Gordon Beds

Class 3 - Rabbit Gully Beds and Trig. N Beds

Class 4 - Clifton Conglomerate and 110 ft. Conglomerate

Class 5 - Te Awanga Beds

Class 1 is characterised by the general absence of conglomerate.

Class 2 is characterised by the association of conglomerates with volcaniclastic sediments and by a uniform lateral formational thickness.

Class 3 is characterised by large variation in conglomerate distribtuion and by an intimate association with sandy and silty units and with lignites.

Class 4 is characterised by the absence of any lithology other than extensive greywacke conglomerate, and by a marked increase in formational thickness towards the coast.

Class 5 is characterised by a uniform lateral formational thickness and by the predominance of conglomerate over associated fossiliferous sandy and silty units.

Within these formational associations, many conglomeratic lithotypes have been recognised which are now considered.

2-6 CONGLOMERATIC LITHOTYPES

There are significant differences between some conglomerates in the Kidnappers Group. A small number of lithotypes have been established to emphasise the distinctive features of different conglomerates. It is anticipated that each of these lithotypes is environmentally sensitive.

Lithotype 1 - Imbricated, Inverse to Normally Graded Conglomerate

From a distance the Clifton Conglomerate appears to be crudely horizontally-stratified (Fig. 2-17.), which upon

close inspection is a reflection of changes in clast size, sorting and fabric (Fig. 2-18.). These changes define two types of sedimentation units consistently recognised as a couplet (Fig. 2-18.) throughout most of the formation.

The lower unit is polymodal, clast-supported and inversely graded, ranging in thickness from one pebble diameter to 30 cm. Inverse grading is typically recognised by an increase in size of the larger clasts (cobbles, Fig. 3-2.) and a corresponding decrease in the percentage of smaller clasts (granules, Section 6-1.), so that towards the top of the unit the framework becomes decidedly more open. This is paralleled by an improvement in the degree of clast imbrication. Clasts are often in contact, although the close stacking of pebbles against one another, observed by Rust (1972) in the Donjek River, was not a striking feature here.

In comparison the upper unit, which ranges in thickness from 10 to 40 cm, shows a slight tendency towards normal grading (Fig. 2-18.). This unit is composed of small pebbles and occasional larger, erratic pebbles. The lower contact with the lower unit is typically conformable although the upper contact with the overlying couplet is often erosional, showing slight angular truncation.

The most distinctive feature of the couplet is clast imbrication, the nature and origin of which is extensively discussed in Chapter 5. The couplets have variable lateral persistence, the imbricated lower unit often being traceable for 15 - 20 m. Laterally the couplets either fade-out, are truncated, or pass into massive, polymodal,

Fig. 2-17. A typical view of the Clifton Conglomerate showing the dominance of crude horizontal stratification and the absence of cross-stratification. The strata dip towards the right (north-west) at 8°. The vertical height in view is approximately 6 m.

Fig. 2-18. A close-up view of Lithotype 1 in the Clifton Conglomerate. A and B represent couplets of Lithotype 1. C and D represent the lower inversely graded unit and E and F the normally graded unit. Clast imbrication is clearly evident in the upper parts of C and D. Unit G is a single clast diameter thick imbricated unit corresponding to units C and D and it angularly truncates unit F. Scale (bottom left) is 33 cm high.


G
F
B
D
E
A
C

clast-supported, weakly imbricated units. Occasionally overlying these unstratified units (Fig. 2-19.) are highly eroded remnants of sandy units. These display small, asymmetrical, straight crested or sinuous ripples having a ripple index of 7 (Fig. 2-19; Reineck & Singh 1973).

Lithotype 1 occurs exclusively in the Clifton Conglomerate, although sporadic cross-bedding (Lithotype 2) is also found at the base of the formation on the coast and inland.

Fig. 2-19. Current ripples within massive conglomerate in the Clifton Conglomerate. Scale 11 cm long.

Lithotype 2 - Planar Cross-stratified Conglomerate

Lithotype 2 is characterised by distinct stratification, comprising sets or cosets of planar cross-bedded units (Fig. 2-11.). Set thickness ranges from 60 cm to 2 m. Individual sets may persist laterally for up to 10 m before they are lost by the lack of outcrop exposure, and as many as 10 overlying sets occur without forming a coset. Set boundaries are mainly erosional (Allen 1963) in cosets (Figs. 2-11 and 2-20.), but solitary sets have non-erosional lower boundaries (Fig. 2-21.). Pebble-sized clasts predominate within the profusely cross-stratified conglomerates, although solitary sets are frequently finer-grained with sand deposition at the down-stream end of sets. Associated with the solitary sets are polymodal, clast-supported and unstratified conglomerate (Fig. 2-21.). Current directions from foreset dips are highly variable (see Section 5-3.).

Mudstone lenses occur only rarely in the 110 ft. Conglomerate. Where they do occur they are highly disrupted (Fig. 2-22.) which points up the possible origin for intraformational mudstone clasts elsewhere in conglomerates.

Lithotype 3 - Thin, Massive to Stratified Conglomerate

Conglomerate units, ranging in thickness from 5 to 12 m on the coast and up to 15 m inland, are a common lithology in the Mt. Gordon, Rabbit Gully and Trig. N Beds. Internally, no single feature characterises the units, rather, they appear to be massive, especially in

Fig. 2-20. Sets of planar cross-stratified conglomerate of Lithotype 2. They occur here in the conglomerate immediately beneath tephric Unit E_1 in the Rabbit Gully Beds (Fig. 2-9.).

Fig. 2-21. A solitary, sandy conglomeratic, planar cross-stratified unit of Lithotype 2, surrounded by polymodal, clast-supported and unstratified conglomerate. Scale is 25 cm long.


0·5m

weathered outcrops, with occasional cross-bedding and interstratified sands. However, within the context of underlying and overlying lithologies these conglomerates form a distinctive deposit.

The lower contact of these conglomerates may be one of three types:

(1) *Rip-up Clasts* - The lower contact of conglomerates is most frequently an erosional one, the underlying mudstone, sandstone or lignite having been ripped-up and incorporated into the base of the conglomerate (Fig. 2-23.). The contacts have distinctly irregular bases with relief locally up to 45 cm. This structure suggests that the underlying lithology has undergone some consolidation before erosion.

(2) *Load Structures* - These penecontemporaneous deformation structures (Fig. 2-24.) sometimes characterise a contact where conglomerate overlies mudstone, and indicate the deposition of conglomerate over an unconsolidated muddy layer (Reineck & Singh 1973).

(3) *Small Channels* - These occur eroded into underlying sandy mudstones and have depths of 1 m and widths of 1.5 m (Fig. 2-25.). Typically they are infilled with cross-stratified pebbles.

Within Lithotype 3 two subtypes are recognised on the basis of association of conglomerate with other lithologies.

Fig. 2-22. Mudstone lenses in the 110 ft. Conglomerate. A disrupted lense, now present as mudstone clasts of intraformational conglomerate can be seen in the bottom right. In the centre a mudstone lense has been penecontemporaneously deformed into flame structures, caused by loading of the overlying conglomerate (Reineck & Singh 1973). Vertical height shown is approximately 8 m.

Fig. 2-23. Rip-up clasts derived from the underlying mudstone and incorporated into the base of a conglomerate. The current direction indicated is towards the right.

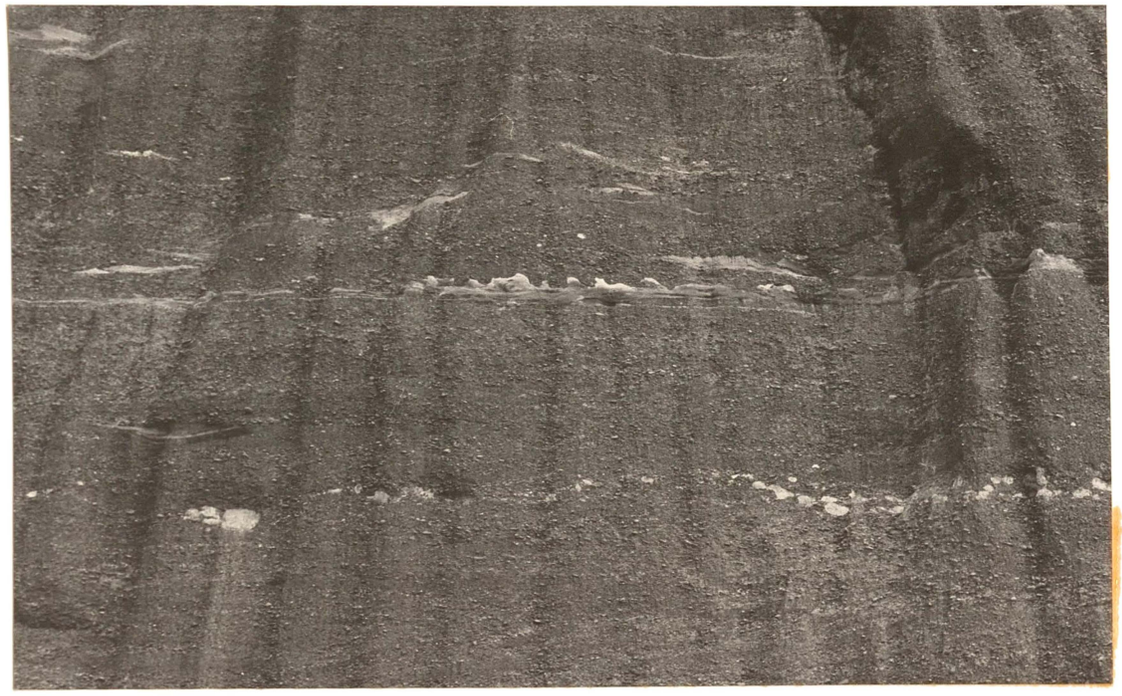

Fig. 2-24. Spectacular load structures where conglomerate has penetrated mudstone. Scale is 19 cm long.

Fig. 2-25. A small channel cut into mudstone and infilled with conglomerate at the base of Lithotype 3A. Channel depth here is approximately 1 m.

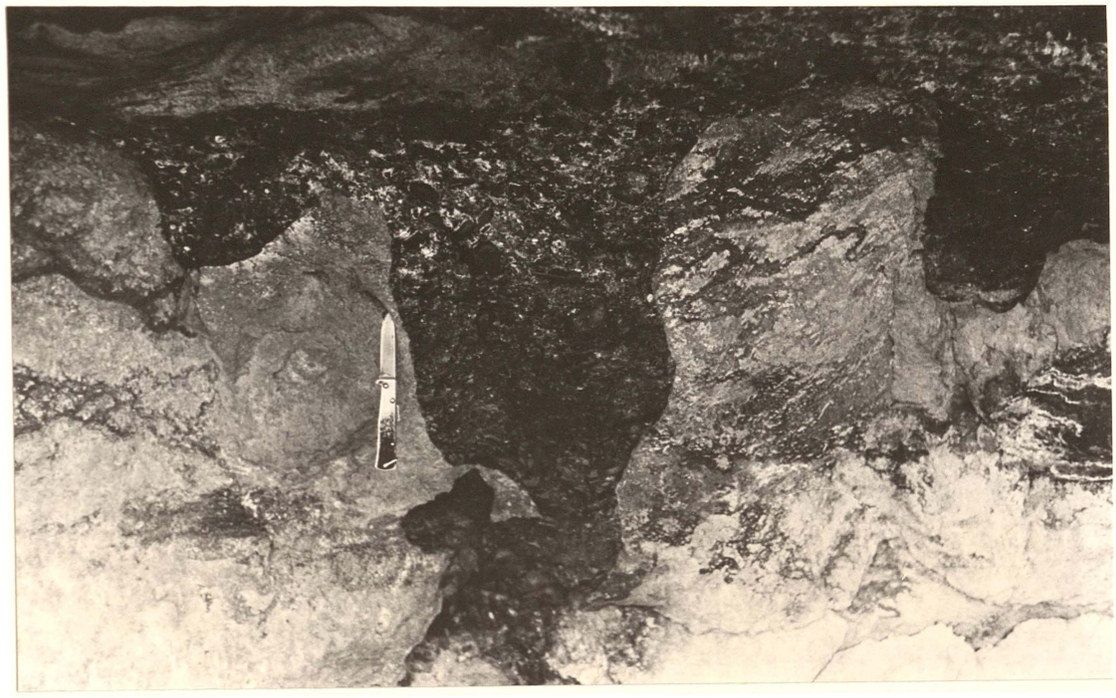

(a) *Lithotype 3A - Conglomerate with Interstratified Volcaniclastic Sediment and Overlying Paleosols*

Lithotype 3A occurs in the Mt. Gordon Beds and is characterised by the association of conglomerate with pumiceous sediment and with overlying paleosols (Fig. 2-10.). The common textures and structures found in these conglomerates are summarised in an idealised column in Fig. 2-26. Massive, poorly sorted and poorly imbricated conglomerate passes upwards into cross-bedding similar to that in Lithotype 2. Above, the conglomerate often becomes finer with units of small pebbles separated by horizontally and cross-bedded pumiceous sand and gravel. The conglomerate is often overlain by volcaniclastic sand and silt upon which a paleosol may be developed.

Conglomerates in the inland sections differ from this idealised column by showing an increase in the amount of planar cross-bedding towards the middle and upper parts of units, and by the general absence of paleosols.

The association of pumiceous and greywacke gravel in a small, planar cross-stratified set is illustrated in Fig. 2-27. Not uncommonly there is a decrease in grain-size and density of particles down the foresets, with the larger greywacke clasts being concentrated at the top of foresets and pumice granules at the base. Similar occurrences within cross-stratified gravelly sand units of the Upper Pleistocene Hinuera Formation

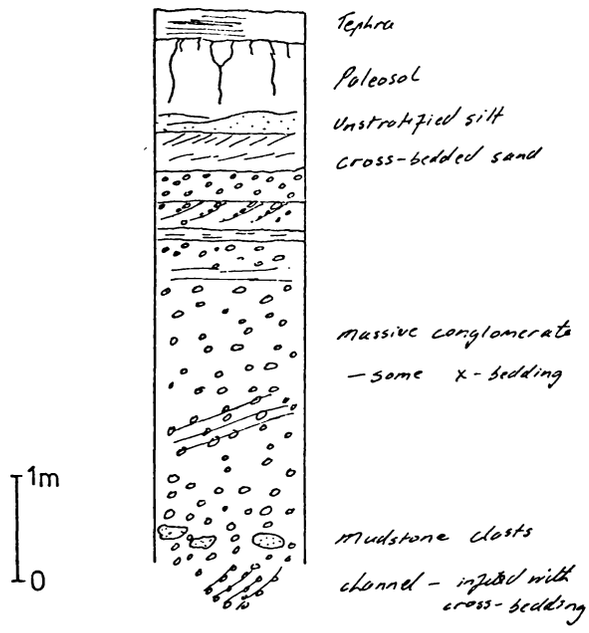

Fig. 2-26. Idealised Stratigraphic Column of Lithotype 3A on the Coast.

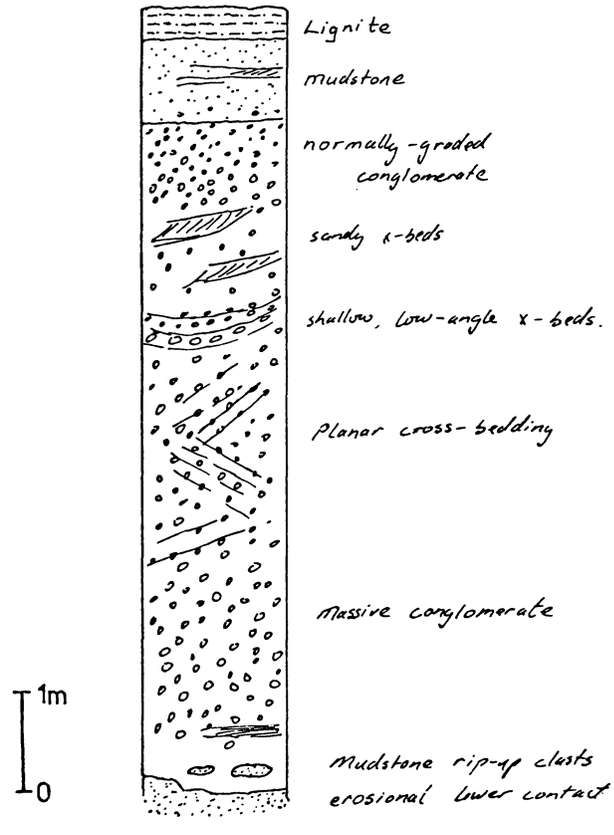

Fig. 2-28. Idealised Stratigraphic Column of Lithotype 3B.

in the Hamilton Basin are explained by Hume *et al.* (1975) as resulting from extremely rapid deposition of successive foreset laminae, trapping the coarse fraction at the top of the foreset before slip-off occurs.

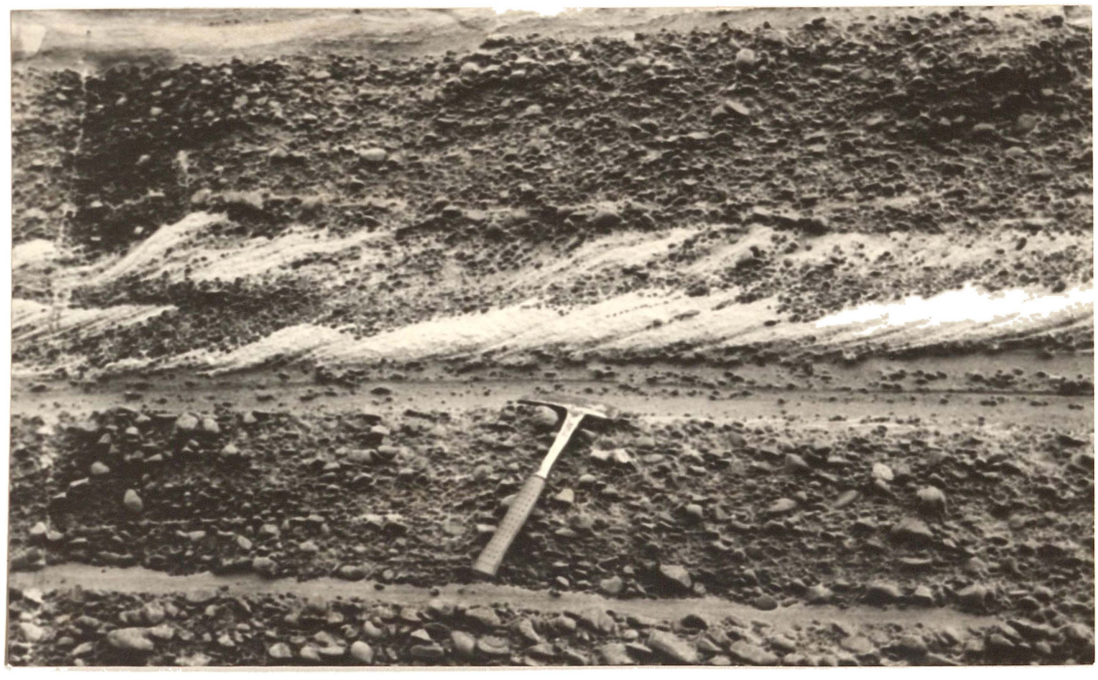

Fig. 2-27. Cross-stratified set composed of greywacke pebbles and pumice granules in Lithotype 3A of the Mt. Gordon Beds. The association of internally unstratified conglomerate (behind hammer) passing upwards into plane bedded sand and sporadic pebbles and then above into cross-bedded pebbles, may correspond to a transition from flow in the upper part of the upper flow regime into the lower part of the upper flow regime, and then into the upper part of the lower flow regime (Fahnestock & Haushild 1962).

(b) *Lithotype 3B - Conglomerates with Overlying Mudstones and Lignites*

An idealised column through Lithotype 3B conglomerates in the Rabbit Gully and Trig. N beds is illustrated in Fig. 2-28. This lithotype is characterised by a similar fining-upwards sequence from massive conglomerates, through planar cross-stratified conglomerate, low-angle cross-stratified conglomerate, isolated sandy cross-beds and into well sorted unstratified pebbles. The units then grade above into mudstone with some inter-stratified sandy lenses and finally into lignite.

Where planar cross-stratified sets occur they are neither as large nor as extensive as in Lithotype 2. Sets are now 2 - 3 m long and up to 30 cm thick. Low-angle cross-stratified conglomerate (Fig. 2-29.) is often the most common form of bedding. These structures resemble broad shallow channels up to 3 m across and 30 - 60 cm deep in sections normal to current direction. In the upper parts of the conglomerates isolated sandy cross-beds infill some of the broad shallow channels.

Where a similar sequence is immediately repeated, the upper mudstone unit is thin (1 m) and Type 2 lignites predominate. However, where Lithotype 3 is not immediately repeated the sequence is followed by more extensive mudstones and by Type 1 lignites. Three successions of Lithotype 3 occur in the Rabbit Gully Beds in the coastal section. Two successions associated with more extensive mudstones, sandstones and Type 1 lignites occur in the Trig. N Beds. The inland correlatives of these formations

show repeated successions of Lithotype 3.

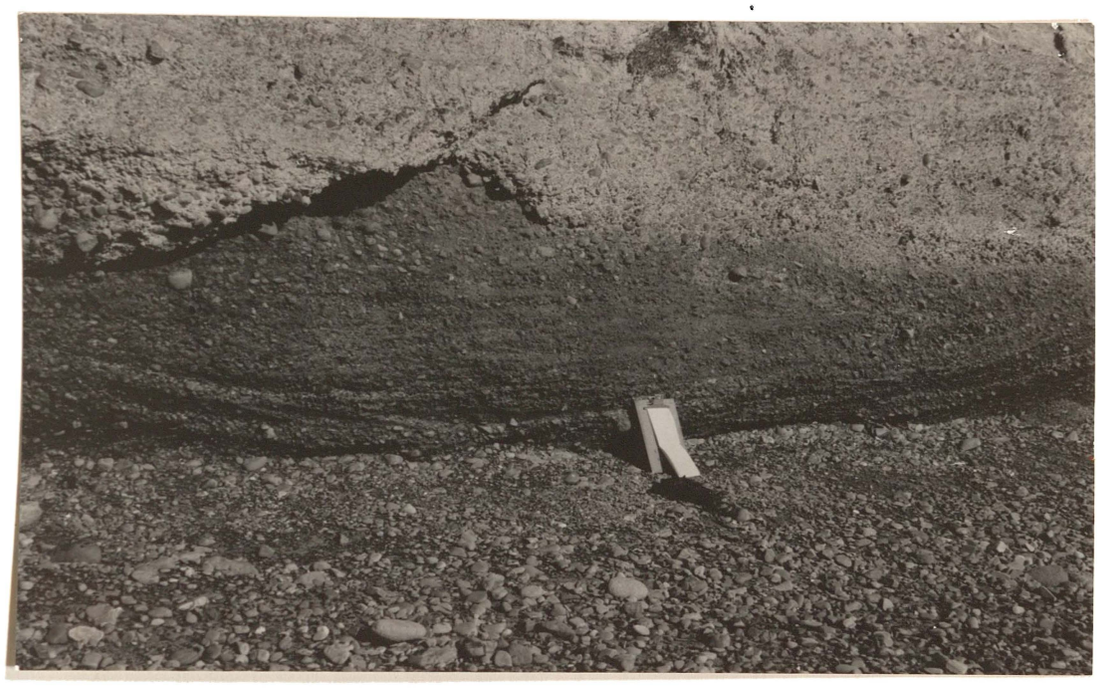

Fig. 2-29. Low-angle cross-stratification resembling a broad shallow channel in Lithotype 3B. Scale is 30 cm high.

Lithotype 4 - Planar Cross-stratified, Shelly, Sandy Conglomerate

Lithotype 4 is of limited extent in the Kidnappers Group occurring only in south-western exposures of the Maraetotara Sand where it is manifested as a 2 m thick planar cross-stratified set with west-dipping foresets. Clast sizes are strikingly bimodal, involving fine sand and pebble modes (Section 6-1.), the pebbles being highly spherical (Section 4-5.). An important constituent of this lithotype is smashed shells. These along with under-

lying and overlying fossiliferous sediments indicate deposition in a marine environment.

Lithotype 5 - Thin, Massive to Low-Angle Cross-stratified, Shelly Conglomerate.

This unstratified and low-angle cross-stratified conglomerate, together with its occasional sandy lenses, is similar to Lithotype 3B. However, the abundance of broken shell fragments identifies the depositional environment as marine. Further, the deposits have a higher matrix concentration so that they are less consistently clast-supported. Lithotype 5 occurs as lensoid deposits interbedded with finer-grained fossiliferous sediments in the Clifton Sand and Te Awanga Beds.

Summary of Lithotype Distribution

The distribution of conglomeratic lithotypes in the Kidnappers Group, and their relationship to the formational classes, are summarised in Table 2-1.

From Table 2-1 formational Class 4, established on the basis of conglomerate content and distribution, is monospecifically Lithotype 1 in the Clifton Conglomerate, and Lithotype 2 in the 110 ft. Conglomerate. Formational Class 3 is wholly made-up of Lithotype 3B and mainly occurs in the Rabbit Gully and Trig. N Beds. Similarily, Class 2 is exclusively made-up of Lithotype 3A. Other associations are also evident in Table 2-1.

The conglomeratic lithotypes are of importance in paleoenvironmental reconstruction, and the formational classes are of significance in understanding paleoenvironmental succession (Chapter 7).

Formation	Lithotype		Formational Class
	Coast	Inland	
Te Awanga	5 & (3B)	5 & (3B)	5
Clifton Conglomerate	1	1	4
Clifton Sand	5	-	1
Trig. N Beds	3B & (2)	3B & (2)	3
Rabbit Gully Beds	3B & (2)	3B & (2)	3
110 ft. Conglomerate	2	-	4
Mt. Gordon Beds	3A & (2)	3A & (2)	2
Maraetotara Sand	4	4	1

Table 2-1. Summary of Conglomeratic Lithotype distribution in the Kidnappers Group. Brackets indicate subordinate importance.

2-7 AGE

On the basis of its macrofauna Fleming (1957) attributed a Putikian age to the Maraetotara Sand. The presence of *Pecten, Xymene* aff. *plebeius, Tawera wanganiensis, Stiracolpus delli murdochi,* and *Xenogalea,* and the absence of characteristic extinct Nukumaruan genera, was the main evidence for this age (Kingma 1971). The presence of several genera in the Maraetotara Sand not previously reported in sediments as young as the Putikian was explained in terms of provincial differences.

The microfaunal age in one sample from the Maraetotara Sand appears to show a discrepancy with the macrofaunal age (Kingma 1971). The presence of *Haeuslerella*

parri, not previously reported for the Castlecliffian, and in particular the common abundance of *Uvigerina* aff. *miozea* suggest either an older age for the formation or the persistence of these genera into the Castlecliffian Stage (Kingma 1971).

Seward (1975) determined fission-track ages on glass shards from four tephras in the coastal section (Fig. 2-30.). From the fission-track age of tephras in the Wanganui Basin, Seward (1974b) dated the base of the Putikian Substage as 0.45 ± 0.09 m.y. B.P. Hence the Maraetotara Sand, which underlies the Kidnapper Tuff (0.85 ± 0.10 m.y. B.P.), is much older than Putikian, and more likely to belong to the Okehuan Substage (Seward 1975). The base of the Okehuan has been dated at 1.06 ± 0.16 m.y. B.P. (Seward 1974b).

The Kidnapper Tuff may be correlated on the basis of its ferromagnesian assemblage with a deep-sea tephra paleomagnetically dated in two cores at 0.87 and 0.86 m.y. B.P. (Ninkovich 1968; Seward 1975). A Lower Okehuan age is favoured here for the base of the Maraetotara Sand in view of consistency in the fission-track age of the Kidnapper Tuff, and inconsistency in the paleontologic age.

As an independent check on the fission-track age of Unit F (Figs. 2-8 and 2-9.), a sample was dated by the uranium-thorium dating technique. Although only glass shards were used (ideally zircon and/or titanomagnetite should also be analysed to enable an isochron to be constructed), the age determined is approximately 0.3 m.y.

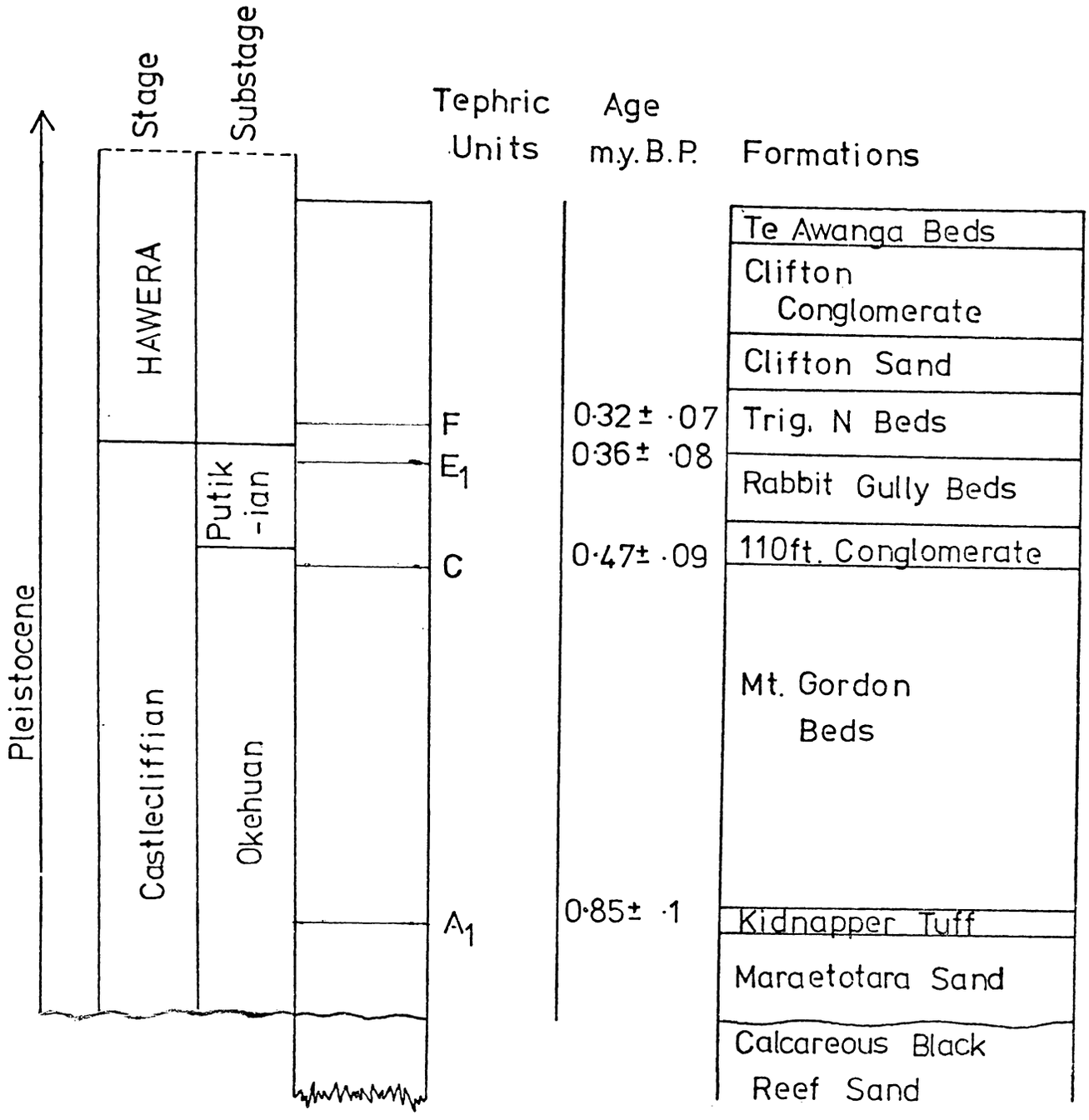

Fig. 2-30. Fission-track ages of selected tephras in the Kidnappers Group (after Seward 1975). Formational ages are recorded alongside, the boundaries being established assuming constant sedimentation rates from the base of the 110 ft. Conglomerate upward (see Fig. 7-6.).

B.P. (Prof. A. Wilson, pers. comm.). This date is not greatly different from the fission-track age obtained by Seward (1975) of 0.32 ± 0.07 m.y. B.P.

Unit C, the top tephra in the Mt. Gordon Beds, with an age of 0.47 ± 0.09 m.y. B.P. occurs immediately beneath the Okehuan/Putikian boundary (Fig. 2-30.). The Castlecliffian/Hawera boundary at 0.34 m.y. B.P. (Boellstorff & Te Punga 1977) occurs between units E and F (Fig. 2-30.) and therefore the boundary approximates the Rabbit Gully/Trig. N Beds formational contact.

In view of the older age accepted here for the Maraetotara Sand (Fleming 1957 c.f. Seward 1975), the widespread hiatus envisaged by Kingma (1971) as following the Nukumaruan, does not occur in the Kidnappers area. Also, the group has a greater stratigraphic thickness of Hawara sediment than it has Castlecliffian sediment (c.f. Kingma 1971).

It is difficult to determine precisely the date when sedimentation of the group ended. However, a wave-planed last-interglacial surface pre-dating extensive uplift of the group is believed to have an age of 0.12 m.y. B.P. (Lewis 1971).

CHAPTER 3: TECHNIQUES AND METHODS OF ANALYSIS

3-1 INTRODUCTION

Several techniques were used in this study to establish the texture, mineralogy, shape and orientation of clasts in conglomerates. In addition the heavy mineralogy of tephras was established by optical techniques. Apart from the measurement at outcrop of clast orientation and field texture, all other analyses were made in the laboratory.

As many of the techniques used are standard in earth sciences the emphasis here is placed on new methods of data analysis. Wherever possible, attempts have been made to make these methods applicable also to laboratory studies from other geological settings.

The computer programmes written for this study are in Fortran IV and were developed initially for the Burroughs 6700/7700 computer. Subsequently most programmes have been adapted for use on the P.D.P. 1130 computer which has the facility of visual display unit terminals.

3-2 CLAST SHAPE MEASUREMENT AND DATA ANALYSIS

Sampling Procedure

The validity of paleoenvironmental interpretations from clast shapes are very dependent on the sampling procedure. The problems of representative sampling, not the least of which are the number of clasts to be measured, have been considered by many workers (e.g. Steinmetz 1962; Evans 1969). Not only is shape dependent on the internal anitrophism and original shape of the primary rock particle (Folk 1968), but also on differential rates of physical and chemical weathering of various rock types during transport (Bradley 1970). Blatt *et al.* (1972) showed that the processes modifying pebble shape were strongly dependent on grain size. Further, a close relationship between size-sorting and shape-sorting was emphasised by Bradley (1970). To isolate the effect of pebble shape it is essential that the number of variables be limited. Consequently the constraints on the sampling procedure were:

(i) Intra-sample and inter-sample clast size (long axis) was as much as possible restricted to the pebble size class.

(ii) Only pebbles of greywacke composition were measured.

(iii) Samples collected from within a conglomerate unit came from a restricted stratigraphic area; usually 30 cm^2. In this area all clasts within the pebble size range were collected.

(iv) The sample population ranged in size from 85 to 270; the number collected being sufficiently

large so as to ensure with confidence that the shape attributes of the total pebble population was represented.

Clast Measurement

A total of approximately 4000 individual measurements were made on the pebbles collected. Three measurements were taken from each pebble; the long, intermediate and short axes (Fig. 3-1.), as defined by Sneed & Folk (1958). Measurements were made with vernier calipers to an accuracy of 0.5 mm.

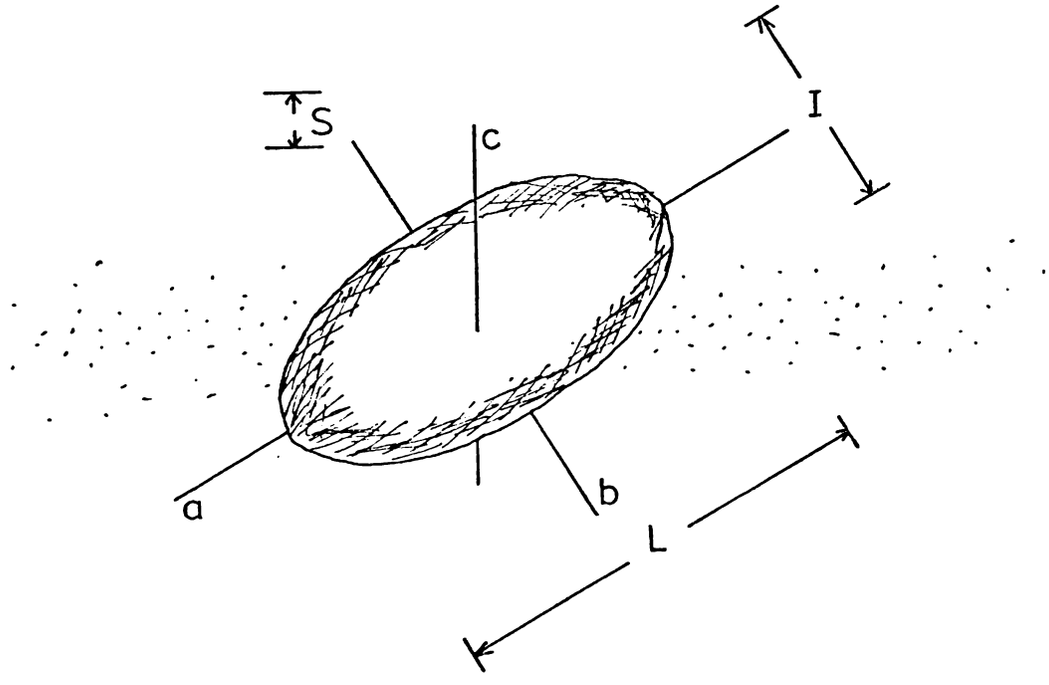

Fig. 3-1. Diagramatic representation of the dimensional axes of a clast. The long axis 'a' is the longest dimension 'L' of the pebble, the intermediate axis 'b' is the largest dimension 'I' in the plane perpendicular to 'L' and the short axis 'c' is the longest dimension 'S' at right angles to the maximum projection plane.

Computer Programme for Shape Data Analysis

Determination of the numerical values of clast shape indices is ideally suited to analysis by computer as the same calculations have to be repeated for each clast.

Programme Input and Output:

The input data required for the shape programme (Appendix I i) are the three axial lengths of each clast, the number of samples, the *t* values from the 2-tailed student's *t*-distribution at P = 0.05, and the range of values for the axes of the triangular graph. The output of the programme includes the value of each shape index for each clast, a statistical summary of the distribution of each sample for each index, and a plot on a triangular sphericity-form diagram (Sneed & Folk 1958) of the clasts within each sample.

Programme Logic:

The logic of the shape programme is represented by a flow chart (Fig. 3-2.) which entails a main programme with two subroutines. The main programme is responsible for calculating four shape indices, defined in Chapter 4. Subroutine Stat (Fig. 3-2.) calculates the statistics for the distribution of each shape index and subroutine plot (Fig. 3-2.) is responsible for positioning pebbles on a sphericity-form diagram. Subroutine plot is an adaption of another subroutine (Lumsden 1973) rewritten to position the points on a sphericity-form diagram where each axis has a different scale.

The writer feels that part of the reason for the paucity of shape studies is the tedious nature of data analysis,

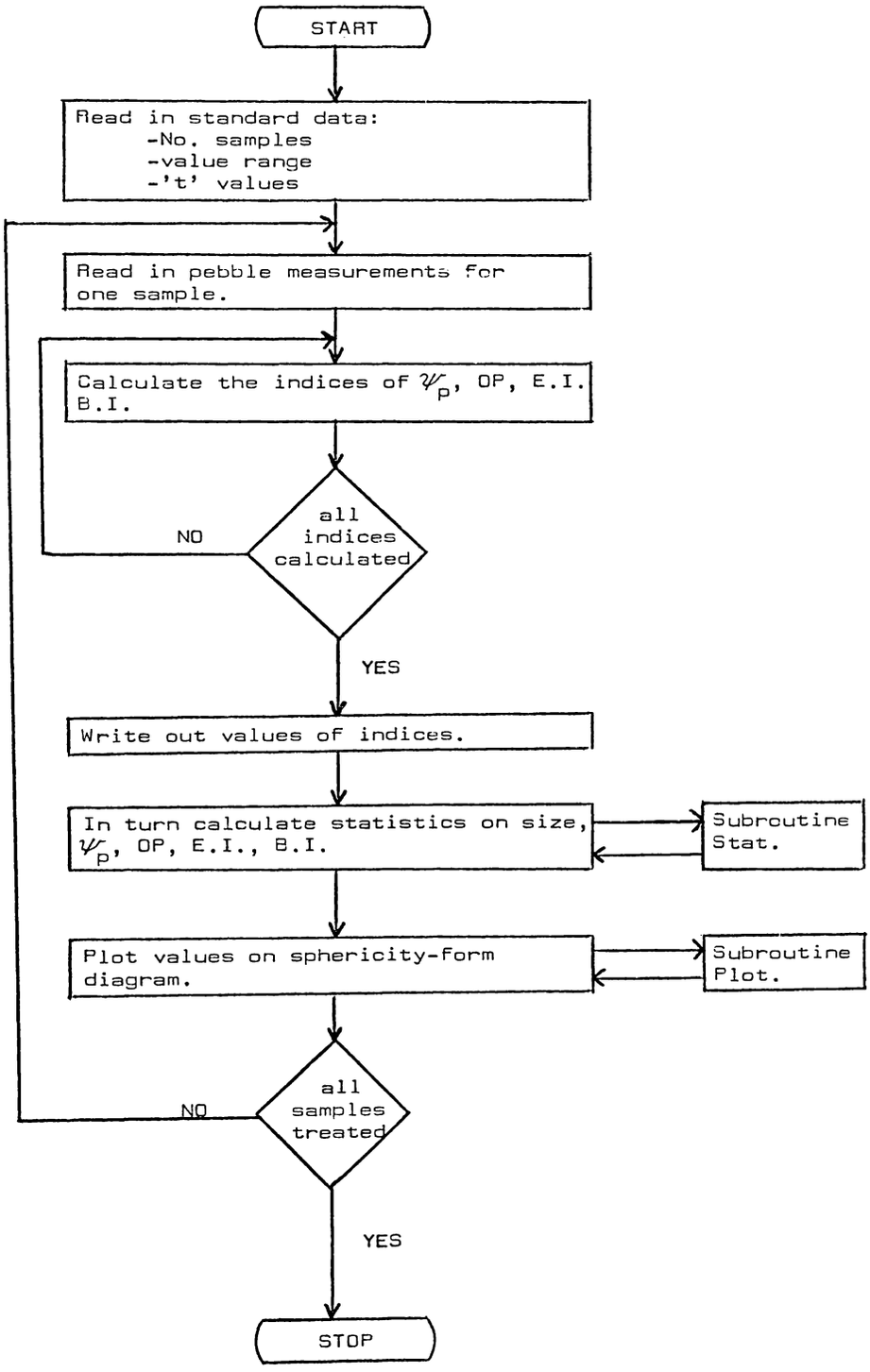

Fig. 3-2. Flow chart of logic for Shape programme.

compounded by the large number of clasts which must be considered to obtain confident results. In this respect the programme is especially advantageous as it eliminates the need for any manual computation or plotting of results. The method is extremely rapid, analysis of all the data in this study being completed in only 10 minutes. Further, the graphic plots are as accurate as manual plots and are immediately suitable for reduction and publication.

Test of Statistical Significance

Significance testing is a valuable statistical aid for establishing whether or not there is a significant difference between samples at particular levels of probability (Hayslett & Murphy 1967). The student's *t*-test (Turner 1970) was employed to test the difference between the means for the shape indices. In hypothesis testing, initially the null or alternative hypothesis is formulated, namely whether the means are equal or unequal:

$$H_o: \mu = \mu_o \quad \text{versus} \quad H_1: \mu \neq \mu_o$$

Where H_o is the null hypothesis, H_1 the alternative hypothesis and μ represents the sample mean (Hayslett & Murphy 1967).

If the means for the two samples are unequal one requires to know whether the difference is due to error in sampling the same population where $H_o: \mu = \mu_o$, or whether the difference is due to sampling of different populations where $H_1: \mu \neq \mu_o$. To determine which hypothesis is correct it is necessary to choose a level of confidence at which one is satisfied that there is or is not a significant difference.

This is known as the probability level.

If P is 0.05 or less the differences are considered real. If P >0.05, that is there are more than 5 chances in 100 that the differences could be due to chance sampling of the same population, it is the view of statisticians that no decision can be made as to which hypothesis holds (Turner 1970). Nevertheless if P is <0.20 and >0.05 there may be real differences present but if P >0.20 differences are insignificant (Folk 1968).

3-3 CLAST ORIENTATION MEASUREMENT AND DATA ANALYSIS

Clast orientation was established by measuring the dip and direction of dip of the maximum projection of the ab plane and the trend and plunge of the a-axis. Trend (Fig. 3-3.) is defined as the strike of the vertical plane containing a line and the plunge as the vertical angle between a line and the horizontal (Ragan 1973).

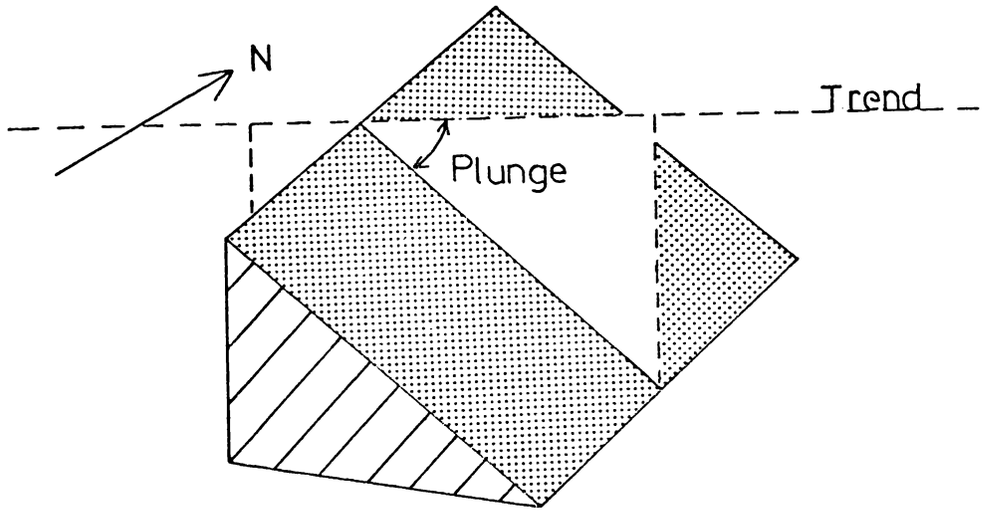

Fig. 3-3. Trend and Plunge of a lineation on a plane. (After Ragan 1973).

The maximum projection of the ab plane is that plane (Fig. 3-4.) within the clast which projects the greatest surface area.

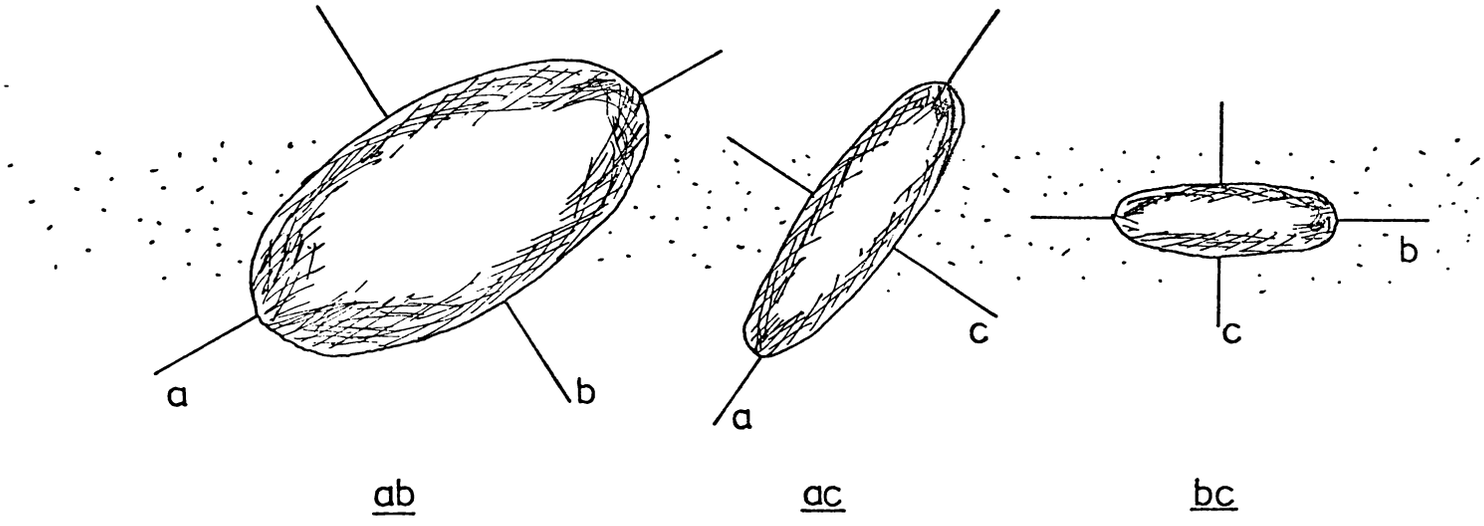

Fig. 3-4. The principal planes of a clast.

Clast Measurement

The orientation of approximately 500 clasts were measured with a silva compass. To identify the a-axis and ab plane it was often necessary to carefully remove the clast and re-position it before the measurements could be made. Many sources of error in orientation measurements have been identified. Some of these are: inconsistencies between various operators, inconsistencies in the performance of an individual operator, errors resulting from the removal of a pebble for identification of the a-axis and ab plane, the selection of clasts with different shapes, and measurement errors (Holmes 1941; White 1952; Bonham & Spotts 1971; Harris 1969; Pittam & Parkinson 1971; Drake 1974, 1977). In an attempt to minimise many of the above errors, all measurements were carefully made by the writer. No attempt was made to

discriminate against particular clast shapes.

To ensure that the data collected were not time transgressive, which may have introduced the possibility of polymodal current directions, measurements were restricted stratigraphically within one sedimentation unit and were usually taken within a vertical range of 30-40 cm and a horizontal distance of 1-2 m.

Correction for Tectonic Tilt

As the units from which the clasts were measured are now tilted (N 60 E, 8 NW) the measured orientations of clasts do not represent the original orientations. Ten Haaf (1959, in Potter & Pettijohn 1963) and Ramsay (1961) have demonstrated that the trend of a linear structure such as that of the a-axis is altered less than 3° in beds tilted up to 25°. On the other hand the strike of a planar structure such as the ab plane of a clast, depending on how closely the strike approximates the structural dip, may change significantly with low structural dips. Similarly the imbrication angle may change dramatically.

As a detailed analysis of clast orientation was intended each a-axis and ab plane measurement was corrected for tectonic tilt following standard procedures (Turner & Weiss 1963; Potter & Pettijohn 1963; Phillips 1971). Stereographic corrections were made using the Wulff stereonet in preference to the Smidtt equal area stereonet as it was found the former allows greater accuracy in the positioning of values near the north and south stereographic poles.

The Kidnappers Group being structurally very simple, corrections were made only for structural tilting about the

horizontal axis, as it proved difficult to appreciate any rotation about a vertical axis. Further, the difficulty of identifying bedding planes in the Clifton Conglomerate necessitated correction with respect to an average plane through the formation, essentially determined by the dip of the upper and lower formational boundaries. It was also assumed that the depositional surface was horizontal, although it was shown by White (1952) for the Keweenawan Conglomerate in northern Michigan that paleostream gradient may be as much as 3^{o}.

Methods of Petrofabric Analysis

Two broad methods of petrofabric analysis have been developed, namely by stereographic petrofabric diagrams and by mathematics (Krumbein 1939).

Petrofabric Diagrams:

In the construction of petrofabric diagrams, standard practise was followed in plotting (planes as poles and lineations as points) and contouring (Turner & Weiss 1963; Phillips 1971). Smidtt equal area paper was used in preference to polar equal area paper because of greater accuracy found with the former in plotting of poles close to the centre of the stereonet. In figures where plots are contoured, the uninterpreted data are presented alongside as a visual check on the validity of the contouring.

Several alternative contouring methods have been developed (Kamb 1959; Mellis, in Flinn 1958; Denness 1970, 1972; Starkey 1977) which are especially suitable for the identification of weakly preferred orientation. Kamb's method in particular has been used in the study of fabric in glacial tills (e.g.

Lindsay 1970a; Drake 1974), although most petrofabric diagrams of conglomerates (e.g. Sedimentary Petrology Seminar 1965) have used the contouring method outlined by Turner & Weiss (1963). As strongly preferred clast orientation was apparent in the field, the method chosen for its simplicity was that outlined by Turner & Weiss (1963).

Mathematical Treatment:

Mathematical analyses of the data were also made for comparative purposes. The vector mean and vector magnitude were calculated for a circular distribution of the data (Curray 1956), while the standard deviation and confidence limits were derived as if the data formed a linear distribution (Barrett 1970). The analysis was facilitated by computer where a computer programme (Seward 1974) was slightly modified (Appendix I ii) and adapted for use at the University of Waikato.

The significance of differences between sample vector means was established by the student's *t*-test (Rust 1972). In addition graphical representation of current directions was established by grouping the data into circular histograms (or rose diagrams).

The fundamental difference between stereographic and 2-dimensional mathematical treatment of orientation data is that concentrations in petrofabric diagrams reflect weighting by the number of common plunge and trend orientations, while rose diagrams or vector means merely reflect weighting by the number of common trends.

Recent Developments in Methods of Orientation Data Analysis Applicable to Conglomerates

Most of the standard methods of orientation data analysis involve either the use of stereographic projections or calculations of 2-dimensional vectors and associated tests of statistical significance (Potter & Pettijohn 1963; Kock & Link 1970; High & Picard 1971). These methods have manifest themselves in the analysis of clast orientation in glacial tills (e.g. Harris 1969) and fluvial gravels (e.g. Rust 1972).

However, 2-dimensional vector calculation is limited to the horizontal plane which at times may cut through the principal cluster, and therefore reduce the length of a vector mean and possibly indicate the wrong paleocurrent direction and strength. To overcome this problem a method of 3-dimensional vector calculation is available (Andrews & Shimizu 1966). Nevertheless, application of this approach to a sequence of tills at Llanduwg by Pittam & Parkinson (1971) was not successful in the detection of the direction of ice advance. This study agreed with the findings of Flinn (1958) who had earlier established the inadequacy of statistical tests of significance of preferred orientation based on the vector method.

Subsequently, a procedure claimed to be able to determine more accurately a 3-dimensional vector mean was developed which uses a series of planes of reference called rotations, rather than a horizontal plane (Mark 1971). The statistical tests relating to the rotational vector procedure were found to be invalid and in place the eigenvalue method was proposed (Mark 1973).

Eigenvalue Method:

In this method each clast orientation, regarded as a unit vector, is used to calculate the directional cosines and sums of cross products of a 3 x 3 matrix (Mills 1977). The three mutually orthogonal eigenvectors (V_1, V_2, V_3) are computed, where V_1 corresponds to the direction about which the moment of inertia is minimised and is therefore an estimate of the distribution mean (Woodcock 1977). On the other hand, the eigenvector V_3 corresponds with the largest moment of inertia and is therefore an estimate of the pole to the fabric pattern. The eigenvector V_2 is perpendicular to both V_1 and V_3.

Indices of fabric strength, analogous to vector magnitude, are defined by eigenvalues (S_1, S_2, S_3) where they measure the spread of data about the respective eigenvectors (Woodcock 1977). Hence the position (eigenvector) and strength (eigenvalue) of an orientation fabric may be defined. Further, the significance of a preferred fabric pattern can be established by testing S_1 against V_1 and S_3 against V_3 where larger S_1 values and smaller S_3 values indicate greater preferred orientation (Mills 1977).

Mark (1974), in the comparison of till fabrics, recognised that eigenvalues are directly related to fabric shape (the shape of a distribution on a stereonet) and proposed a triangular plot with the three eigenvalues at each apex. This approach has also been used by Mills (1977) in comparison of till fabrics from alpine and lowland glaciers. Woodcock (1977), by proposing a two-axis ratio plot and a three-axis ratio plot, has tremendously

improved the capability of the eigenvalue method to compare orientation fabrics.

Advantages of the Eigenvalue Method:

The great advantage of the eigenvalue method is that by quantifying an orientation fabric, it enables comparison of a large number of petrofabric diagrams. Had the writer been aware of this method and in particular of the recent developments outlined by Woodcock (1977), at the time clast orientation was analysed, conclusions similar to those found by graphical cross-correlation (Chapter 5) may have been more simply derived.

Limitations of the Eigenvalue Method:

It is however, appropriate to note the limitations recognised by Woodcock (1977) of eigenvalues as shape-fabric indicators. For symmetry classes with orthogonal crystallographic axes (spherical, axial, orthorhombic) Turner & Weiss 1963), the directions of the axes correspond with the orthogonal eigenvectors. Hence co-axiality occurs where the eigenvectors coincide with the axes of greatest and least moment of inertia. However, for monoclinic symmetry, the case at sites 1 to 5 (Figs. 5-6; 5-10; 5-12; 5-14; 5-16.), co-axiality does not occur and although eigenvalues may still be derived they must be interpreted with caution. Further, problems of interpretation also arise with bimodal distributions also found to be the case at site 1. (Fig. 5-6A.). In any event, it is suggested (Woodcock 1977) that all orientation data should be checked on an equal area projection to identify the gross shape of the fabric.

3-4 TEXTURAL ANALYSIS

There are several problems in determining the texture of conglomerates which are briefly considered now:

(1) In sampling conglomerate units involving clasts of pebble, cobble and boulder size (Table 3-1.) it is frequently difficult to collect a representative sample from a particular unit. Invariably one is faced with the problem of exactly how much of the matrix, itself often of granule and pebble size, is associated with the larger clasts.

(2) The established techniques of laboratory textural analysis are most suited to sand and silt fractions. Hence sampling may be biased towards textures which are able to be analysed.

(3) There are few published analyses of modern gravelly sediments to which conglomerates may be compared in assisting in the interpretation of paleoenvironments.

(4) One must consider whether a detailed knowledge of the grain-size distribution is in fact necessary or whether an appreciation of the field texture and its stratigraphic variation are more environmentally important.

In the light of the foregoing discussion, gross textural variation of conglomerate units was emphasised over laboratory analysis. Nevertheless selected conglomerate samples were analysed in detail.

Millimetres	Phi (ϕ)	Wentworth Size Class		General Terms for Size Fractions
			BOULDER	GRAVEL
256	−8			
			COBBLE	
64	−6			
			PEBBLE	
4	−2			
			GRANULE	
2	−1			
		very coarse sand		SAND
1	0			
		coarse sand		
0·5	1			
		medium sand		
0·25	2			
		fine sand		
0·125	3			
		very fine sand		
0·0625	4			MUD
		coarse silt	SILT	
0·031	5			
		medium silt		
0·0156	6			
		fine silt		
0·0078	7			
		very fine silt		
0·0039	8			
			CLAY	

Table 3-1. Grain-size Scale (After Wentworth, 1922) showing the millimeter and equivalent Phi (ϕ) unit limits to each size class (after Folk et al. 1970).

Laboratory Analysis of Texture

The laboratory techniques used to establish the grain-size distribution of samples are standard (Folk 1968; Carver 1971). Samples were wet sieved using a 4ϕ screen and the mud was retained and concentrated. Conglomerate samples with shells were digested in 10% HCL and subsequently washed several times to remove the remaining acid. Sandy samples were split to an average weight of 40 g although conglomerate samples frequently exceeded 500 g. Conglomerates were sieved at ½ϕ intervals and sandy samples at ¼ϕ intervals in a Ro-tap sieve shaker. Sieving time was usually 10 minutes but where the samples contained pumice this was reduced to 5 minutes to prevent excessive size modification (Walker 1971).

The mud concentrate was dispersed with small quantities (10 ml) of calgon and after vigorous stirring a subsample of 1-5 mls, depending on the concentration of mud, was extracted and retained for silt analysis. The weight of mud was established by removing 20 ml of the fluid after 20 sec. at 20 cm depth and drying before weighing.

Silt analysis was performed by hydrophotometer (Jordan *et al.* 1971). The times calculated by C. Tilly (pers. comm.) at which transmission readings should be taken were used in the present study, as the times suggested by Jordan *et al.* (1971) have recently been found to be in error (Tilly 1977). It is appropriate here to make two further points regarding the recent notes of Tilly (1977) and Jordan (1977):

(i) The small errors in some of the original times (Jordan *et al.* 1971) become insignificant for

predominantly sandy or gravelly sediments, as the total amount of clay is low.

(ii) Although the original Jx value of 0.56 for the interval 8-14ϕ is not a geometric progression, as suggested should be the case by Tilly (1977), it was used in the computer programme as it gave realistic results. The reason the new value of 0.14 (Jordan 1977) gives unrealistically low amounts of clay stems from the large range of phi intervals (8-14) the final reading covers. Therefore the geometric mid-diameter is very much smaller and does not approximate the arithmetic mid-diameter as is the case in preceding $\frac{1}{2}\phi$ intervals.

Despite these inconsistencies the method, originally demonstrated as being 4-5 times more accurate than the pipette method (Jordan *et al.* 1971), is still considered to be of comparable accuracy to the pipette method of silt analysis (D. Lowe, pers. comm.).

Computer Programme for Grain-size Data Analysis

The method of grain-size analysis now used at the University of Waikato relies on a combination of sieves and hydrophotometer. The analytical advantage of this technique is however, offset by the amount of calculation required to convert the raw data into a common form. The extent of this calculation together with subsequent graphical and statistical characterisation of the grain-size distribution, makes computer analysis an extremely suitable method.

Existing Programmes:

Over the past 15 years a number of grain-size programmes have been written and mentioned in publications discussing sediment texture, but few programmes have been published; two notable exceptions are the programmes of Kane & Hubert (1963) and Slatt & Press (1976). The features of most programmes written to date are as follows:

(i) The programmes are peculiar to the method of textural analysis and/or the computer available.

(ii) They are used primarily for the calculation of statistical parameters.

(iii) Parameters are calculated by the method of moments.

(iv) Most programmes only analyse data down to the 4ϕ boundary.

Since most of the grain-size programmes have been written, developments in computer hardware, and in particular software, have made many programmes obsolete in both logic and efficiency.

Up to this point two texture programmes are available at the University of Waikato, one to calculate statistical parameters (Marks 1975) and the other to convert the hydrophotometer transmission readings to percent weights within ½ϕ intervals of the silt fraction (Jordan *et al.* 1971). The former programme had the disadvantage of only analysing data down to the 4ϕ boundary and in ½ϕ intervals, and the latter only partly fulfills the present requirements.

Programme Input and Output:

The texture programme (Appendix I iii) requires three

sets of raw input values:

(i) The cumulative weights for successive ¼ϕ sieve intervals.

(ii) The transmission readings from the hydrophotometer.

(iii) The weight of mud in the sample.

The programme has the potential to output the following information of a grain-size distribution:

(i) A plot of three superimposed graphs, namely a histogram and two cumulative curves, one with arithmetic ordinate and the other with probability ordinate.

(ii) A list of the values for each of the graph positions.

(iii) The percent gravel, sand, silt and clay and the ratio of clay/silt and sand/mud.

(iv) The textural class for gravel-free and gravel-bearing detrital sediments (Folk *et al.* 1970).

(v) The Folk and Ward statistics of mean, sorting, skewness and kurtosis (Table 3-2.).

(vi) The median and C statistic (Passega 1957).

(vii) The verbal classification for each of the statistical parameters (Table 3-2.).

An example of the programme output is included in Appendix I iii.

Programme Logic:

The programme was deliberately designed as a main programme with a number of subroutines which may be included

Graphic Mean

$$M_z = \frac{\phi 16 + \phi 50 + \phi 84}{3}$$

Inclusive Graphic Standard Deviation

$$\sigma_I = \frac{\phi 84 - \phi 16}{4} + \frac{\phi 95 - \phi 5}{6.6}$$

Verbal Classification:

σ_I under 0.35ϕ	very well sorted (vws)
0.35 to 0.50ϕ	well sorted (ws)
0.50 to 0.71ϕ	moderately well sorted (mws)
0.71 to 1.0ϕ	moderately sorted (ms)
1.0 to 2.0ϕ	poorly sorted (ps)
2.0 to 4.0ϕ	very poorly sorted (vps)
over 4.0ϕ	extremely poorly sorted (eps)

Inclusive Graphic Skewness

$$Sk_I = \frac{\phi 16 + \phi 84 - 2\phi 50}{2(\phi 84 - \phi 16)} + \frac{\phi 5 + \phi 95 - 2\phi 50}{2(\phi 95 - \phi 5)}$$

Verbal Classification:

Sk_I from	+1.00 to +0.30	strongly fine-skewed (sfs)
	+0.30 to +0.10	fine-skewed (fs)
	+0.10 to -0.10	near-symmetrical (ns)
	-0.10 to -0.30	coarse-skewed (cs)
	-0.30 to -1.00	strongly coarse-skewed (scs)

Graphic Kurtosis

$$K_G = \frac{\phi 95 - \phi 5}{2.44(\phi 75 - \phi 25)}$$

Verbal classification:

K_G	under 0.67	very platykurtic (vpk)
	0.67 to 0.90	platykurtic (pk)
	0.90 to 1.11	mesokurtic (mk)
	1.11 to 1.50	leptokurtic (lk)
	1.50 to 3.00	very leptokurtic (vlk)
	over 3.00	extremely leptokurtic (elk)

Table 3-2. Statistical Parameters (after Folk, 1968).

depending on the information required. In line with this approach the programme logic has been represented by a number of simplified flow charts (Figs. 3-5. to 3-7.). The main programme Fig. 3-5.) is responsible for the conversion of the transmission values, their combination with sieve data and the plotting of graphs. Subroutine R value (Fig. 3-6.) calculates the percent gravel, sand, silt and clay and establishes the textural class of the sediment. The Folk and Ward parameters and their verbal classification (Table 3-2.) are determined by subroutine Stat (Fig. 3-7.).

A number of difficulties were encountered in writing the programme and these are briefly discussed below:

(1) Often in textural analysis the mud fraction is analysed in larger phi intervals than the coarser fractions. This introduces complications in the plotting of graphs and the calculation of statistical parameters. Part of the logic developed to overcome this difficulty is apparent in the first half of subrountine Stat (Fig. 3-7.).

(2) Whether to consider the distribution as open-ended or closed is a difficulty presently unresolved in the Literature (Griffiths 1967; Folk 1968; Pettijohn 1975). As the statistical parameters in this programme are calculated by the graphic method there is frequently no need to close the distribution. Nevertheless in muddy samples, it may be more realistic to close the distribution when establishing the depositional environment from the grain-size distribution of coarser

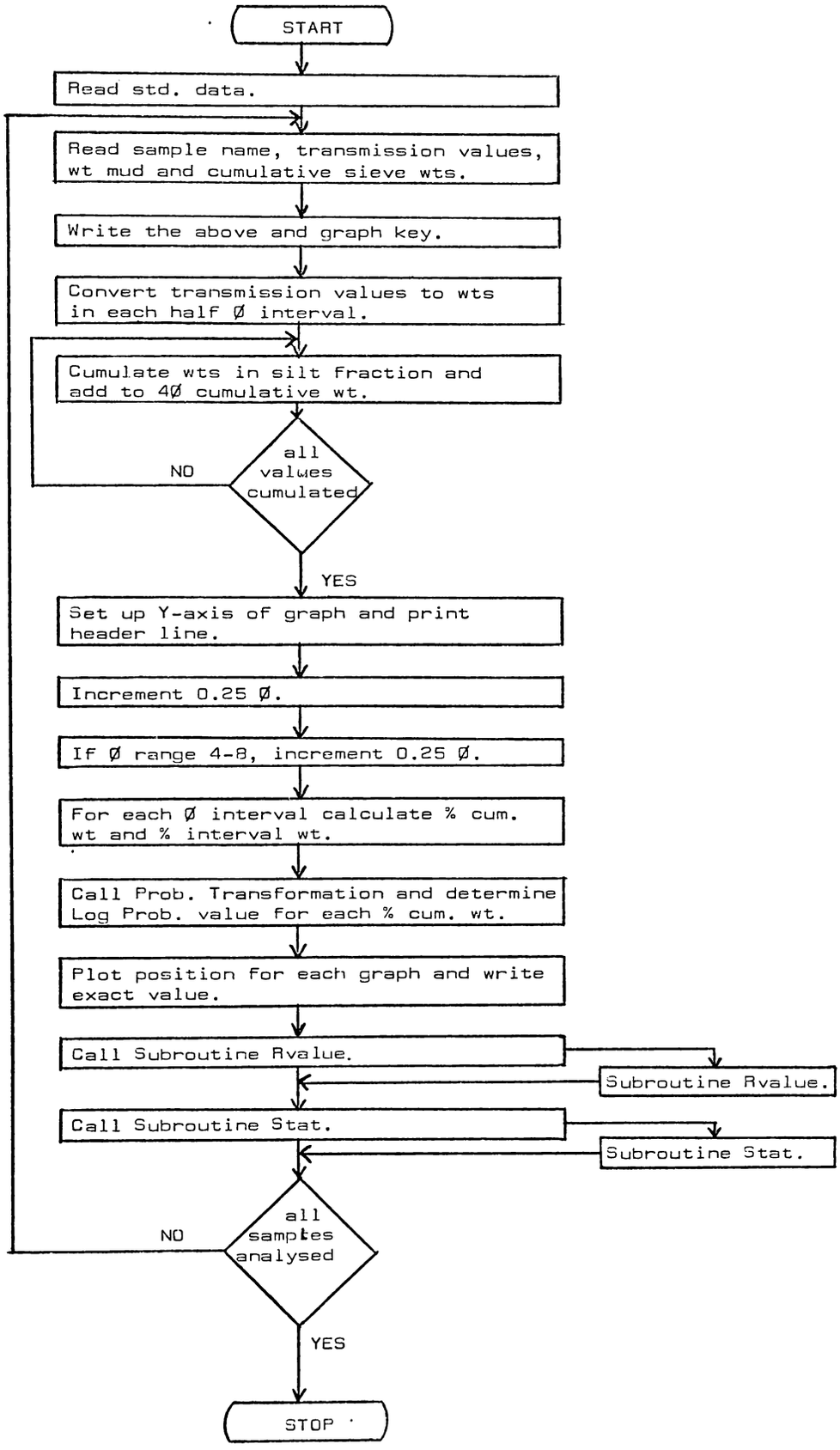

Fig. 3-5. Flow chart of the main texture Programme.

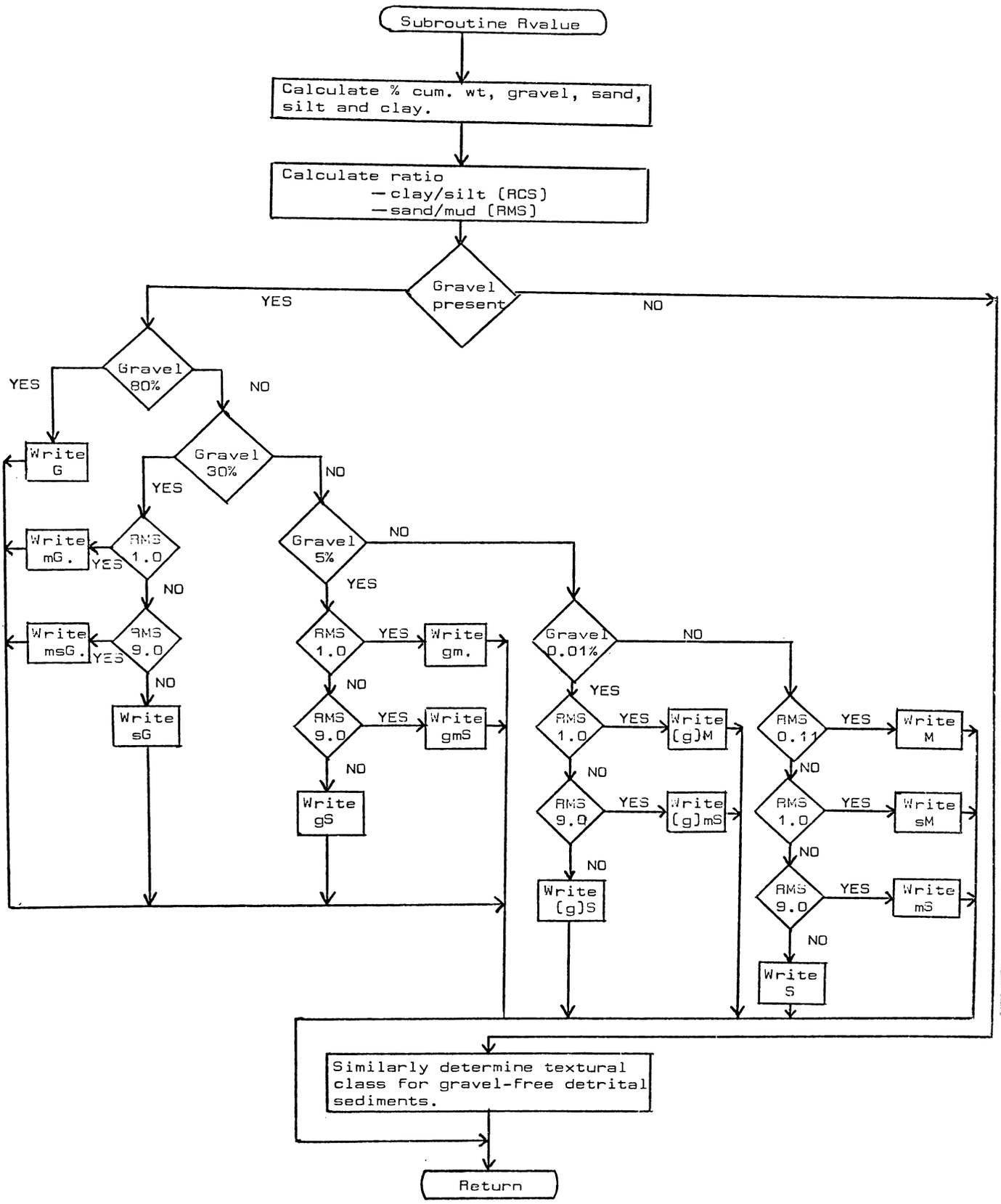

Fig. 3-6. Flow chart of Subroutine Rvalue.

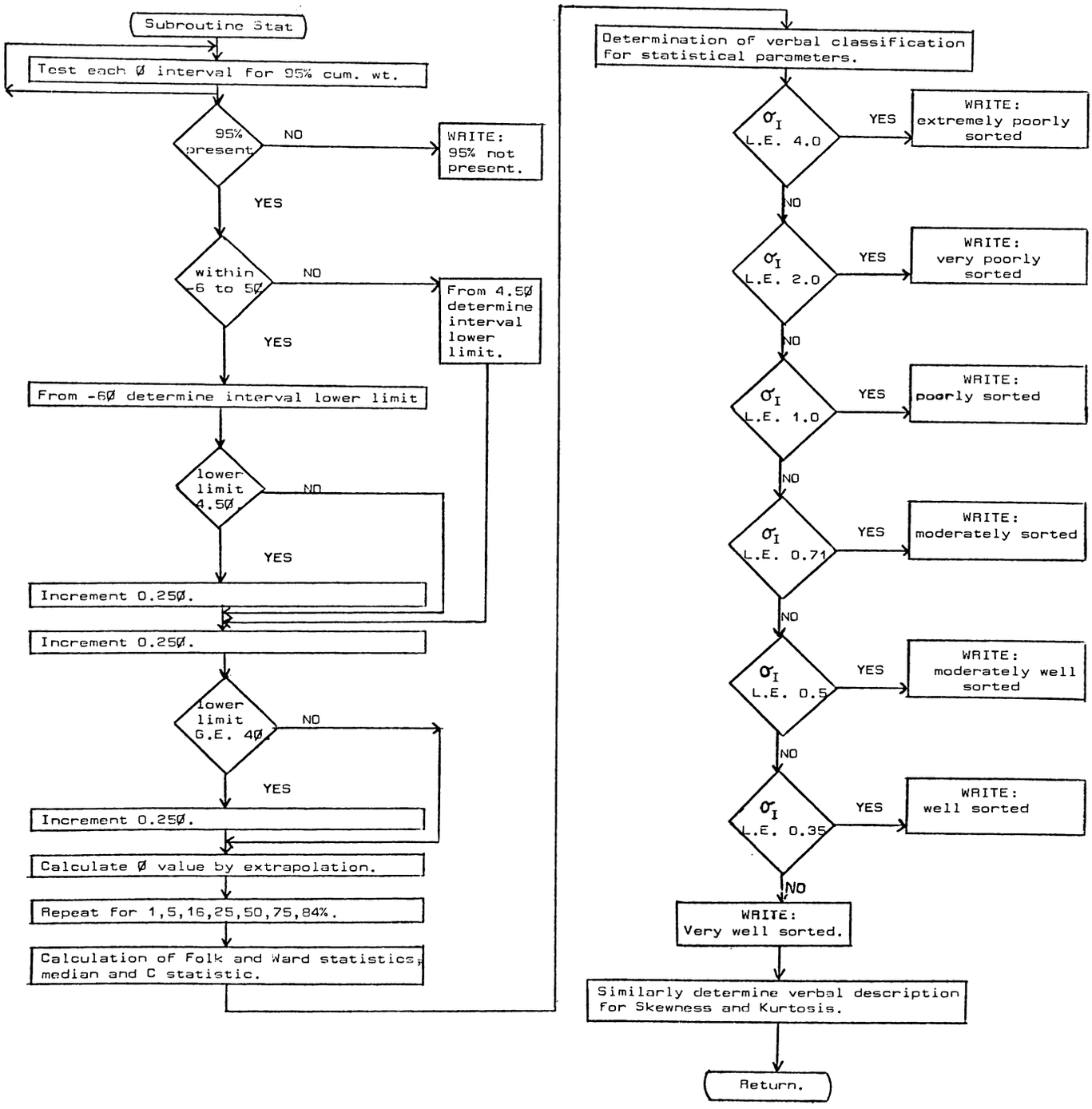

Fig. 3-7. Flow chart for Subroutine Stat.

fractions alone (Nelson 1977). Further, the clay may originally have been present as flocculated particles of silt size or the clay may represent weathering or diagenetic products (Visher 1969).

(3) Frequently the phi range and the phi intervals for which analysis is made has been varied depending on the grain-size distribution of the sample. Variation of thiskind is difficult to accommodate in a single programme, however a large degree of versatility has been achieved by writing a number of variations on the central programme. The following variations are accounted for:

(i) Data input within the range - 6.0 to 8.0ϕ or 14ϕ
(ii) Data input within the range - 3.25 to 8.0ϕ or 14ϕ
(iii) Data input within the range - 6.0 to 4.0ϕ
(iv) Data input within the range - 3.25 to 4.0ϕ

Each of these variations may be further adapted to accommodate ½ϕ sand intervals and whole phi mud intervals. In addition the critical percentiles may be extrapolated off the percent cumulative weight arithmetic curve or the log probability curve. Although only a standard programme from -6.0 to 8.0ϕ is included here (Appendix I iii), the above variations, as well as an adaption to accept pipette weights in place of hydrophotometer readings, are available (Kamp, in prep.).

Advantages of the Texture Programme:

Advantages of the texture programme can now be listed:

(1) The analysis is rapid. A complete graphic and statistical summary of the grain-size distribution for 100 samples is available in approximately 15 minutes. The location of a Visual Display Unit terminal in the sediment laboratory will enable the raw data to be analysed instantaneously.

(2) The analysis is contained on a single page of print-out.

(3) A percent cum. wt. curve on a probability ordinate is plotted for grain-size data. The truncation points in the curve (Visher 1969) may easily be read off the graph.

(4) Whereas most programmes calculate statistical parameters by the method of moments (Griffiths 1967), this programme calculates them by the graphic method (Folk 1968). The reasons for the preference of the latter are the amount of data in the literature on the interpretation of grain-size distributions derived by this method, the problem of the open-ended distribution, and the comparable accuracy in determining the mean, sorting and skewness parameters of both methods (Folk 1966; Jaquet & Vernet 1976).

(5) Programmes which calculate the parameters by the graphic method (Kane & Hubert 1963; Marks 1975; Slatt & Press 1976) do so by extrapolation off cumulative curves with an arithmetic ordinate. It is felt by some that critical percentiles are more accurately read off cumulative curves on probability ordinate (Folk 1968). However, as it has been found in some

muddy samples that the probability curve distorts the fine end of the distribution, which together with experimental weighing errors produces an inferior result, the cumulative curve on arithmetic ordinate is sometimes favoured (Slatt & Press 1976). This programme accommodates both views as the critical percentiles may be extrapolated off either curve.

(6) The versatility of the programme is ensured by the availability of a number of variations.

(7) The textural class and the verbal classification for the statistical parameters are printed out and are immediately available for interpretation.

(8) The advantage of not having to punch cards with the Hewlett-Packard desk top calculator (Slatt & Press 1976) is maintained by the option to feed the data directly into the P.D.P. 1130 through the keyboard of a Visual Display Unit terminal. In particular, the advantages of this system are that the data are retained on disc file once processed and is immediately available for reprocessing without having to feed the data in again; rapid correction of data errors using the edit mode is possible; and the program and data may be punched and feed in on cards which maintains a hard copy and overcomes the problem of occasional loss of disc storage.

There are several advantages in the Burroughs over the P.D.P. computer in using this programme:

(i) Greater core storage enables a larger number of samples to be analysed in one run.

(ii) The programme may be used by people with no computing experience.

(iii) Operation of this computer model by all other New Zealand Universities and some Government Departments which enables the programmes to be immediately available for use by other institutions.

Disadvantages of the Programme:

(1) The positions in the graphic plots are only to an accuracy of 0.5% and are required to be sketched in by joining the points. This does have the advantage however, of allowing a certain amount of interpretation especially in determining the exact position of the mode(s) and truncation points.

(2) The critical percentiles are extrapolated as straight line segments. This error is very small as most of the distribution is in ¼ϕ intervals.

It is felt the advantages of the texture programme far outweigh the disadvantages and for the reasons given above, this programme is thought to have new capabilities over and above existing programmes.

3-5 COMPOSITIONAL ANALYSIS

X-Ray Diffraction Analysis

X-Ray diffraction analysis of bulk powder samples is a common technique used to identify and semiquantitatively estimate sample mineralogy (Nelson & Cochrane 1970). Analysis of selected samples was undertaken using a Phillips PW 1130/00 X-Ray diffractometer.

Sample Preparation:

Conglomerate samples washed clean of surficial mud were reduced to pea size in a standard rock crusher. Samples were ground in a 12 cm twin head Gilko (model LRM) ring mill for 30 secs. which reduced the material to a particle size between 8-40 microns, the optimum size for powder X-Ray analysis (Nelson & Cochrane 1970). The powder was loaded into sample holders by the back-filling technique with sufficient care being taken to prevent orientation of the particles. To assist in semiquantitative estimation of the major minerals at least three subsamples of each sample were scanned from 4° - 35° 2θ. The machine settings used were: K.V. 35.0, mA. 8.5, range 400 cps, time constant 4 sec., high voltage 56% (1.5 K.V. on the rate meter), lower level 17%, and attenuation 2.

A Computerised Method of Mineral Identification:

The procedure to interpret the diffractometer trace is one of converting the degrees 2θ peak values to angstroms, and comparing the values to those of reference minerals published in the X-Ray powder diffraction file (1967). For common minerals, such as quartz and feldspars, this is a simple procedure. However, where sample mineralogy is largely unknown the process of associating observed peaks with standard peaks becomes involved and tedious. A computer programme (Appendix I iv) has been developed which is capable of identifying minerals represented by peaks on an X-Ray diffractometer trace.

Two sets of input values are required, namely a list of reference mineral peaks in angstroms and the value in degrees

2θ of the observed peaks on the trace. The programme output includes the angstrom values of the observed peaks and the minerals identified (Appendix I iv).

Programme Logic:

It is apparent in the flow chart (Fig. 3-8.) that the logic of the programme is based on the initial agreement of an observed with a reference mineral peak, and then the coincidence of subsequent peaks for a reference mineral with other observed peaks. Hence, in the identification of an unknown mineral where the equivalent reference mineral has two standard peaks, both must agree, whereas if the reference mineral has three peaks there must be three observed peaks with the same angstrom values.

A complication common to both manual and computer mineral identification is the difficulty of accurately obtaining the degree 2θ values at which peaks occur. This may be due to either the incorrect positioning of the pen on the trace or internal machine drift. This difficulty has largely been accounted for by allowing a standard error range in the comparison of angstrom values for observed with standard peaks. In the present example (Appendix I iv) an error range of 0.02 angstroms is sufficient to correctly identify the minerals.

The present list of reference minerals is limited to 30 but this may be increased many times, the only limit being the amount of computer storage required in execution of the programme.

Advantages of the Mineralogy Programme:

The major advantage of using this computer programme

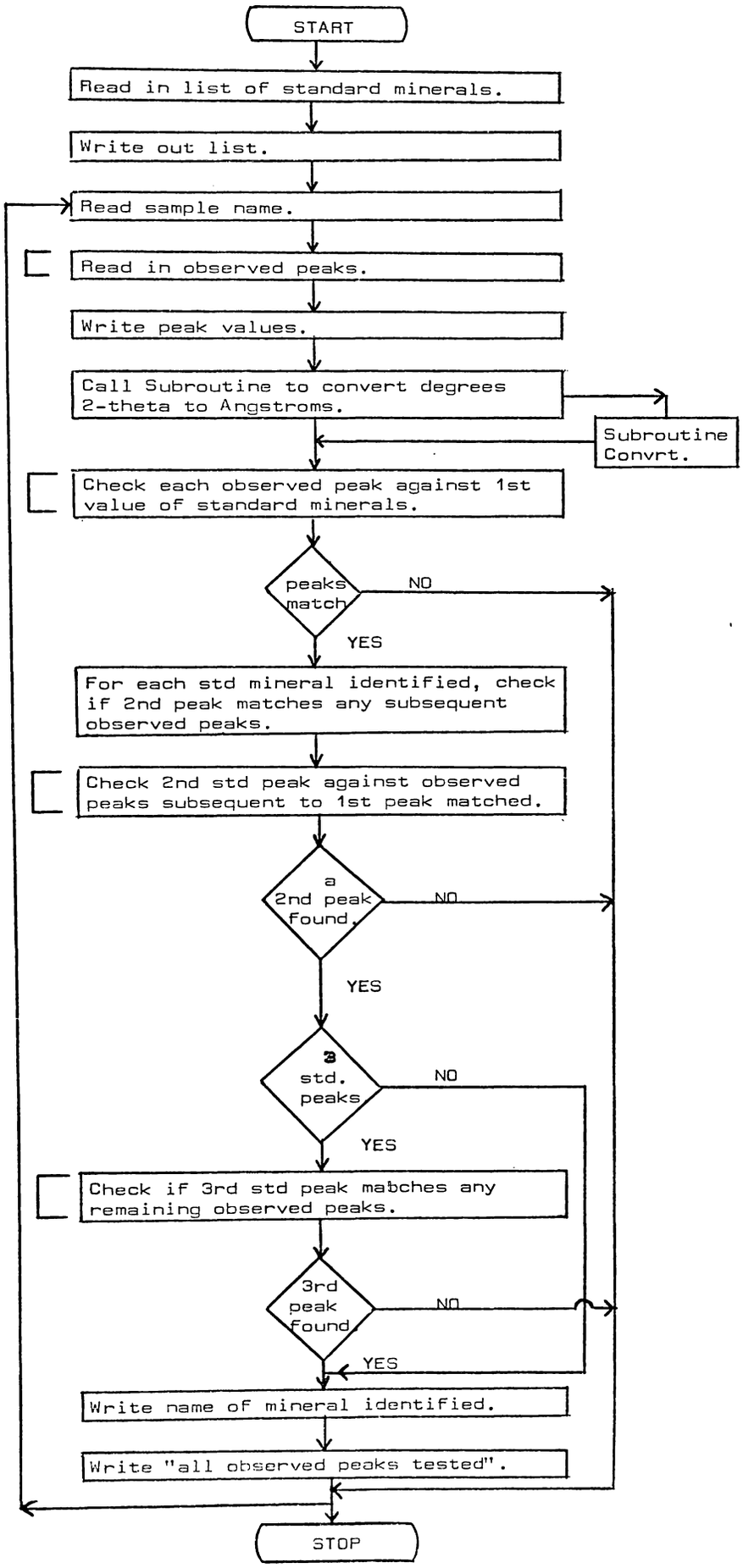

Fig. 3-8. Flow chart to identify sample mineralogy.

is the elimination of the tedious work required in mineral identification. Approximately 100 samples may be identified in 10 minutes. It also enables concise storage of sample mineralogy and largely eliminates the need to work with rolls of trace. Location of a V.D.U. terminal in the X-Ray room would allow direct entry of peak positions into the computer, with almost instantaneous identification of minerals. It is not unrealistic to speculate that future X-Ray diffractrometers will have an attached computer capable of internal mineral identification. Although such a system would be preferable, the use of this programme effectively modernises the capability of the present X-Ray diffractrometer at no extra cost.

Semiquantitative X-Ray Analysis:

Semiquantitative determinations of wt.% quartz was made using the primary peak at 3.34Å, of wt.% plagioclase at 3.20Å, wt.% potash feldspar at 3.35Å and wt.% clay minerals at 4.46Å. The weight percent of each mineral was established by measuring the peak heights above background and reading the value off intensity-concentration curves (Hume 1978). Two ranges in plagioclase composition were identified using the criterion of Hume (1978):

Plagioclase A	3.18Å	Oligoclase - Andesine
Plagioclase B	3.21Å	Andesine - Labradorite

Petrography and Mineralogy

Thin-Sections:

Thin-sections of selected conglomerates were made using standard techniques. Normal optical procedures were followed in thin-section description.

Heavy Mineralogy:

Heavy minerals were extracted from the 2 to 4ϕ fraction of tephras by heavy liquid separation using tetrabromoethane (S.G. 2.95 to 2.96). The relative abundance of non-opaque minerals was established by point-counting 300 - 500 grains/slide depending on the dominance or otherwise of one particular ferromagnesian mineral.

CHAPTER 4: SEDIMENT SHAPE

4-1 THE CONCEPT OF SEDIMENT SHAPE

The complex nature of grain morphology, and the inherent difficulties in its description and measurement, has resulted in several different interpretations of the concept of particle shape. Particle morphology is interpreted by most writers (e.g. Griffiths 1967; Folk 1968; Dobkins & Folk 1970; Pettijohn 1975; Geode 1975) as including the properties form, sphericity, roundness and surface texture. In comparison, Blatt *et al.* (1972) discussed shape under the headings of surface texture, roundness and sphericity. In keeping with general usage grain shape is defined in this study as including particle form and sphericity. Roundness and surface texture, although recognised as aspects of grain morphology, are viewed as distinct from particle shape. Thus shape is conceived in terms of those aspects of external morphology which enable a 3-dimensional appreciation of form and which permit comparison between forms.

4-2 *PREVIOUS STUDIES ON THE ENVIRONMENTAL SIGNIFICANCE OF SHAPE*

Most previous studies of clast shape have been concerned with documenting either downstream changes in pebble shape, or changes in pebble shape with transition from one environment to another. The most important literature on both of these aspects has been reviewed by Dobkins & Folk (1970) and Bradley *et al.* (1972). As the intended emphasis in this study of pebble shapes is on characterisation and identification of fluvial and marine environments, a brief discussion of the literature on this aspect follows.

Folk (1968), contrary to the belief of others, considered that prolonged abrasion did not increase sphericity, and that rivers tended to develop rod-like pebbles while beaches produced disk-like ones. To resolve the controversy Dobkins & Folk (1970) studies basalt pebble morphology in rivers and on beaches in Tahiti - Nui. Convincing evidence was presented to show that with increasing energy levels on beaches there was definite shape modification by abrasion. They now believed that given sufficient wave energy, beach abrasion and fluvial abrasion mechanisms are so different that shape modification occurs independent of lithology, thus refuting the earlier evidence of Folk (1968).

Most workers now recognise that pebble shape is environmentally sensitive, provided clasts have been in the one environment for some time. A contentious point, however, is whether this is due to shape modification, as above, or selective sorting. Milner (1962) has suggested that environments may be more effective in selecting and concentrating

clasts of particular shape, rather than modifying the shapes. Further, Bradley *et al.* (1972) suggests that this may occur indirectly through size sorting.

Nevertheless, regardless of whether shape modification or selective sorting is responsible for the shape attributes of clasts in conglomerates, it is generally agreed that marine and fluvial environments may be distinguished on the basis of pebble shape. This statement is qualified by Sames (1966) in that this will only occur if the marine environment is markedly different from the fluvial, as in the case of a beach compared with an estuary.

4-3 THE MEASURES AND CLASSIFICATION OF CLAST SHAPE

The shape attributes of clasts within conglomerates were measured and classified in the following way:

Sphericity

Sphericity is a measure of how nearly clast shape approximates that of a sphere. The derivation of an index of sphericity originally required the surface area of particles to be calculated. For a sphere the surface area is calculated simply from the diameter, but as the clast becomes more irregular an increasingly large number of measurements is required. It has been demonstrated however, that any three orthogonal axes will enable this property to be determined with some 98% precision (Griffiths & Smith 1964). Determination of sphericity then, requires the measurement of three mutually perpendicular axes which need not pass through the same point (Fig. 3-1.).

Since Wadell developed the concept of sphericity in 1932 many formulae for its calculation have been proposed. The most successful measure is the maximum projection sphericity (ψ_p) of Sneed & Folk (1958):

$$\psi_p = \sqrt[3]{\frac{S^2}{L.I}}$$

This formula is a more actualistic concept of sphericity than earlier proposals as it accounts for the dynamic behaviour of a particle when it orients its maximum projection area normal to the fluid medium.

Oblateness - Prolateness

To enable a distinction to be made between clasts

with equal sphericity but different form, such as a thin roller (or rod) and a thick disk (Fig. 4-1.), a measure of oblateness and prolateness (*OP*) was introduced by Dobkins & Folk (1968):

$$OP. = \frac{\frac{L-I}{L-S} - 0.5}{\frac{S}{L}}$$

Oblateness - prolateness is a measure of how nearly a clast shape approximates the shape of a disk or a rod, and it is loosely referred to as the bladed nature of a clast. Using this formula, all perfect blades have *OP.* = 0.0; disks have negative *OP.* values and rods give positive *OP.* values.

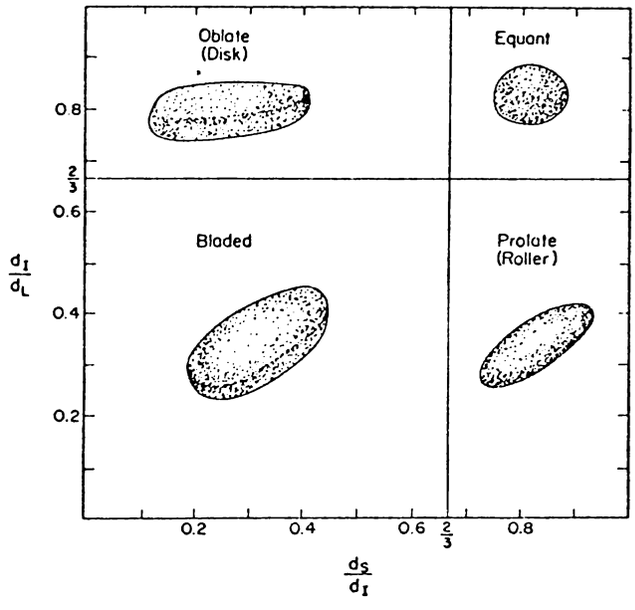

Fig. 4-1. Zingg's classification of shapes of pebbles. The terms oblate and platy are essentially synonymous. (After Blatt et al. 1972).

Elongation Index

The Elongation Index (*E.I.*) was initially described by Schneiderholm in 1954 (in Pryor 1971) but modified by Folk (1968) as the ratio of the greatest width to the greatest length:

$$E.I. = \frac{I}{L}$$

The *E.I.* is only a 2-dimensional measure of clast shape, however, despite its simplicity it is useful as a rapid measure of clast elongation.

Bladed Index

An alternative method of establishing the bladed nature of a clast is by the formula for the basal axis of the sphericity-form diagram (Fig. 4-2A.) of Sneed & Folk (1958).

$$\text{Bladed Index } (B.I.) = \frac{L-I}{L-S}$$

Both the *E.I.* and *B.I.* are a measure of the degree to which a clast approaches the shape of a perfect disk and therefore they are an approximation to the *OP.* index.

Schemes for the Classification of Shape Form

As three possible end member shapes (spheres, rods and disks) cannot be represented on a single scale, rarely can the shape of a clast be defined uniquely by any one of the above measures on its own. In 1935 Zingg (Blatt *et al.* 1972) proposed a classification based on the ratios of axial lengths and devised four shape classes (Fig. 4-1.). This scheme was modified by the superposition of lines of equal sphericity by Krumbein (1941). On the basis of too few

classes and the disproportionally small rod-like class, Sneed & Folk (1958) proposed the now well known sphericity-form diagram (Fig. 4-2A.). On this diagram lines of equal maximum projection sphericity were constructed. The shapes of particles falling at various points on the triangle are illustrated in Fig. 4-2B. Subsequently contours for *OP.* index have been added to this diagram (Fig. 4-2C.) (Dobkins & Folk 1970).

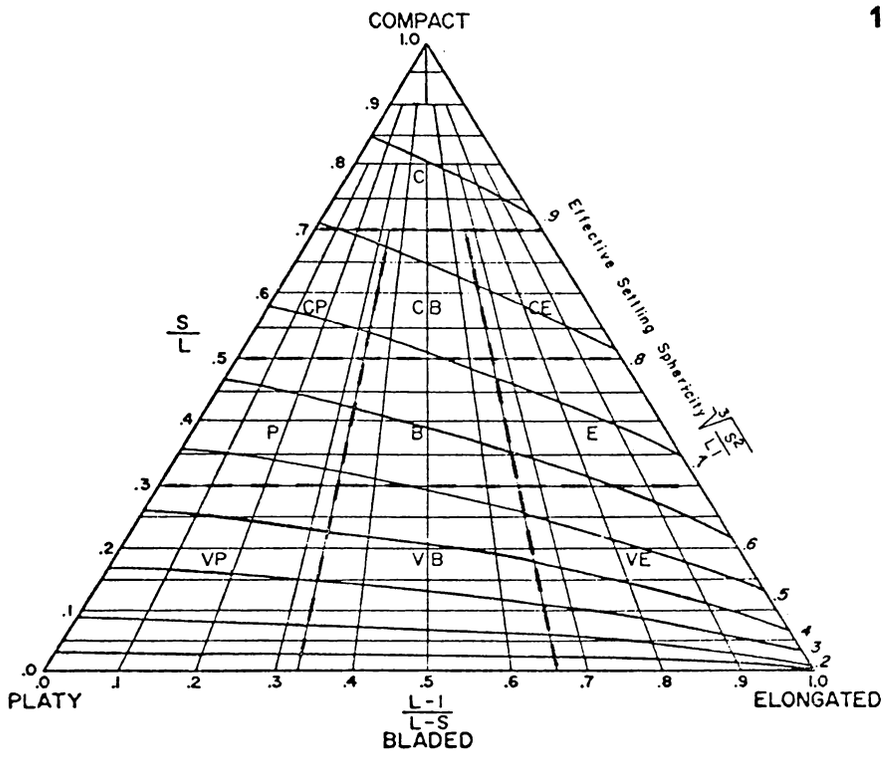
COMPACT
1.0
.9
.8
.7
.6
.5
.4
.3
.2
.1
.0
C
CP
CB
CE
P
B
E
VP
VB
VE
S/L
Effective Settling Sphericity
PLATY
ELONGATED
L-I / L-S
BLADED

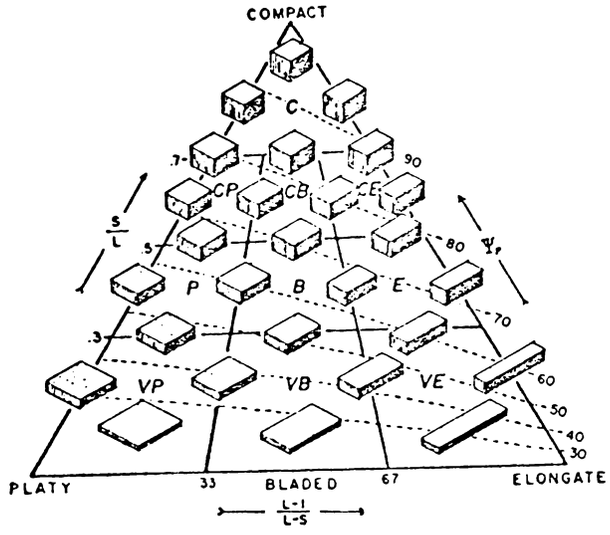
COMPACT
C
CP
CB
CE
P
B
E
VP
VB
VE
S/L
90
80
70
60
50
40
30
PLATY
33
BLADED
67
ELONGATE
L-I / L-S

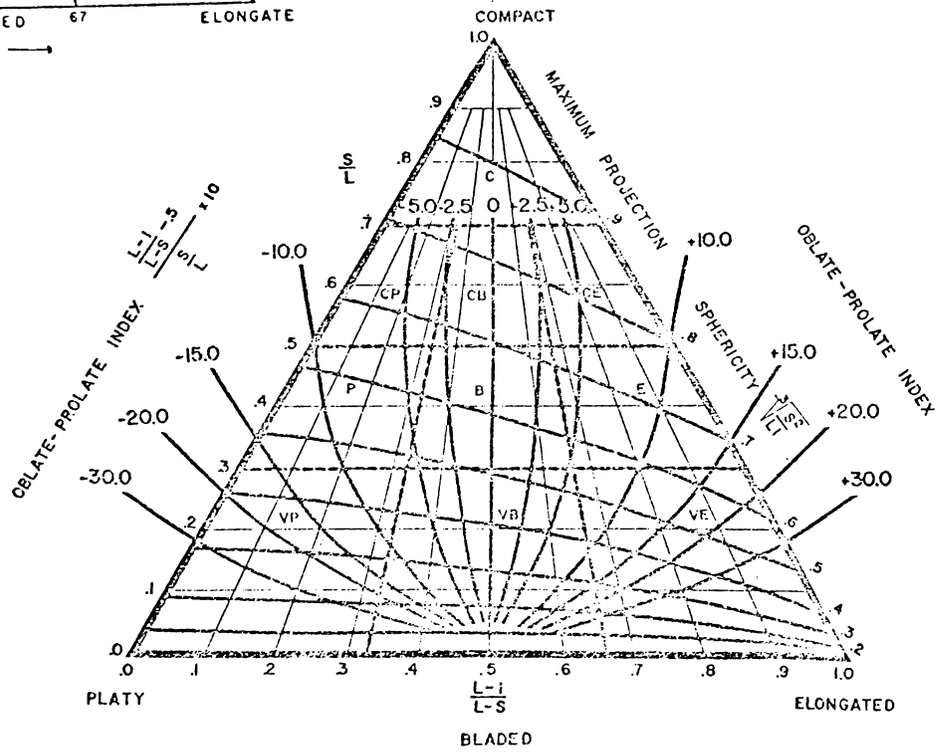
COMPACT
1.0
.9
.8
.7
.6
.5
.4
.3
.2
.1
.0
S/L
C
CP
CB
CE
P
B
E
VP
VB
VE
MAXIMUM PROJECTION
5.0 2.5 0 2.5 5.0
-10.0
-15.0
-20.0
-30.0
+10.0
+15.0
+20.0
+30.0
OBLATE-PROLATE INDEX
SPHERICITY
PLATY
ELONGATED
L-I / L-S
BLADED

4-4 SAMPLING DESIGN

To help meet the objectives outlined in Chapter 1, conglomerate units sampled were selected to cover a significant vertical stratigraphic range of the Group (Fig. 4-3.) and to represent units for which the inferred environment of deposition was either known or unknown. A summary of the field data is included in Table 4-1.

Stratigraphic position	Sample No.	No. of Clasts	Inferred environment
Clifton Conglomerate			
70 m	013	270	Fluvial
30 m	012	225	Fluvial
15 m	011	20	Fluvial
15 m	010	40	Fluvial
15 m	009	40	Fluvial
15 m	008	55	Fluvial
15 m	007	25	Fluvial
15 m	006	45	Fluvial
Clifton Sand 18 m	005	100	Marine
Trig. N. Beds 75 m	004	170	Unknown
Rabbit Gully Beds 50 m	003	85	Unknown
110 ft. Conglomerate 15 m	002	210	Fluvial
Maraetotara Sand 11 m	001	145	Marine

Fig. 4-3. The units sampled for clast shape. Measurements are taken from the base of respective formations where they occur in the coastal section, except the Maraetotara Sand (N135/386167). The sample numbers are prefixed with W.T. 14. to indicate Waikato Thesis numbers.

Although the units sampled are of different ages this probably introduces little bias as they are located within a restricted geographic area and presumably therefore the clasts had all travelled about the same distance from source.

Initially discussion is centred on samples 001 to 005, 012 and 013. In section 4-6 the effect of selective sorting of particular clasts on the basis of shape is investigated in samples 006 to 011.

4-5 *SHAPE CHARACTERISTICS OF PEBBLES IN THE CONGLOMERATES*

Classification of Form

Pebble shapes for samples 001 to 005, 012 and 013 are presented in Figs. 4-4 to 4-10. Comparison by visual inspection of the sphericity-form diagrams indicates that the units sampled have generally similar form characteristics, there being little difference in the shapes of pebbles from the different environments. Approximately 50% of the pebbles are shared between bladed and elongate forms. Fewer than 5% of the pebbles occur in the forms very platy, very bladed or very elongate. Of the remainder almost subequal amounts occur in one of the platy, compact elongate, compact bladed or compact platy classes.

Fig. 4-11 summarises the form data for fluvial, marine and unknown environments. The differences between marine and fluvial samples are too few to draw significant conclusions about. However, fluvial pebbles tend to be more elongate and marine ones more platy. Also the unknown samples group more with the fluvial samples than they do the marine.

The forms of fluvially shaped pebbles reported elsewhere (Dobkins & Folk 1970) appear to be more compact than those in this study. This may reflect lithological differences in that the former study measured basalt pebbles, compared with greywacke pebbles in this study.

Results Derived from Shape Indices

Table 4-1 summarises the statistics for each of the ψ_p, *OP*, *E* and *B* indices. Sample mean values of ψ_p are

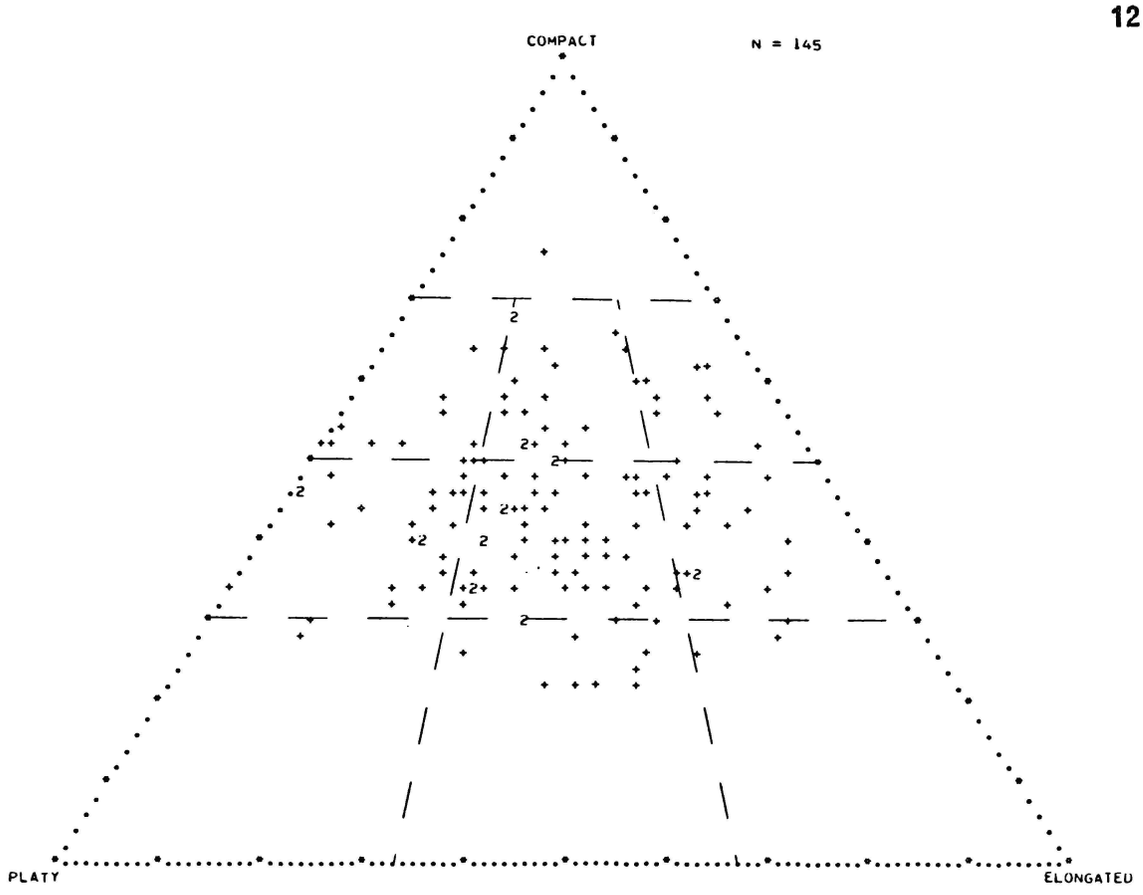

Fig. 4-4. Distribution of pebble form in sample 001 on a sphericity-form diagram.

Note: a number indicates 2 or 3 pebbles have the same form.

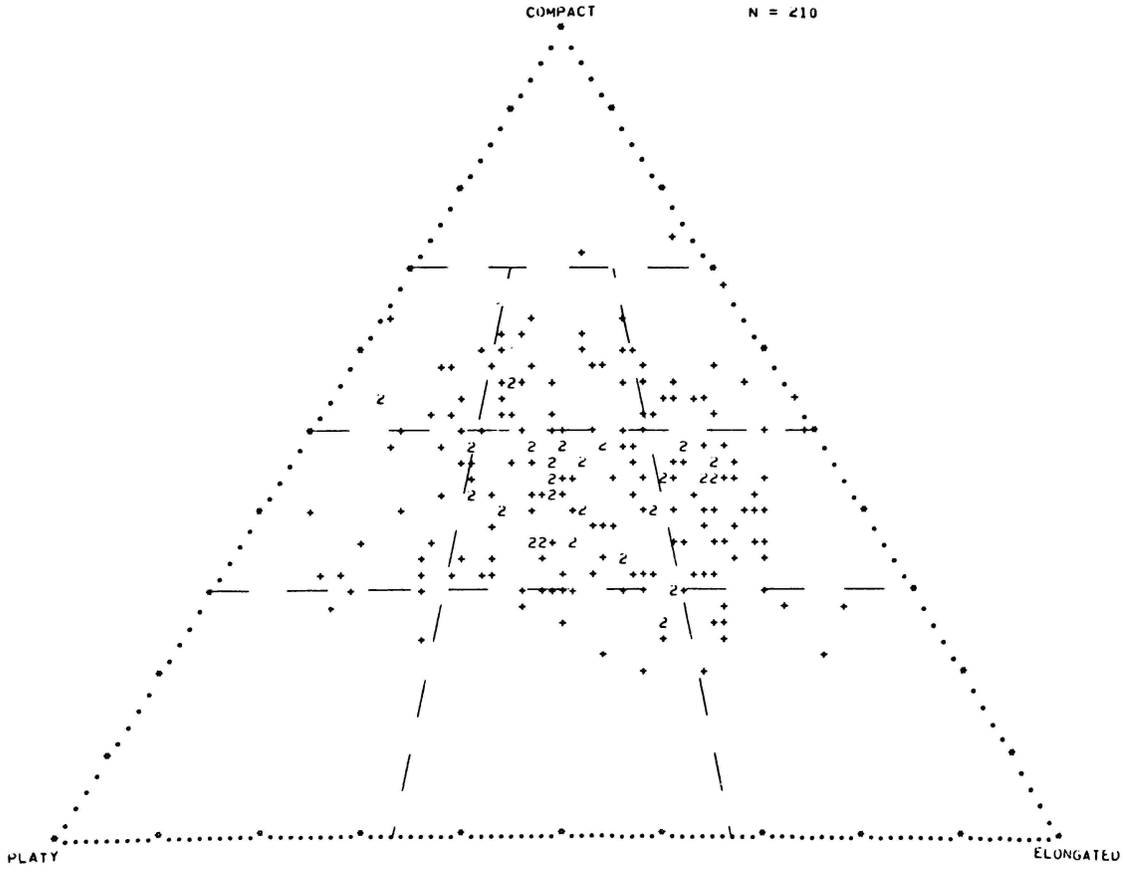

Fig. 4-5. Distribution of pebble form in sample 002 on a sphericity-form diagram.

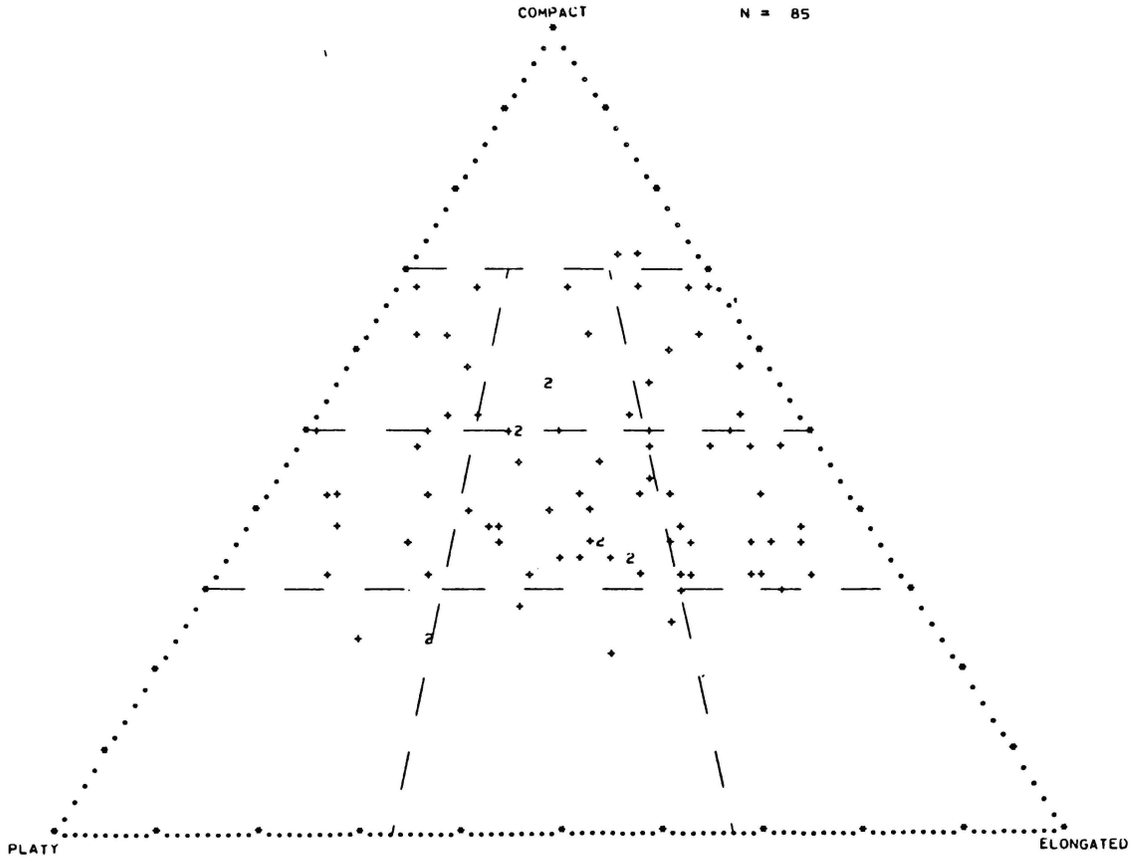

Fig. 4-6. Distribution of pebble form in sample 003 on a sphericity-form diagram.

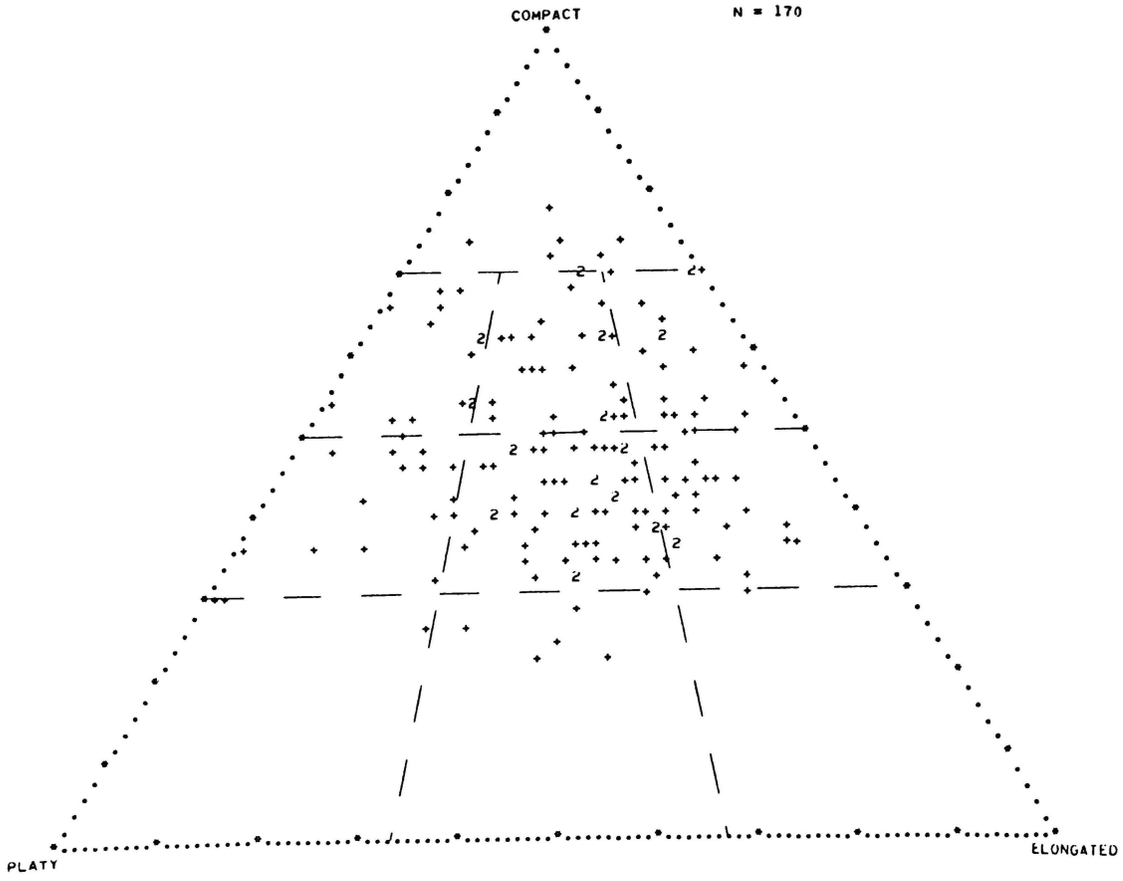

Fig. 4-7. Distribution of pebble form in sample 004 on a sphericity-form diagram.

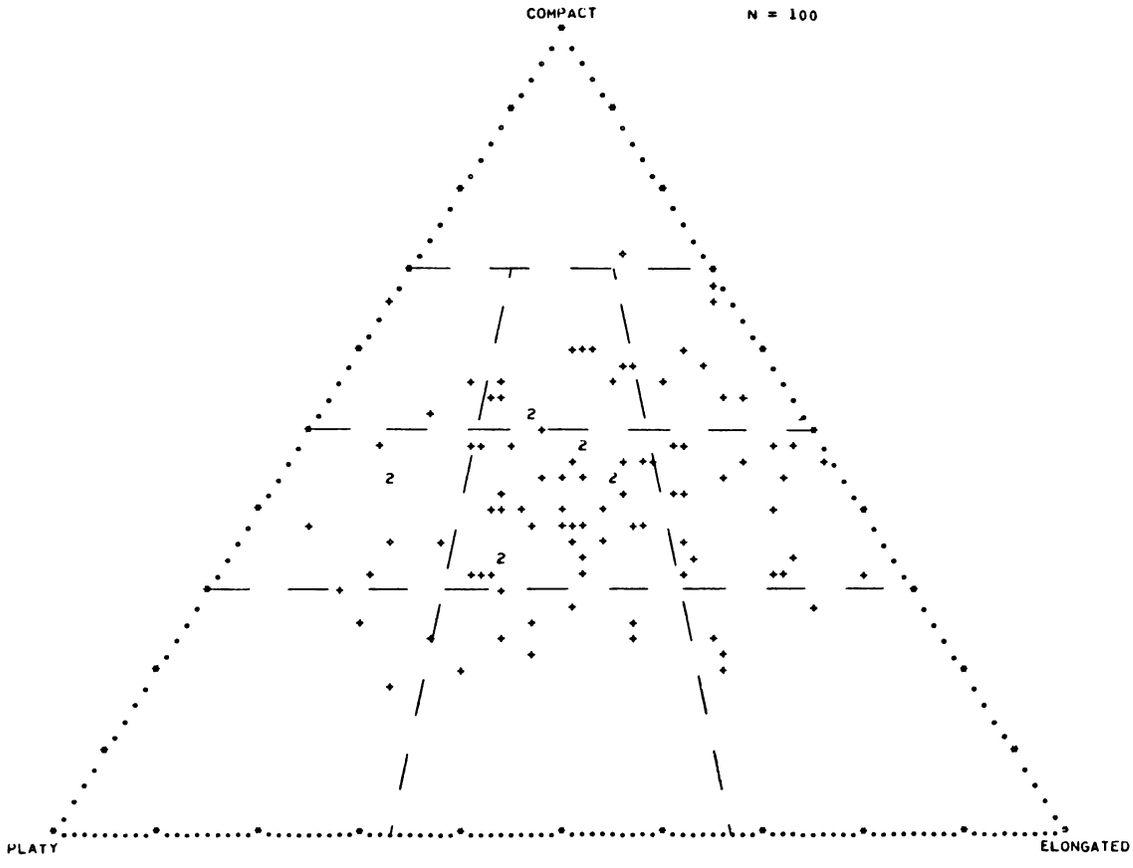

Fig. 4-8. Distribution of pebble form in sample 005 on a sphericity-form diagram.

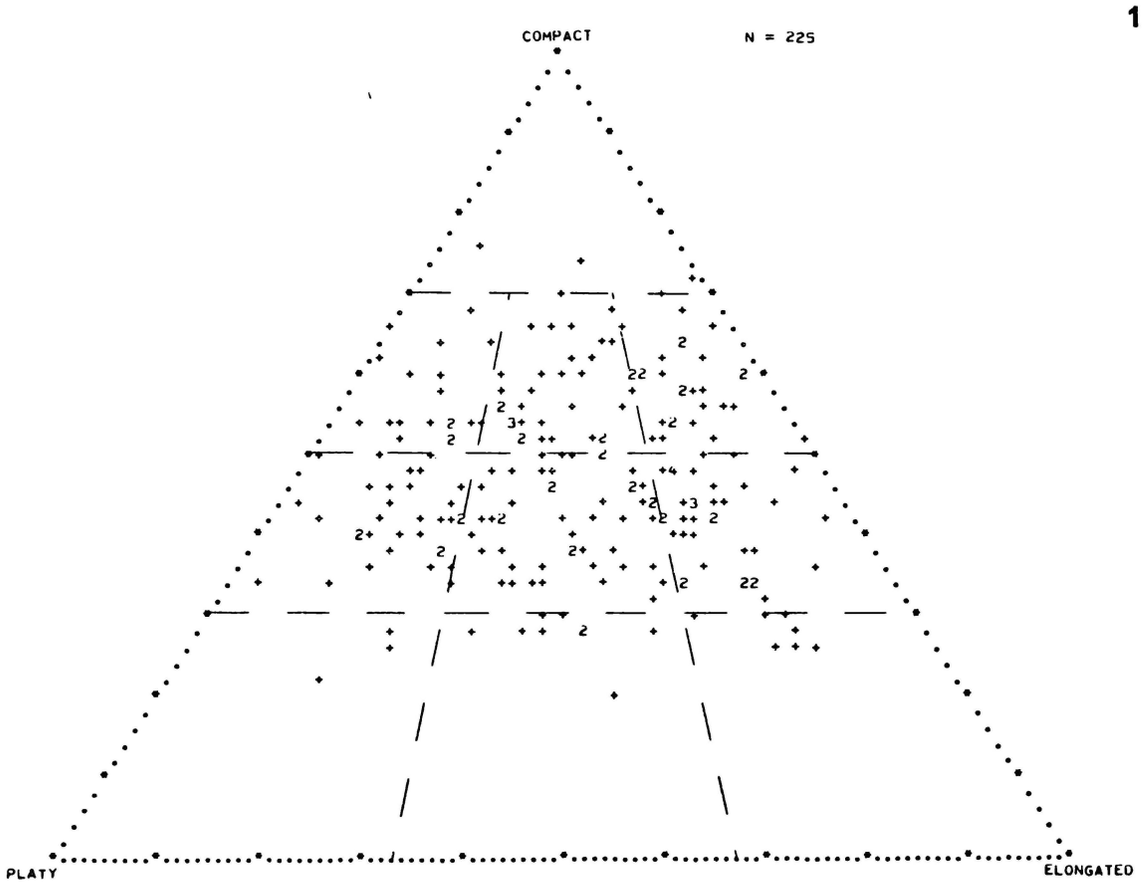

Fig. 4-9. Distribution of pebble form in sample 012 on a sphericity-form diagram.

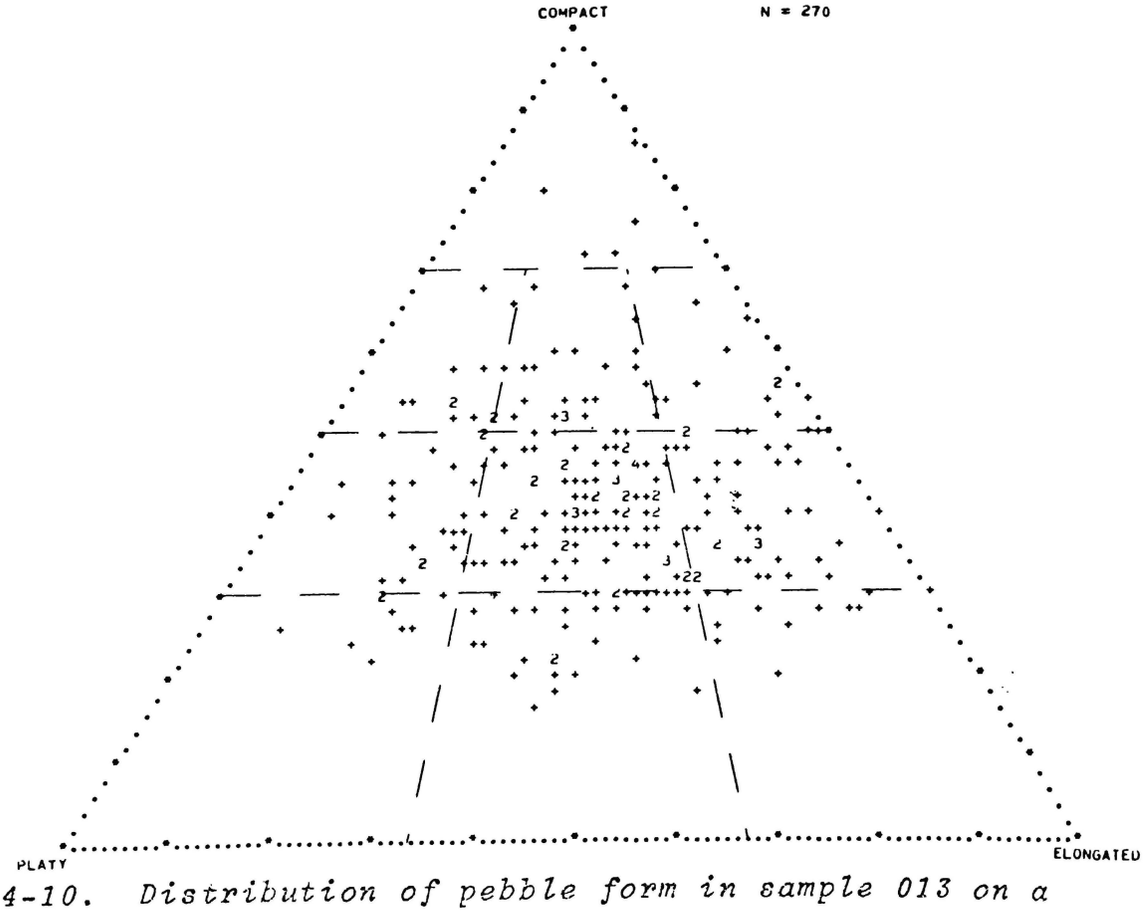

Fig. 4-10. Distribution of pebble form in sample 013 on a sphericity-form diagram.

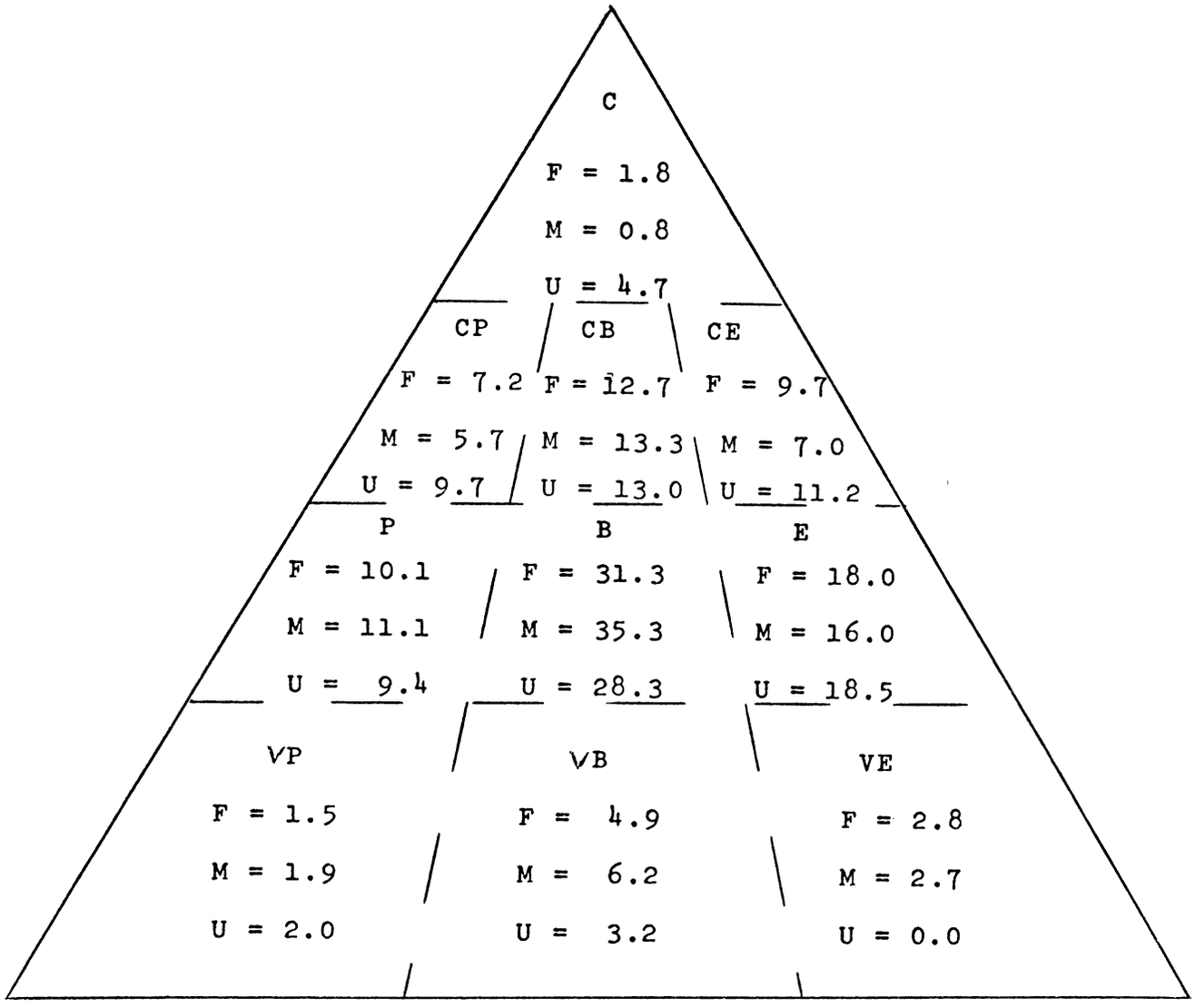

Fig. 4-11. Percentage of pebbles in each of the 10 form classes. The sum of F (fluvial), M(marine) and U (unknown environment) pebbles equals 100%. Abbreviation for form classes: C - compact, P - platy, B - bladed, E - elongate, V -very.

surprisingly uniform. For fluvial units ψ_p = 0.647 ± 0.001, in marine units ψ_p = 0.635 ± 0.007, and in unknown units ψ_p = 0.665 ± 0.001. The average standard deviation for fluvial samples of 0.099 is slightly lower than that for marine samples where σ = 0.103. This statistic for the unknown units is 0.104. The confidence limits reflect the low sample variance and confirm that most pebbles occur within a restricted number of sphericity-form classes.

The statistics suggest that pebble sphericity is similar irrespective of environment, and that marine samples are no less variable than fluvial samples. Contrary to other studies of pebble shape, ψ_p would appear to be a poor environmental discriminator.

A wide range in the mean *OP*. index values exists with most being positive and one (001, marine) negative. The average of the fluvial mean *OP*. index values is *OP*. = +1.030 ± 0.205 and for the unknown units *OP*. = 0.855 ± 0.320. There is a wide difference in *OP*. index values for the two samples known from independent evidence (shells) to be marine. One of these, 005, occurs within the range of all the other units. The mean *OP*. index values indicate that most units have the attributes of fluvially shaped pebbles, 001 being the exception as it has pebble shapes characteristic of a low energy beach (Dobkins & Folk 1970). The large standard deviations and confidence limits about the mean reflect the high sample variance, indicative of significant pebble to pebble variation.

A graphic plot of ψ_p versus *OP*. index for each unit (Fig. 4-12.) indicates that Dobkins & Folk's (1970) river/

Sample	No.	Maximum Projection Sphericity Mean	Var.	Stdev.	95 Con.	Oblateness - Prolateness Index Mean	Var.	Stdev.	95 Con.	Inferred Environment
013	270	0.63	0.011	0.105	0.013	1.14	26.48	5.150	0.61	Fluvial
012	225	0.67	0.009	0.097	0.013	0.47	27.25	5.22	0.68	Fluvial
005	100	0.63	0.012	0.111	0.022	0.89	28.99	5.39	1.07	Marine
004	170	0.68	0.010	0.101	0.015	0.70	22.18	4.71	0.71	Unknown
003	85	0.65	0.012	0.108	0.023	1.01	30.33	5.510	1.20	Unknown
002	210	0.64	0.009	0.094	0.013	1.49	35.61	5.968	0.81	Fluvial
001	145	0.64	0.009	0.095	0.015	0.67	24.19	4.92	0.80	Marine
		Bladed Index				Elongation Index				
013	270	0.55	0.039	0.197	0.023	0.68	0.017	0.129	0.015	Fluvial
012	225	0.52	0.052	0.229	0.030	0.72	0.018	0.134	0.018	Fluvial
005	100	0.54	0.044	0.210	0.042	0.69	0.016	0.127	0.025	Marine
004	170	0.54	0.045	0.212	0.032	0.72	0.015	0.124	0.019	Unknown
003	85	0.54	0.039	0.197	0.023	0.68	0.017	0.129	0.015	Unknown
002	210	0.57	0.193	0.439	0.059	0.69	0.019	0.138	0.019	Fluvial
001	145	0.47	0.043	0.207	0.034	0.74	0.017	0.129	0.021	Marine

Table 4-1. Summary of the statistics describing the shape distribution of pebbles in each unit sampled. The depositional environment inferred from other evidence is entered alongside.

beach environmental boundary line discriminates 001 from the other tightly grouped samples. Although the samples have similar sphericity values, the *OP.* index allows a separation to be made with confidence. The data strongly suggest that six of the units sampled consist of pebbles displaying fluvial shape attributes and one unit has pebbles characteristic of a low energy beach environment.

Results for *E.I.* and *B.I.* confirm the separation of samples into two groups and fail to yield consistent differences in shape within the larger, apparently non-marine group (Table 4-1.).

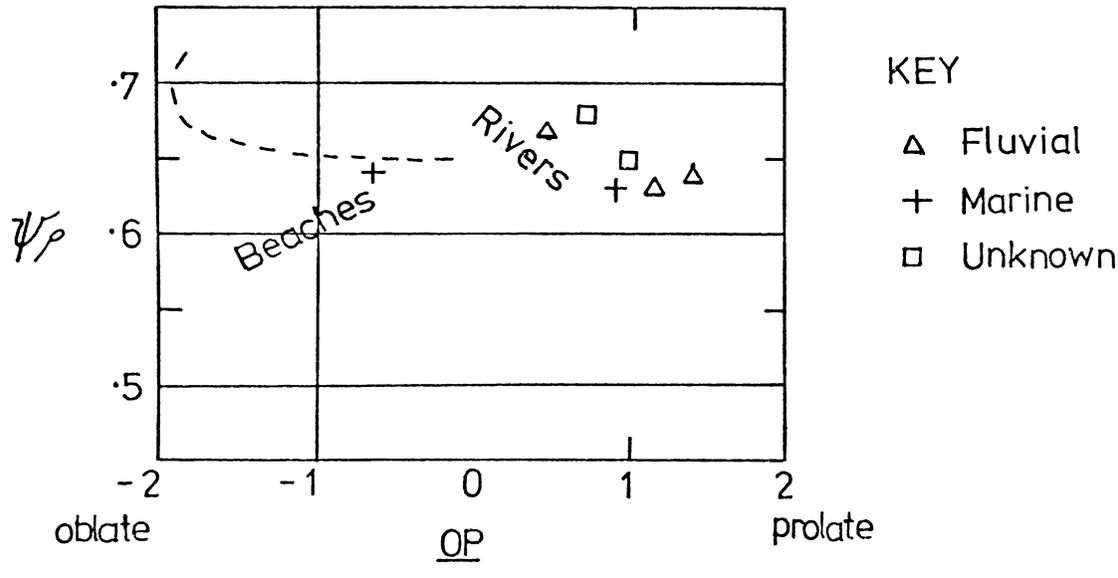

Fig. 4-12. A plot of sphericity vs. OP. index for each sample. Each point is the average of all pebbles in the sample. In general the fluvial pebbles are less spherical than fluvial pebbles reported by Dobkins & Folk (1970). Nevertheless, there is a confident separation between one beach sample (005) and all other samples (inferred fluvial and environmental unknowns).

Comparison of Significance Within Known Marine and Fluvial Conglomerates

A summary of significance testing of samples from within and between known environments is shown in Table 4-2. In general significance levels are consistently either very high or very low.

It appears that irrespective of index, significant differences occur within the marine and within the fluvial units. Furthermore, the marine samples are not always found to be significantly different from the fluvial samples. This suggests that intra-environmental differences are as significant as inter-environmental differences. The inconsistencies are less apparent when it is appreciated that although 005 on the basis of field characteristics is a marine conglomerate, the pebbles have fluvial shape attributes (Fig. 4-12.).

Comparison of Fluvial and Marine Conglomerates with Environmentally Unknown Units

Table 4-3 summarises significance testing of known against unknown environments to help determine which group the unknown units belong. In general the differences between the two unknown units are not significant (Table 4-3). Frequently however, there are significant differences between 001 (marine) and the unknown units. Nevertheless, compared to the fluvial samples the unknown units show few significant differences.

Again with disregard for any particular index, the data in Table 4-3 is in agreement with that in Table 4-2 and both are consistent with the environmental interpretation of the units presented in Fig. 4-12.

Sample No.	ψp t value	ψp S.	ψp S. at 5%	O. - P. Index t value	O. - P. Index S.	O. - P. Index S. at 5%	Elongation Index t value	Elongation Index S.	Elongation Index S. at 5%	Bladed Index t value	Bladed Index S.	Bladed Index S. at 5%
Comparison within Marine Conglomerates												
005 / 001	0.750	>20%	No	2.337	<2>1%	Yes	2.985	<1>0.2%	Yes	2.579	∿1%	Yes
Comparison within Fluvial Conglomerates												
013 / 012	4.348	<0.1%	Yes	1.451	<20>10%	No	3.365	<0.1%	Yes	1.560	20>10%	No
012 / 002	3.259	<0.2%	Yes	1.915	<10>5%	No	2.296	<5>2%	Yes	2.038	5>2%	Yes
002 / 013	1.077	>20%	No	.687	>20%	No	0.815	>20%	No	2.689	1>2%	Yes
Comparison of Fluvial and Marine Conglomerates												
012 / 005	3.26	0.2>0.1%	Yes	0.677	>20%	No	1.568	<20>10%	No	0.743	>20%	No
005 / 002	0.815	>20%	No	0.851	>20%	No	0.0	N.S.	No	0.643	>20%	No
012 / 001	2.916	1>0.2%	Yes	2.073	<5>2%	Yes	1.416	<20>10%	No	2.122	5>2%	Yes
001 / 002	0.0	N.S.	No	3.586	<0.1%	Yes	3.435	<0.1%	Yes	3.37	<0.1%	Yes

Table 4-2. Comparison of the significance of differences between mean values of shape indices within Fluvial and Marine Samples and between Fluvial and Marine samples. S. refers to Significance Level.

Maximum projection sphericity				O. - P. Index			Elongation Index			Bladed Index		
Sample No.	t value	S.	S. at 5%	t value	S.	S. at 5%	t value	S.	S. at 5%	t value	S.	S. at 5%
A.												
003												
	2.170	5>2%	Yes	0.466	>20%	No	1.151	>20%	No.	0.0	No	No
004												
B.												
005												
	1.229	>20%	No	0.149	>20%	No	0.503	>20%	No	0.0	N.S.	No
003												
	0.732	>20%	No	2.380	<2>1%	Yes	1.175	>20%	No	2.36	2>1%	Yes
001												
C.												
005												
	3.757	<0.1%	Yes	0.302	>20%	No	1.896	<10>5%	No	0.0	N.S.	No
004												
	3.579	<0.1%	Yes	2.513	<2>1%	Yes	1.394	<20>10%	No	2.949	1>0.2%	Yes
001												
D.												
013												
	4.905	<0.1%	Yes	0.900	>20%	No	3.203	<0.2>0.1%	Yes	0.500	>20%	No
004												
	3.309	<0.1%	Yes	0.471	>20%	No	0.0	N.S.	No	0.884	>20%	No
012												
E.												
012												
	1.564	20>10%	No	0.812	>20%	No	1.149	>20%	No	0.612	>20%	No
003												
	0.788	>20%	No	0.637	>20%	No	0.558	>20%	No	0.595	>20%	No
002												

Table 4-3. Comparison of the significance of differences between mean values of shape indices for known environments (Marine and Fluvial) and samples from unknown environments. S refers to Significance Level.

4-6 EVALUATION OF SHAPE INDICES

On the assumption that in Fig. 4-12 samples are correctly grouped with respect to shape, it is possible to evaluate the success rate of an index in establishing the correct grouping of pebble shapes into fluvial and purely marine environments (Fig. 4-13.).

	ψ_p	*OP* index	*B.* index	*E.* index
Total No. of cases	17	17	17	17
No. correct predictions	7	17	15	11
% Success	41%	100%	88%	65%

Fig. 4-13. A summary of the success rate of shape indices at consistently establishing the correct grouping of pebble shapes. The data are derived from Tables 4-2 and 4-3.

Dobkins & Folk (1970) found in $\frac{2}{3}$ of the localities studied on Tahiti-Nui that both *OP.* and ψ_p gave a correct and clear environmental discrimination if used alone, and in the remainder each was correct ½ of the time. This study has revealed however that the *OP.* index is correct all of the time and ψ_p correct approximately ½ of the time.

Considering that together the *OP.* index and ψ_p uniquely identify pebble form (Dobkins & Folk 1970), it is to be expected that as one parameter becomes more sensitive the other must become less sensitive in discriminating form. The discrepancy with Dobkins & Folk's (1970) evaluation is partly a reflection of the pebbles in this study having

lower sphericity. In certain regions of the triangle the sphericity parameter does not differentiate well platy from elongate forms because the sphericity contours become more or less parallel to the triangle base (Fig. 4-14.). The difference is also partly a reflection of the fact that most pebbles in this study are either bladed or elongate (Figs. 4-4 to 4-10.) and therefore span only one sphericity contour interval while several *OP.* index contour intervals are crossed.

Following on further from Dobkins & Folk (1970) the distribution of the sample population, and in particular the mean position, will be important in determining which of the two indices will be the best discriminator. Fig. 4-15 indicates the directions in which both *OP.* index and ψ_p become more consistent at establishing similar shapes, for constant sample variance, because of the increase in contour density.

Movement of the sample shape distribution in the vertical direction is more significant than movement horizontally due to the curved nature of the *OP.* index contours and an increase in contour concentration. Hence the *OP.* index becomes more successful as a shape-discriminatory index away from an $\frac{S}{L}$ ratio of 0.6 (Fig. 4-15.). It is more difficult to determine the position where ψ_p shows maximum efficiency as it is complicated by the fact that an increase in contour concentration is offset by the contours becoming subparallel to the triangle base and vice versa. The region where ψ_p is most effective is around $\frac{S}{L} = 0.5$. In general, the region of the triangle where the *OP.* index is most

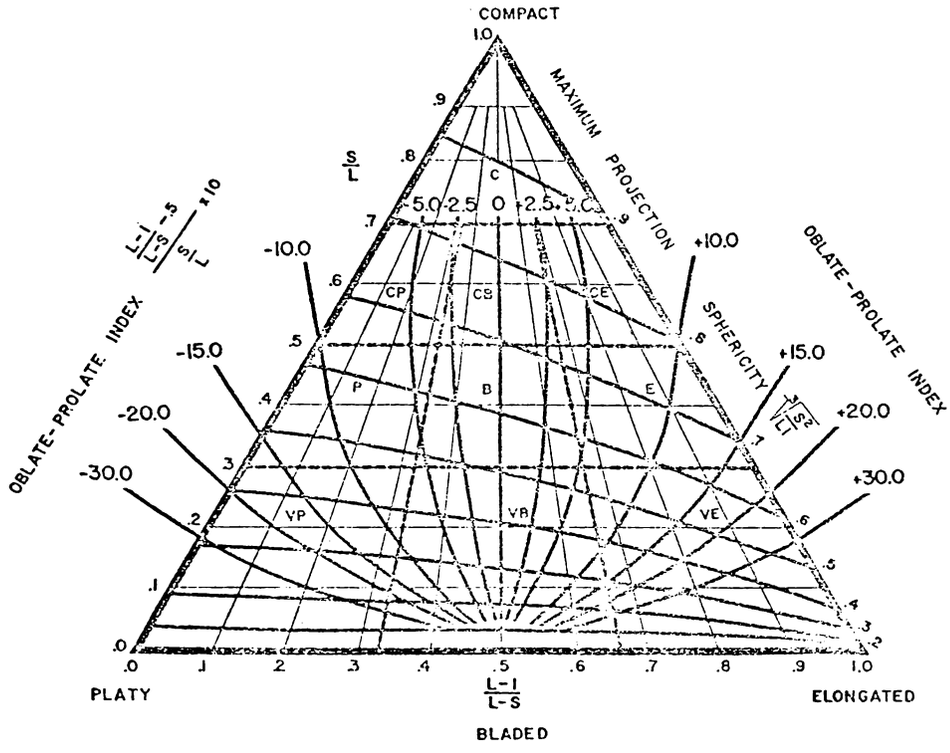

Fig. 4-14. Sphericity, oblate - prolate index, form diagram. (After Dobkins & Folk 1970).

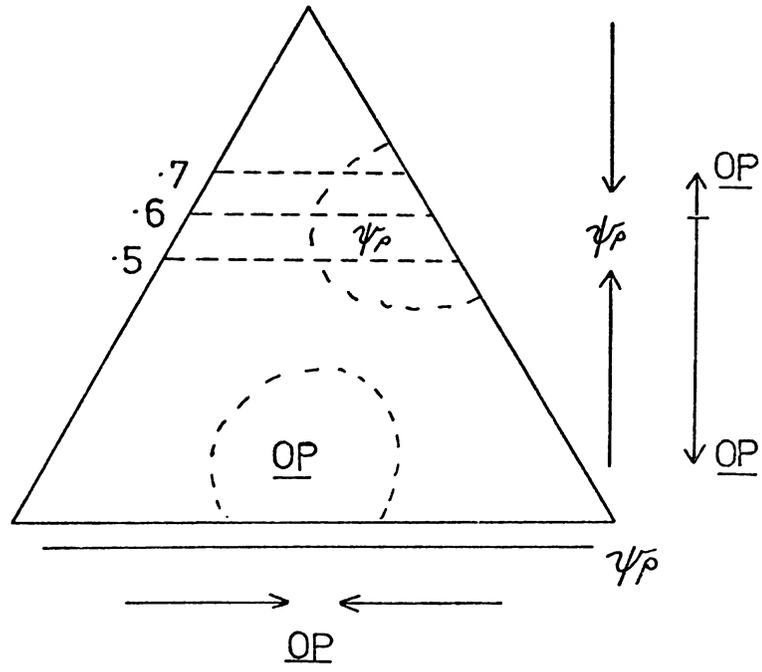

Fig. 4-15. A triangular diagram indicating the direction in which the indices ψ_p and OP become improved shape discriminators, for sample distribution on a sphericity, oblate - prolate index, form diagram. The most successful region for each index is indicated.

consistent is the lower centre, and the most successful region for ψ_p will be right of centre at approximately $\frac{S}{L} = 0.5$ (Fig. 4-15.).

Although the theoretical situation described above is strictly correct, the *OP.* index will always be more consistent in differentiating purely marine from fluvial pebbles for larger areas of the triangle as it is a more sensitive measure of platy versus elongate shapes. The reason is the larger range in numerical values from one end of the scale (prolate +30.0) to the other (oblate -30.0) compared with the ψ_p range of 0.0 to 1.0. Hence, there is a large difference in the mean values between purely marine and fluvial pebbles for *OP.* index than for ψ_p. The larger the difference between mean values, the more likely the alternative hypothesis holds.

In addition, the *OP.* index, by determining how oblate a pebble may be, gives an estimate of the amount of shape modification which has occurred and therefore the amount of energy which has been expended on the pebble. Together with other evidence this may be narrowed down to one of two possibilities; a short time in a high energy environment, or a longer time in a lower energy one.

The bladed and elongation indices (Fig. 4-13.) showed varying degrees of success, essentially proportional to the spread of mean values between the two extremes of their respective scales. Of the two, the more complicated bladed index is a better measure. Although the elongation index is less successful, it is a very simple and rapid method suitable for use in the field. For a difference in mean

values similar to that between 005 and the fluvial pebbles in this study, only 100 clasts of a unit need be measured to be confident at the 95% level from which of the environments the unit can be excluded.

4-7 SHAPE SELECTIVE SORTING

Selective movement of particular clast shapes in rivers has been observed by many workers. The order of increasing clast transportability reported in the literature is summarised below:

Russell (1939)	rods, spheres
Krumbein (1942)	disks, spheres, rods
Unrug (1957)	spheres, rods, blades, disks
Bradley *et al.* (1972) and Spalletti (1976)	compact, elongated, platy

$\longrightarrow$

increasing transportability

Hence, it is evident there is disagreement regarding the clast shape that is most likely to be transported furthest, although this may be explained in part by the mode of transport. Bradley *et al.* (1972) consider that platy clasts are transported in saltation with an erratic tumbling motion. This arises from the large cross-sectional area in contact with higher-velocity flows, and therefore platy clasts moved furthest. Similarly, Spalletti (1976) found that a decrease in the $^{S}/_{I}$ ratio below 0.67, corresponding to an increase in platy nature, indicates the predominance of saltation transport. Conversely, an increase in the ratio above 0.67 corresponds to a more prolate character, and therefore an increase in traction over saltation transport.

To determine whether selective sorting of pebble shapes occurs in the Clifton Conglomerate, six sedimentation units were sampled (Fig. 4-16.) within a restricted stratigraphic range at the base of the Clifton Conglomerate (Fig. 4-3.).

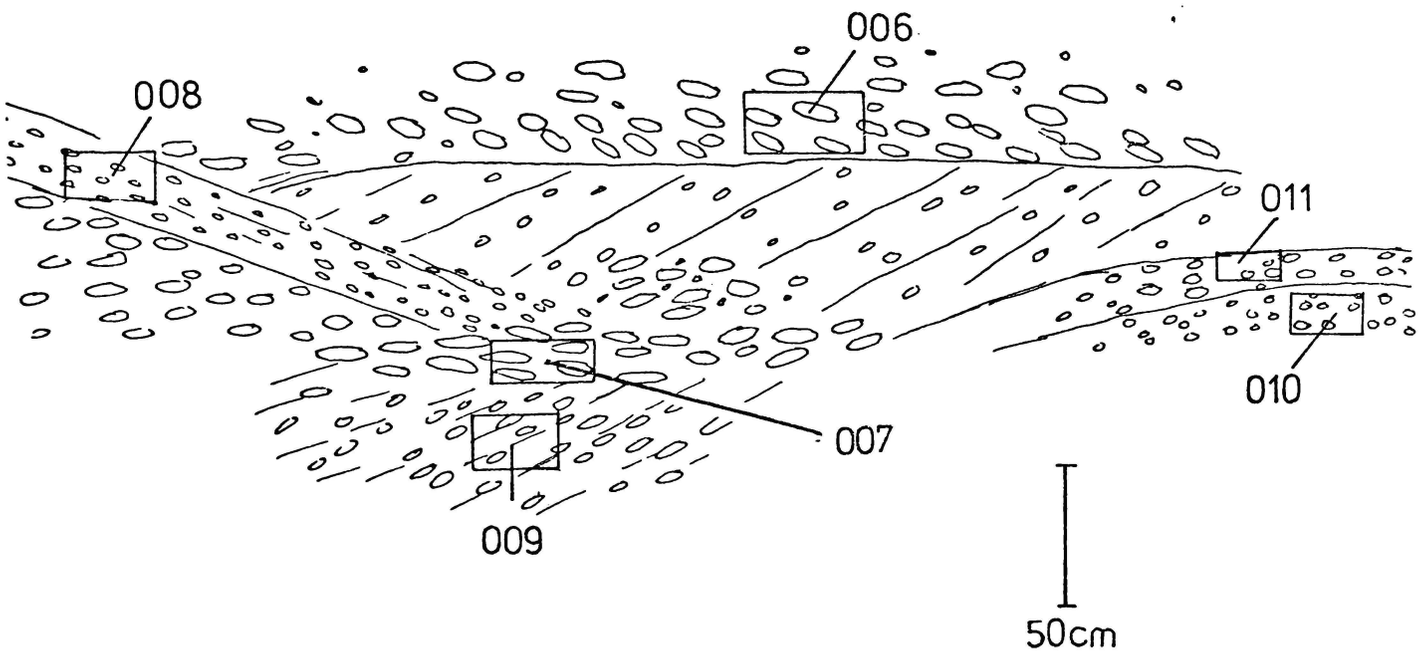

Fig. 4-16. Sketch of the outcrop 15 m from the base of the Clifton Conglomerate in the coastal section (N135/423204). Sampling areas and numbers are indicated.

Results Derived from the Measurement of Pebble Shape

The pebble shape distributions for each sample are presented in Figs. 4-17 to 4-22, and the percentage pebbles in each of the 10 form classes are summarised in Table 4-4. The data indicate that samples are generally bimodal.

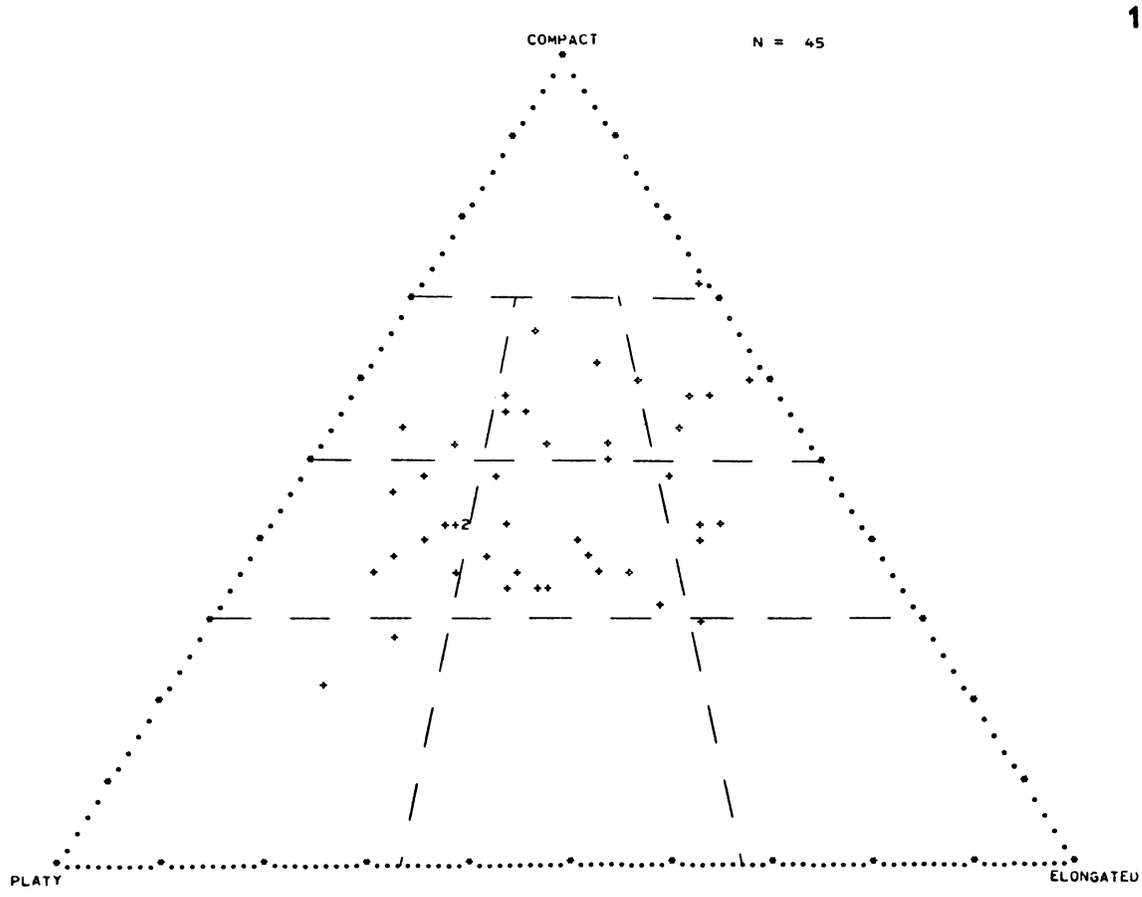

Fig. 4-17. Distribution of pebble form in sample 006 on a sphericity-form diagram.

Note: a number indicates 2 pebbles have the same form.

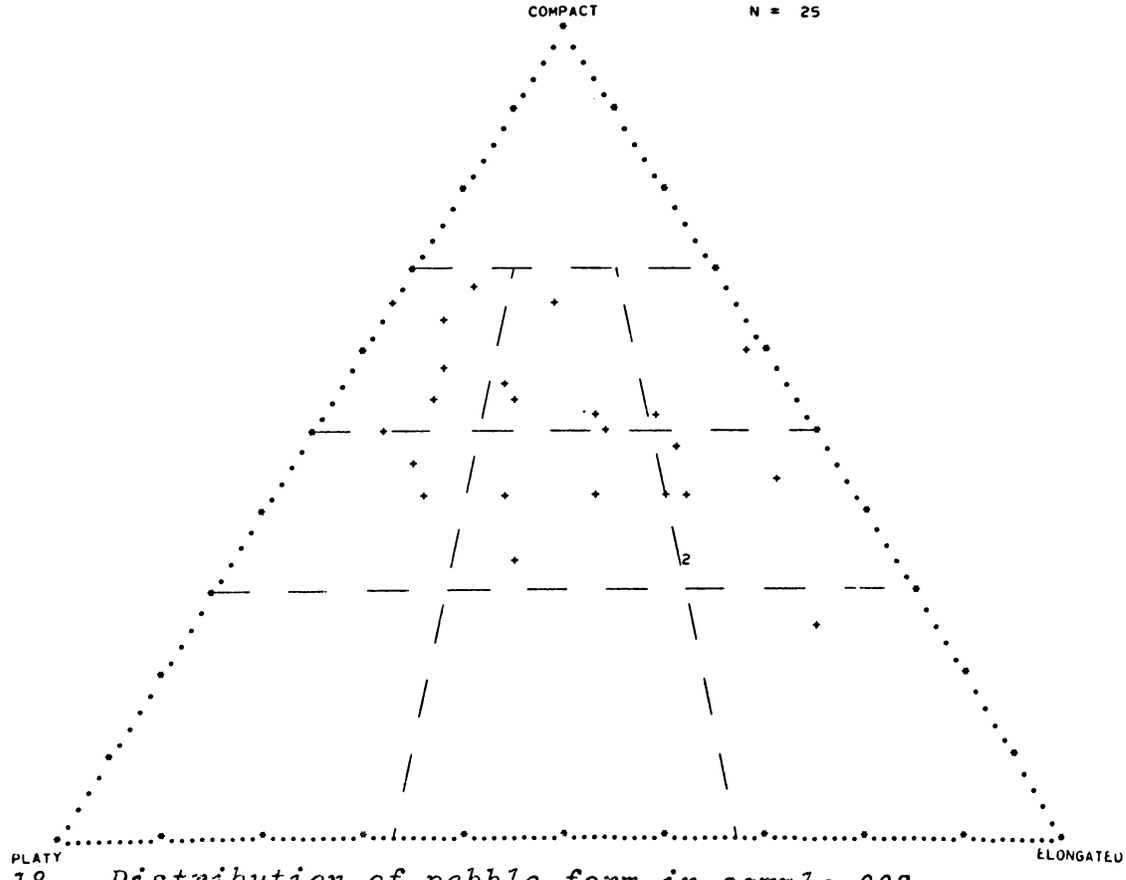

Fig. 4.18. Distribution of pebble form in sample 007 on a sphericity-form diagram.

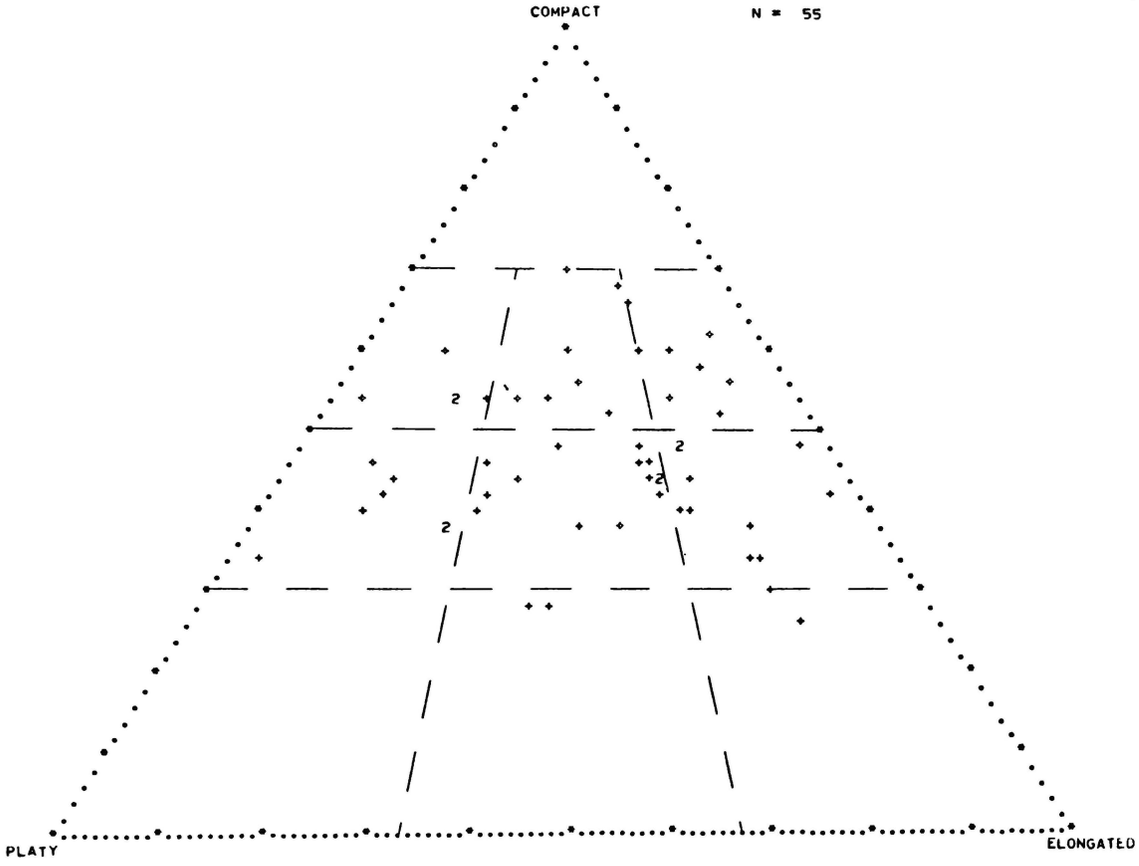

Fig. 4-19. Distribution of pebble form in sample 008 on a sphericity-form diagram.

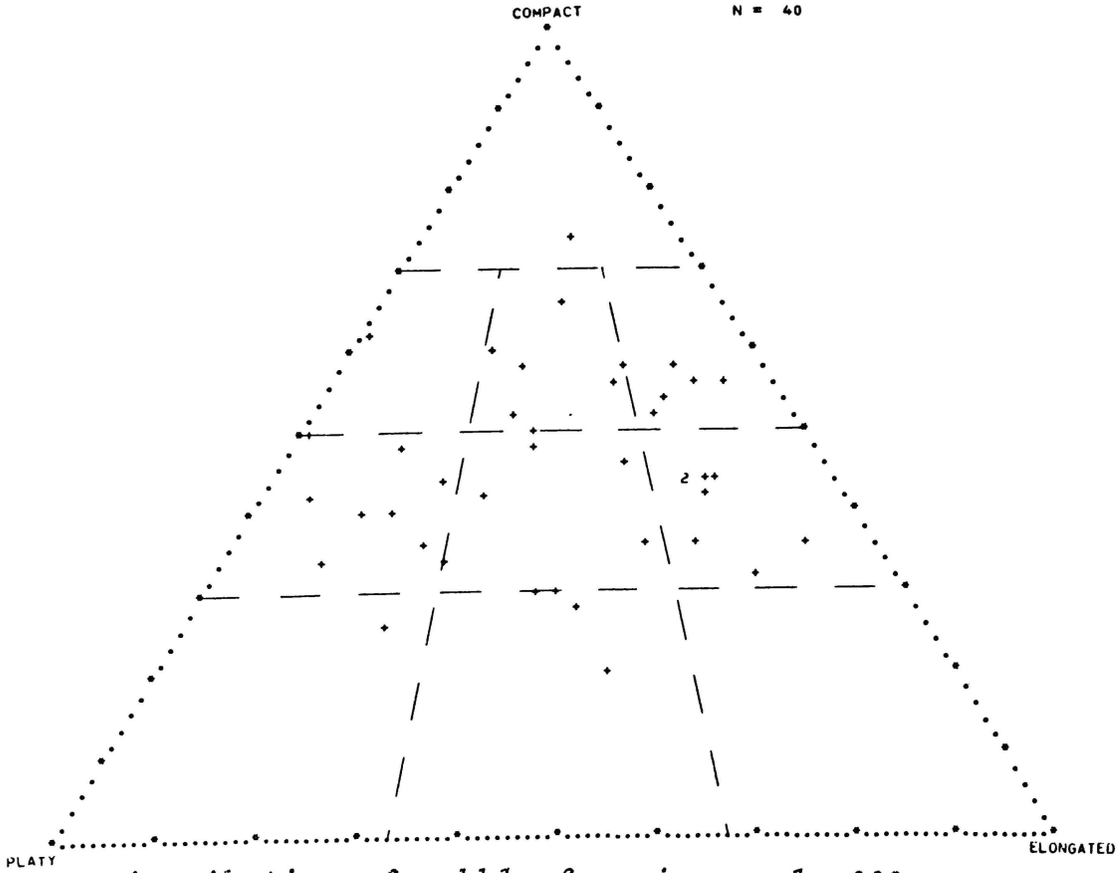

Fig 4-20. Distribution of pebble form in sample 009 on a sphericity-form diagram.

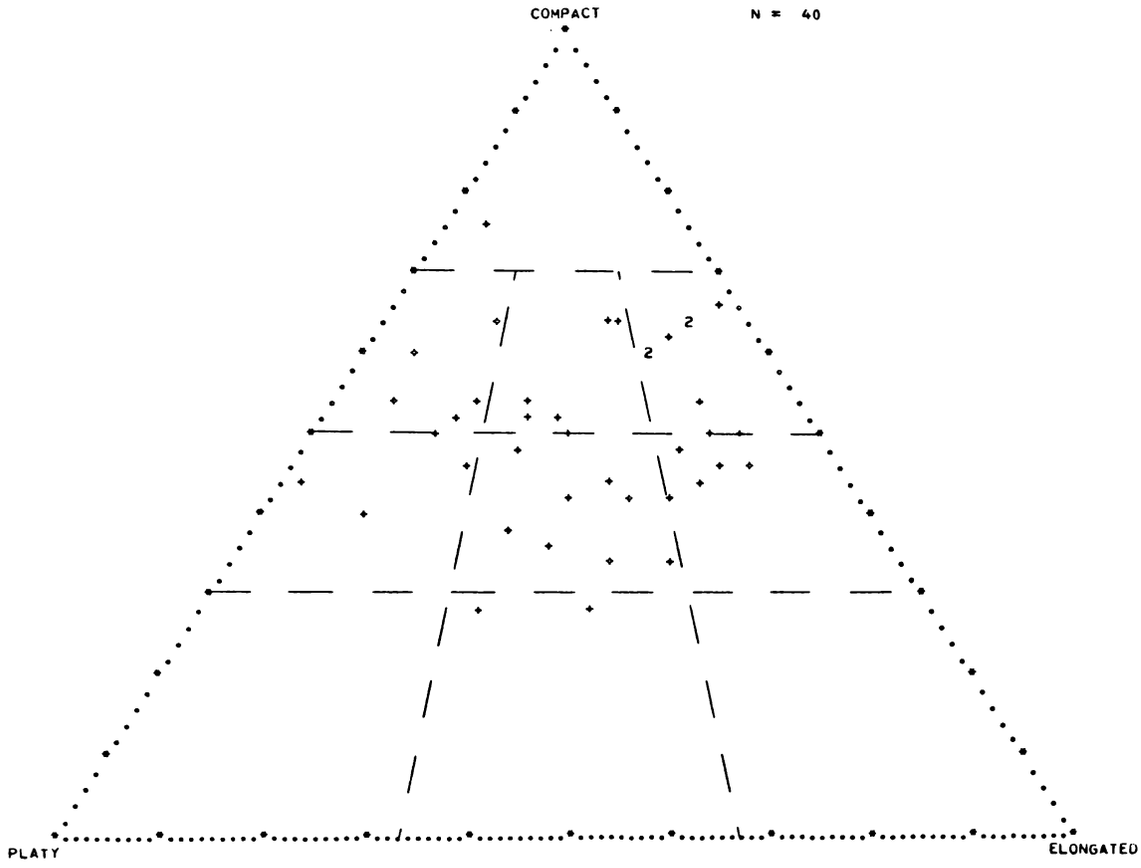

Fig. 4-21. Distribution of pebble form in sample 010 on a sphericity-form diagram.

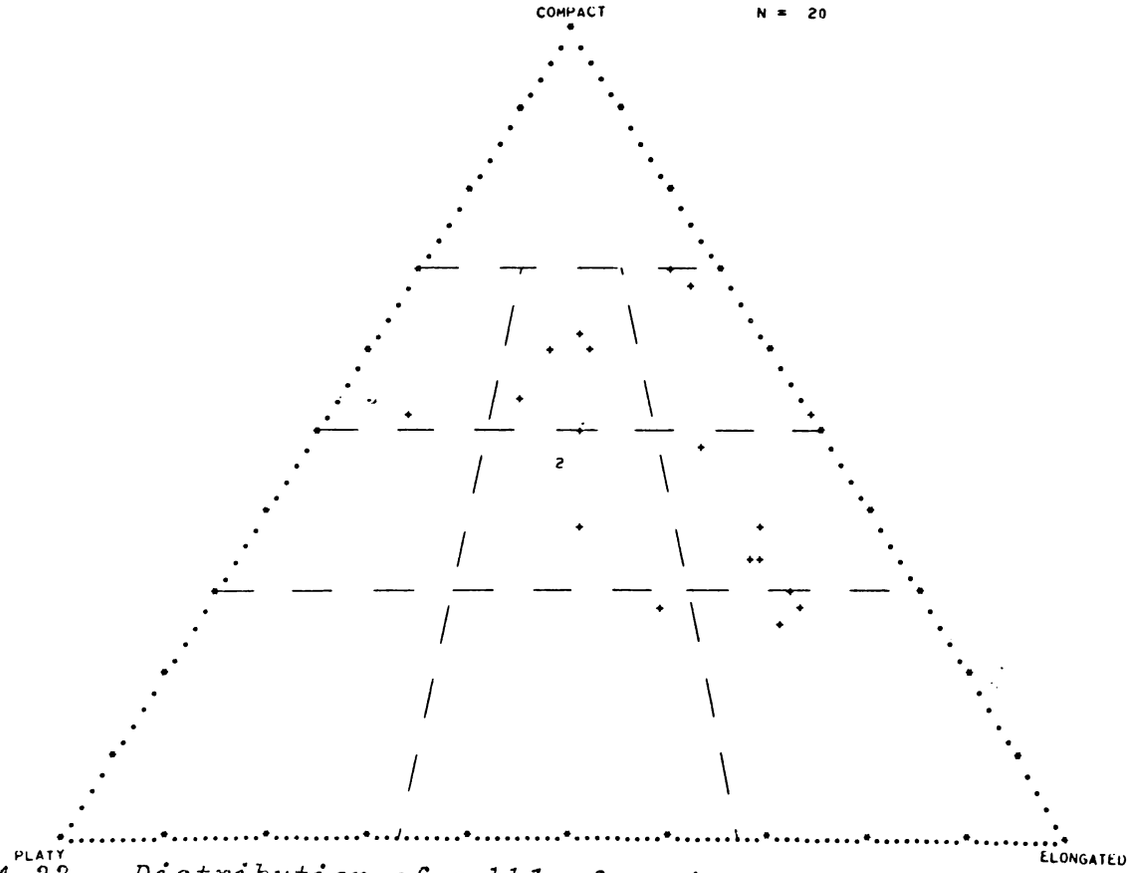

Fig. 4-22. Distribution of pebble form in sample 011 on a sphericity-form diagram.

Sample No.	Form Classes (Sneed & Folk 1958)									
	C	CP	CB	CE	P	B	E	VP	VB	VE
006	2.2	4.4	17.8	11.1	22.3	*26.7*	11.1	4.4	-	-
007	-	*25.0*	20.0	8.0	8.0	12.0	*23.0*	-	-	4.0
008	2.6	5.1	15.4	12.8	*20.5*	15.4	*20.5*	2.6	5.1	-
009	-	9.0	12.7	14.6	12.5	*25.5*	20.0	-	3.6	1.8
010	2.5	15.0	15.0	*22.5*	7.5	*20.5*	12.5	-	5.0	-
011	-	5.0	*25.0*	15.0	-	15.0	*25.0*	-	5.0	10.0

Table 4-4. Percent pebbles in each form class. The principal modes are in italics. The bimodality evident in this table is less apparent in the original distributions (Figs. 4-17 to 4-22.). Hence the form class boundaries in the sphericity-form diagram may only be arbitary and may not reflect natural associations of pebble shapes. For example, an essentially unimodal cluster (Fig. 4-21.) statistically becomes bimodal (sample 010). Zingg's shape classes (Fig. 4.1), although fewer in number, may be more natural divisions of pebble shapes.

The shape measures of ψ_p, *OP*, *E.I.* and *B.I.* were calculated for each sample, and statistical analyses of the distributions undertaken (Table 4-5.). The mean ψ_p values are remarkably similar, having a range of only 0.04, and are in close agreement with the fluvial average of Dobkins & Folk (1970, 0.67 c.f. 0.68). On the other hand, the extreme range in *OP* index values is sufficiently large to identify a significant difference between a random combination of cases (Table 4-5.). Results derived from *E.I.* and B.I. are not

	Maximum Projection Sphericity (ψ_p)						Oblateness - Prolateness Index						
Sample No.	N	Mean	DMean	Var.	Stdev	95 con.	N	Mean	DMean	Var	Stdev	95 con.	Mean Size
006	45	0.65	0.474	0.011	0.103	0.031	45	-1.00	1004.88	22.33	4.73	1.42	2.76
007	25	0.68	0.142	0.006	0.077	0.032	25	0.13	703.40	29.31	5.41	2.23	2.69
008	40	0.65	0.457	0.011	0.107	0.034	40	0.05	1237.68	30.94	5.56	1.78	1.49
009	55	0.68	0.426	0.008	0.088	0.024	55	0.96	1553.39	28.24	5.31	1.44	1.35
010	40	0.69	0.352	0.009	0.094	0.030	40	0.32	804.23	20.11	4.48	1.43	1.57
011	20	0.68	0.197	0.010	0.102	0.048	20	3.83	479.84	25.26	5.03	2.35	1.53

	$\underline{t}$ value	S.	S. at 5%	$\underline{t}$ value	S.	S. at 5%
006	1.264	>20%	No	-0.904	>20%	No
007	1.207	>20%	No	0.057	>20%	No
008	1.482	<20>10%	No	0.799	>20%	No
009	0.526	>20%	No	0.612	>20%	No
010	0.375	>20%	No	2.724	<1>0.2%	Yes
011	1.082	>20%	No	-3.702	<0.1%	Yes

Table 4-5. Comparison of the significance of differences between mean values of shape indices to establish whether shape selective sorting occurs in a fluvial conglomerate. S. refers to Significance Level.

included here, as the data merely confirms that derived from the *OP* index.

Shape versus Size Selective Sorting

The mean ψ_p and *OP* index values have been graphed in Fig. 4-23. The spread of values in the graph, together with significant differences between a random combination of *OP* index values (Table 4-5.), shows that the samples have been selectively sorted.

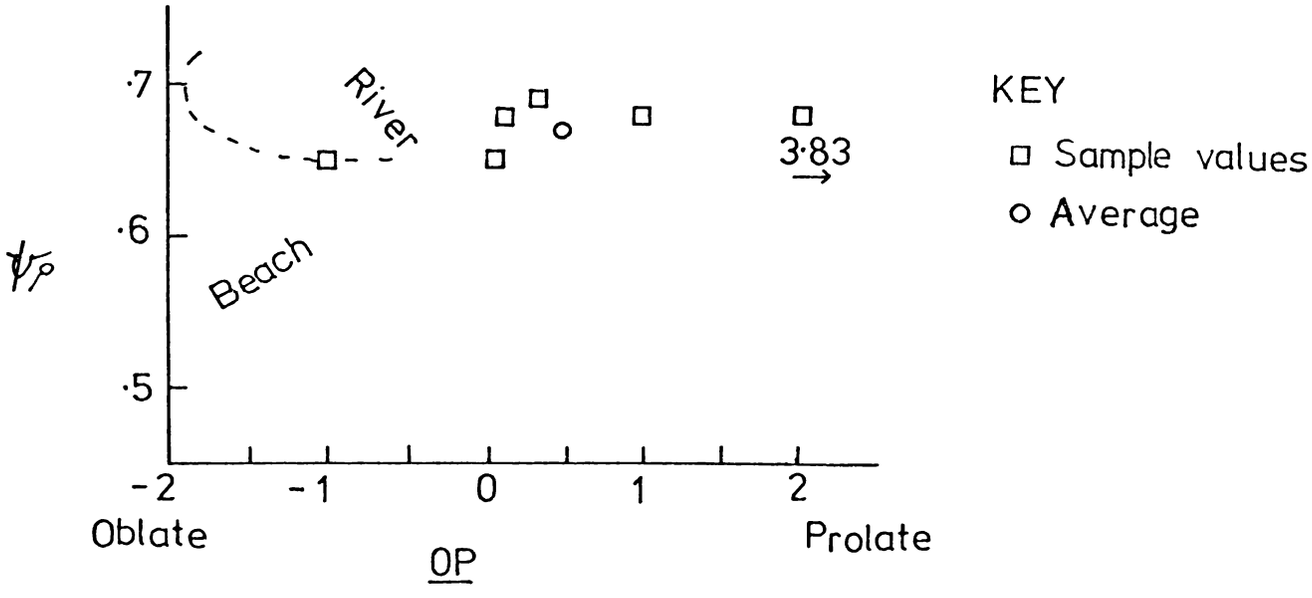

Fig. 4-23. A graph of ψ_p versus OP index for each sample together with the average value.

To establish whether the sorting is a function of shape and/or size, the mean size for each sample was plotted against *OP* index (Fig. 4-24.).

Two groups are recognised, one where the larger pebbles are oblate to bladed, and the other where the smaller pebbles are bladed to prolate. In the latter group, pebbles (uniformly about 1.5 cm, Fig. 4-24.) may be either bladed

to prolate, or markedly prolate (e.g. 011, Table 4-5.). Hence, larger pebbles tend to be oblate (a size-dependent shape), but smaller pebbles appear to have shapes independent of size (size-independent shapes).

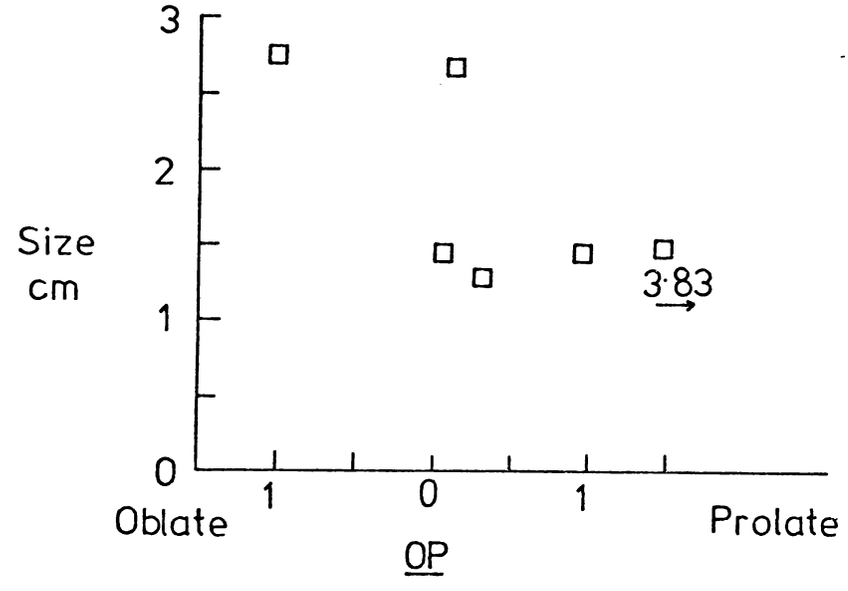

Fig. 4-24. A graph of mean size in cm (length of b-axis) versus OP index. The consistently similar ψ_p values (Fig. 4-23.), irrespective of oblateness or prolateness, indicates a fine balance between reduction in size and change in shape. For instance, as a large oblate pebble reduces in size, it becomes more prolate yet maintains the same ψ_p value (Fig. 4-23.).

The associations of size and shape are meaningful in the context of the facies sampled (Fig. 4-16.). Samples 006 and 007 are interpreted as imbricate channel lag deposits, and 011 and probably also 010, come from a broad in-channel bar deposit. Samples 008 and 009 were derived from foreset beds formed by the downstream migration of a channel bar.

Two sorting processes are responsible for the size-shape dependent and independent relationships:

(i) For a given flow velocity there is selective movement, and subsequent accumulation, of particular pebble shapes independent of size.

(ii) The flow is only competent to move the smaller pebbles, leaving the large oblate pebbles. These consequently accumulate as lag deposits after washing-out the smaller pebbles.

The first sorting process is probably responsible for deposition of 011, and the second sorting process for accumulation of 006 and 007. As 011 has the most prolate character, it provided least resistance to flow, and therefore, at non-uniform and subcritical flow (i.e. turbulent, tranquil flow of Spalletti 1976), pebbles would be selectively sorted with respect to shape independent of size, as would be anticipated on a low channel bar. 008 and 009 represent non-selective accumulation on a foreset bed where gravity is an additional force. By comparison, 006 and 007 consist of oblate pebbles which provide most resistance to flow, and therefore smaller bladed to prolate pebbles, if deposited at all, have been subsequently washed-out.

The shape selective sorting evident in the Clifton Conglomerate is in agreement with the views of Bradley *et al.* (1972) in that sorting processes are as much responsible for downvalley changes in size and shape, as clast modification by abrasion. Also, the oblate clasts have probably been transported by saltation and the bladed to prolate clasts by traction (Bradley *et al.* 1972; Spalletti 1976).

CHAPTER 5: SEDIMENT FABRIC

5-1 INTRODUCTION

The Concept of Sediment Fabric

Two kinds of fabric occur, namely deformation and apposition (Pettijohn 1975). The former, produced by external stress, is most apparent in metamorphic rocks while the latter, formed at the time of deposition, is a primary fabric. Two aspects of appositional sediment fabric are important:

(i) Orientation - the attitude of an individual particle in space,

(ii) Packing - the mutual relationship of particles to each other.

Any nonspherical grain, the usual case in conglomerates, will possess an orientation. Most often in conglomerates the fabric is dimensional, that is determined by the alignment of similar axes (Fig. 3-1.), rather than crystallographic where there is alignment of crystallographic directions (Pettijohn 1975).

The recognition of an orientation fabric necessitates selection of a unique plane to which the fabric elements (clasts in this discussion) may be compared. A bedding plane, representing the depositional slope, is the most realistic plane of comparison. However, bedding in conglomerates is frequently not obvious and an average plane through a particular sedimentation unit must be assumed. Hence orientation is regarded as the inclination of a fixed direction (axis or plane) within a grain to a fixed direction

(axis or plane) outside it (Griffiths 1967).

Fabric elements within stratigraphic units can display varying degrees of preferred orientation. At one extreme the observed orientations may be completely random and scattered over the whole hemisphere of a stereonet (Toots 1962), while at the other extreme preferred orientation is marked with both trend and plunge restricted (Flinn 1958). Between end members, the fabric elements together reflect varying degrees of preferred orientation. Some confusion in terminology has arisen where fabric elements show preferred orientation with respect to plunge, but random orientation with respect to trend. Such fabric patterns should not be described as random, but rather as displaying no preferred orientation; technically they are preferentially oriented, but the fabric is usually of no environmental significance.

One of the most obvious aspects of clast orientation is imbrication; the tendency for clasts to align with the plane of maximum projection dipping upstream. (Fig. 3-4.).

Some Previous Orientation Studies

The orientation fabric of clasts within sediment deposits has commonly been used to establish paleoflow directions and in some cases to determine the depositional environment. The study of clast orientation in glacial tills has been more intensive than that in clast supported conglomerates of fluvial or marine origin. Hence an understanding of the genesis of clast orientation in tills is more advanced than that of conglomerates; a factor which has assisted the writer in analysis of the Kidnappers Group.

A number of studies, particularly of modern river beds,

have revealed that imbricate clast supported conglomerates may be of two kinds (Fig. 5-1.):

(i) The a-axis transverse to flow and b-axis dipping up stream.

(ii) The a-axis parallel to flow and dipping upstream.

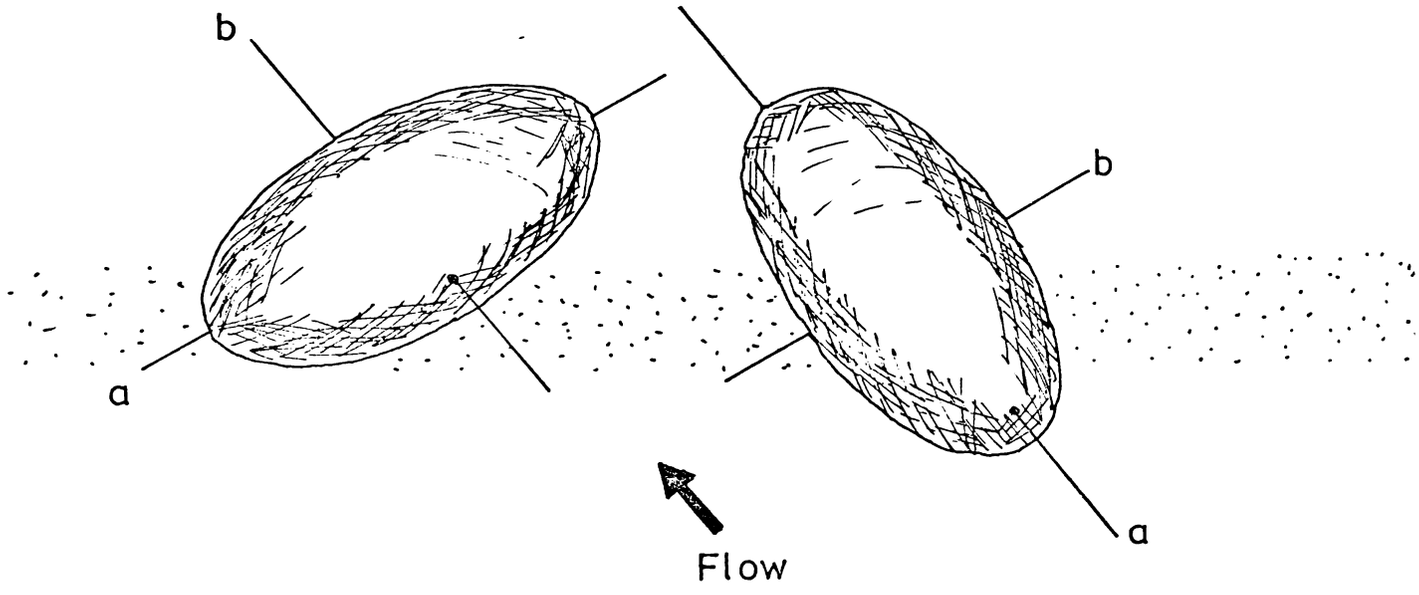

a(t) b(i) a(p) a(i)

Fig. 5-1. Two types of orientation coded as a(t) b(i), meaning a(transverse) and b(imbricate), and a(p) a(i) where a(parallel) and a(imbricate). (After Harms et.al. 1975).

Preferred a-axis orientation parallel to current have been described by many workers including Twenhofel (1932) and Krumbein (1939). However, a-axis orientation normal to flow is now believed to be the predominant orientation in most fluvial settings (Unrug 1957; Doeglas 1962; Sedimentary Petrology Seminar 1965; Kelling & Williams 1967; Rust 1972). Johansson (1963) however found some clasts have a-axis orientations of various angles to flow, emphasising the danger of

of generalizations. The inconsistency in a-axis orientation and the general agreement that flat pebbles are imbricated with the ab plane dipping upstream has lead some workers to suggest that the trend of the maximum projection of the ab plane could be used more reliably as a current direction indicator (Rusnak 1957; Johansson 1963; Potter & Pettijohn 1963).

Apart from a study of resedimented conglomerates where a(p) a(i) is the dominant fabric (Davies & Walker 1974; Walker 1975), and the occasional paper on the orientation of beach pebbles (e.g. Fraser 1935) where the a-axes were found to be aligned parallel to the strand line, there appear to have been few studies on clast orientations in conglomerates from marine environments.

As with fluvial conglomerates, clast orientation in glacial tills may be predominantly normal (Holmes 1941; Andrews & King 1968) or parallel to the direction of glacier movement (Boulton 1970a, 1970b; Lindsay 1970a, 1970b; Mark 1974). Nevertheless, it is generally believed that a primary mode occurs parallel and a secondary mode transverse to the direction of glacier advance (Mills 1977). Further, some workers recognise a dependent relationship between clast shape and its orientation (Holmes 1941; Andrews & King 1968; Drake 1974, 1977) and/or size characteristics and orientation (Lindsay 1970c), although it should be noted the influence of size and shape on clast orientation has been refuted (Mills 1977). There is also disagreement as to whether clasts are imbricated with upglacier dips (Harrison 1957; Boulton 1970a, 1970b; Lindsay

1970a, 1970b; Mark 1974; Mills 1977), whether they dip downglacier or whether they have no preferred orientation (Holmes 1941; West & Donner 1957; Harris 1969).

In a combined theoretical and experimental study of sand grains under conditions of unidirectional fluid flow, Rusnak (1957) considered processes for orienting grains with the flow, and found that the orientation is partly dependent on the complex inter-relationships of size, shape, roundness and density. The results for sand grains are in agreement with the reported influence of size and shape on the orientation of pebbles (Unrug 1957), where elongate pebbles in particular, roll on the a-axis developing a transverse mode. In comparison, smaller and more spherical pebbles show less distinct transverse orientation and are more influenced by irregularities in the bed surface; a view which concurs with that of Laronne and Carson (1976). Johansson (1963), in a field study, found pebbles less than 2 cm consistently parallel to current and pebbles greater than 2 cm equally transverse and parallel. A flume study on the reorientation of clasts (Kelling & Williams 1967) found similar results to Johansson apart from the influence of size, now thought to be independent of orientation. On the other hand, the Sedimentary Petrology Seminar (1965) found no correlation between the orientation of various clast sizes and shapes and stream direction.

Several factors other than the attributes of clasts may also determine the orientation fabric, as given by

Rusnak (1957) as: the velocity of the fluid flow, the distribution of eddies in turbulent flow, the roughness of the bottom, the eddies shed by adjacent particles, the packing of adjacent particles and the rate of sediment supply.

For some time glacial sedimentologists have realised that clast orientation in tills is not only a function of the size/shape characteristics of clasts, but also the nature of the ice-sediment interface and the processes operative during transport, deposition, and subsequent to deposition of clasts. This concept has lead to several models on the genesis of clast fabric in tills (Glen *et al.* 1955; Harrison 1957; Lindsay 1970b, 1970c; Mark 1974; Shaw 1977). Although interactions of a clast with the transporting medium are complex (e.g. Mark 1974), and several combinations of processes may lead to the same orientation fabric, it is now possible to establish whether clast orientation is primarily the result of englacial or subglacial fabric-forming processes (Lindsay 1970b, Mark 1974). However, in the study of conglomerates, few workers have recognised the potential of clast orientation in recording the transportational, depositional and post-depositional processes operative at the depositional interface, and no model equivalent to that for glacial tills has been developed.

Approach to Clast Orientation in the Kidnappers Group

A review of the literature shows that orientation studies can be approached at two levels, one to derive paleocurrent directions and the other to determine the

depositional environment. In line with this approach and to help meet the objectives outlined in Chapter 1, 6 sites within conglomerates of the Clifton Sand and Clifton Conglomerate were selected (Fig. 5-2.) and clast measurements made (Table 5-1.).

Site	Dip ab	Dip Direction ab	Trend a	Plunge a	L	I	S	No. Clasts	Litho-type
1	✓	✓	✓	✓	✓	✓	✓	120	1
2	✓	✓						54	1
3	✓	✓						100	1
4	✓	✓						56	1
5	✓	✓						51	1
6	✓	✓	✓	✓	✓	✓	✓	100	5

Table 5-1. A summary of the measurements made on each clast at each site. The 'ab' refers to the plane, 'a' to the axis, 'L' to length of the a-axis, 'I' the b-axis and 'S' the c-axis.

Each orientation measurement was corrected for tectonic tilt following the procedure outlined in Chapter 3. The original and corrected values of ab plane measurements made at sites 1 to 6 and the a-axis plunge and trend together with the axial lengths and shape indices for site 1 and 6 are included in Appendix II. Although all data were treated mathematically and approximately 70 petrofabric diagrams were constructed, only the most relevant information is included here.

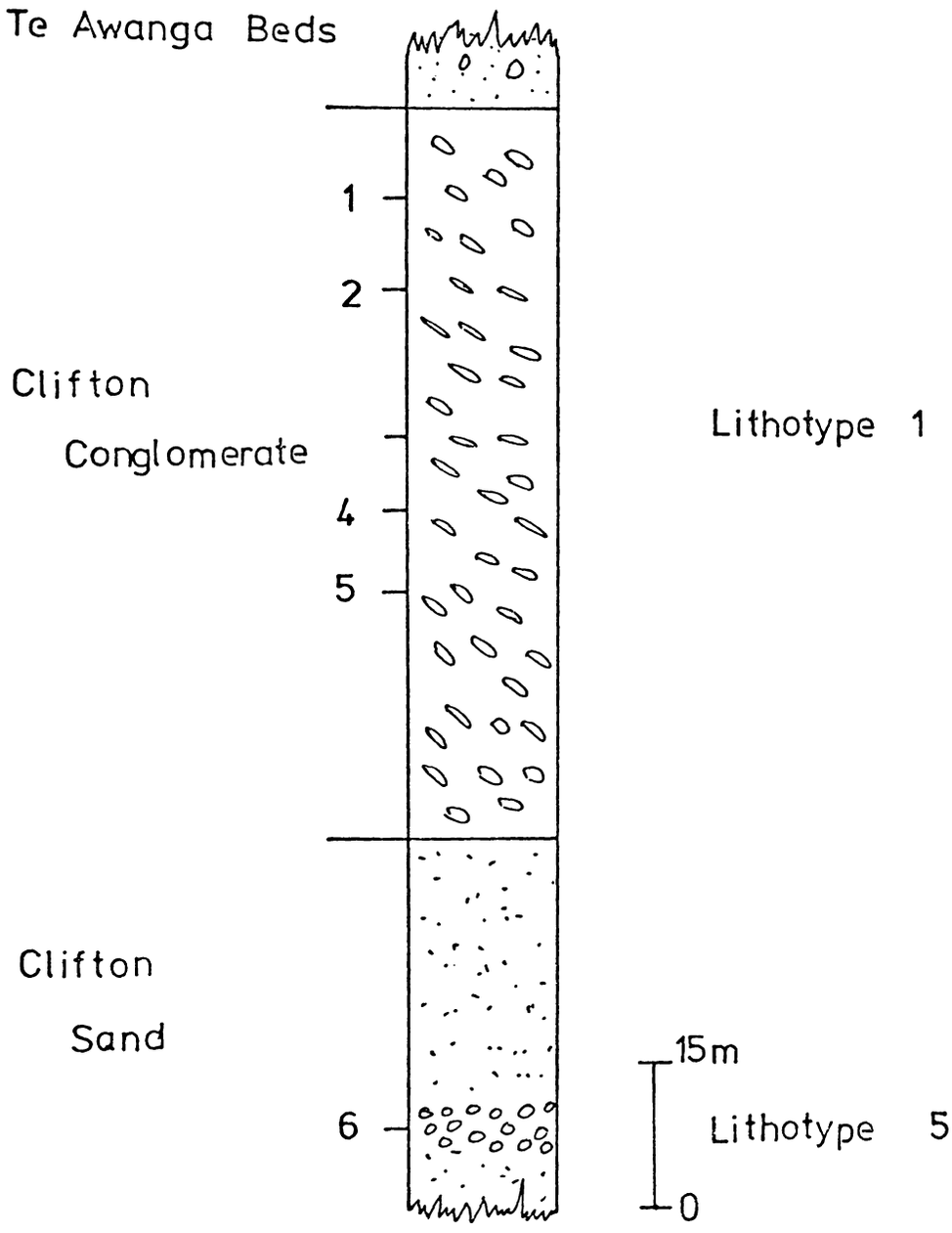

Fig. 5-2. Stratigraphic column indicating the position of Sites 1 to 6 and lithotypes 1 and 5 in the coastal exposure (N135/416207 to 424202) of the Kidnappers Group.

5-2 *ORIENTATION FABRICS OF CLASTS FROM MARINE AND FLUVIAL CONGLOMERATES*

Comparison of Petrofabric Diagrams

Orientation fabrics of a-axes and ab planes of clasts at site 6 (marine) and 1 (fluvial) are plotted in Figs. 5-3 to 5-6. The a-axes at site 6 (Fig. 5-3A.) define a sub-horizontal girdle with two sets of modes each 180° apart. The direction normal to one set of modes (F-F') is 120° and the other (G-G') 80°. Minor concentrations also occur approximately 90° from the modes F-F'. Surprisingly, a-axes orientations at site 1 (Fig. 5-5A.) also have two sets of opposing modes, however the girdle is no longer subhorizontal but gently dips towards the south. The direction normal to one set of modes (P' - P'_2) is 116° and the other (R' - R'_2) is 139°. In addition, there is an appreciable concentration of more steeply plunging a-axes trending north-west.

The orientation of ab planes at each site is, however, quite different as emphasised by their distribution. At site 6 (Fig. 5-4A.) the poles to the ab planes appear to be distributed about the c-axis describing an orthorhombic symmetry. As indicated by elongation of this fabric pattern there is slight imbrication of clasts in an easterly and westerly direction. In comparison, poles to ab planes of clasts at site 1 (Fig. 5-6A.) have well defined bimodality with maxima offset from the c-axis. This fabric describes a monoclinic symmetry characteristic of the action of gravity plus a unidirectional current (Potter & Pettijohn 1963).

Paleocurrent directions within the marine conglomerate at site 6 were determined independently from 3 small-scale

Fig. 5-3A.: Equal area plot of a-axes orientations of clasts at site 6. Number of points = 100. Contour intervals: 9%, 6%, 4%, 2%, 1%, per 1% area. Modes F-F' have a direction normal to trend of 120° and modes G-G' of 80°. The trends of the cross-stratification indicated by arrows are 318° and 80°.

Fig. 5-3B.: Point distribution of the trends of a-axes at site 6. Number of points = 100.

Fig. 5-4A.: Equal area plot of poles to maximum projection (ab) planes of clasts at site 6. Number of poles = 100. Contour intervals: 18%, 11%, 6%, 2%, 1%, per 1% area.

Fig. 5-4B.: Distribution of poles to maximum projection (ab) planes of clasts at site 6. Number of poles = 100.

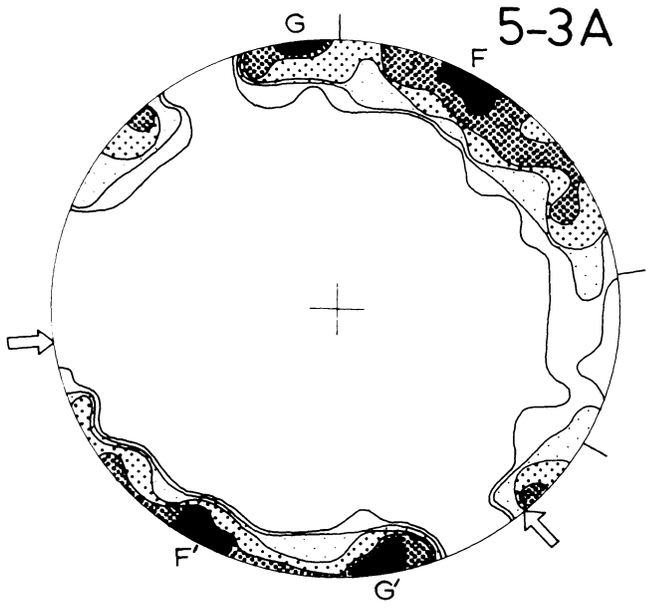

5-3A

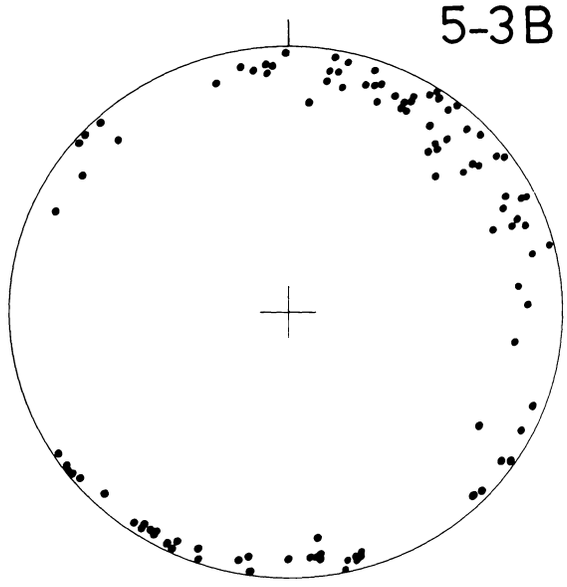

5-3B

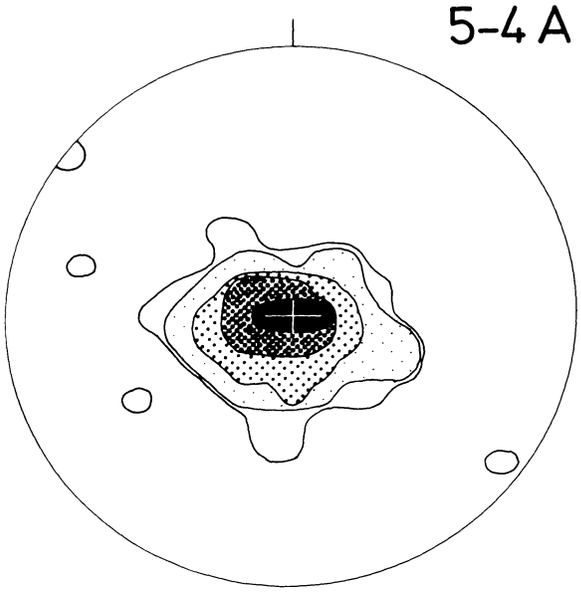

5-4A

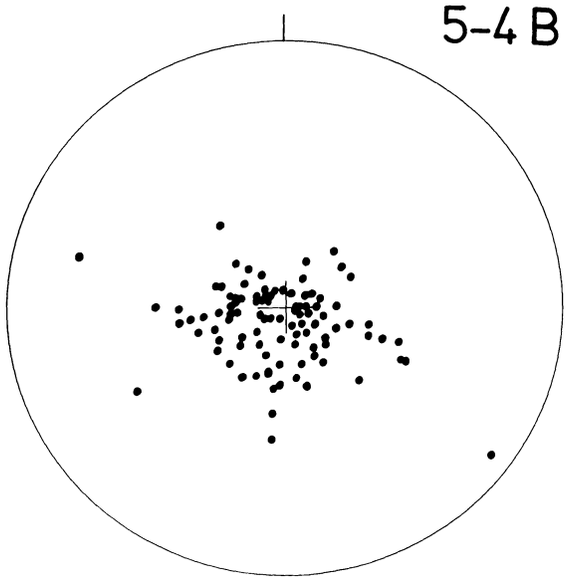

5-4B

tabular cross-beds and these directions are included in Fig. 5-3. The paleocurrent directions indicated by cross-bedding are 105° apart and match those normal to the trends of a-axes orientations. The position in outcrop where the clast orientations were measured was within several metres of the cross-bedding but site 6 itself lacked evidence of cross-stratification. If the current directions indicated by the cross-bedding are accepted, then the a-axes aligned transverse to current. Further, bimodality in the a-axes orientation fabric may be a function of the wide divergence in current directions, where some clasts have oriented transverse to one current direction and other clasts transverse to a different current direction. This may also explain the orientation fabric of ab planes (Fig. 5-4A.) where the effect of different current directions has been to disorient the ab plane with respect to dip direction but maintain some preferred orientation with respect to dip.

Paleocurrent directions measured from occasional cross-beds in the Clifton Conglomerate are consistently from the west between 070° and 150°. As the directions normal to the trend of a-axes orientations at 116° and 139° (Fig. 5-5A.) are comparable to paleocurrent directions indicated by cross-bedding, it supports the view that the a-axis of a clast aligns transverse, rather than parallel to current flow. Paleocurrent directions from the west and north-west are also consistent with imbrication of the maximum projection of the ab plane in an upstream direction. As a whole, monoclinic symmetry is characteristic of clast orientation in the Clifton Conglomerate as evident from the orientation fabrics of poles to ab planes at other sites (Figs. 5-10; 5-12; 5-14; 5-16).

Fig. 5-5A.: Equal area plot of a-axes orientations of clasts at site 1. Number of points = 100. Contour intervals: 6%, 4%, 3%, 2%, 1%, per 1% area. Modes P' - P_2' have a direction normal to trend of 116° and modes R' - R_2' of 139°.

Fig. 5-5B.: Point distribution of the trends of a-axes at site 6. Number of points = 120.

Fig. 5-6A.: Equal area plot of poles to maximum projection (ab) planes of clasts at site 1. Number of poles - 120. Contour intervals: 6%, 4%, 3%, 2%, 1%, per 1% area. The current direction indicated by the direction through the girdle axis is 143°.

Fig. 5-6B.: Distribution of poles to maximum projection (ab) planes of clasts at site 1. Number of poles = 120.

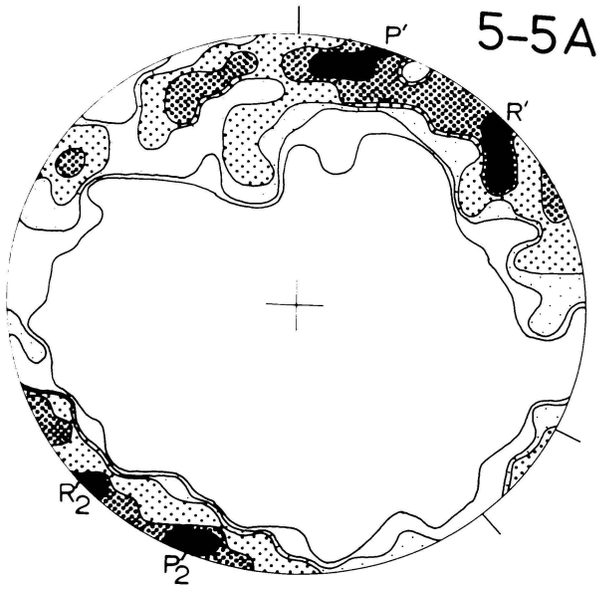

5-5A

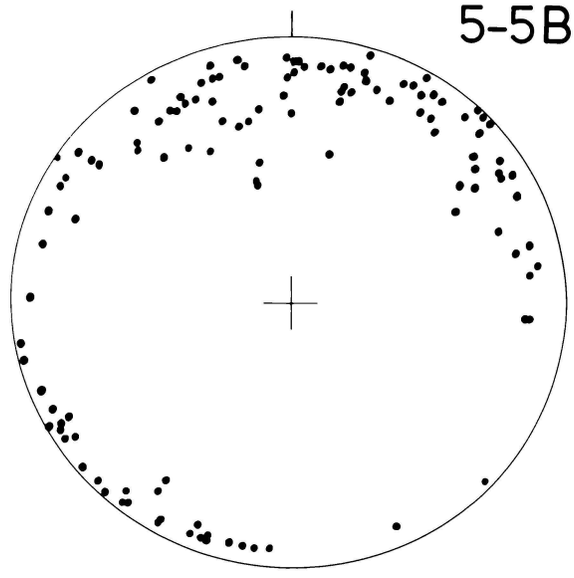

5-5B

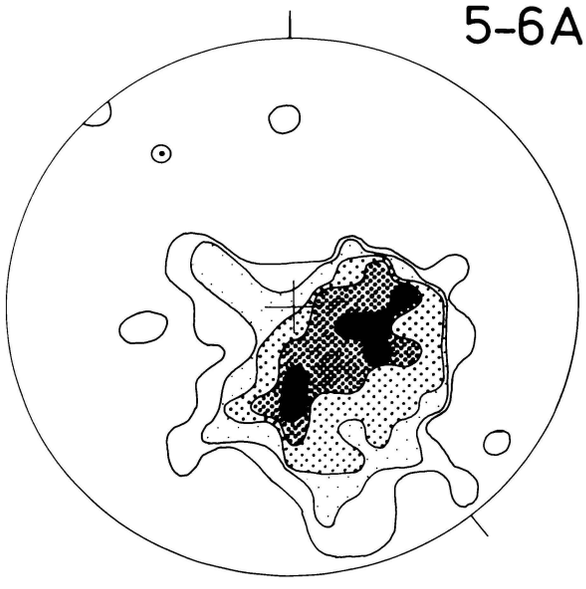

5-6A

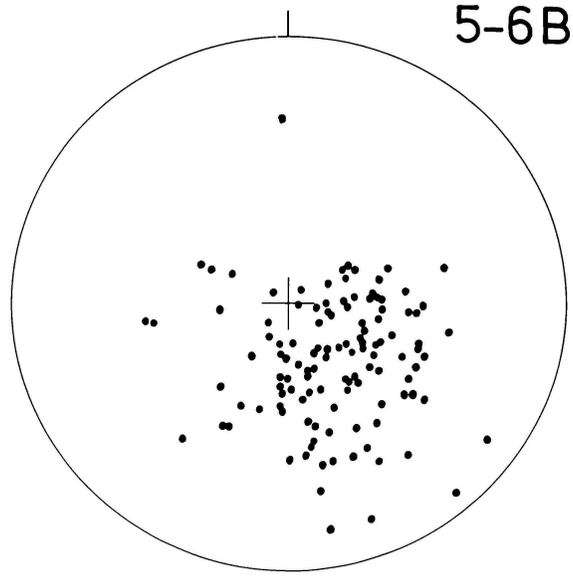

5-6B

Comparison of Imbrication Angles

Imbrication angles for the pebbles measured at sites 1 and 6 show significant differences in the positions of modes (Fig. 5-7.). The smallest difference between modes is 10° and the average difference is 15°. Pettijohn (1975) reported the mean upstream inclination of pebbles in fluvial deposits ranges from 15° to 30° while the mean inclinations for marine deposits is only 2° to 15°. The range of inclinations of the clasts in this study are on average 5° higher than those reported by Pettijohn for both the deposits at sites 1 (fluvial) and 6 (marine).

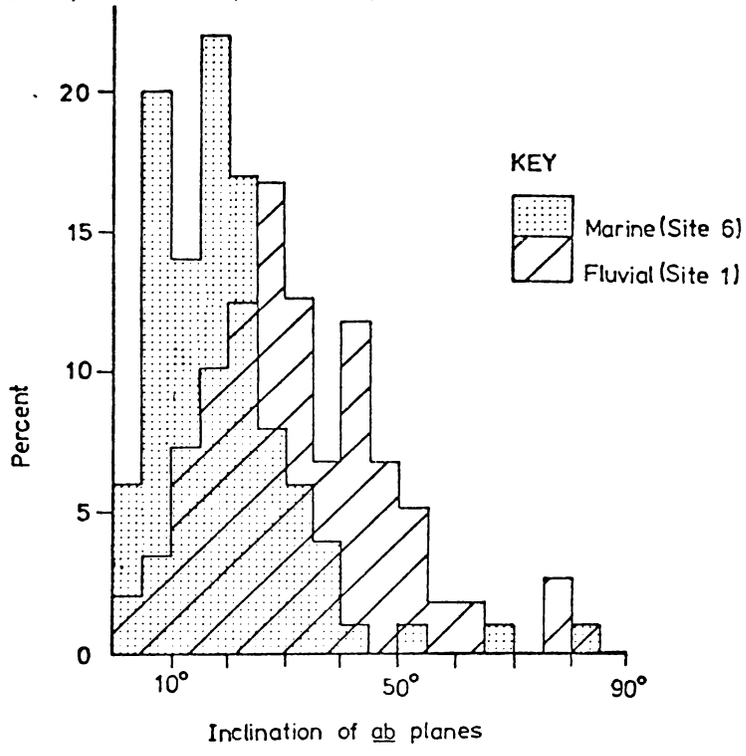

Fig. 5-7. Comparison between imbrication angles for site 1 (fluvial) and site 6 (marine).

The difference in imbrication angles between sites 1 and 6 may reflect the persistence and strength of unidirectional versus polydirectional currents, an interpretation consistent with the petrofabric diagrams and evidence of

paleocurrent directions from cross-bedding. Also, from a consideration of orientation theory and flume experiments, a decrease in fluid velocity is known to lower the imbrication angle (Rusnak 1957; Jizba 1971).

Although, for the Clifton Conglomerate, monoclinic symmetry and a-axes orientation transverse to current, do not exclude a marine origin, these features, together with the larger imbrication angles, strongly suggest a fluvial origin for this formation. This hypothesis is further strengthened by considering the fluvial shape characteristics (Fig. 4-12), the absence of marine fossils, and the markedly different orientation fabric of a conglomerate unit known to be marine.

5-3 *PALEOCURRENTS*

Paleocurrent directions in conglomerates of the Kidnappers Group have been determined on the basis of clast orientation and dip direction of foreset beds. Where possible, directions derived from clast orientation have been corroborated by directions from cross-bedding. As the conglomerates exposed inland are mainly inaccessible, a regional pattern of paleocurrent directions could not be established. Therefore paleocurrents in the coastal conglomerates were determined, and their directional variability used in paleoenvironmental reconstruction.

Paleocurrent Directions in the 110 ft. Conglomerate

In this formation paleocurrent directions have been determined from dip directions of planar cross-stratified sets (Lithotype 2, Section 2-6). The principal modes of current directions are represented as vector means in Fig. 5-8, and all paleocurrent directions measured in the formation are incorporated in Fig. 5-9 and Appendix III. A feature of the current directions is their bimodality. There is a definite trend for the angular separation of modes to increase, and for directions to become more easterly with time through the formation. The three principal modes evident in Fig. 5-9 are deceptive, in that at any one stratigraphic level there are at most, only two modes, and these are generally less than 90° apart (Fig. 5-8.). Nevertheless, Fig. 5-9 shows that at times during deposition of the formation, currents flowed in various directions between 240° west to 40° east.

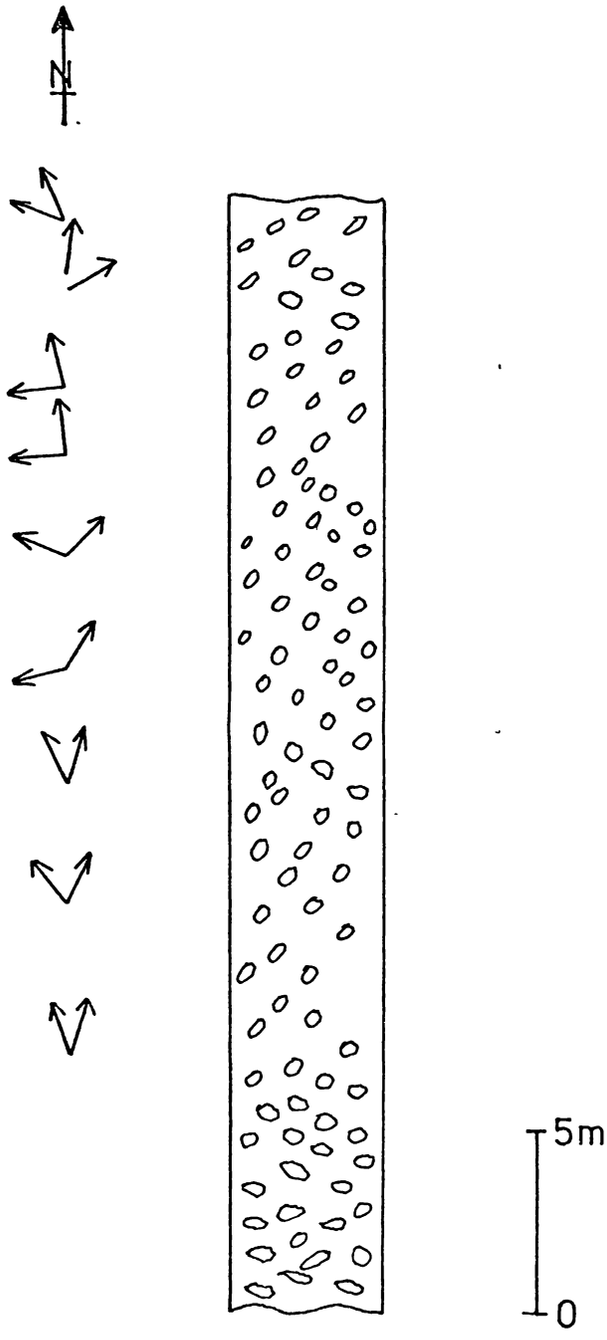

Fig. 5-8. Paleocurrent directions indicated by foreset dip directions in the coastal exposure of the 110 ft. Conglomerate (N135/437197 to 453203). Principal modes represented by vector means are indicated as arrows. The paleocurrent directions are bimodal and from the south.

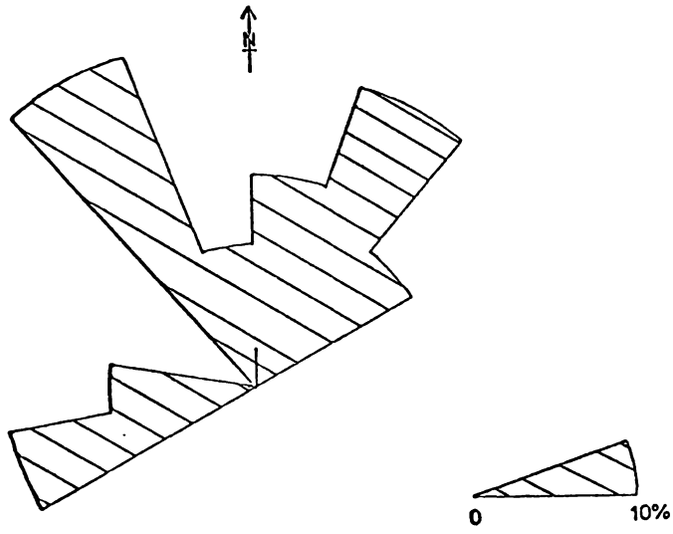

Fig. 5-9. Rose diagram of paleocurrent directions derived from the dip direction of foreset beds in the 110 ft. Conglomerate in the coastal section.

Paleocurrent directions from cross-bedding in conglomerates in the Mt. Gordon Beds are similar to those in the 110 ft. Conglomerate, although directions in conglomerates of the Rabbit Gully and Trig. N. Beds are more westerly (Appendix III).

Paleocurrent Directions in the Clifton Conglomerate

In view of the paucity of cross-bedding in the Clifton Conglomerate, paleocurrent directions were established from clast orientation measurements at five localities (Fig. 5-18.). Petrofabric diagrams were constructed from the dip and dip directions of clast ab planes (Figs. 5-25, 5-16, 5-14, 5-12, 5-10 for sites 1 to 5 respectively). Vector means were also calculated and rose diagrams constructed to illustrate the paleocurrent data in the standard format (Figs. 5-19, 5-17, 5-15, 5-13, 5-11 for sites 1 to 5 respectively). The paleocurrent directions measured from each of the analyses are summarised in Fig. 5-18.

The paleocurrent directions indicated by the petrofabric

Fig. 5-10A.: Equal area plot of poles to maximum projection (ab) planes of clasts at site 5. Number of poles = 51. Contour intervals: 12%, 8%, 6%, 4%, 2%, per 1% area. The current direction indicated by the direction through the girdle axis is 135°.

Fig. 5-10B.: Distribution of poles to maximum projection (ab) planes of clasts at site 5. Number of poles = 51.

Fig. 5-11.: Rose diagram of the directions 180° opposite to the dip directions of maximum projection (ab) planes of clasts at site 5. Number of values = 51. The vector mean indicated by the arrow is 144° and the midpoint of the principal mode 130°. The class intervals are 20° and the scale represents 10% of the values.

Fig. 5-12A.: Equal area plot of poles to maximum projection (ab) planes of clasts at site 4. Number of poles = 56. Contour intervals: 14%, 10%, 7%, 3%, 2%, per 1% area. The current direction indicated by the direction through the girdle axis is 102°.

Fig. 5-12B.: Distribution of poles to maximum projection (ab) planes of clasts at site 4. Number of poles = 56.

Fig. 5-13.: Rose diagram of the directions 180° opposite to the dip directions of maximum projection (ab) planes of clasts at site 4. Number of values = 56. The vector mean indicated by the arrow is 105°. The midpoints of the two principal modes are 70° and 130°.

5-10 A

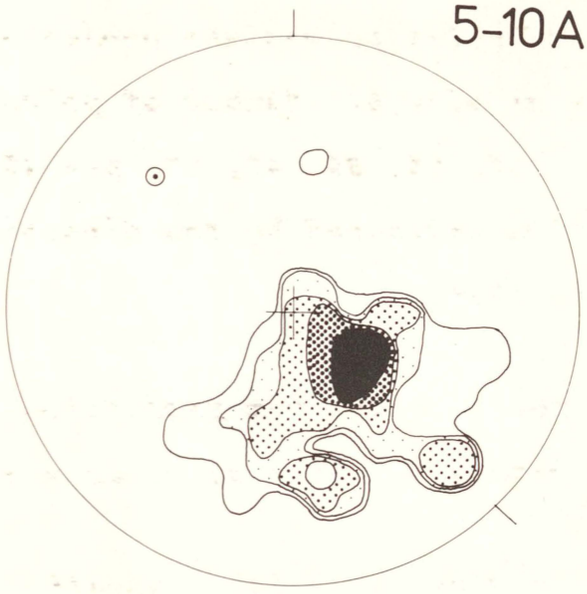

5-10 B

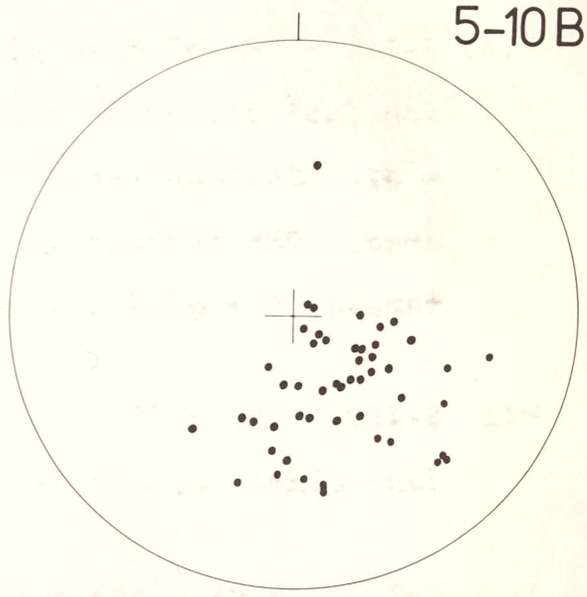

5-11

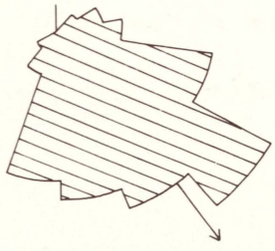

5-13

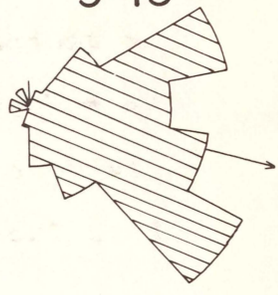

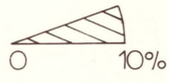

5-12 A

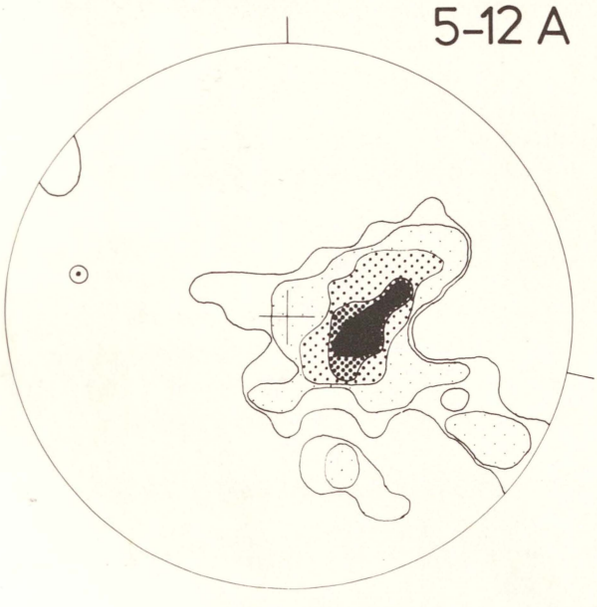

5-12 B

Fig. 5-14A.: Equal area plot of poles of maximum projection (ab) planes of clasts at site 3. Number of poles =100. Contour intervals: 10%, 7%, 5%, 2%, 1% per 1% area. The current direction indicated by the direction through the girdle axis is 118°.

Fig. 5-14B.: Distribution of poles to maximum projection (ab) planes of clasts at site 3. Number of poles = 100.

Fig. 5-15.: Rose diagram of the directions 180° opposite to the dip directions of maximum projection (ab) planes of clasts at site 3. Number of values = 100. The vector mean indicated by the arrow is 132° and the midpoint of the principal mode 120°. Class intervals are 20° and the scale represents 10% of the values.

Fig. 5-16A.: Equal area plot of poles of maximum projection (ab) planes of clasts at site 2. Number of poles = 54. Contour intervals: 18%, 13%, 7%, 3%, 2%, per 1% area. The current direction indicated by the direction through the girdle axis is 98°.

Fig. 5-16B.: Distribution of poles of maximum projection (ab) planes of clasts at site 2. Number of poles = 54.

Fig. 5-17.: Rose diagram of the directions 180° opposite to the dip directions of maximum projection (ab) planes of clasts at site 2. Number of values = 54. The vector mean indicated by the arrow is 103°. The midpoints of the two principal modes are 70° and 130°.

5-14 A

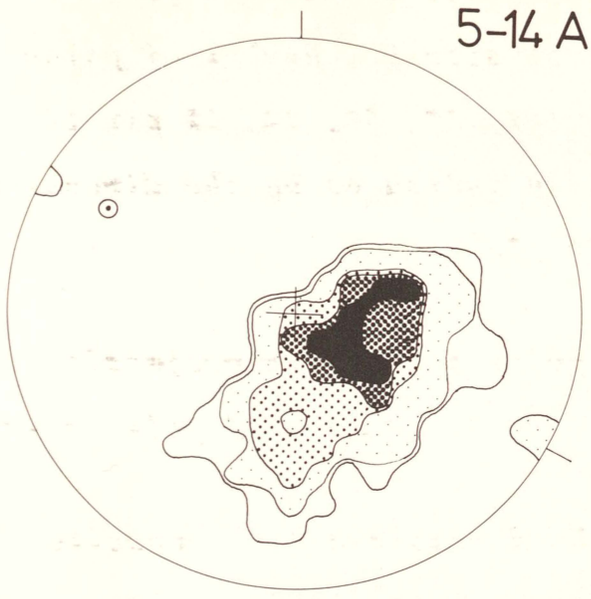

5-14 B

5-15

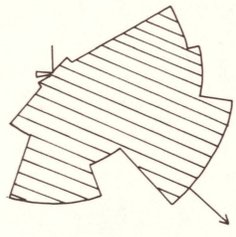

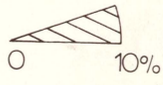

5-17

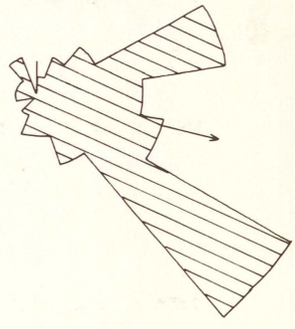

5-16 A

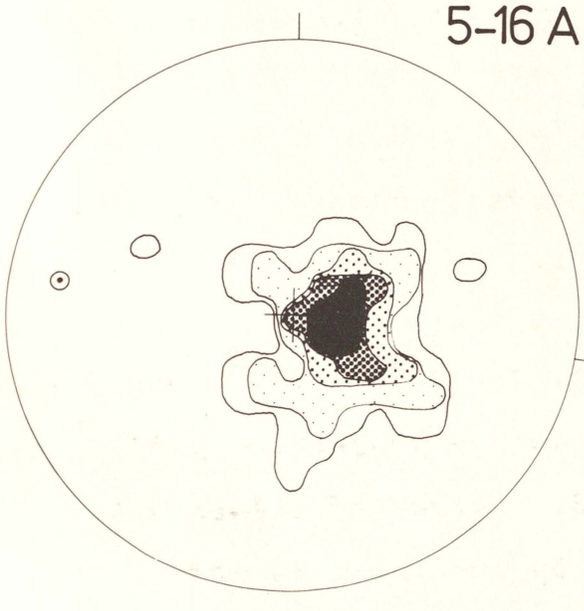

5-16 B

Fig. 5-19. Rose diagram of the direction 180° opposite to the dip direction of maximum projection (ab) planes of clasts at site 1, corrected by removing the influence of a-axis plunge (see Section 5-4). Number of values = 120. The vector mean indicated by the arrow is 133° and the mid-point of the principal mode is 130°.

Fig. 5-20. Rose diagram of the directions normal to the trend of the a-axes at site 1. Number of values = 120. The mid-point of the principal mode is 100°.

diagrams are unimodal and flowed from the west and northwest with only 37° of directional variance. Although paleocurrent directions could not be confirmed at sites 1 to 5 by the dip directions of foresets, where cross-bedding does occur in the formation (Section 2-6) the directions indicated are between 070° and 150° from the west. Hence the current directions shown in Fig. 5-18A are in agreement with those from cross-bedding.

The paleocurrent directions and environmental significance in conglomerates of either marked paleocurrent variability or uniformity, are considered more fully in Chapter 7.

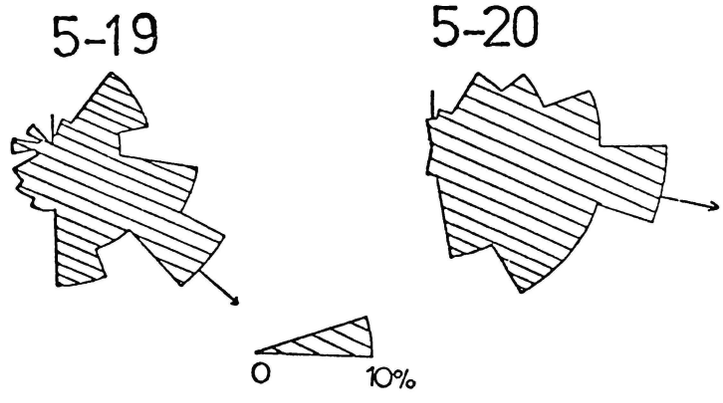

Comparison of Petrofabric and Mathematic Analysis of Paleocurrent Directions

Palecurrent directions measured from petrofabric diagrams (Figs. 5-25, 5-16, 5-14, 5-12, 5-10.) are in close agreement with vector means (Appendix III), except for site 3 where there is a discrepancy of 18° (Fig. 5-18.). However, the directions indicated by the principal modes in the rose diagrams (Figs. 5-19, 5-17, 5-15, 5-13, 5-11) are sometimes similar and some-

times different from petrofabric and vectorial analysis (Fig. 5-18.). For a symmetrical, monoclinic, orientation fabric (e.g. Fig. 5-25.), the paleocurrent direction is more precisely determined by vectorial analysis than by measurement off the petrofabric diagrams, since it is difficult to place a monoclinic distribution on a great circle. Vectorial analysis is further advantaged by its rapidity and the additional statistical information (e.g. vector magnitude) which quantifies current variance, therefore facilitating comparison of paleocurrent directions.

However, where the distribution is non-normal, the vector mean may indicate an incorrect direction (e.g. site 3, Fig. 5-15 c.f. 5-14.). The other form of mathematic analysis, rose diagrams, are also often inadequate as a near-symmetrical distribution (e.g. 5-16) has been shown to become bimodal (Fig. 5-17.). An explanation for these discrepancies may lie in the nature of the current direction indicator. Possibly more than with any other paleocurrent indicators, clasts as indicators do not have an equivalent ability to correctly predict the paleocurrent direction. Invariably, a proportion of the clast orientations are not related to the current direction because of bed irregularity and lodgement effects. In petrofabric diagrams the extraneous orientations may be visually eliminated but in mathematic analysis all directions, including the erratic ones, are equally weighted. Hence, construction of petrofabric diagrams is required to inspect and evaluate the distribution for such irregularity.

The paleocurrent direction at Site 1 was deliberately

derived from Fig. 5-25, rather than from Fig. 5-6, because of marked bimodality in the distribution of ab plane poles. The reason for the bimodality is considered fully in the following section.

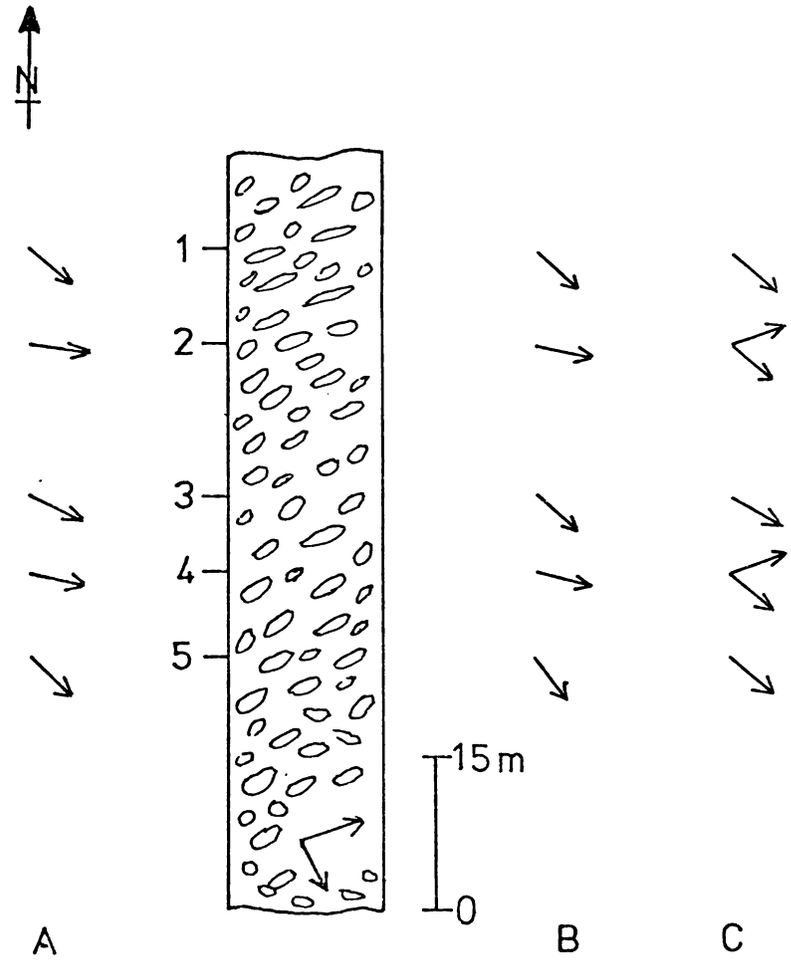

Fig. 5-18. Paleocurrent directions indicated by clast imbrication in the coastal exposure of the Clifton Conglomerate (N135/418207 to 423203). Numbers refer to measurement sites of clast orientation. The arrows above A are current directions measured from petrofabric diagrams (the direction through the girdle axis and the centre of the stereonet). Arrows above B are vector means and those above C are principal modes in rose diagrams. Current directions derived from foreset dip directions of occasional cross-beds are indicated within the column where they occur. Paleocurrent directions are consistently from the west.

5-4 COMPLICATIONS IN THE DETERMINATION OF PALEOCURRENT DIRECTIONS FROM CLAST IMBRICATION IN CONGLOMERATES

From the study of modern rivers and flume experiments, other workers (e.g. Rusnak 1957; Potter & Pettijohn 1963; Rust 1972) have concluded that the direction of dip of the maximum projection of the ab plane of clasts is a more consistent current direction indicator than the a-axis of clasts. However, this has not been adequately tested in conglomerates. Awareness of potential complications in the measurement of paleocurrent directions from clast orientation in conglomerates, arises from an attempt to explain the bimodality in the distribution of the poles to the ab planes of clasts at site 1 (Fig. 5-6A.).

Bimodality in the Distribution of ab Plane Pole Orientations at Site 1

Fig. 5-29 (located as a fold-out on p.181) shows the maxima of a-axes points and ab plane poles from Figs. 5-5A. and 5-6A. Reservations have been expressed about using maxima divorced from the total distribution (Turner & Weiss 1963), but this has been done initially to simplify the situation. The total distribution will be considered later in this section. Three great circles may validly be described taking into account the maxima for the a-axes points and ab plane poles:

(i) Points P' - Q_1' - P_2' lie on great circle (1) which is defined by the girdle axis Q_A.

(ii) Points P' - P_1' - P_2' similarly lie on great circle (2) about a girdle axis P_A.

(iii) Points R' - P_1' - Q_1' - R_2' lie on great circle (3) and define a girdle axis R_A.

A girdle axis is located at the pole of a great circle.

For an orientation fabric a(t) b(i) (Fig. 5-21.), b is always 90° from a. In this case the pole to the ab plane and the points of the a-axis will lie on the same great circle, where the ab plane pole is 90° along the great circle from each point. Hence the ab plane pole and girdle axis should lie in a plane which passes through the centre of the stereonet.

In considering Fig. 5-29 it appears this condition is satisfied for great circle (2). It also satisfies great circle (3) if one accepts Q_1' - P_1', as a continuous girdle with R_1' as the midpoint. However, for great circle (1) the condition is not satisfied as the maxima Q_1' is not in the same vertical plane as the girdle axis Q_A and the centre of the stereonet, as it is further removed from P' than from P_2'.

The Implication of Bimodality in the Distribution of ab Plane Poles in Determination of Paleocurrent Directions

If one determines the paleocurrent direction normal to the a-axes maxima R' - R_2', i.e. the direction through the midpoint of the girdle Q_1' - P_1', then the current has a direction of 139° (Fig. 5-29.). Similarly, if the current direction is taken as that normal to the a-axes maxima P' - P_2' and therefore corresponding to the direction of dip of the ab plane pole maxima P_1', the paleocurrent would have a direction of 116°. Marked bimodality in ab plane

orientations at any site has not been reported elsewhere and appears to be inconsistent with the evidence derived from modern rivers by Bluck (1974, 1976). Simply recording a mean direction of 127° will not resolve whether the bimodality is due to bimodal current directions or whether it is due to some effect other than clast interaction with the current.

A Theoretical Explanation for Bimodality in the ab Plane Pole Distribution at Site 1

To better understand bimodality in the maxima of the ab plane poles and the reason that in only one of the three great circles the respective maxima and girdle axis occur in a plane through the centre of the stereonet, it is necessary to consider a theoretical situation. The stereographic position of the pole to the ab plane for a clast with an orientation fabric a(t) b(i) is shown in Fig. 5-21. Alternative positions of the pole for increasing imbrication angles (θ) are shown as crosses. Consider modification of the orientation fabric a(t) b(i) by imposing a plunge of α degrees on the a-axis (Fig. 5-22.). A new pole position is defined shown as the square mark. If for a number of clasts the dip on the ab plane is held constant (i.e. the dip on the b-axis) but the a-axis plunge is varied (α degrees), a simple ab plane pole distribution will no longer be defined. If the a-axes trending in opposite directions have similar plunge, the poles to the ab planes will describe a girdle which lies on the same great circle as the a-axis and is symmetrically distributed about the mid-point, 90° from the trend on the a-axis. Further, if the plunge on the a-axes

trending in one direction is greater on average than that trending in the opposite direction, a girdle will be described. However, the girdle will now be distributed about a point on the great circle that is further removed from the a-axes maxima with the greater a-axes plunge, than from the opposing a-axes (Fig. 5-22.).

From inspection of Fig. 5-29., it is immediately apparent that asymmetry exists about great circle (1), where the mode Q_1' is asymmetrically distributed about its girdle axis Q_A. Hence a current direction normal to the a-axes and therefore through the girdle axis and the centre of the great circle will not coincide with the direction through the ab plane pole girdle.

An hypothesis is suggested that the asymmetry in the distribution of the ab plane poles at site 1 is a function of plunge on the a-axes. Also, it is probable that the bimodality is a function of the same effect and that Q_1' in particular, is an apparent mode only.

A measure of the distribution asymmetry, is gained by how far the ab plane poles are removed from a position equidistant from the a-axis maxima (e.g. the distance that Q_1' is from Q_2' in Fig. 5-29.). Hence by only plotting the ab plane poles it is not possible to detect asymmetry in the distribution which will, if present, introduce error in the determination of paleocurrent directions. This can only be established accurately if the a-axes trends and plunge are also plotted.

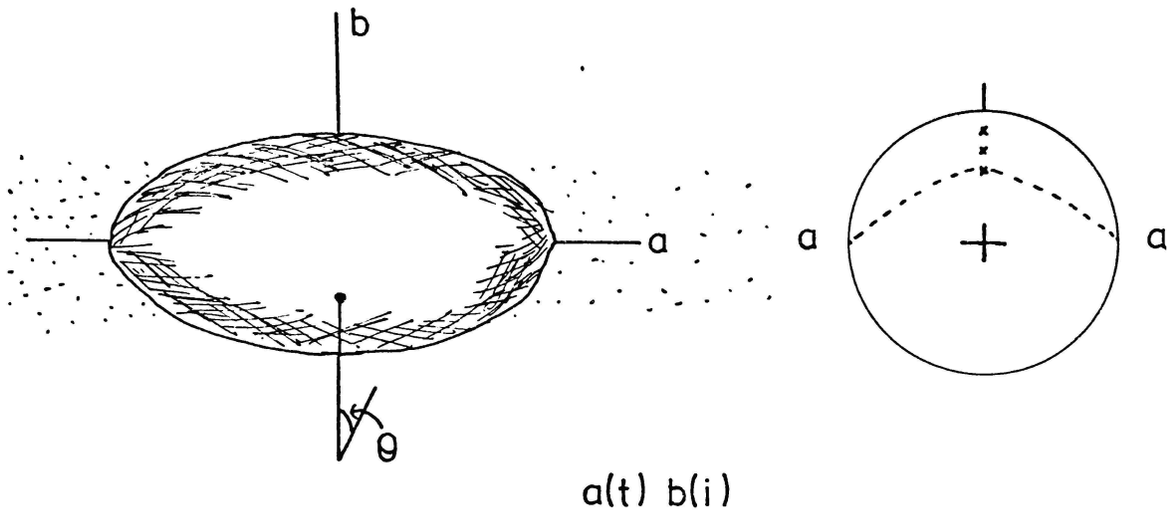

Fig. 5-21. Diagramatic and stereographic representation of the orientation fabric a(t) b(i). The a-axis is represented by 2 points where the great circle meets the primitive. The crosses represent the positions of the poles to the ab plane for increasing imbrication angles (θ), where the distance of the pole from the centre increases with θ.

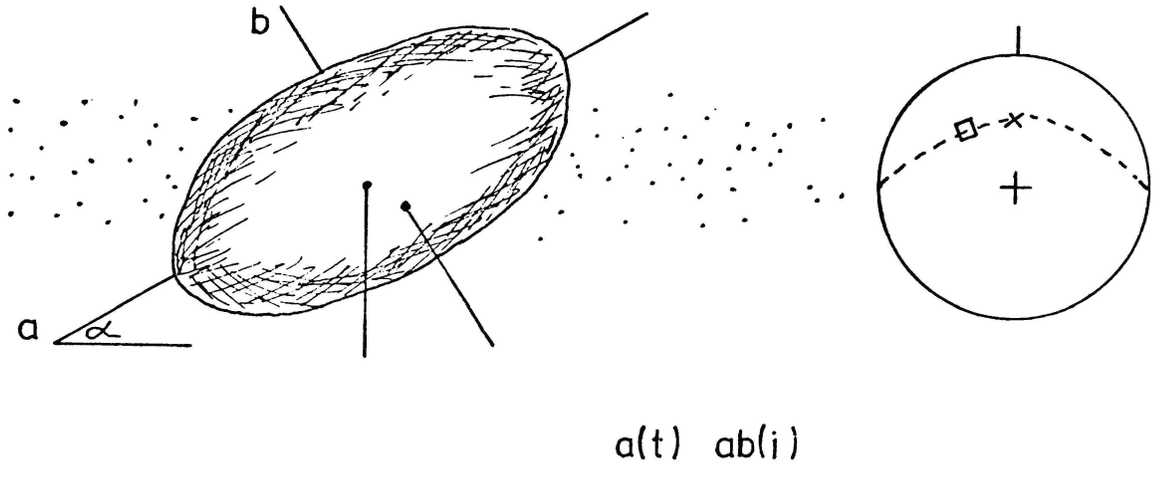

Fig. 5-22. Diagramatic and stereographic representation of the orientation fabric a(t) ab(i). Imposing a tilt on the a-axis of the clast rotates the pole to a new position marked by a square. The new pole position is now more than 90° from the trend of the a-axis now projected upwards.

Correction of the ab Plane Orientation for a-axis Plunge at Site 1

An analysis of the a-axis plunge on clasts at Site 1 with respect to their trend, shows that the north-easterly trending axes have on average 10° greater plunge than the south-westerly trending axes (Fig. 5-23.). Thus the potential exists for the theoretical situation outlined above to occur.

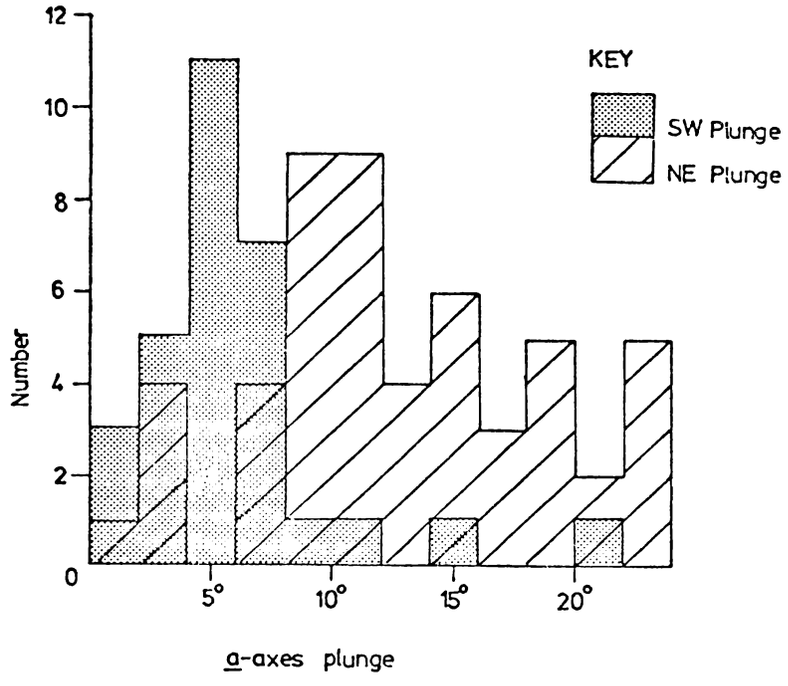

Fig. 5-23. Histogram of the plunge on north-east and south-west trending a-axes of clasts at Site 1.

To remove the effect of the a-axis plunge, this hypothesis was tested by stereographically rotating selected ab plane pole positions about the normal to the trend of the a-axis.

Rotation of Selected ab Plane Pole Positions:

Clasts with ab plane poles in the mode Q_1' and an a-axis

plunge and trend typical of those in the a-axis maxima R' were rotated. The new positions are represented by black dots on Fig. 5-24. Likewise clasts with ab plane poles in the north-east part of the mode P_1' and an a-axis plunge and trend typical of those in the a-axis maxima P_2' were also rotated to new positions marked as white dots. Appendix IV i gives the initial and new positions for the ab plane poles. The greater the plunge on the a-axis the further the rotation of the ab plane poles; conversely, the lower the dip on the ab plane the greater the angular rotation of the ab plane pole.

The effect of removing a-axis plunge is to reduce the bimodality and, more especially, to rotate the ab plane poles away from Q_1'. It seems reasonable therefore, on the basis of some selected positions, to tentatively suggest that the hypothesis is correct. A new great circle may be drawn in reservedly as S' - S_1' - S_2' which has a girdle axis S_A and defines a paleocurrent direction of 129° (Fig. 5-24.).

Rotation of all ab Plane Poles at Site 1:

To test whether or not the theoretical situation, which only dealt with selected cases in the maxima, does reflect the true situation, all clasts measured at site 1 were stereographically rotated about the normal to the trend of the a-axis to remove the plunge on the a-axis. Recorrected values are shown in Appendix IV ii and the new orientation fabric (Fig. 5-25.) is displayed alongside the original (Fig. 5-26.). The ab plane pole distribution is no longer bimodal but rather displays monoclinic symmetry typical of

Fig. 5-24. Rotation of selected ab plane poles about the normal to the trend of the a-axis. The current direction indicated by the direction through the girdle axis S_A is 129°.

5-24

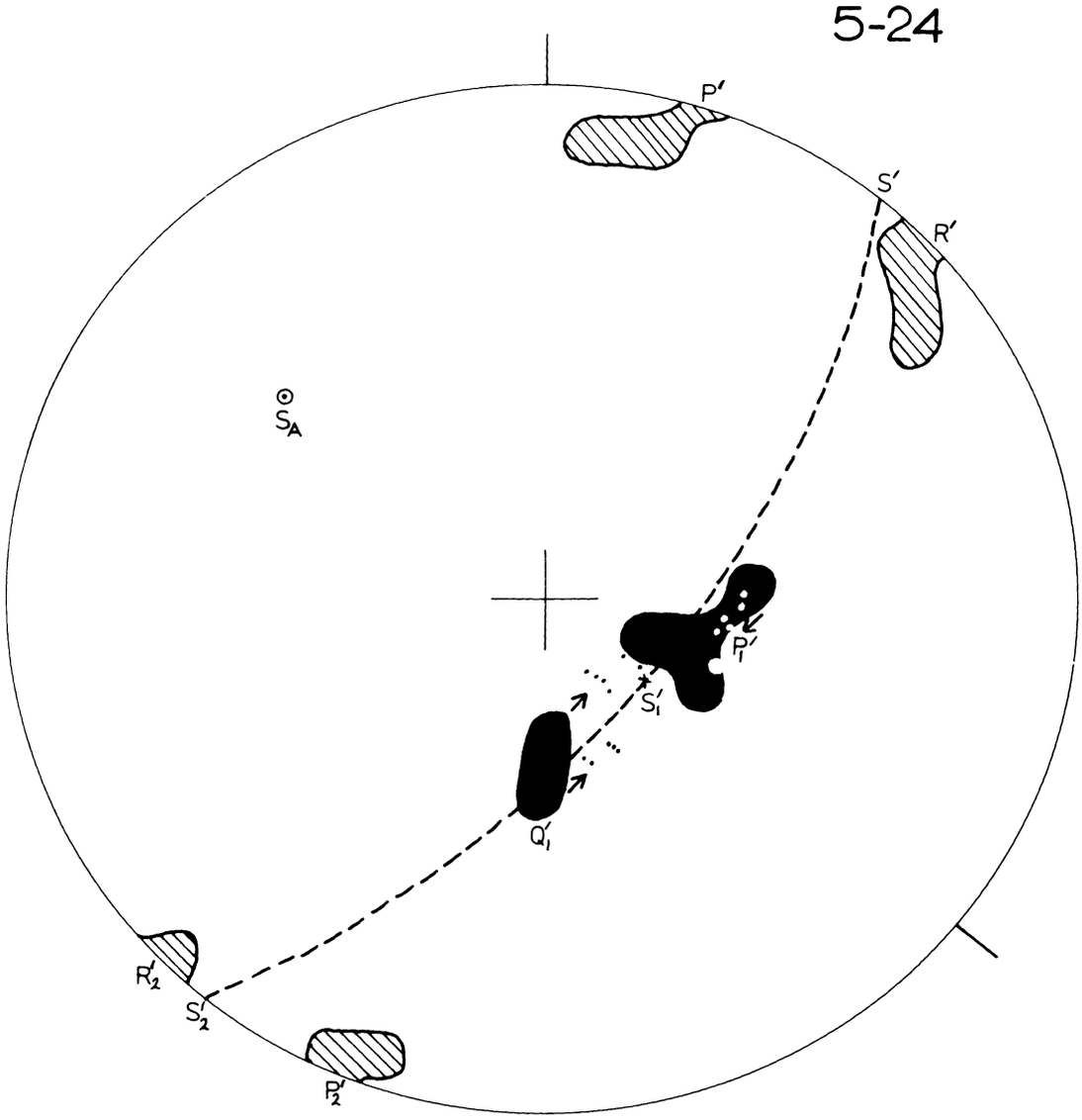

a unidirectional current. The distribution centred about the maxima is now almost exactly equidistant from the trend of the a-axes, thereby describing a symmetrical distribution. On this basis it is felt the hypothesis can be accepted.

It is difficult to determine the current direction from such a symmetrical distribution; however a value of 132° found by centring the distribution on a great circle is acceptable by visual inspection. The original bimodal character of the direction of dip of the ab plane is also apparent in the rose diagram Fig. 5-27. However, removal of the a-axis plunge restores a principal mode as shown in Fig. 5-28, the mid-point of which gives a current direction of 130°. Similarly, calculation of the vector mean for the recorrected ab plane poles gives a value of 133°. Hence for the reasons outlined in discussion of Fig. 5-29, a paleocurrent direction in the range 129° - 132° is thought to be the most accurate estimate.

A New Orientation Fabric a(t) ab(i)

If a symmetrical or an asymmetrical distribution occurs a new fabric can be postulated, namely that of a(t) ab(i) (Fig. 5-22.). The reason for this is that the dip and direction of dip of the ab plane has elements in common with the plunge on the a-axis and the b-axis. The fabric a(t) b(i) is reserved for describing the pattern where the a-axis has no plunge and the imbrication is due only to the plunge on the b-axis.

In the ideal situation where all the a-axes are transverse to current, a(t) ab(i) will describe a girdle and

Fig. 5-25A.: Equal area plot of poles of maximum projection (ab) planes of clasts at site 1. Recorrected by removing the influence of a-axis plunge. Number of poles = 120. Contour intervals: 13%, 8%, 4%, 2%, 1%, per 1% area. The current direction indicated by the direction through the girdle axis is 132°.

Fig. 5-25B.: Distribution of poles to maximum projection (ab) planes of clasts at site 1. Recorrected by removing the influence of a-axis plunge. Number of poles = 120.

Fig. 5-26.: Equal area plot of poles to maximum projection (ab) planes of clasts at site 1. Number of poles = 120. Contour intervals: 6%, 4%, 3%, 2%, 1%, per 1% area. The current direction indicated by the direction through the girdle axis is 143°. Note: a duplicate of Fig. 5-6A.

Fig. 5-27.: Rose diagram of the directions 180° opposite to the dip directions of maximum projection (ab) planes of clasts at site 1. Number of values = 120. The vector mean indicated by the arrow is 140°. The midpoints of the two main modes are 110° and 170°. Class intervals are 20° and the scale represents 10% of the values.

Fig. 5-28.: Rose diagram of the directions 180° opposite to the dip directions of maximum projection (ab) planes of clasts at site 1. Recorrected by removing the influence of a-axis plunge. Number of values = 120. The vector mean indicated by the arrow is 133° and the midpoint of the principal mode is 130°.

5-25 A

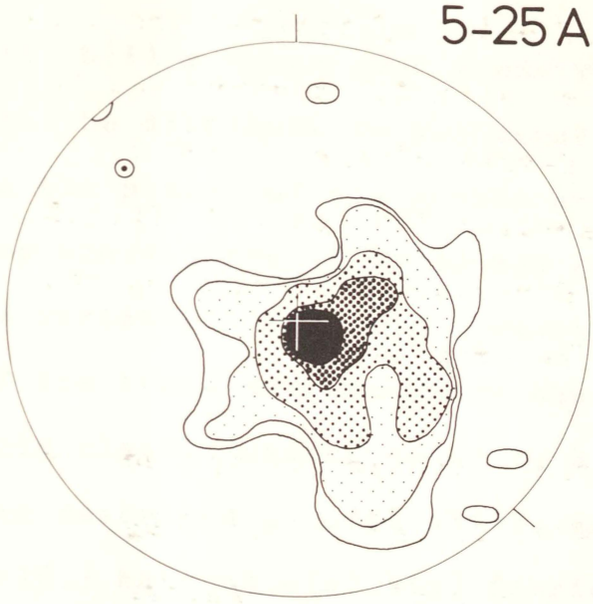

5-25 B

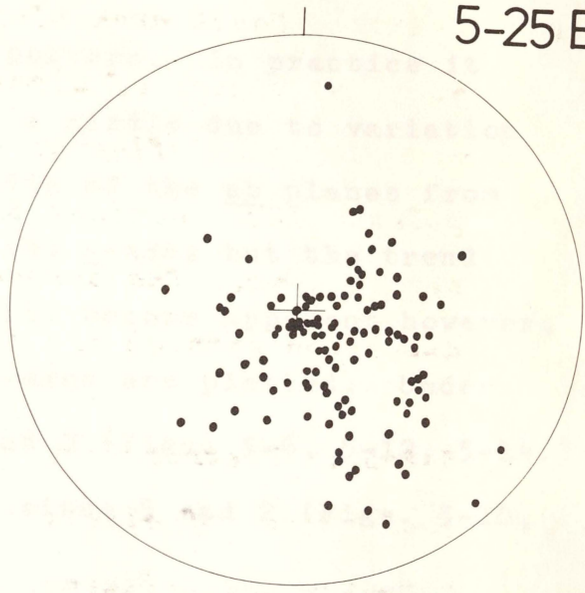

5-26

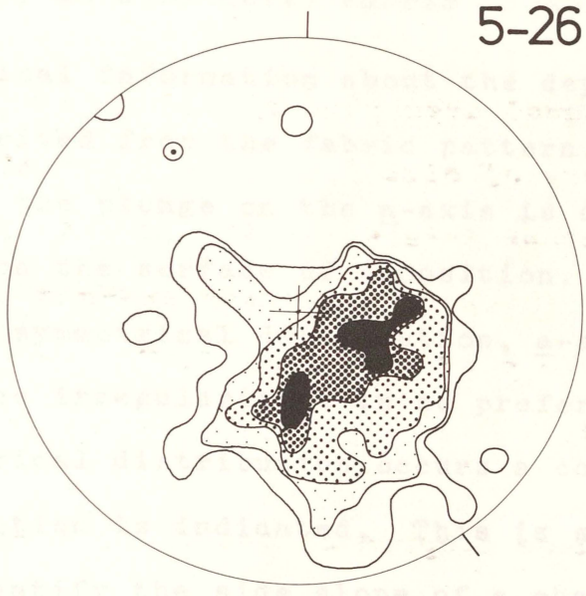

5-27

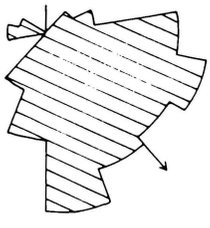

5-28

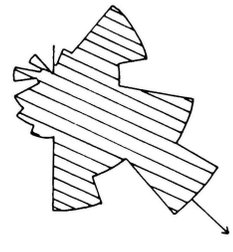

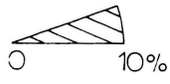

a(t) b(i) a monoclinic symmetry pattern. In practice it will be difficult to distinguish a girdle due to variation in the plunge of the a-axes and dip of the ab planes from one where there is no plunge on the a-axes but the trend is variable. This will immediately become apparent however, if the trend and plunge on the a-axes are plotted. Under this classification sites 1, 4 and 3 (Figs. 5-6, 5-12, 5-14.) are described as a(t) ab(i), and sites 5 and 2 (Figs. 5-10, 5-16.) have an a(t) b(i) fabric.

The Significance of an a(t) ab(i) Fabric

Sedimentological information about the depositional surface may be derived from the fabric pattern. In the a(t) ab(i) fabric the plunge on the a-axis is due to a transverse slope on the surface of deposition. If the fabric reflects a symmetrical distribution, a-axis plunge may reflect surface irregularities in no preferred direction, but if an asymmetrical distribution occurs a consistent slope in one direction is indicated. This is significant in that it may identify the side slope of a channel or channel bar which may otherwise not be discernable.

The recognition of an inclined bedding surface in the Clifton Conglomerate is important in view of the initial assumption expressed in Section 5-1 that because of difficulty in identifying bedding planes, it was necessary to assume an average horizontal plane as a depositional surface. This study has however rejected a horizontal depositional plane at site 1 because the fabric elements do not have an orientation fabric consistent with this. Furthermore, the validity of deriving paleocurrent directions by only measuring the

orientation of the ab plane, as commonly suggested by others (Rusnak 1957; Porter & Pettijohn 1963), is now questioned. This arises because the slope of the depositional surface will have a significant effect on the orientation of the clast. However, if the trend and plunge on the a-axis is also measured, the effect of the dip of the original depositional surface on the ab plane orientation may be eliminated.

Most published petrofabric diagrams of pebble ab plane orientations in modern braided rivers (e.g. Sedimentary Petrology Seminar, 1965, Fig. 1.) display perfect monoclinic symmetry. This perhaps reflects that many sedimentologist, preferring not to get their feet wet, have biased the sample by choosing flat bar tops to measure pebble orientation. In a braided fluvial sub-environment a flat bar top may not be the most typical position and therefore to always expect a monoclinic symmetry pattern, as suggested in the literature, is rather misleading.

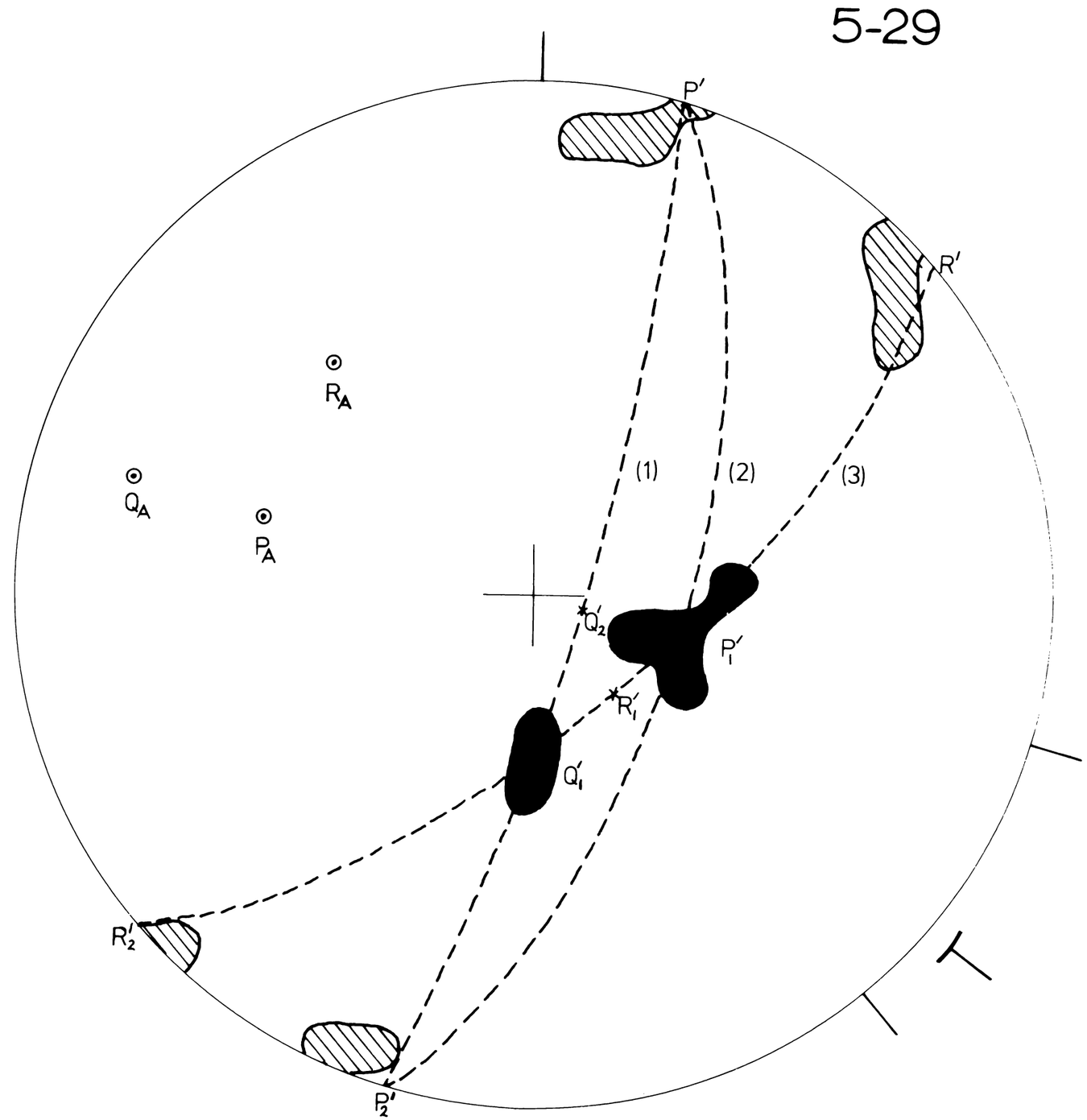

Fig. 5-29. Petrofabric diagram showing the maxima for poles to maximum projection (ab) planes of clasts (from Fig. 5-6A.) as solid black, and the maxima of a-axes orientations of clasts (from Fig. 5-5A.) as hatching. The dotted lines represent great circles on which lie ab plane pole and a-axes maxima. The poles to the great circles are the girdle axes Q_A, P_A and R_A. The direction through Q_A, P_A and the centre of great circles (1) and (2) is 116^o. The direction through R_A and the centre of great circle (3) is 139^o.

It is apparent in the diagram that ab plane pole mode Q_1' is asymmetrically distributed about great circle (1). Hence a paleocurrent direction through the ab plane pole girdle $Q_1' - R_1' - P_1'$ is not coincident with that normal to the a-axes maxima. Correction of the ab plane direction of dip by removing the influence of plunge on the a-axis, rotates the ab plane poles into a single mode, the paleocurrent direction through the mode now being in the range $129-132^o$ (indicated).

Hence it is important that the trend and plunge of the a-axis of clasts should be measured in addition to the dip and direction of dip of the maximum projection of the ab plane, as slope on the depositional surface has an influence on the orientation of the ab plane.

5-5 *ORIGIN OF CLAST ORIENTATION*

To help establish whether clast orientation in conglomerates of the Kidnappers Group relates primarily to orientation during transport or to post-depositional reorientation, the scalar properties of clasts in relation to their orientation were studies. In this context post-depositional reorientation is taken to mean the reorientation of a clast while it remains either in contact with the fluid medium, or in contact with other clasts in the processes of transport and depostion.

Method

For sites 1 and 6 (Fig. 5-2.) the clasts were grouped into three classes on the basis of size (taken to be the length of the b-axis), three on the basis of sphericity (maximum projection sphericity), and three on the basis of the elongation index (Table 5-2, Appendix V).

Class	A	B	C
size	≥8cm	<8 >6cm	≤6 >3cm
sphericity	≥0.6	<0.6 ≥0.5	<0.5
E.I.	≥0.8	<0.8 ≥0.6	<0.6

Table 5-2. A summary of the class limits for each of the size, sphericity and elongation indices classes.

The clasts were approximately equally distributed within each of the three classes for size, sphericity and elongation

index. The orientation of each clast within each class was plotted graphically and analysed mathematically. This procedure was followed for both a-axis and ab plane orientations at sites 1 and 6, although only the most relevant information is presented here (Figs. 5-30 to 5-32, Table 5-3 and 5-4).

The Influence of Clast Attributes on the Orientation of a-axes at Site 1.

Petrofabric Analysis of Size, Sphericity and Elongation Index Classes:

In Figs. 5-30A, B, C the a-axes distributions are plotted with respect to each of the size classes of pebbles at site 1. Similarily Figs. 5-31A, B, C represent the distribution of the sphericity classes and Figs. 5-32A. B. C the distribution of the elongation classes. Incorporated in Table 5-3 is a summary of the statistics for each of the nine classes. The trend values of clasts within each class are included in Appendix V.

The petrofabric diagrams in general show little preferred orientation with no one class completely explaining the tendency for clasts in the total distribution (Fig. 5-5A.) to have a-axis orientations either normal or parallel to current flow. The same comment can be made from the mathematical analysis where most classes fail to find a significant difference between the vector means at P = 0.05. Despite this general statement, Fig. 5-30A shows that the largest size class contains the greatest number of clasts aligned parallel to the flow direction. Conversely, pebbles in the

Fig. 5-30A.: Point distribution of the trends of a-axes in size class A. Size ≥ 8 cm. Number of points = 34.

Fig. 5-30B.: Point distribution of the trends of a-axes is size class B. Size <8 cm. >6 cm. Number of points = 36.

Fig. 5-30C.: Point distribution of the trends of a-axes in size class C. Size ≤6 cm. >3 cm. Number of points = 50.

Fig. 5-31A.: Point distribution of the trends of a-axes in sphericity (maximum projection sphericity) class A. Sphericity ≥0.6. Number of points = 44.

Fig. 5-31B.: Point distribution of the trends of a-axes in sphericity class B. Sphericity <0.6 ≥0.5. Number of points = 47.

Fig. 5-31C.: Point distribution of the trends of a-axes in sphericity class C. Sphericity <0.5. Number of points = 29.

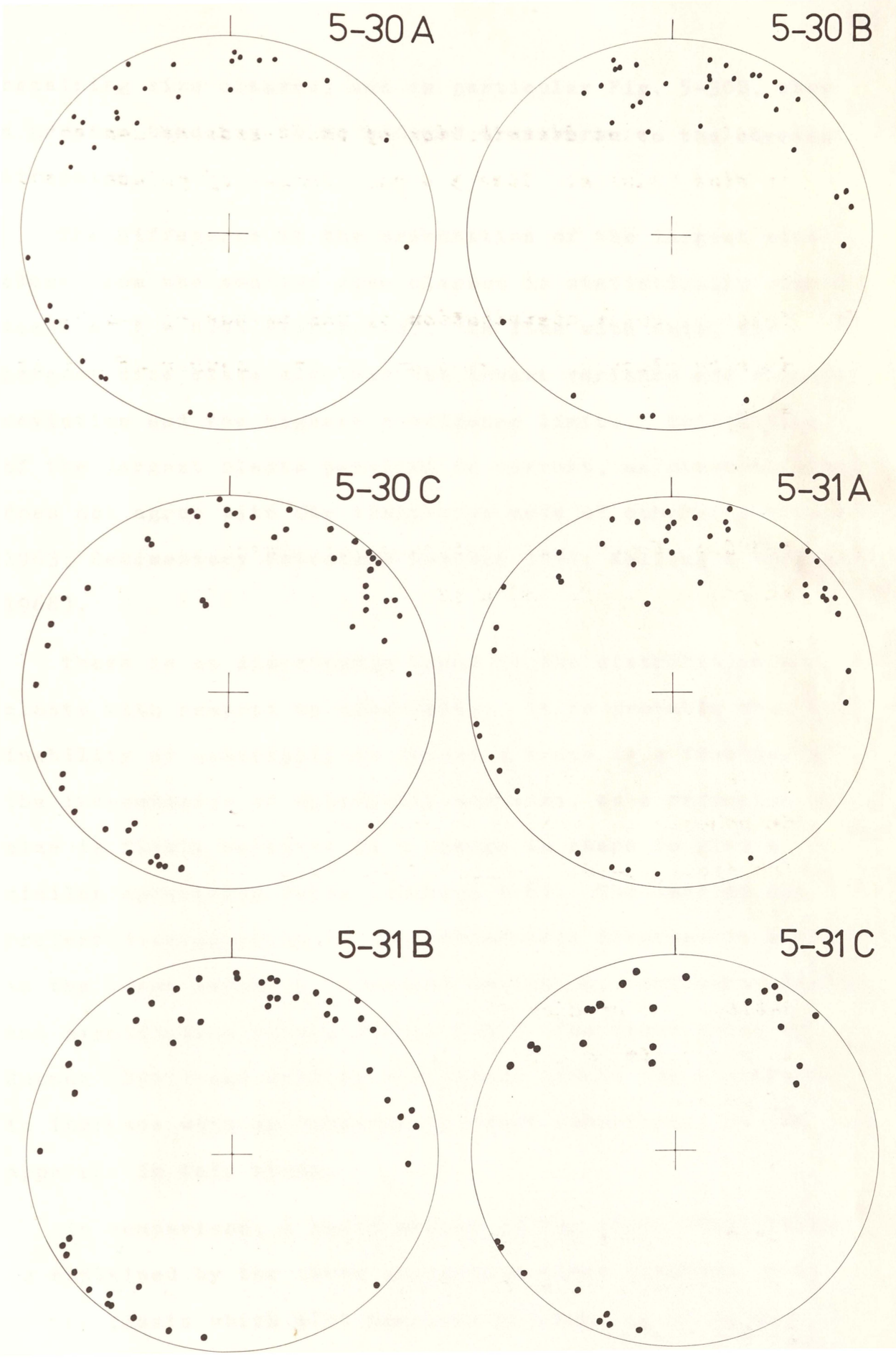
5-30 A
5-30 B
5-30 C
5-31 A
5-31 B
5-31 C

remaining size classes, and in particular Fig. 5-30B, show a greater tendency to be aligned transverse to the current direction.

The difference in the orientation of the largest size class from the smaller size classes is statistically significant at P = 0.05 (Table 5-3). In line with this, the largest size class also has the lowest variance and standard deviation and the highest confidence limits. Orientation of the largest clasts parallel to current, as observed above, does not agree with the transverse mode of others (Johansson 1963; Sedimentary Petrology Seminar 1965; Kelling & Williams 1968).

There is no discernable trend in the distribution of clasts with respect to sphericity. It is probable that the inability of sphericity to impose a trend is a function of the independence of sphericity and size, as a reduction in size is finely balanced by a change in shape to give a similar sphericity value (Section 4-6). The lack of any preferred orientation in the petrofabric diagrams is mirrored in the large variance, standard deviation, confidence limits and significance values (Table 5-3). The trend noted by Rusnak (1957) and Kelling & Williams (1968) for dispersion to increase with an increase in clast sphericity, is not apparent in this study.

In comparison, a small amount of the total distribution is explained by the three elongation index classes. Most of the clasts which plot parallel to flow, occur in the large and intermediate elongation classes (Fig. 5-31A & B). This is not however, statistically significant (Table 5-3).

Fig. 5-32A.: Point distribution of the trends of a-axes in elongation index class A. Elongation index value ≥0.8. Number of points = 37.

Fig. 5-32B.: Point distribution of the trends of a-axes in elongation index class B. Elongation index value <0.8 >0.6. Number of points = 55.

Fig. 5-32C.: Point distribution of the trends of a-axes in elongation index class C. Elongation index value ≤0.6. Number of points = 28.

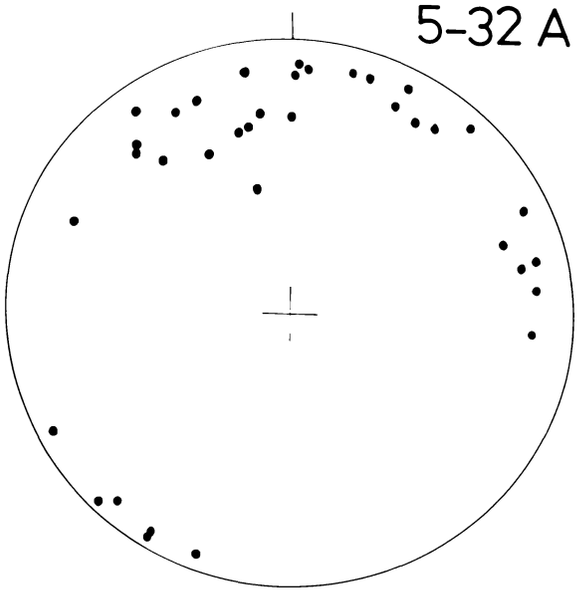
5-32 A

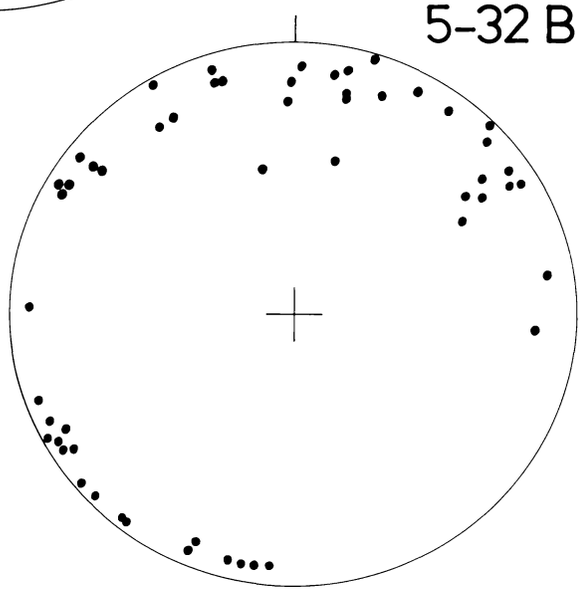
5-32 B

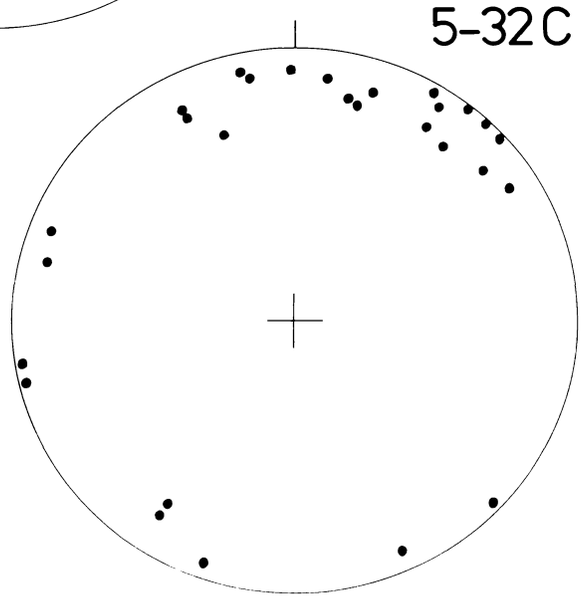
5-32 C

			n	Mean	Var.	Stdev.	Vec. Mag.%	95% con.	99% con.	S.
TOTAL			120	349	5893	77	39.24	14	19	
Size	≥8cm		34	315	3708	61	55.75	21	28	<0.1%
	<8 >6cm		36	15	4465	67	59.55	23	31	>20%
	≤6 >3cm		50	353	7554	87	24.46	25	33	5>2%
Ratio I/L	≥0.8		37	353	4254	66	54.64	22	30	20%
	<0.8 >0.6		55	333	6166	79	30.86	22	29	10>5%
	≤0.6		28	5	6010	78	44.00	31	41	>20%
Sphericity	≥0.6		44	359	5817	77	42.48	24	32	>20%
	<0.6 ≥0.5		47	351	6205	79	35.45	24	32	>20%
	<0.5		29	332	5394	74	42.31	28	38	20>10%
Cross-correlation		LL	14	343	1804	43	78.74	25	35	
		LM	17	280	4124	65	52.41	34	46	
		LS	3	340	6085	79	47.17	194	248	
		ML	13	2	4467	67	57.12	41	57	
		MM	17	15	3097	56	71.52	29	40	
		MS	5	44	3470	59	68.86	74	122	
		SL	11	22	11880	109	14.98	74	105	
		SM	20	313	8059	90	10.31	42	58	
		SS	19	350	5094	72	48.88	35	48	
Grouped correlation	LL, LM, ML, SL		55	330	4889	70	44.03	19	26	10%
	LS, MS, SM, SS		47	355	6952	84	30.73	25	33	

Table 5-3. Summary of the statistics resulting from the vector analysis of a-axes orientation data at Site 1. S. refers to Significance Level. A complete summary of the data is included in Appendix V.

			n	Mean	Var.	Stdev.	Vec. Mag.%	95% con.	99% con.
TOTAL			120	140	3139	57	64.27	12	14
Size	≥8cm		34	133	1625	41	77.72	14	19
	<8 >6cm		36	143	1953	45	74.30	15	21
	≤6cm		50	150	4701	69	50.91	20	26
Ratio	≥0.8		37	150	2829	54	68.04	18	24
	<0.8 >0.6		55	133	3303	58	62.35	16	21
	≤0.6		28	143	2628	52	70.00	20	27
Sphericity	≥0.6		44	144	2748	53	66.52	16	22
	<0.6 ≥0.5		47	142	3206	57	63.00	17	23
	<0.5		29	135	3351	58	67.35	23	30
Cross-correlation		LL	14	135	1206	35	84.39	21	28
		LS	3	164	38	7	99.62	16	35
		LM	17	117	2050	46	73.85	24	33
		ML	13	152	1559	40	79.84	24	34
		MM	17	140	2525	51	70.29	26	36
		MS	5	128	1412	38	84.10	47	78
		SL	11	160	6823	83	33.30	56	79
		SM	20	148	5024	71	49.48	34	46
		SS	19	144	3431	59	62.17	29	39
Grouped correlation		LL, ML	27	143	1412	38	81.26	15	21
"	"	LM, LS, MM, MS, SL, SM, SS	92	139	3593	60	60.21	13	17
Total-axis plunge removed			120	133	4515	68	52.03	13	17

Table 5-4. Summary of the statistics resulting from the vector analysis of ab plane pole orientations at Site 1. The directions used in calculation are 180° opposite to the direction of dip of the ab plane.

A complete summary of the data is included in Appendix V.

Nevertheless, this does agree with the findings of Johansson (1963) and Kelling & Williams (1968) who observed more elongate pebbles transverse to current flow.

Part of the reason the Sedimentary Petrology Seminar (1965) did not find a relationship between clast shape and orientation, may lie in their use of the 3-dimensional flatness ratio rather than the elongation index. Fluvial sedimentologists have been reluctant to use this simple 2-dimensional measure, although glacial stratigraphers have realised its environmental sensitivity and have put it to good effect in recognising transverse and parallel clast orientations (Drake 1977).

Petrofabric Cross-correlation:

By simply analysing the clast orientations with respect to size, sphericity, and elongation classes, insuffient of the total orientation pattern is explained. It therefore appears that either the orientation is more subtly related to size and shape, or in fact there is no relationship. The difference in the orientation of the large size class and the large and intermediate elongation classes from other classes, prompted the plotting of various size/elongation cominations as a cross-correlation. The matrix is illustrated below:

LL	LM	LS
ML	MM	MS
SL	SM	SS

The notation used to characterise each of the nine subclasses in the cross-correlation is as follows: L, M and S

refer to the large, intermediate and small size and elongation classes. The first letter in the two letter abbreviation, refers to the size class and the second letter to the elongation class. For instance LL is the large size large elongation subclass, while SM is the small size intermediate elongation subclass.

The orientations for clasts in the nine subclasses were plotted on petrofabric diagrams but although not included here, the trend values for each subclass are included in Appendix (V) and a mathematical summary of the results is included in Table 5-3. Certain trends are apparent. The subclasses LL and LM consistently plot in the north-west quadrant and LS in the north-east and south-west quadrants. Other combinations also have a tendency to plot either predominantly transverse or parallel to current flow. As the number of pebbles in each subclass was not statistically significant, combinations which showed similar trends were grouped into two diagrams, one of LL, LM, ML and SL in Fig. 5-33 and the other of LS, MS, SM and SS in Fig. 5-34. The combination MM was not plotted as it did not fall directly into one or other of the patterns.

Each of the two grouped correlations have factors in common. In Fig. 5-33A not only do clasts have a-axis orientation transverse to current direction, but also this group contains most of the pebbles oriented parallel to flow. On the other hand, in Fig. 5-34A orientations are predominantly transverse to current flow. The effect of the graphical cross-correlation has been to sort and stress

Fig. 5-33A.: Equal area plot of a-axes orientations of clasts in the grouped correlation of subclasses LL, LM, ML, SL. Number of points = 55. Contour intervals: 8%, 6%, 4%, 2%, per 1% area.

Fig. 5-33B.: Point distribution of the trends of a-axes of clasts in the grouped correlation of subclasses LL, LM, ML, SL. Number of points = 55.

Fig. 5-34A.: Equal area plot of a-axes orientations of clasts in the grouped correlation of subclasses LS, ML, SM, SS. Number of points = 47. Contour intervals: 7%, 5%, 3%, 2%, per 1% area.

Fig. 5-34B.: Point distribution of the trends of a-axes of clasts in the grouped correlation of subclasses LL, LM, ML, SL. Number of points = 47.

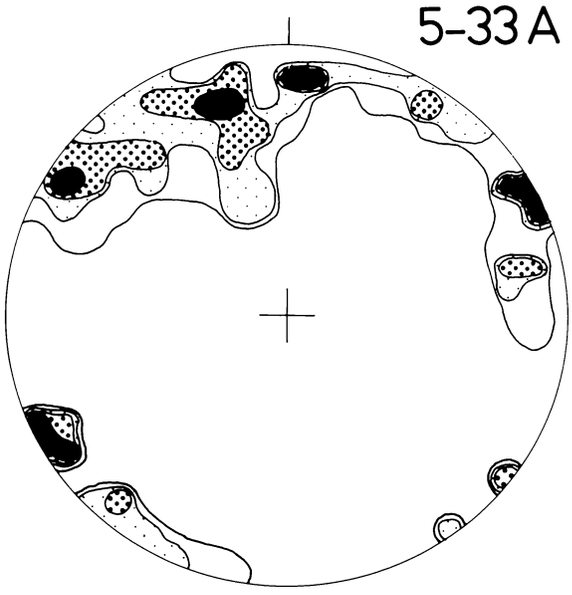

5-33 A

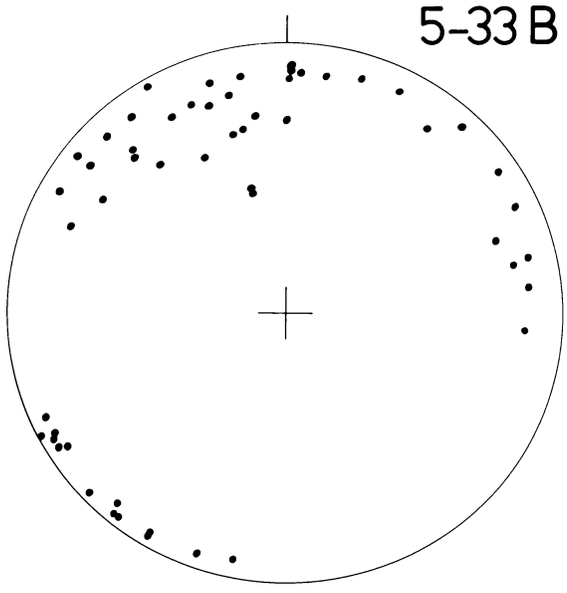

5-33 B

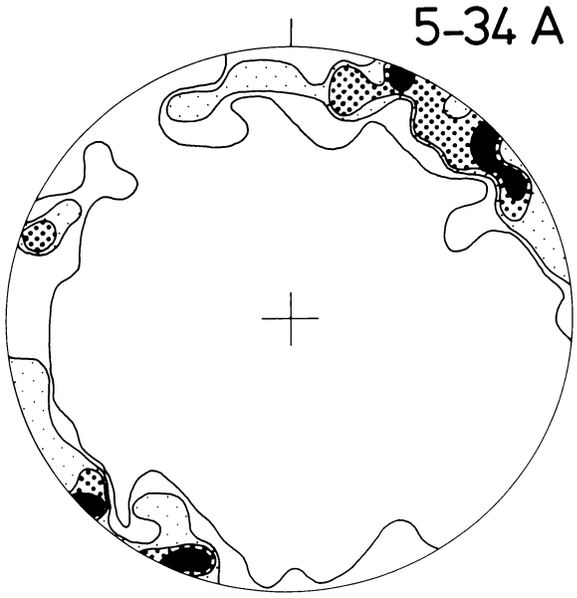

5-34 A

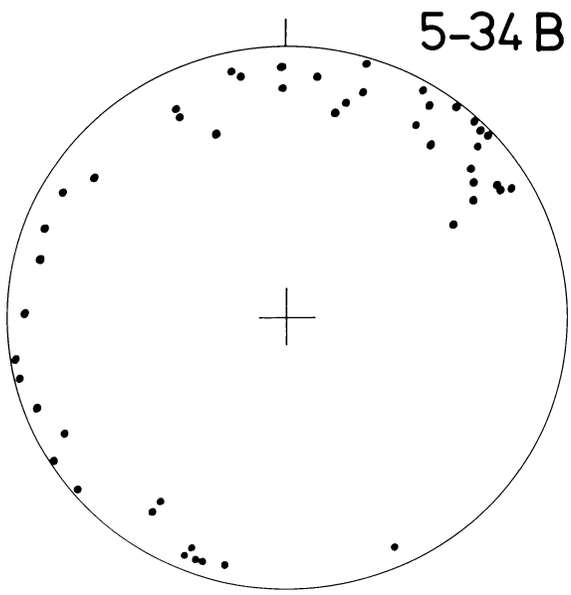

5-34 B

the slight tendency for each size and elongation class to explain the total distribution. The result is that although the greatest tendency is for pebbles to be oriented normal to flow, those that are parallel to flow have large sizes and large elongation values. This explains in part the orientation of some large clasts parallel to current flow (c.f. Johansson 1963; Kelling & Williams 1968).

The Influence of Clast Attributes on the Orientation of ab Planes at Site 1

Modification of the dip direction of the ab plane by the external factor of channel slope, has already been established (Section 5-4.). As the distribution of the ab plane poles is closer to the c-axis in Fig. 5-25A. than in the original distribution (Fig. 5-26.), it appears that removal of dip on the a-axis reduces the imbrication angle. Although this occurs, clast imbrication is still present irrespective of depositional slope.

An analysis similar to that for the a-axes was undertaken to establish whether the influence of scalar properties was recorded in the orientation of ab planes (Appendix V). No discernable trend, either on the basis of petrofabric diagrams or mathematical treatment (Table 5-4), was evident for any particular class to explain parts of the total orientation fabric (Fig. 5-6A.)

A cross-correlation between size and elongation was also developed and it was found that certain subclasses gave concentrations in similar regions of the stereonet. Grouping the subclasses yielded two diagrams, one of LL and ML in Fig. 5-35 and the other of LM, LS, MM, MS, SL, SM and SS in

Fig. 5-36. Neither of these orientation fabrics is able to explain the bimodality in the original fabric (Fig. 5-26A.) and therefore reinforces the influence of channel slope.

The inability to detect a significant influence of scalar properties on orientation is understandable, as most pebbles irrespective of size and shape are imbricated. The least spread in the two distributions occurs in Fig. 5-35A which also has, on average, lower imbrication angles. A lower standard deviation, higher vector magnitude and higher confidence limits (Table 5-4.) confirms the reduced spread. For this reason the larger size/elongation clasts are more attractive as paleocurrent direction indicators. However, the vector mean for these clasts is 143° (Table 5-4.), more removed from the correct range of 129-132° (Section 5-4.) than the value 139° for the alternative grouped correlation. Therefore it appears larger size/elongation clasts are more affected by slope of the depositional surface. If for these pebbles it can be established that the a-axis has no plunge, or if it is measured and a correction made, an accurate indication of the paleocurrent direction may be derived by measuring a reduced number of these clasts.

The Influence of Clast Attributes on the Orientation Fabric of Site 6

The same method of analysis outlined for site 1 was repeated at site 6, but neither the individual size, sphericity or elongation index classes, nor a cross-correlation gives any indication of a relationship between a-axis and ab plane

Fig. 5-35A.: Equal area plot of poles to maximum projection (ab) planes of clasts in the grouped correlation of subclasses LL and ML. Number of poles = 27. Contour intervals: 22%, 15%, 11%, 7%, 4%, per 1% area.

Fig. 5-35B.: Distribution of poles to maximum projection (ab) planes of clasts in the grouped correlation of subclasses LL and ML. Number of poles = 27.

Fig. 5-36A.: Equal area plot of poles to maximum projection (ab) planes of clasts in the grouped correlation LM, LS, MM, MS, SL, SM, SS. Number of poles = 92. Contour intervals: 8%, 6%, 4%, 2%, 1%, per 1% area.

Fig. 5-36B.: Distribution of poles to maximum projection (ab) planes of clasts in the grouped correlation of subclasses LM, LS, MM, MS, SL, SM, SS. Number of poles = 92.

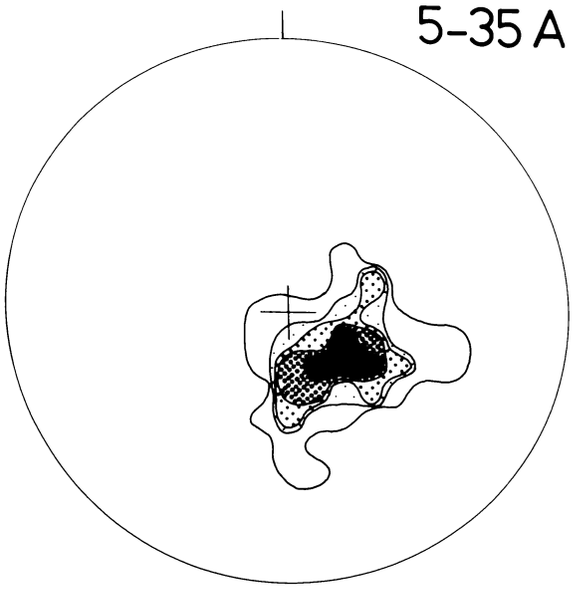

5-35 A

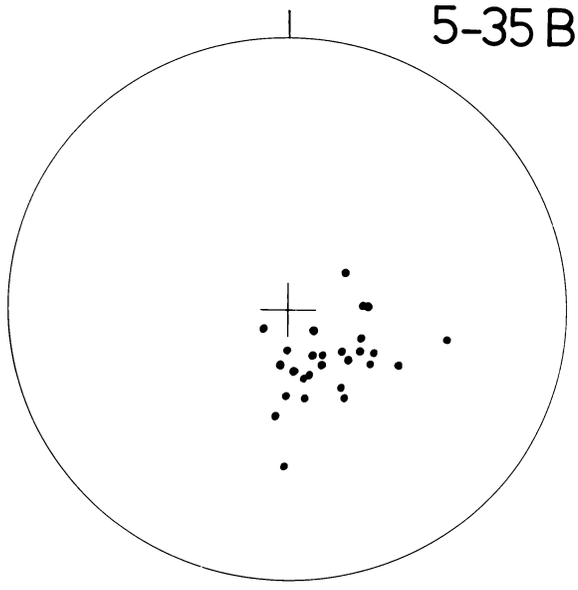

5-35 B

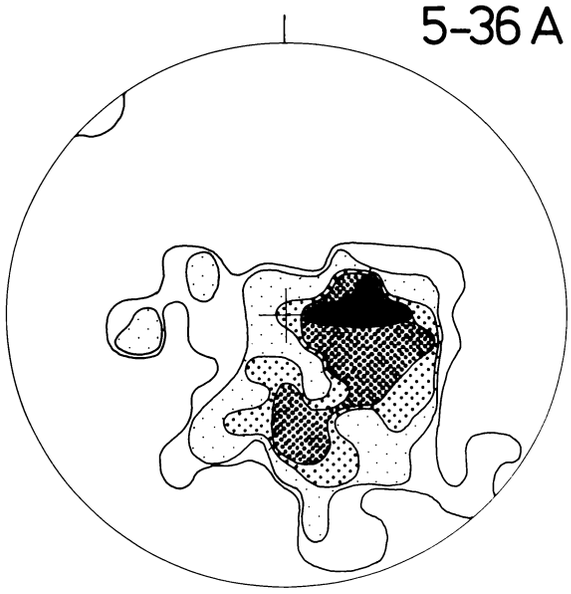

5-36 A

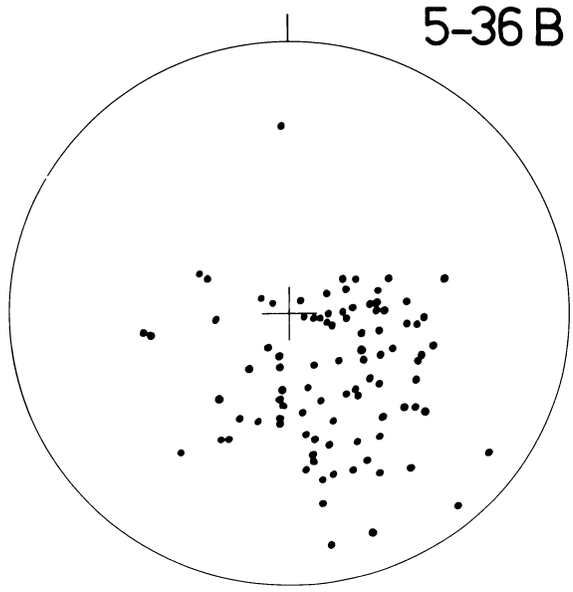

5-36 B

orientations and clast attributes. Evidently, the influence of polydirectional currents is to confuse pebble orientations, particularly the direction of dip of the ab plane, and complicate the effect on orientation of clast shape and size.

The Theory of Grain Orientation Development during Transport and Deposition

Jizba (1971) believes that the preferential alignment of clastic particles in sedimentary rocks can best be explained by studying the phenomena of tumbling in free fall and hydrodynamic drag. This view, supported in part by Rusnak (1957), echoes the minimum energy hypothesis developed by Jeffery (1922), in a study of the motion of ellipsoidal particles immersed in a viscous fluid, and Taylor (1923) has provided experimental verification of this. The following is a brief summary of fluid forces acting on a clast based on Rusnak (1957) and Jizba (1971).

Orientation due to Angular Momentum:

A clast in motion has an angular momentum which is the product of the moment of inertia about the axis of rotation and the angular velocity. A pebble will only maintain its angular momentum if it rotates about the c-axis or a-axis (Fig. 5-37.), where this corresponds respectively to a maximum and a minimum moment of inertia. A clast is unable to rotate about the b-axis (Fig. 5-37.) when it has a forward velocity, and consequently randomly tumbles when in free motion.

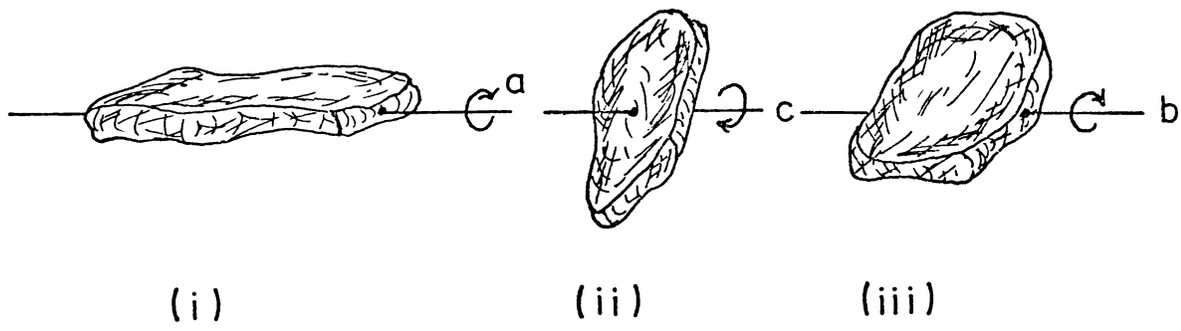

Fig. 5-37. Rotation about the a-axis (i) and c-axis (ii) and tumbling about the b-axis (iii) when a clast is in free motion.

Upon deposition, the orienting force due to angular momentum will cease and therefore the orientation of the pebble will reflect the axis about which the pebble tumbled. Consequently, these pebbles which tumbled about the b-axis will be randomly oriented, compared with those which rolled around the longest axis and are now transverse to current direction. However, clast motion is constrained within a fluid and therefore drag and lift may play a greater role than angular momentum in determining particle orientation (Jizba 1971).

Orientation due to Fluid Drag:

The drag of a particle is given by the formula:

$$D = \tfrac{1}{2} C_D V^2 S_1$$

Where D is drag, C_D the drag coefficient (related to shape), fluid density, V fluid velocity, and S_1 area of the grain as projected on a plane perpendicular to the fluid flow. The drag will be at a minimum when the grain's long axis

is aligned parallel to flow. For a platy clast the most stable orientation is one with the ac or ab plane projecting into the current. Where a grain is in an inherently unstable position, the fluid drag will reorient the pebble so as to present the least surface area to the current and produce the least fluid drag.

Orientation due to the Lift Force:

The force acting on a grain in a direction perpendicular to fluid flow is called lift. The amount of lift is given by the formula:

$$L = \tfrac{1}{2}C_L V^2 S_{LL}$$

Where L is the lift, C_L is the lift coefficient of the particle (related to shape) and S_{LL} is the plan area of the grain as projected horizontally. The most stable grain orientations are those that have a negative (downward) lift. This corresponds to a position where the clast is facing into the current in an imbricate fashion.

In summary, the preferred orientation of a pebble in response to interaction with the flow, will depend on the relative importance of each of the three fluid forces. This in turn is dependent on the size and shape of the clast, where the larger and more elongate a clast the more likely a preferred orientation at right angles to flow (greater influence of inertial forces) and conversely, the smaller a pebble the more likely it is parallel to current (drag forces).

Factors of Clast Reorientation

Collisions:

It has long been recognised in the application of theory to the understanding of clast orientation in glacial tills, that the preferred orientations reflect processes other than just the forces exerted by the transporting medium (c.f. Jizba 1971). Manley *et al.* (1955) and Glen *et al.* (1957) have pointed out that reorientation of clasts results from interaction between clasts. Glen *et al.* (1957) envisaged that the collisions of particles in motion was a mechanism by which clasts moved towards an orbit of minimum energy (Jeffery 1922). For instance, a prolate clast rolling in an orbit of minimum energy would "sweep out the least volume", thereby coming into contact with a minimum of other clasts which could disrupt this preferred orientation. In the same way, the orbit of a clast in an unstable rotation would occupy a larger volume and therefore have a greater chance of colliding and changing orbit. Thus a transverse orientation would be favoured for prolate clasts whereas for an oblate clast, for which the minimum energy hypothesis favours a transverse mode, would on the basis of collisions favour the parallel direction.

In support of this idea Manley *et al.* (1955) observed that the orbit of a single rod remained constant for a long time, whereas when the density was increased the transverse orientation developed. These views do not completely concur with the experimental and field evidence of Johansson (1963) and Rust (1972) who found collisions

caused rotation from the transverse mode; an effect which increased with pebble concentration. This did however, mainly occur with collisions of moving and stationary clasts (c.f. Glen *et al.* 1957). An opposite relationship holds for imbrication which improves with pebble concentration (Rust 1972).

Velocity:

Apparently an increase in current strength results in improved clast imbrication (Rusnak 1957). On flow velocity, the Sedimentary Petrology Seminar (1965, p.278) commented that "the currents that orient gravel during floods in Wolf Run are evidently so intense that variation in size and flatness has virtually no influence on the hydrodynamic response of the particles". Rust (1972) noted that as a-axis orientation parallel to current represented the saltation mode of transport, a-axis orientation could be used to infer the magnitude of ancient stream velocities. Kelling & Williams (1968) found reorientation to be an *in situ* process and primarily a function of flow velocity. An increase in current strength reorients pebbles with a transverse mode but at low velocity ranges, the attitudes of pebbles is directly controlled by the geometry of the bedforms; an effect similar to lodgement of small particles in irregularities of a depositioned surface (Hendry 1976; Laronne & Carson 1976).

A Synthesis of the Origin of Clast Orientation

A synthesis of the theoretical views and experimental and field observations of others would suggest that the

processes orienting clasts may include interaction with the fluid forces, interaction between particles, and between a particle and the depositional surface. Further, the opportunity for interaction may occur during transport and/or after deposition (Fig. 5-38.). In line with this, the terms transportational orientation and post-depositional orientation are used to respectively describe the groups of forces responsible for clast orientation while in motion, and orientation imposed on the clast while it remains in contact with the current or other particles transported by the current.

Influence	*a*-Axis		*ab* Plane
	Saltation	Traction	
Angular Momentum	Parallel*	Transverse*	N.P.O.*
Drag	parallel*+		conformable*+
Lift	imbricate+		imbricate+
Collisions	transverse*		N.P.O.*
Bedform	transverse+		N.P.O.+
Lodgement	N.P.O.+		N.P.O.+
Particle Density	transverse/parallel+		imbricate+

Fig. 5-38. A summary of the preferred orientation of the a-axis and ab plane of a clast likely to develop under each influence.
N.P.O. means no preferred orientation.
** means influence operative during transport.*
+ means a post-depositional influence.

A-axis orientation parallel or transverse to current may result either from the transportational orientation or its post-depositional modification (Fig. 5-38.). However, imbrication of the ab plane is exclusively a post-depositional orientation fabric, hence it has potential in establishing the importance of transportational versus post-depositional influences on the origin of clast orientation.

The Origin of Clast Orientation at Site 1

In the graphical cross-correlation those clasts parallel to current were mainly large sizes with large elongation index values (Fig. 5-33A.). According to Fig. 5-38, such an orientation may develop through angular momentum or reorientation parallel to flow by fluid drag once deposited. The second alternative is unattractive especially as the smaller clasts do not seem to have reoriented under this force (Fig. 5-34A.). Hence the most probable origin of the parallel modes in Fig. 5-33A is one of orientation due to transport where the clasts tumbled about the b-axis in a random fashion.

As the smaller clasts are transverse to flow, this evidently reflects movement by rolling on the a-axis, an orientation reinforced by post-depositional processes (Fig. 5-38.). An apparent contradiction is highlighted in that larger clasts moved by saltation and smaller clasts by traction. A possible explanation drawn from Figs. 5-33A and 5-34A lies in the movement of the largest clasts at high flood stages with subsequent deposition. With falling flood stage, the remaining population continues to be transported until a critical velocity is reached immediately above which

a clast is in traction transport, and below which a particular size is no longer transported. Therefore, although a total population may at some stage have moved in saltation/suspension, only the largest clasts are most likely to maintain this orientation, with most others recording a traction orientation prior to deposition.

No trend in clast size or shape was evident in the preferred orientation of ab planes at site 1 (Figs. 5-35A & 5-36A.). Ubiquitous however, is imbrication, evident from Fig. 5-38 to be a post-depositional modification. Imbrication is predominantly due to the lift force and particle density effects (Blatt *et al.* 1972; Hendry 1976). For a given lift force the larger clasts have a lower angle of imbrication, consistent with that found in Fig. 5-35A & 5-36A. The very high imbrication angles and in particular the inclination of clasts in a downstream direction, reflect lodgement effects. Hence, the predominance of upstream imbrication strongly suggests that clasts have suffered reorientation by rotation of the ab plane upstream. This process most likely occurs during falling flood stages and normal stream flow, when the current is largely incompetent to move the sediment, but of sufficient strength to reorient clasts *in situ*.

5-6 A MODEL OF CLAST ORIENTATION

Clast orientation may record a spectrum of transportational and post-depositional processes operative on clasts. At one extreme, the orientation fabric may be wholly the result of orientation during transport, preserved by rapid burial, or at the other extreme post-depositional influences may have completely modified the original orientation. Hence clast orientation, at least in the extreme cases, is now thought to be a sensitive environmental indicator in conglomerates.

A model (Fig. 5-39.) is presented which enables the relative importance of the processes operative during transport and after deposition to be evaluated. The model contains two enclosing boxes, an outer one representing the ab plane and an inner one representing the a-axis. Imbrication is largely synomonous with post-depositional modification and hence its recognition is evidence of this; the degree of development indicating the amount of modification. It is evident from the model that most clasts may be imbricated although the smaller more elongate pebbles are most susceptible to lodgement. The a-axis orientation is less sensitive at distinguishing transportational and post-depositional orientation as each may develop the same fabric. However, it may in part explain the hydrological regime and mode of transport. A 3 x 3 matrix of size and elongation index classes improves resolution, where the influence of clast shape is to establish a preferred or a non-preferred orientation during transport. Clast size on the other hand largely determines the post-depositional stability.

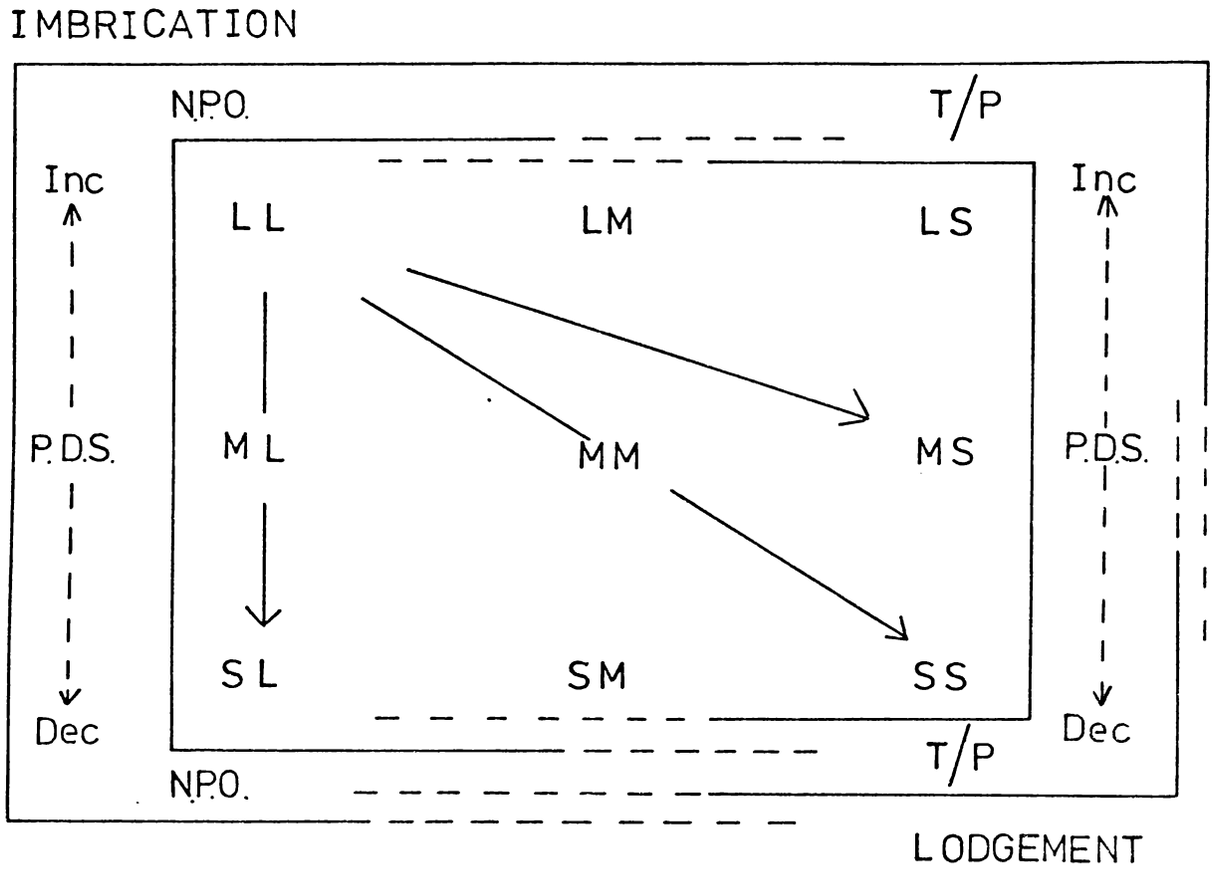

Fig. 5-39. Clast orientation model. For two examples of operation of the model see the text in Section 5-6. N.P.O. means no preferred orientation. P.D.S. means post-depositional stability. T/P means transverse/parallel orientation during transport.

Operation of the model is best explained by two examples. The fabric identified at site 1 had large size/elongation clasts parallel to flow, other clasts transverse to flow, with all clasts imbricated. Clearly, the imbrication indicates significant post-depositional modification. In considering a-axes orientations, the largest sizes are most stable after deposition and although there may have been a slight post-depositional tendency to develop a parallel orientation for LL, the orientation largely indicates deposition from turbulent transport in saltation. The smaller clasts are less stable and have inherited their transverse orientation both from rolling on the a-axis and the reinforcement of this orientation after deposition. As explained earlier (Section 5-5.) a-axis orientations are consistent with a flood and falling-stage regime. Further, it is thought there is a genetic association of large clasts parallel to current and well developed imbrication, both being indications of strong currents.

An alternative fabric is one with poorly developed imbrication with large clasts transverse and small clasts parallel/transverse to flow. The absence of imbrication suggests the unimportance of modification after deposition owing to rapid burial. Hence the a-axis orientation predominantly transverse to flow is developed during transport. A depositional setting in which such a fabric may develop is by avalanche of clasts down the foreset slope of a migrating channel bar.

The above model is intended to illustrate that a spectrum of clast orientations exist which relate to the processes of

sediment transport and deposition. In its extremes the model is valuable, although the natural variability of clast orientation may preclude further refinement.

CHAPTER 6: SEDIMENT TEXTURE AND MINERALOGY

Sediment texture is interpreted here as the particle-size distribution of the solid, inorganic constituents of deposits. Textural analyses generally have been used to describe grain-size distributions, to characterise or identify depositional environments, and to interpret the hydrodynamic regime of sediments. Studies by Friedman (1961), Allen (1965), Visher (1965, 1969) and others have, however, been concerned mainly with sandy deposits. Few textural studies of conglomerates have been reported, and where they have, the deposits have been predominantly sandy gravels (e.g. Bork 1970; Hume *et al.* 1975). For the reasons outlined in Section 3-4 detailed textural analysis to identify the depositional environments has not been attempted. Rather, hydrodynamic interpretations are emphasised here.

In view of the limited applicability of the usual forms of lithostratigraphic correlation, tephrostratigraphy, largely determined by the ferromangesian mineral assemblages, was investigated to establish, if possible, correlation of coastal and inland exposures of conglomerates.

6-1 TEXTURAL ANALYSES OF SOME CONGLOMERATES

Twelve gravelly samples (014-025) were analysed following the procedure outlined in Section 3-4 and the results are summarised in Fig. 6-1. Most samples are true gravels with 014, 015 and 024 being muddy, sandy gravels and 025 a sandy gravel (terminology after Folk *et al.* 1970).

Contrary to the results of Visher (1969), the cumulative size frequency curves on probability paper (Fig. 6-1.) do not clearly display separate log-normal subpopulations corresponding to traction, saltation and suspension modes of sediment transport. The slopes of the curves are also decidely more shallow than the average slopes of Visher. This not only refects the more poorly sorted nature of the conglomerates, but also the coarser grain-size and fine skewness, where the abundance of material in the coarse phi intervals has a damping influence on the distribution.

Excluding Fig. 6-1c, samples have mean and median sizes coarser than about -3ϕ, are poorly to very poorly sorted and strongly fine-skewed. The poor to very poor sorting is partly a result of the wide range of grain sizes available for transport, and partly the result of rapid deposition. Similarly, positive skewness may be explained by rapid deposition preventing the washing out of fines (Hume *et al.* 1975 c.f. Friedman 1961). Kurtosis is quite variable and has commonly been found not to be a useful grain-size parameter (Baker 1968).

Hence the absence of meaningful log-probability plots together with the non-normality of these gravels, limits interpretation of the grain-size distribution in terms of

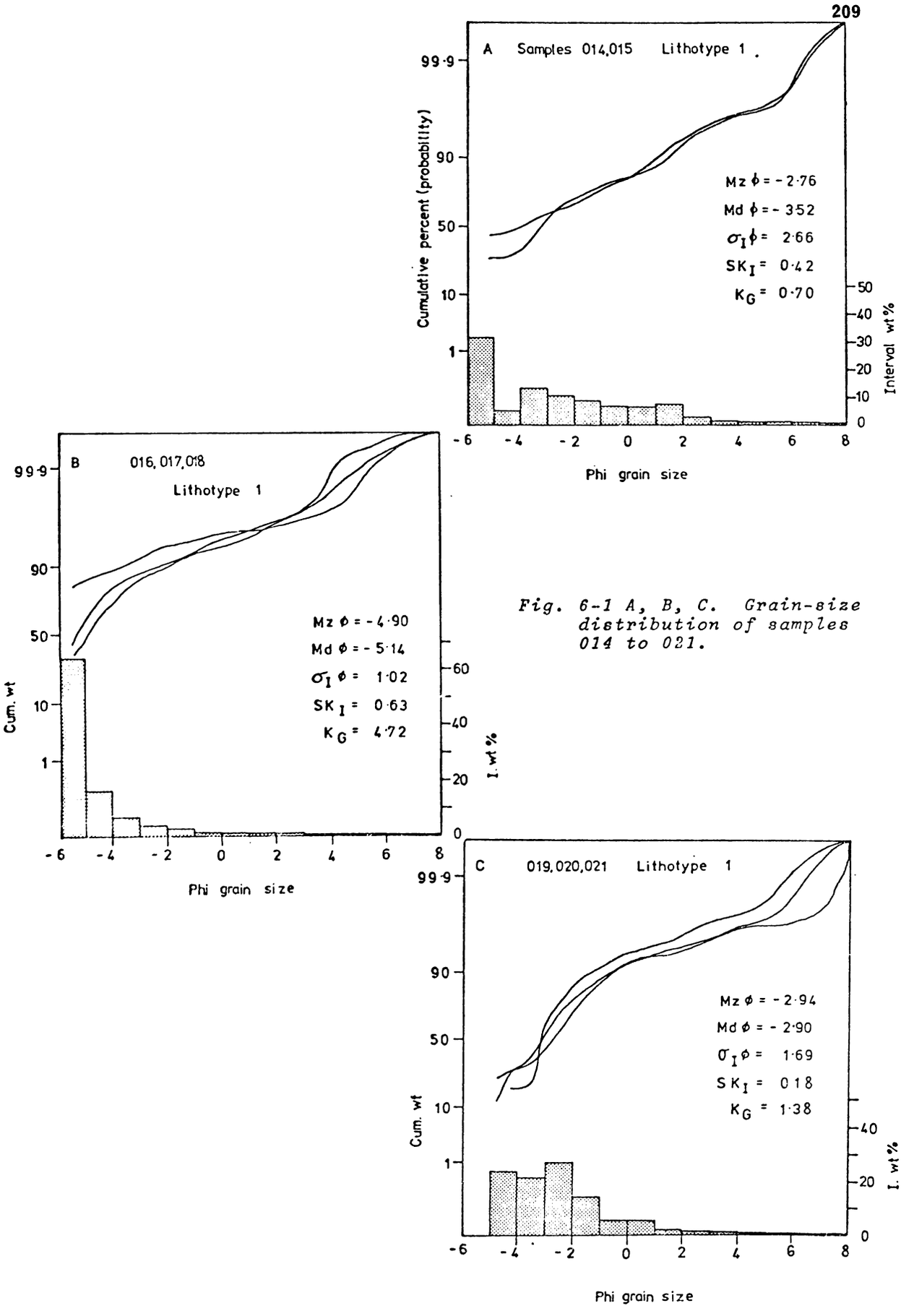

Fig. 6-1 A, B, C. Grain-size distribution of samples 014 to 021.

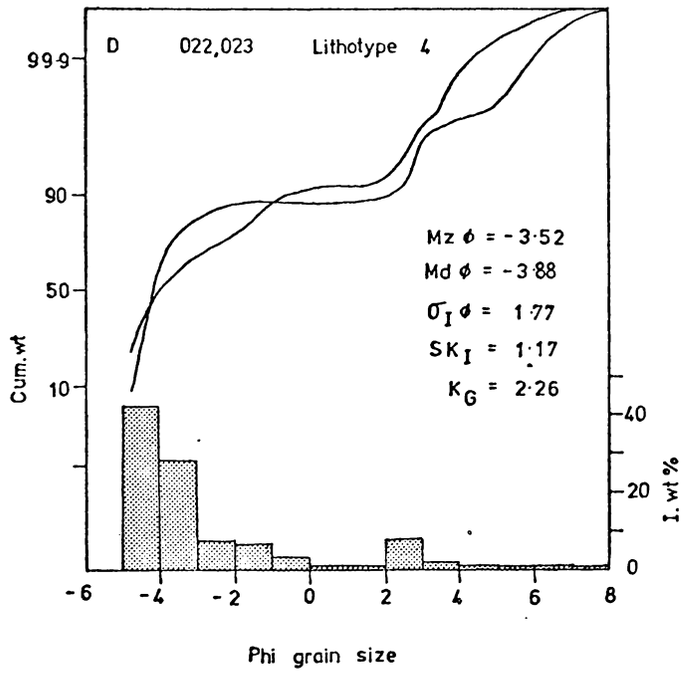

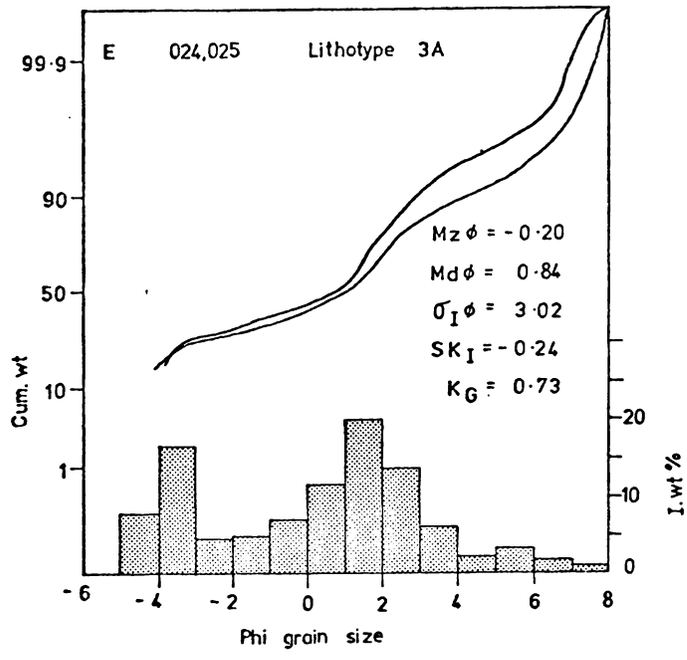

Fig. 6-1c, d. Grain-size distributions of Samples 022 to 025.

depositional environments.

Grain-Size Distribution of Lithotype 1.

The sedimentation units in three couplets of Lithotype 1 were analysed: the lower part of the inversely graded unit (Samples 014, 015, Fig. 6-1A.), the upper part of the inversely graded unit (Samples 016, 017, 018, Fig. 6-1B.), and the normally graded unit (Samples 019, 020, 021, Fig. 6-1C.). Samples in Fig. 6-1A are bimodal (< -5ϕ and -4 to 2ϕ), in Fig. 6-1B are strongly unimodal (< -5ϕ), and in Fig. 6-1C are largely unimodal (-5 to -1ϕ). To interpret these grain-size distributions a shear velocity relationship of bedload to suspended load sediment, developed by Walker (1975) for resedimented conglomerates, has been applied to the couplets of Lithotype 1.

For sediment to remain in suspension the applied shear stress must generate turbulent eddies that can prevent sediment from settling to the bed. Similarly, for rolling of pebbles on a bed, the applied shear stress must be great enough to overcome the rolling resistance of the clasts (Harms *et al.* 1975). Hence, a relationship between the size of clasts transported by rolling and the size of sediment suspended for a given flow velocity has been derived (ibid. p139). Furthermore, Walker (1975) graphed equivalent suspended sediment and bedload clast sizes for various shear velocities (Fig. 6-2.). Mean flow velocities in m/sec. equivalent to shear velocities were also calculated by Walker (1975, Fig. 7A.).

One interpretation of Fig. 6-2 is that relatively small fluctuations above and below a critical shear velocity will

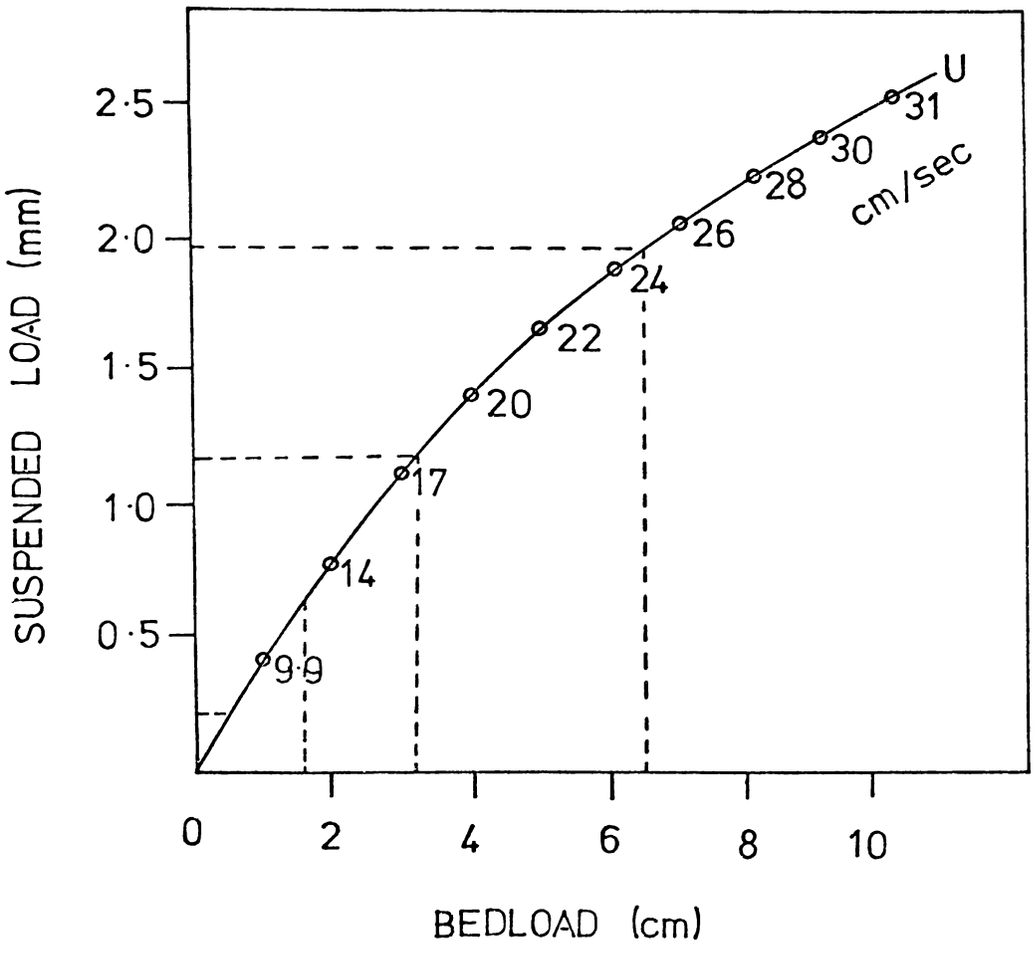

Fig. 6-2. Graph showing the relationship between size of clasts transported by rolling with size of sand suspended by the same flow. For example, if 4 cm pebbles are rolled on the bed (U = 20 cm/sec) sand sizes finer than 1.4 mm (very coarse sand) are maintained in suspension. After Walker 1975.

result in either rolling of gravel on the bed with suspension of sand, or cessation of gravel rolling and deposition of sand for appropriate size distributions (Harms *et al.* 1975). In Fig. 6-1B, cessation of movement of gravel sizes from -5 to -6ϕ (3.2 to 6.4 cm) should result in sand finer than -1.0 to -0.25ϕ (2.0 to 1.2 cm) being maintained in suspension (Fig. 6-2.). However, in Fig. 6-1B there is minimal sediment coarser than -1ϕ associated with this mode.

This may be interpreted in a number of ways. Either no sediment coarser than -1ϕ was available for transport, or it was available but never deposited, or alternatively it was deposited and then removed. The first alternative is unlikely in view of finer grained sediment above and below samples 016, 017 and 018. It is difficult to establish which of the remaining alternatives holds, however, it is significant that the "missing" grain sizes from -5 to -1ϕ abound in overlying unit of the couplet (Fig. 6-1C.). Nevertheless, in view of the larger range of grain sizes in samples 016, 017 and 018 (Fig. 6-1B), it seems unusual that the upper unit (Fig. 6-1C.) is the more poorly sorted. Hence it is possible that at one time a greater quantity of sediment in the range -5 to -1ϕ was deposited, but that it has subsequently been washed out. The presence at the base of the inversely graded unit of a heterogeneous grain-size distribution from -6 to >3ϕ (Fig. 6-1A.) is additional support for this view.

A mean current velocity in the vicinity of 3.5 m/s is indicated for the lower unit of the couplet, and a velocity

of 1.8 m/s for the upper unit (Walker 1975, Fig. 7A.). The environmental significance of textural associations in couplets of Lithotype 1 are considered more fully in Chapter 7.

Grain-Size Distribution of Lithotype 4

Bimodality of pebble and fine sand modes characterises the grain-size distribution of Lithotype 4 (Fig. 6-1D.). Comparison of the average pebble size (1.6 cm) with the fine sand mode (0.2 mm) in Fig. 6-2 establishes marked disparity, indicating suspension of sand until the current velocity had decreased significantly from that when pebble transport ceased. However, the intimate associate of pebbles and sand in the lithotype indicates their contemporaneous deposition. An alternative explanation is that in deposition on a foreset slope (Section 2-6.) the shear velocity relationship may not hold, as gravity is now also a significant force.

Grain-Size Distribution of a Unit in Lithotype 3

Two samples from cross-bedded units, one illustrated in Fig. 2-27, were texturally analysed and the results are presented in Fig. 6-1E. The distribution is clearly bimodal with a greywacke mode from -5 to -3ϕ, and a pumice mode from 0 to 3ϕ. The mean current velocity derived from the greywacke mode is in the vicinity of 1.0 to 1.5 m/s, which compares favourably with the >1.0 m/s suggested by Hume *et al.* (1975) for similar units in the Upper Pleistocene Hinuera Formation.

6-2 COMPOSITION OF CONGLOMERATES

Conglomerates in the Kidnappers Group consist predominantly (>95%) of clasts of indurated sandstone, or "greywacke", typical of that forming much of the axial ranges of the North Island. Of the remaining pebble lithologies chert is by far most important. Hard white Whangai argillite, first noted by Beu & Taylor (1975), and limestone fragments, occasionally occur in the upper most conglomerates of the group, especially the Clifton Conglomerate.

Petrography of Greywacke Pebbles

Thin-sections were made of five pebbles (samples 026 to 030) selected from conglomerates of the Mt. Gordon Beds, 110 ft. Conglomerate, and Clifton Conglomerate. The texture and composition of the pebbles range from well sorted fine sandstones - feldsarenite and lithic feldsarenite - to poorly sorted medium coarse sandstone - feldspathic litharenite. Too few sections were described to confirm the association of increasing lithic content with increasing grain-size and decreasing sorting; nevertheless, it is apparent that the sandstones are highly variable, both in texture and composition.

The greywackes consist of detrital grains of quartz, feldspar, mica and lithic fragments imbedded in a finer grained matrix. Detrital quartz usually forms 10 to 20% of the rock, occurs as angular grains with undulatory extinction, and often has inclusions. Anhedral to rectangular euhedral crystals of detrital feldspar dominate, forming up to 35% of the rock. Plagioclase feldspar displaying multiple twinning dominates by 3:1 over microcline and

untwinned orthoclase. Brown biotite is the dominant ferromagnesian mineral forming amounts of 2 to 5%. Green chlorite with anomalous blue interference colours is a common accessory mineral, occurring mainly as chloritised biotite. Small, colourless or yellowish green epidote, colourless sphene, and blue/green hornblende are sometimes present. Lithic fragments, probably mainly of volcanic origin, form up to 30% of the rock. The lithic fragments are mainly rounded but are often difficult to detect as they grade imperceptibly into the matrix of interstitial silt and clay.

Distinctive intergrowths of quartz and feldspar are present as veinlets up to 1 mm thick, and although zeolite veins are present in hand specimens, none were observed in thin-sections. Detrital feldspars are often highly weathered to kaolin and sericite. This is especially noticeable in poorly sorted coarse arenites where grains have sometimes been completely altered.

X-Ray Diffraction Analysis of Greywacke Pebbles

The bulk mineralogy of eight greywacke pebbles (samples 031 to 038) selected from five formations was determined by X-ray analysis (Section 3-5.). Invariably plagioclase A dominated over plagioclase B and the total wt.% plagioclase feldspar exceeded potash feldspar by 2 to 4 times. The bulk mineralogy of greywacke pebbles is best expressed by the ratios of quartz, feldspar, and clay minerals, since most of the lithic fragments are mainly composed of quartz and feldspar, while the matrix typically consists of clay minerals. The pebbles X-rayed have a generally similar

bulk mineralogy averaging 30 to 50% total feldspar, 20 to 40% quartz, and 25 to 35% clay minerals. On the basis of these samples there appears to be no systematic change in the bulk mineralogy of greywacke pebbles with time through the group.

X-ray analysis, as a rapid means of semiquantitatively determining bulk mineralogy and hence source rock provenance, is limited by the inability to distinguish detrital quartz and feldspar from that in associated lithic fragments. However, where the bulk mineralogic composition of the lithic fragments can be determined, their influence in sediments may be evaluated. For example, it would be of value to determine by X-ray analysis whether greywacke rock fragments, so dominant in the conglomerates, persist into the sands and silts of the Kidnappers Group.

Thirty-nine coarse sand to fine silt samples from the group were X-rayed and the ratio of quartz, feldspar and clay minerals plotted (Fig. 6-4.). An unusual feature is the high relative amount of clay minerals in moderately to well sorted coarse to fine sands. The bulk composition of the coarse to fine sands is only slightly more quartz rich (30 - 45%) than the greywacke pebbles (Fig. 6-3.), and feldspars (30 - 45%) and clay minerals (20-30%) are slightly less. As clay size material is of low abundance in the sandy samples, the clay minerals must be inherited from the greywacke rock fragments. This indicates the importance of the latter in the sands as well as in the conglomerates of the group. Because 35% of the greywacke pebbles (Fig. 6-3.) and 25% of the sands (Fig. 6-4.) consist of clay minerals,

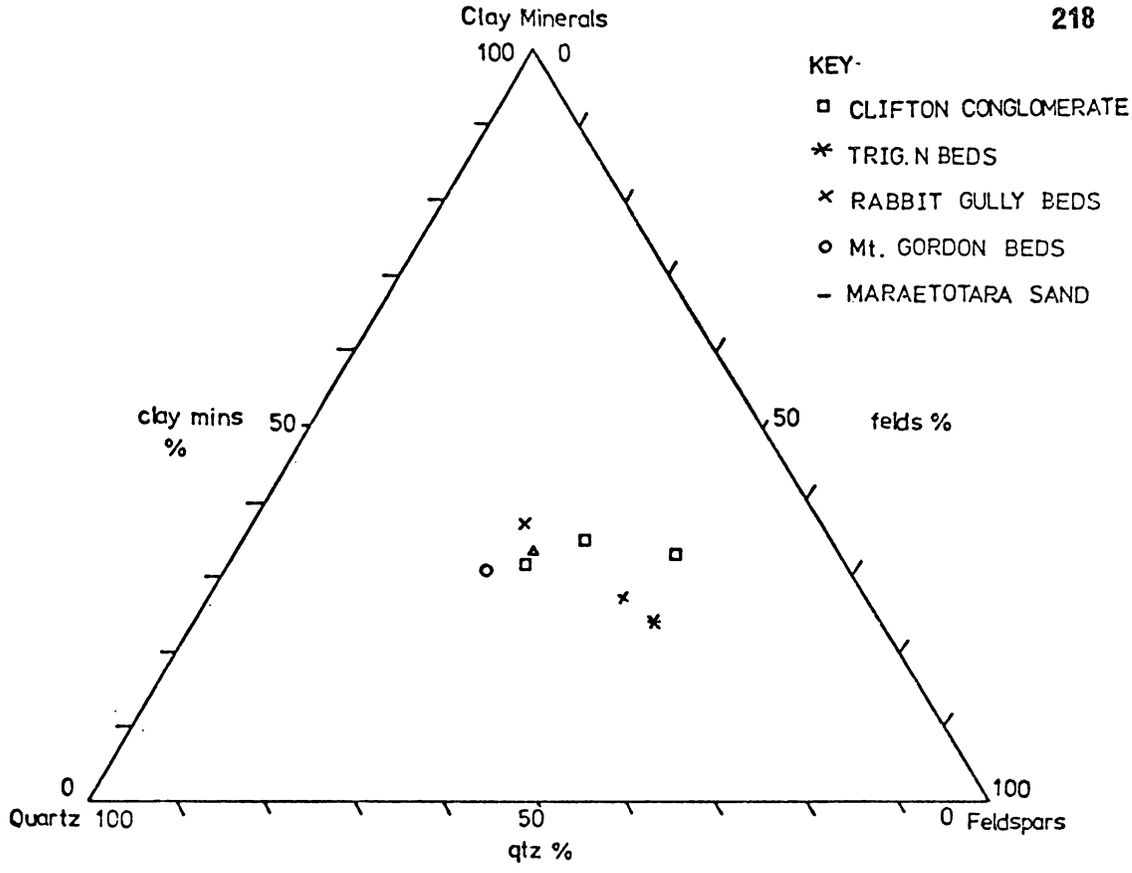

Fig. 6-3. Bulk mineralogy of greywacke pebbles.

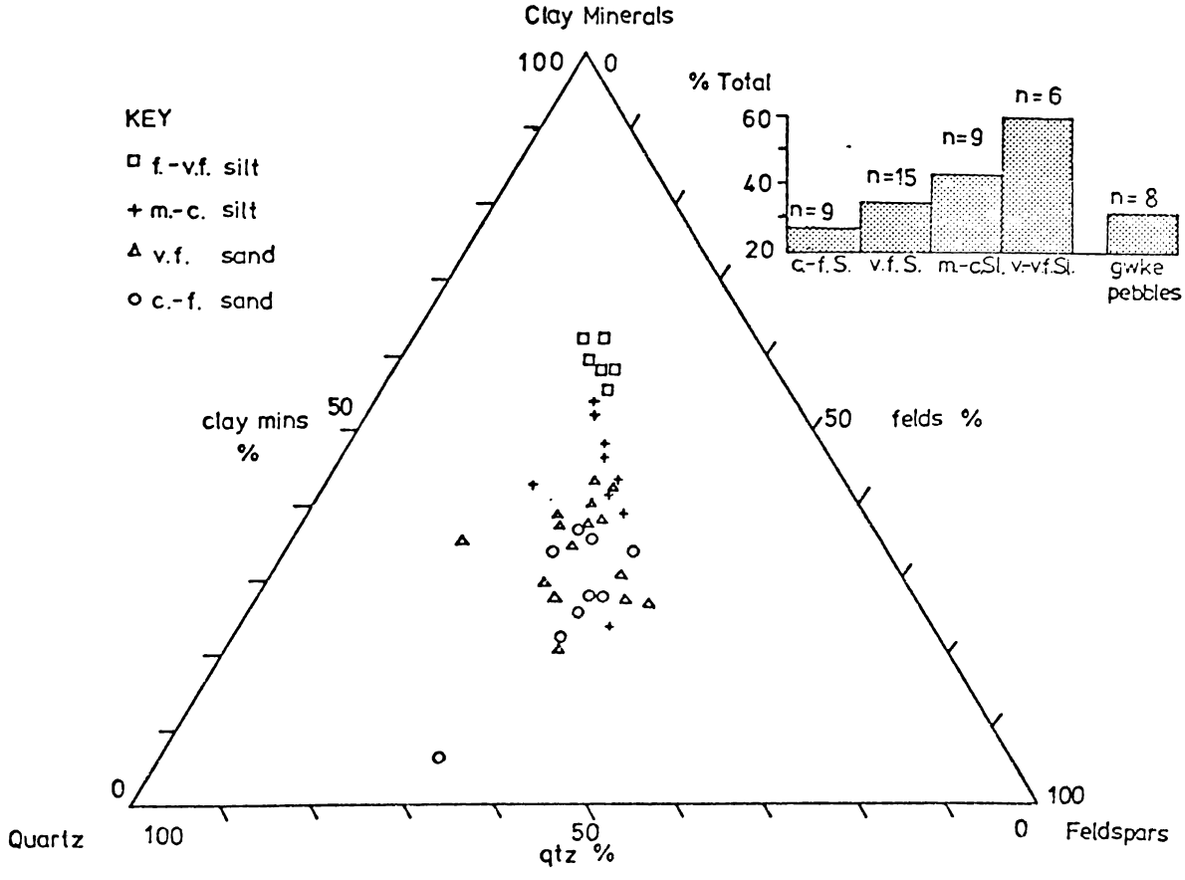

Fig. 6-4. Bulk mineralogy of sandy and silty samples.

then, together with some detrital clay minerals, the sands must contain more than 50% by weight rock fragments.

The mineralogy of the coarse to fine sands was checked optically and by field of view method these grains were composed of 40 - 60% rock fragments (Table 6-1.). It is also apparent in Fig. 6-4 that a linear decrease in rock fragments with grain-size corresponds with a linear increase in the relative abundance of clay minerals.

Sample No.	Rock Fragments %	Felsics %	Others
081	45 - 50	∿40	10
082	40 - 50	∿50	1
083	55 - 60	∿40	2-4
084	48 - 52	∿50	2-4
085	45 - 55	∿50	2
086	55 - 60	∿40	2
087	48 - 50	∿40	4-6
088	55 - 60	∿40	2
089	55 - 60	∿40	2

Table 6-1. Optical determination of percentage rock fragments in coarse to fine sandy units of the Kidnappers Group.

6-3 HEAVY MINERALOGY OF TEPHRIC UNITS

Ferromagnesian Minerals Identified

Ferromagnesian minerals were identified in the 2-4ϕ fraction of samples 039 to 054 using the criteria of Kerr (1959) and Heinrich (1965). Mineralogic notes for heavy minerals follow. Colours are for transmitted light.

Hypersthene:

Colourless to yellow-green, euhedral and subhedral, occasionally well rounded grains. Two pleochroic

schemes are recognised, one strongly pleochroic from bright yellow-orange to mid-green (samples 050 ,051 ,052), and the other colourless or pale green to pale yellow-pink. Straight to slightly angular extinction (1-3°), high relief, with low to moderate interference colours. Occasional inclusions of apatite, magnetite, and glass. Grains in some samples show multiple, needle-like pyramidal terminations. The origin of the sharp terminations is attributed to post-depositional solution along planes of weakness (Seward 1974a). Biaxial -ve.

Hornblende: Predominantly dark-green, elongate, euhedral to subhedral smaller grains and often fractured subhedral to anhedral larger grains. Extinction angles from 1 - 20°, moderate relief with low to moderate interference colours. Pleochroic from light-green to dark-green and occasionally green to brown. Biaxial -ve.

Augite: Colourless to very pale-green stubby grains with some subhedral faces giving the minerals a slight degree of elongation. High relief, with very high interference colours and an extinction angle of 40 - 45°. Some shown to be Biaxial -ve.

Magnetite: Small euhedral to anhedral opaque grains, often exhibiting good crystal faces defining a hexagonal form.

Biotite: Large grains forming irregular to pseudo-hexagonal plates resembling a stack of cards. Green-brown colour, slightly pleochroic. Low relief, low interference colours and a low 2V angle. Incipient alteration to chlorite sometimes observed.

Zircon: Clear and colourless, varying from long acicular euhedral grains to stubby triangular-shaped grains. Straight extinction. Extremely high relief and interference colours which often have a washed-out appearance. Invariably inclusions, possibly apatite, are present.

Calcic-Amphibole: Brown to black or dark brown to burnt orange if oxidised, these grains are slightly larger than hornblende. Interference colours commonly 2nd order greens.

Epidote: Small, euhedral, well rounded grains. Distinctly pistacchio green. Pleochroic from yellow-green to green. Derived from mesozoic rocks.

Apart from epidote the heavy mineral assemblage of the tephras is typically that characterising the rhyolitic deposits derived from the Taupo Volcanic Zone (Ewart 1966; Seward 1976).

Distribution of Heavy Minerals within Different Size Grades

To establish whether mineralogy varies with grain-size and with modification by water action, two trough cross-bedded sets (samples 039 and 040) in the volcaniclastic unit overlying tephra Unit A (Fig. 2-9.) were sampled, separated into ¼ϕ and ½ϕ intervals in the 2-4ϕ fraction,

and the relative heavy mineral abundances determined (Section 3-5.). The results are illustrated in Fig. 6-5 and the data are included in Appendix VI i.

Heavy minerals occur in the sand through coarse silt fractions but are most abundant in the fine and very fine sands. The presence of heavy minerals in the whole sand fraction, and especially their abundance, highlights the mineralogic immaturity of the volcaniclastic sediments.

From Fig. 6-5 it is evident that the trend in mineralogic changes with grain-size are similar for both samples. More importantly, however, there is a large increase in the relative abundance of opaques, mainly at the expense of hypersthene, in the very fine sand fraction. Hornblende shows less relative decrease in abundance with augite also showing little variation. In general the combined 2-4ϕ mineralogy is most similar to the modal class (Fig. 6-5.).

Fig. 6-6 shows there is little difference in the 2-4ϕ heavy mineralogy of samples 039 and 040 compared with that in the parent tephra (041), despite the large difference in wt.% heavies. Therefore, under the influence of water action sufficient to form trough cross-bedded sets, the relative abundance of the major heavy minerals has not changed. On this basis the mineralogy of slight to moderately reworked tephra is probably preserved, and providing there are differences in the abundance of major heavy minerals with successive tephras, valid correlation is possible, However, specific minerals such as biotite are susceptible to selective sorting (Fig. 6-6.).

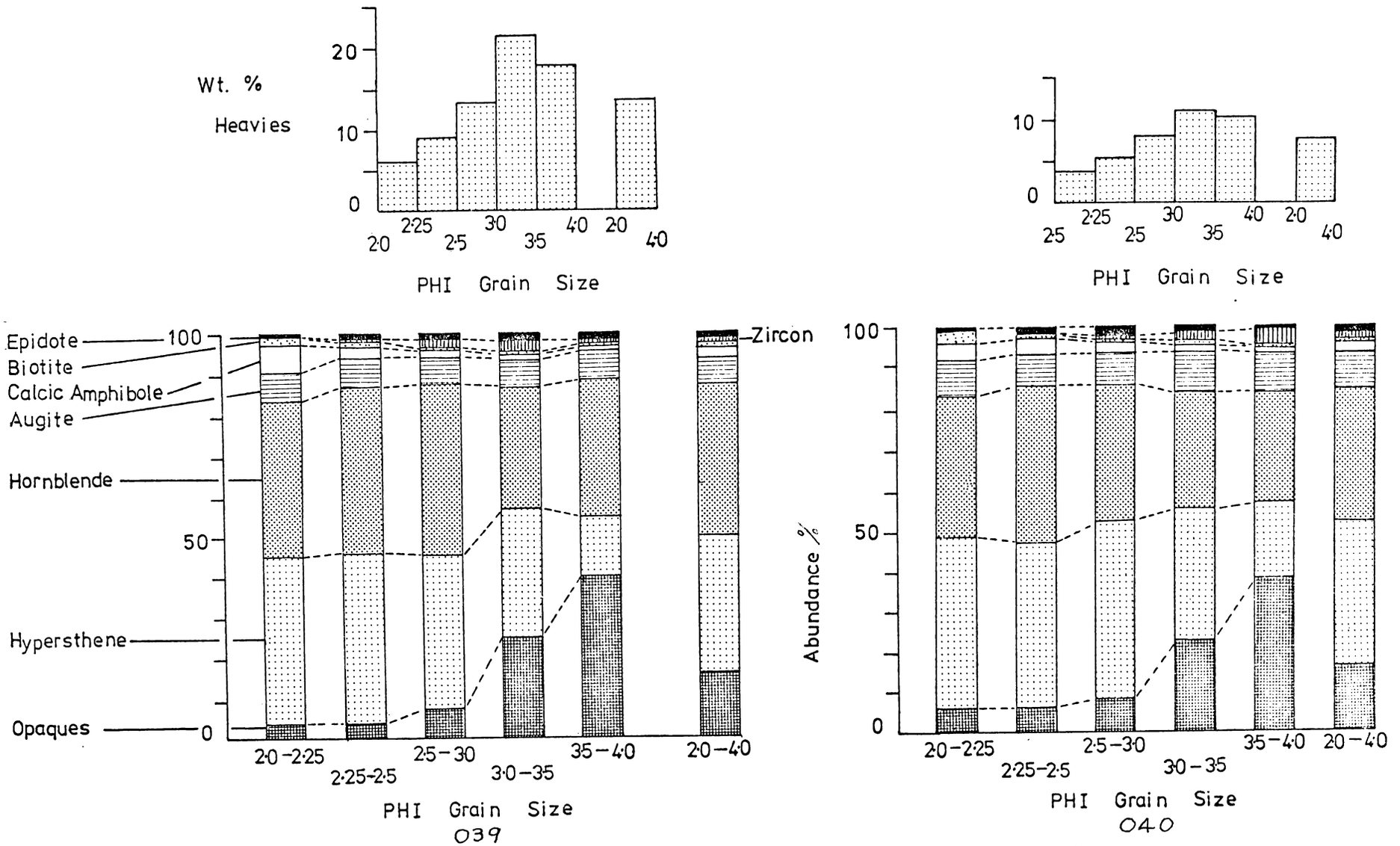

FIG. 6-5. Distribution of Heavy Minerals within Different Size Grades.

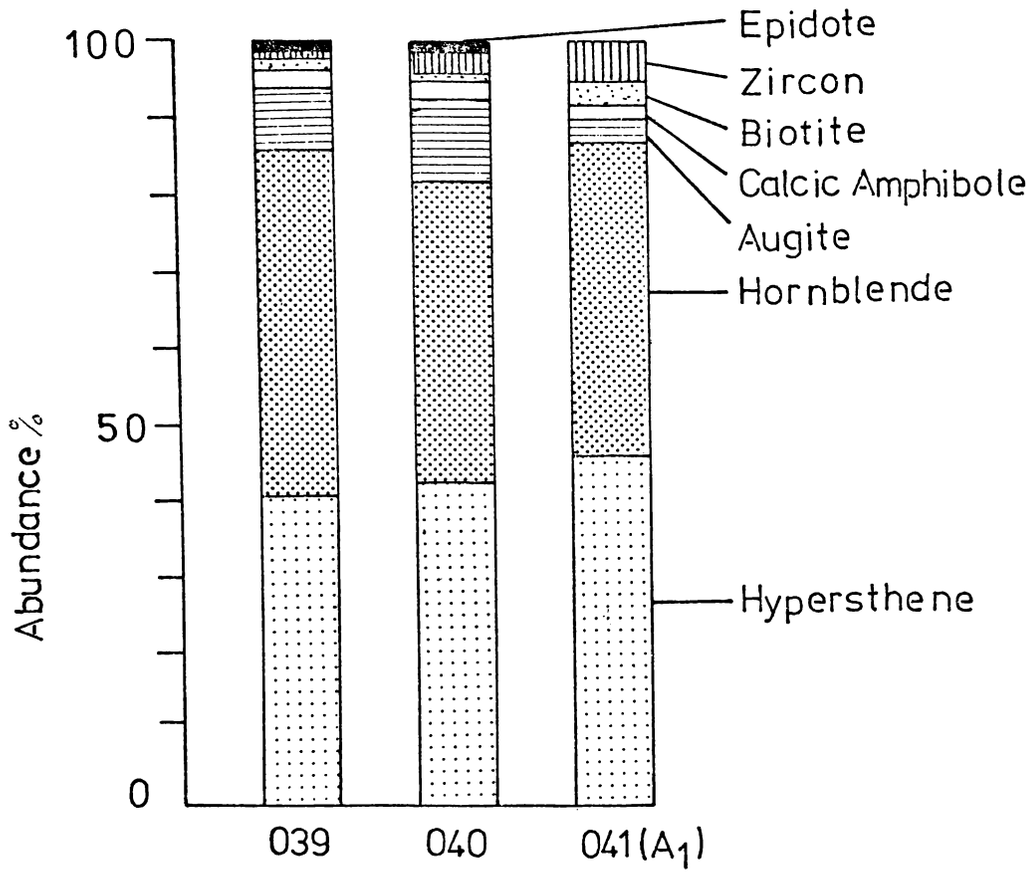

Fig. 6-6. Comparison of the heavy mineralogy of tephric Unit A (041) with its reworked equivalents (039, 040).

Ferromagnesian Mineralogy of the Tephras

Details of the ferromagnesian assemblages of the tephras are summarised in Fig. 6-7 and the data are included in Appendix VIii. A large relative difference in wt.% heavies and opaques occurs between some tephras. This occurrence, and an inverse relationship between wt.% heavies and opaques, may reflect one of a number of influences, such as differences in the eruptive mineralogy of tephras, differential weathering, differences in grain-size and hence mineralogy, or modification due to water action.

As the percent heavy minerals in rhyolitic tephras is normally low, rarely exceeding 5% (Fieldes & Weatherhead 1966), the first alternative is unlikely to explain the magnitude of inter-tephra differences. Differential weathering is not supported as an explanation as normally

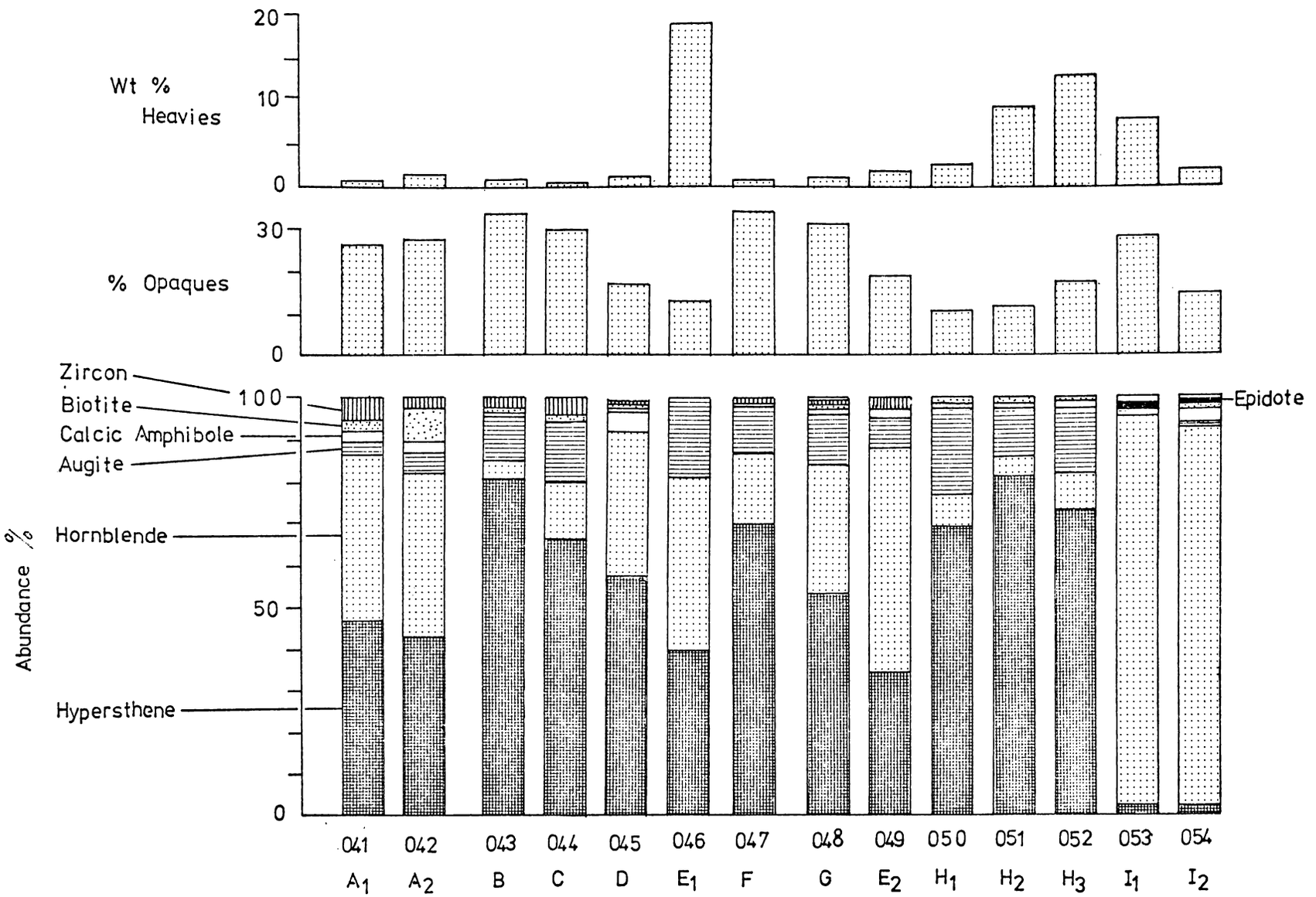

FIG. 6-7 HEAVY MINERALOGY OF TEPHRAS IN THE KIDNAPPERS GROUP

an increase in both wt.% heavies and opaques would occur and not an increase in one and the reverse with the other. Further, the abundance of glass shards, which are readily weathered materials, precludes significant relative enrichment of heavy minerals.

However, modification by sorting may increase the wt.% heavies as demonstrated in Fig. 6-6. Also, an increase in heavy mineral grain-size will concomitantly depress the percent opaques, a corollary of Fig. 6-5. This has occurred in sample 046 (Fig. 6-7.). Current-bedded and flame structures in Unit E_1 are evidence of water action, and the average size of heavy minerals in this unit is 1ϕ larger than the average heavy mineral sizes in all other tephras in the group. Therefore, abnormally high amounts of heavy minerals and lower than average percent opaques probably reflect reworked tephra. This situation for tephras in the group (Fig. 6-7.) is supported by field observations where samples 046, 053, 051, 052 and, to a lesser extent, 050 and 054, show some evidence of current bedding.

Tephra Correlation

Correlation of tephras in the Kidnappers Group was established on the basis of similarity in the relative abundance of hypersthene, hornblende and augite, and on field characteristics (Chapter 2). Coastal and inland tephras can be confidently grouped in three cases (Fig. 6-8.). Correlation of Units A_1 and A_2 (samples 041 and 042) is also supported by the biotite content which agrees with its reported occurrence by Seward (1975) in sample 217 from the same unit.

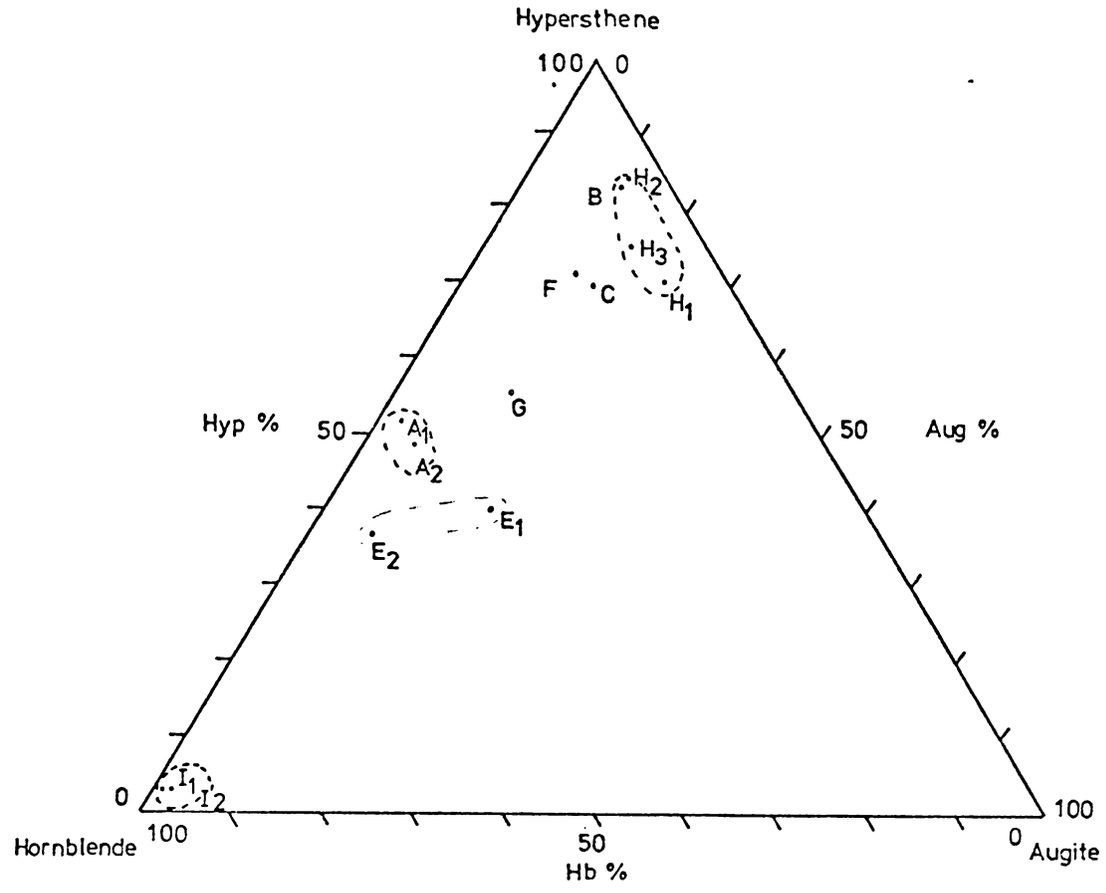

Fig. 6-8. Correlation of tephric units on the relative abundance of hypersthene, hornblende and augite.

The dominance of hypersthene in Units H_1, H_2 and H_3 (samples 050, 051, 052) and exclusion on a stratigraphic basis (Fig. 2-9.) of Units B, C and F affords good correlation across the basin (Fig. 2-9.). Similarly Units I_1 and I_2 (samples 058 and 059) are correlated on their hornblende abundance. Although samples 050 and 054 may have been slightly reworked, it is believed differences in the mineralogy of units H and I reflect real difference in eruptive mineralogy of the tephras.

A tentative correlation is made between Units E_1 and E_2 (samples 046 and 049) Fig. 6-8.). On the assumption that all tephras in the inland sections are present on the coast, then E_2 approximates E_1 more closely than any other coastal tephra.

CHAPTER 7: PALEOENVIRONMENTS

> *Facies models for environments of conglomerate deposition are poorly developed, mainly because of the general absence of a descriptive framework - that is, there is little agreement as to the features that must be observed and recorded in outcrops of conglomerate.* (Harms *et al.* 1975, p133).

In this chapter an attempt is made to determine the depositional environments of conglomerates in the Kidnappers Group. The various lithotypes established earlier correspond to environmentally sensitive facies. The depositional history of the group is interpreted from the succession of these facies and from the alternation of conglomeratic and finer-grained lithologies.

7-1. MARINE AND FLUVIAL CONGLOMERATES IN THE GROUP.

Marine and fluvial conglomerates have been distinguished in this study on the basis of their fossil content, their clast orientation fabric and clast shape, and their stratigraphic relation to adjacent beds of known marine origin.

Fossil Content

Inclusion of marine fossils in conglomerates in a whole or smashed condition in sufficient concentration to preclude transport by birds is nearly always an indicator of marine deposition. Shell fragments are a constituent of Lithotypes 4 and 5 only. The absence of fossils, however, does not necessarily preclude a marine origin as, for example, the coarseness of the substrate may have prevented organism growth.

Clast Orientation Fabric

The ab planes of clasts in Lithotype 1 (Clifton Conglomerate) consistently dip west and north-west. The monoclinic symmetry displayed by the ab plane poles (Figs. 5-6, 5-10, 5-12, 5-14 and 5-16) is characteristic of fluvial gravels deposited under the action of gravity plus a unidirectional current (Potter & Pettijohn 1963). Upstream imbrication is confirmed by paleocurrent directions derived from the dip direction of foreset beds (Section 5-3.). In comparison, the ab plane poles of clasts at Site 6 (Clifton Sand) show orthorhombic symmetry (Fig. 5-4.). This fabric is interpreted as forming from the action of widely diverse currents periodically reorienting clasts in a marine environment (Section 5-2.). Marine deposition for Lithotype 5 (Site 6) is supported by the abundance of marine fossil fragments, and by the widely opposing current directions indicated by cross-bed directions.

An average difference in imbrication angles of 15° between Sites 1 and 6 (Fig. 5-7) is comparable with the difference between the inclination of clasts in modern fluvial and marine environments (Pettijohn 1975; Rust 1975).

Clast Shape

The interpretation made from clast shapes of inferred fluvial, marine and unknown conglomeratic environments (Section 4-5.) is that pebbles from Lithotypes 1, 2, 3, and 5 have typically fluvial shapes while those from Lithotype 4 have shapes more characteristic of a low energy beach (Dobkins & Folk 1970). However, as discussed above, Lithotype 5 is most probably a marine deposit. The environmental significance of this dichotomy is discussed more fully in Section 7-4.

Stratigraphic Context

In a number of cases fossiliferous marine units bound the upper and lower extent of conglomerates (Log I). Where conglomerates are thin and lense-like, the depositional environment is probably marine (e.g. Lithotypes 4 and 5 in the Maraetotara Sand and Clifton Sand respectively). Conversely, where conglomerates are thick and continuous, the environment of deposition is probably non-marine (e.g. Lithotype 1 in the Clifton Conglomerate). As Lithotypes 2 and 3 are bounded, at most, by only one contact with fossiliferous marine units, their depositional origin is most probably non-marine.

Summary:

From these various lines of evidence any one feature of the conglomerate cannot be confidently identified as being marine or fluvial. Nevertheless, the evidence taken together points towards a fluvial origin for Lithotypes 1, 2 and 3, and a marine origin for Lithotypes 4 and 5.

7-2. BRAIDED RIVER ENVIRONMENT

In view of the coarseness of conglomerates in Lithotypes 1, 2 and 3, the depositional setting anticipated for the greywacke conglomerates of the group, is one of a braided fluvial environment.

Braided streams are characterised by high width/depth ratios, steep slopes and generally low sinuosities (Miall 1977). They consist of a series of rapidly shifting channels and mid-channel bars, the whole environment being flooded during periods of high discharge. The deposits of braided rivers are

normally coarser than those of other river types, and are dominated by sand or gravel (Miall 1977).

Environmental interpretation of ancient braided stream deposits has been aided by establishing the relationship of bar types to stratification in modern braided rivers (Smith 1974; Boothroyd & Ashley 1975; Harms *et al.* 1975; Hein & Walker 1977).

Common Associations of Features in Conglomeratic Lithotypes 1, 2 and 3.

The common associations of features which define Lithotypes 1, 2 and 3 (Section 2-6) are summarised in Fig. 7-1. Noticeable differences between these Lithotypes identify a proximal-distal sequence within the braided fluvial environment. Each of Lithotypes 1, 2 and 3 encompasses facies characteristic of their position in this sequence.

Gravel Bar Terminology

Gravel accumulations in braided rivers are collectively called bars. Where they divide the flow and cause the braided pattern they are informally referred to as braid bars (Allen 1965; Rust 1972a). Braid bars may have a simple depositional history, in which case they are known as unit bars (Smith 1974; Hein & Walker 1977), but more typically they have a complex history of multiple episodes of deposition and erosion. Four types of unit bars have been commonly recognised in modern braided rivers (Fig. 7-2.).

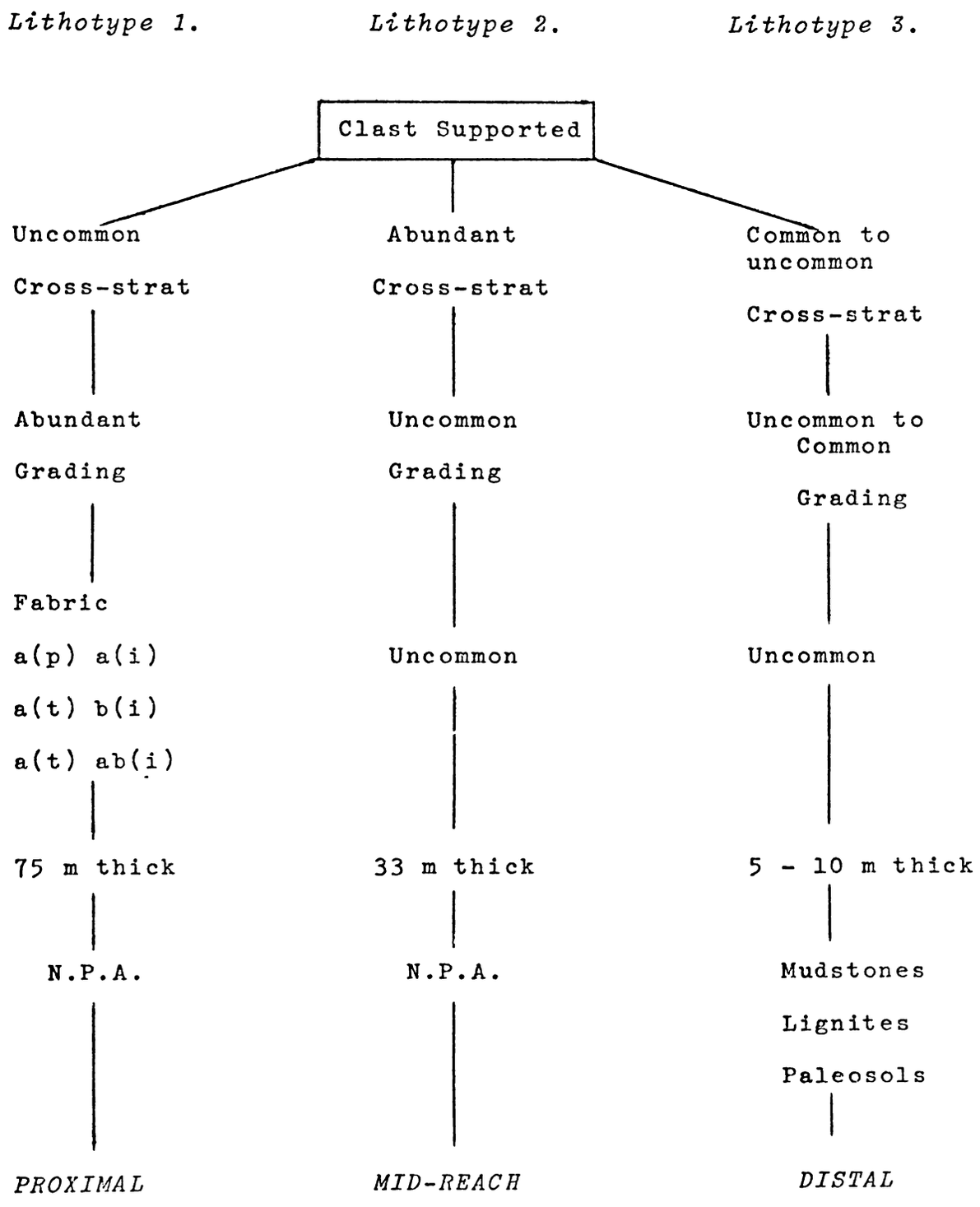

Fig. 7-1. Common associations of features in conglomerates which define facies changes from proximal to mid-reach to distal areas of a braided river environment. N.P.A. means no preferred association with other lithologies.

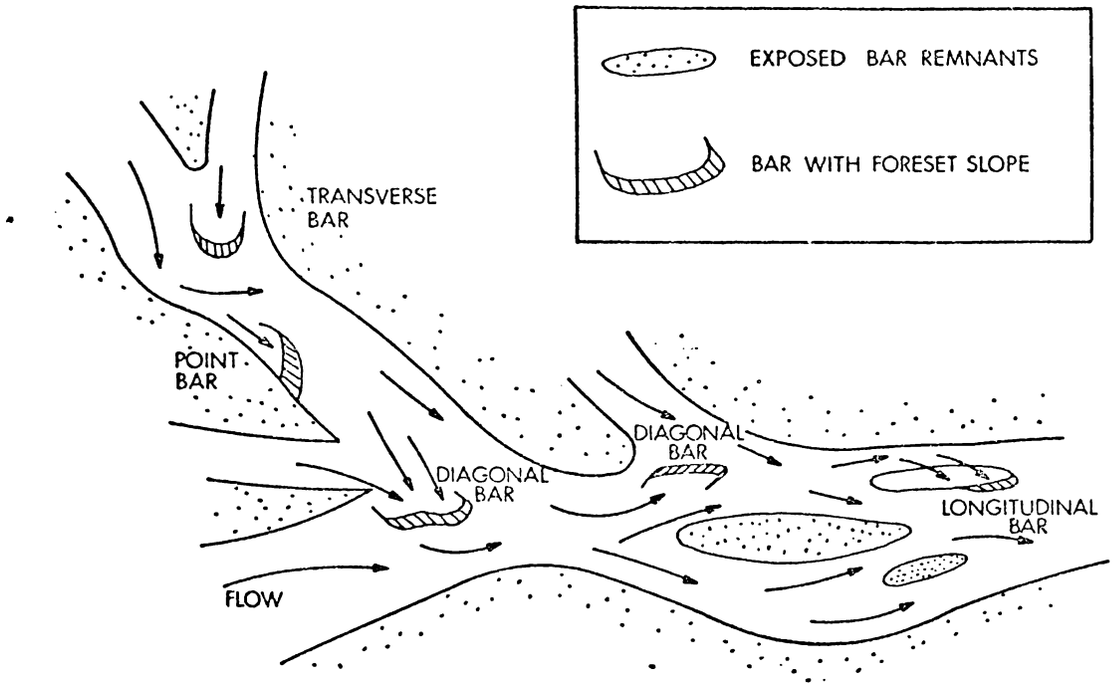

Fig. 7-2. The common gravel bar types in modern braided rivers (After Hein in Harms et al. 1975).

7-3. CONGLOMERATIC LITHOTYPES 1, 2 and 3, AND THEIR FACIES EQUIVALENTS

Lithotype 1 - Channel Lag and Longitudinal Bar Facies.

This lithotype consists of a recurring couplet having a lower inversely graded unit and an upper normally graded unit (Fig. 2-18.). From various lines of evidence, including the features summarised in Fig. 7-1, Lithotype 1 is interpreted as proximal channel and longitudinal bar facies in a braided river environment.

Evidence from Clast Orientation Fabric:

An investigation of the origin of clast orientation at Site 1 (Section 5-5.) revealed the following features:

(i) The a-axes of large clasts are either parallel or transverse to paleocurrent direction.

(ii) The smaller clasts are dominantly transverse to paleocurrent direction.

(iii) Imbrication is primarily developed by post-depositional clast reorientation.

This orientation fabric may have formed during a flood and falling-stage regime. During flood flows the total sediment population moves in traction, saltation and suspension modes. As the flood-stage begins to fall the flow becomes partially incompetent and the larger clasts are deposited. Immediately prior to deposition the large elongated clasts with a-axes transverse to flow move as bedload by rotation about the a-axis. The large oblate clasts, however, having a-axes both transverse and parallel, move in saltation by tumbling about the b-axis. With continued fall in flood-stage the remaining population is deposited. The dominance of a-axes orientations transverse to flow for smaller clasts indicates movement in the traction mode by rotation about the a-axis.

To maintain dispersion of clasts above the bed, strong currents are required, a condition also needed for the development of clast imbrication (Bluck 1976; Rust 1975). Further evidence for strong current activity is found in the low directional variance of paleocurrents in the Clifton Conglomerate (Fig. 5-18.) and the slightly higher than normal imbrication angles (c.f. Pettijohn 1975).

Evidence from Grading, Sorting and Size Distribution:

The lower unit in the couplet of Lithotype 1 may be only one pebble diameter thick or an inversely graded unit up to 30 cm thick (Section 2-6, Fig. 2-18.). Inverse grading in

the lower unit and normal grading in the upper unit is evident both in the field and in textural analyses of selected couplets (Fig. 6-1.). Davies & Walker (1975) related the presence of inverse grading to size sorting within a layer of clasts maintained above the bed by dispersive pressure. The working of smaller clasts down through the layer, the so-called kinetic sieve mechanism, is regarded by Middleton (1970) as the dominant process forming inverse grading, rather than the movement of larger clasts to a region of minimal shear stress. High concentrations of dispersed clasts, a high shear stress, steep slopes and proximal environments are implied by Walker (1975) for the formation of inverse grading.

An improvement in sorting, positive skewness, and the absence of granules and small pebbles in the upper part of the inversely graded unit (see Section 6-1.), is significant in view of the well developed clast imbrication at the same position. The absence of sediment in the size range -1 to -4ϕ, and its abundance in the overlying normally graded unit, suggests sediment has been washed out of the lower unit to form an imbricate open-work deposit.

The washing out of fines concomitant with formation of a lag deposit has been observed in modern braided rivers. Hein & Walker (1977) related bar front migration to velocity increases upstream and to increased jostling of the coarse bedload material washing out the finer clasts. Bluck (1967, 1976) invoked the washing out of fines as the process forming positively skewed coarse lag deposits. Further, Bluck equated reworking to be an indicator of non-uniform flood flows.

Fahnestock & Haushild (1962) observed experimentally that reorientation of pebbles was enhanced by selective erosion of interstitial sand.

Hence, it is suggested that after emplacement of the inversely graded unit continuing strong flows washed out the fines and reoriented clasts *in situ*. A fall in the flood-stage, together with downstream sorting of small pebbles and granules, resulted in deposition of the normally graded unit. Mean flow velocities in excess of 3.5 m/sec. occurred at the time of emplacement of the lower unit in the couplet, and this had fallen to less than 1.8 m/sec. with deposition of the upper unit (Section 6-1.).

Evidence from Shape:

A clast size-dependent and size-independent relationship with shape was established in Section 4-7. In particular, the larger sizes are dominantly oblate and the smaller sizes range from bladed to prolate. Bradley *et al.* (1972) and Spalletti (1976) consider that platy (or oblate) clasts move in suspension with an erratic saltation motion but when deposited are the most stable clast shape, as they provide most resistance to flow. Therefore, concentrations of large oblate clasts may be interpreted as a lag deposit where the smaller pebbles have been washed out. In this case, clast shape is a facies indicator.

Channel Lag and Longitudinal Bar Facies:

From the various lines of evidence discussed above Lithotype 1 is interpreted as a flood and falling-stage deposit. The formation of the lower unit in the couplet is not dissimilar to that postulated for the diffuse gravel sheets described

by Hein & Walker (1977). However, in their study of the Kicking Horse River in British Columbia, diffuse gravel sheets were only a few pebble diameters thick and no mention was made of an inversely graded unit. The difficulty of observing braided rivers in flood, and of trenching gravel bars, may be the reason that inversely graded units have not been previously described.

The development of channel bars from diffuse gravel sheets according to the scheme envisaged by Hein & Walker (1977) is summarised in Fig. 7-3. In view of this model, the crudely horizontally bedded, normally graded unit of Lithotype 1 reflects vertical aggradation and the formation of longitudinal and/or diagonal bar facies. The low paleocurrent directional variance (Fig. 5-18.) suggests that longitudinal bars with symmetrical current flow are the most likely bar facies (Fig. 7-3.). The crude horizontal bedding evident in the upper unit is typical of that described for longitudinal bars (e.g. McDonald, & Banerjee 1971; Smith 1970, 1974; Harms *et al.* 1975; Rust 1975; Church & Gilbert 1975; Hein & Walker 1977; Miall 1977).

The facies associations of Lithotype 1 imply high fluid and sediment discharge in proximal reaches of a braided river. Steep depositional slopes are implied by the dominance of coarse-grained channel and bar facies, and by the absence of any overbank deposits.

Lithotype 2 - Transverse and Longitudinal/Diagonal Bar Facies.

Lithotype 2 consists of planar sets of cross-stratified conglomerate (Section 2-6.). This lithotype occurs mainly in the 110 ft. Conglomerate as solitary sets near the base but

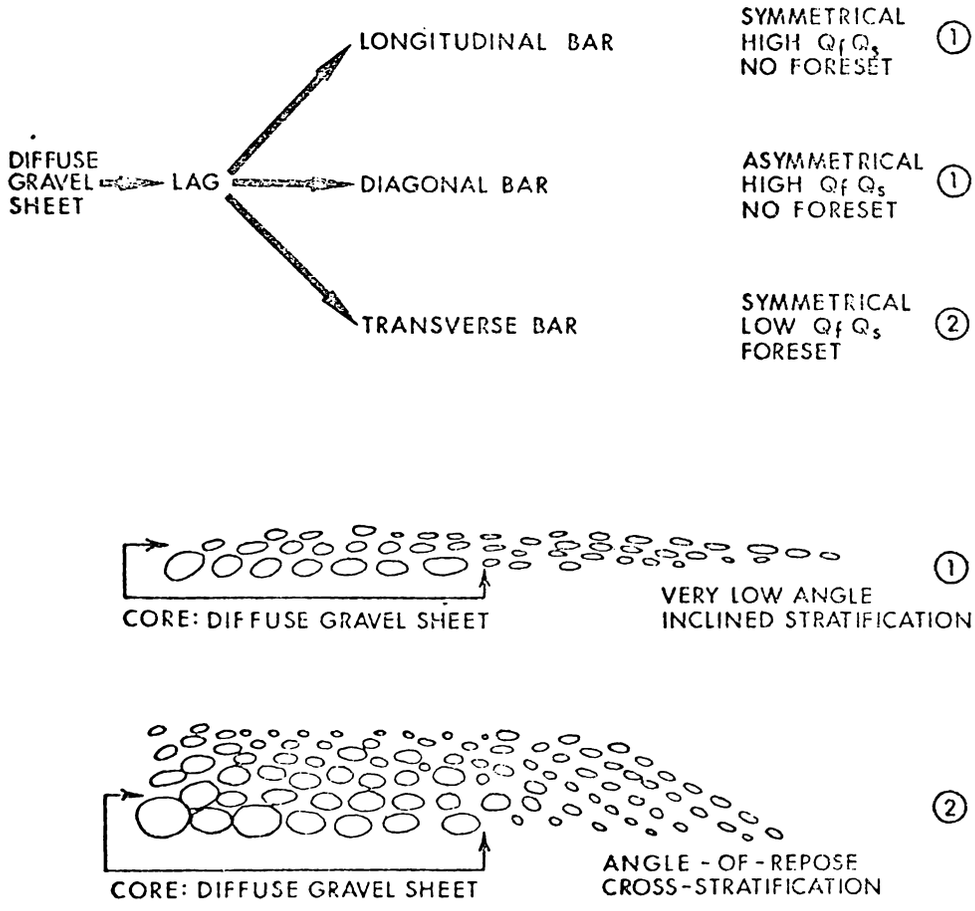

Figure 7-3. Relationship between bar types and stratification. As the diffuse gravel sheet stops moving, it forms a lag, which can develop into a longitudinal bar if flow on either side of the bar is symmetrical. If flow is asymmetrical (higher discharge on one side than the other), the bar will be diagonal to the main stream direction. If fluid discharge Q_f and sediment discharge Q_S are both high, gravel will move across bar top and growth will be downstream. If Q_S and Q_f are low, the bar will tend to aggrade, build a steeper downstream face, and eventually form angle-of-repose cross-stratification. The horizontal or low angle stratification (1 in diagram) is associated with longitudinal and diagonal bars without angle-of-repose foreset slopes. High-angle cross-stratification (2 in diagram) tends to be associated with transverse bars with foresets. *(After Harms et al. 1975; Hein & Walker 1977).*

as cosets higher in the formation. Massive, polymodal, clast supported conglomerates occur throughout the formation but are especially associated with the solitary sets.

The large scale cross-stratification is formed by downstream migration of avalanche faces of migrating transverse bars (e.g. Doeglas 1962; Ore 1964; Collinson 1970; Smith 1970, 1974; Rust 1975; Hein & Walker 1977). The massive to crudely horizontally bedded conglomerate is formed by the aggradation of longitudinal and/or diagonal bars (Smith 1974; Hein & Walker 1977). In modern gravelly braided rivers these bars form by vertical aggradation of a diffuse gravel sheet where transverse bars preferentially form under low flows and longitudinal/diagonal bars under conditions of high sediment and fluid discharge (Fig. 7-3.). Hence, the association of these bars in the lower parts of the 110 ft. Conglomerate relates to formation of different bar types with varying discharge conditions.

Passing upwards through the formation the abundance of planar cross-bedded sets increases markedly. This is paralleled by an increased separation of paleocurrent modes and by a tendency for the paleocurrent directions to become more easterly with time (Fig. 5-8.). The angular separation of modes ranges from 34° to 130°, with the profusely cross-bedded middle and upper parts falling within the range of 90° to 130°. The dip directions of foreset beds in modern braided rivers are also typically bimodal, their separation ranging from 90° to 180° (Ore 1964; Bluck 1976). Therefore, on the basis of current directional variability and internal stratification, Lithotype 2 probably formed by the migration of transverse bars in association with longitudinal/diagonal bar facies.

From Hein & Walker's (1977) model (Fig. 7-3.) an increase in the abundance of transverse bars corresponds to a decrease in fluid and sediment discharge. At periods of low flow the reworking of channel bars, and especially their dissection, are emphasised as the method of forming avalanche faces (Ore 1964; Smith 1974). Also a sudden increase in depth by flooding will result in a height differential and deposition of successive transverse bars (Smith 1974) to form the profusely cross-stratified nature of the 110ft. Conglomerate.

The disrupted mudstone lenses associated with Lithotype 2 in the 110 ft. Conglomerate formed during flood events and attest to periodic deposition of mud in low energy back-water areas during normal flow. The facies associations of Lithotype 2 imply lower fluid and sediment discharges than do those of Lithotype 1, probably on moderately steep slopes in the mid-reach of a braided river system.

Lithotype 3 - Channel and Topstratum Deposits

Any paleoenvironmental interpretation of the thin conglomerates of Lithotype 3 is exceedingly difficult on the basis of their internal characteristics alone. However, recognition of recurring features (Fig. 7-3.) in the conglomerates, and especially their association with other lithologies, has enabled the synthesis of two idealised sequences (Figs. 2-26 and 2-28.).

Lithotype 3 is a fining upward cycle from basal massive, poorly stratified conglomerates, into cross-stratified conglomerates and sands, and then into mudstones. This sequence probably corresponds to a progression in the distal reaches of a braided river environment from channel bar facies through

to topstratum overbank deposits. Within Lithotype 3 two subtypes are recognised on the basis of association with paleosols in Lithotype 3A and with lignites in Lithotype 3B (Figs. 2-26 and 2-28 respectively).

The fully developed fining upward cycle comprises three main parts: a lower coarse-grained division, an upper fine-grained division, and a capping of either a lignite or a paleosol. The conglomeratic member lies on either an erosional or a non-erosional surface (see Section 2-6.).

It was earlier suggested in this Section that massive poorly stratified conglomerates formed by accretion of longitudinal bars and/or diagonal bars, while planar cross-stratification formed by migration of transverse bars. Low-angle inclined stratification in the upper parts of conglomerates (Figs. 2-26 and 2-28.) may reflect infilling of broad shallow channels (Fig. 2-29.) or local scours, or alternatively be the accretion deposits of point bars (Harms *et al.* 1975). On occasions, sandy cross-beds, resulting from the migration of small transverse bars, may infill the paleochannels.

The medium and small scale planar or trough cross-beds and ripple sands in Lithotype 3A formed by the migration of dunes and ripples across bar surfaces during low water-flows (Miall 1977). The upward change in grain-size from conglomerate to sandstone and from conglomerate to mudstone is always sharp. The fine-grained unit in Lithotype 3B is typically mudstone with rare interbedded fine sandy units. The mudstone superficially appears to be massive but on close inspection micro-horizontal laminations are evident. This unit is interpreted as representing deposition of suspended sediment in overbank areas.

Paleosols and lignites as upper members of Lithotype 3 are important as they signify emergence of a flood plain for some time, enabling growth of organic material.

Longitudinal bar migration typifies the upper reaches of braided rivers, but under moderate to high-stage flooding, longitudinal bar growth by slipface migration has also been reported in the lower reaches of outwash fans (Boothroyd & Ashley 1975). Erosional lower contacts and the incorporation of rip-up clasts are further evidence of initially high currents. The increasing vertical incidence of small scale cross-stratification indicates fluid and sediment discharge characteristics more typical for distal reaches of braided rivers.

Braided streams are not characterised by large areas of flood plain. Nevertheless, abandoned areas with variable amounts of vegetation cover have been reported in the distal reaches of modern braided rivers (e.g. Doeglas 1962; Williams & Rust 1969; Smith 1974; Boothroyd & Ashley 1975; Miall 1977) and in ancient analogues (e.g. Bluck 1967; Kelling 1968). Accumulation in modern braided rivers of fine beds up to 2 m thick (Smith 1974; Boothroyd & Ashley 1975) is comparable to the thickness of mudstone units in Lithotype 3 (Section 2-6.). The trapping of fine sediment is encouraged by vegetation which ultimately becomes the source for the lignites (Bluck 1967; Kelling 1968).

The sudden upward change in grain-size above the conglomerate most probably relates to channel shifting by avulsion (Miall 1977). Therefore, where the percent sandstone and mudstone is low and Type 2 lignites predominate, the restricted

upper reaches of a flood plain are suggested. Conversely, where mudstones and sandstones are well developed and Type 1 lignites predominate, lower regions of a flood plain are more probable..

Proximal - Distal Sequence.

The features of Lithotypes 1, 2 and 3 (Fig. 7-1.) define facies typical of those in proximal, mid-reach and distal areas of modern braided rivers. In-channel diffuse gravel sheets and longitudinal bars (Lithotype 1), increasing amounts of transverse bars (Lithotype 2), and fining upward cycles of channel and topstratum deposits (Lithotype 3) are similar to downstream changes in braided rivers reported by Church & Gilbert (1975) and Boothroyd & Ashley (1975).

Included in Fig. 7-4 is a summary of the fluvial conglomeratic paleoenvironments and their stratigraphic position in the Kidnappers Group.

7-4. MARINE CONGLOMERATES OF DELTAIC AND ESTUARINE PALEOENVIRONMENTS

A marine origin for Lithotypes 4 and 5 was established in Section 7-1. Marine conglomerates are only volumetrically important in the Te Awanga Beds.

The high-angle planar cross-beds of Lithotype 4 are interpreted as representing deposition on the foreset slope of a prograding delta. The pebbles have shape attributes typical of those on a low energy beach (Fig. 4-12.), and indicate some wave abrasion of the sediment on a shoreface or barrier spit. The marine conglomerates of Lithotype 4 in the Maraetotora Sand are considered to have formed by progradation

of an alluvial plain from the west, which formed a shallow embayment and eventually estuarine conditions as now evidenced in south-western exposures of the formation (Kamp, in prep.).

In Lithotype 5 the overwhelming evidence for a marine origin (Section 7-1.) contrasts with the fluvial shape characteristics of the pebbles (Fig. 4-12.). This dichotomy is resolved by envisaging deposition in a restricted marine environment where there was insufficient wave energy to modify pebble shapes (Sames 1966). An estuarine/subtidal origin for Lithotype 5 is supported by the paleoenvironmental interpretation of the enclosing fine-grained, fossiliferous marine sediment (Log L). The lenticular shape of the conglomerates indicates that they may have infilled paleochannels of tidal origin.

The stratigraphic position and paleoenvironments of the marine conglomerates are included in Fig. 7-4.

Paleosols

From their horizon colours, compacted nature and subgammate pattern (Section 2-4.), the paleosols in the Mt. Gordon Beds appear similar to modern yellow-grey earths (Gibbs 1969). However, the degree of development and preservation of the paleosols, in view of their age and depth of burial (300 m), require some explanation.

If the concentration of organic material in the uA horizon is a compaction feature resulting from depth of burial, then the original A horizon must have been three or four times thicker than the present uA horizon. This is atypical of yellow-grey earths, whose A horizons generally are poorly developed. Alternatively, the organic material may have been concentrated by leaching of an overlying bed with subsequent movement into the paleosol. This alternative is considered unlikely, however, as there are no organic horizons in the overlying 100 m of sediment, and there is no evidence of organic staining in the tephras immediately overlying the paleosols (e.g. Fig. 2-7.). The most likely explanation for the well developed uA horizons involves selective preservation due to the stability of the humus-allophane colloidal complex, a condition known to cause the persistence of colour and structure in uA horizons of paleosols derived from volcanic parent materials (Gibbs 1971).

A second difficulty in classifying the paleosols as buried yellow-grey earths lies in their extremely indurated nature. A compacted subsurface fragipan is an important feature of New Zealand yellow-grey earths (Gibbs 1971). However, only in exposures subjected to pronounced wetting and drying do

modern yellow-grey earths approach the degree of compaction exemplified by the paleosols in the Mt. Gordon Beds (Prof. H.S. Gibbs, pers. comm.). For the paleosols to represent fossil yellow-grey earths, post-burial induration, which reinforced pedogenic compaction, must be shown to have occurred.

As tephras immediately overlying the paleosols are loose and display undisturbed shower bedding, and as the underlying siltstones are relatively soft (e.g. Fig. 2-7.), the induration cannot be explained by depth of burial. Rather, it is anticipated that dissolution and movement of silica from the overlying tephras into the pore spaces of the paleosols is responsible for the degree of induration. This process probably occurred soon after burial and would have been aided by the extremely porous nature of the overlying conglomerates and the low sedimentation rates in the Mt. Gordon Beds (Fig. 7-6.).

The origin of fragipans in New Zealand yellow-grey earths is not clearly resolved. Some pedologists (e.g. Raeside 1964) attribute the fragipan to compaction during accumulation of parent material, so that time is the dominant factor, while others (e.g. Prof. H.S. Gibbs. pers. comm.), explain the fragipan as being formed by alternate wetting and drying, with climate the dominant factor. If the second hypothesis is correct, and the paleosols in the Mt. Gordon Beds are in fact yellow-grey earths, then they probably formed under a climate similar to that where yellow-grey earths presently occur, namely one characterised by 700 to 1000 mm of rainfall with distinct moist and dry seasons.

Lignite Paleoenvironments

The paleobotany reported here is that discussed by R.A. Cooper in Kingma (1971). Pollen grains of *Nothofagus* (beech) and Podocarpaceae (conifers) are very rare in the Kidnappers Group suggesting that beech and conifer forest was a considerable distance from the site of active sediment accumulation. The vegetation represented is mainly that of alluvial flats with swampy patches. *Podocarpus dacrydioides* (kahikatea) and probably *P. totara*, *Leptospermum* (manuka), *Coprosma*, Cyperaceae (sedges), and Gramineae (grasses) are the main elements. Spores of tree ferns and other ferns, probably growing in nearby gullies, are also abundant.

The flora of the Kidnappers Group indicate a rainfall of probably less than 1000 mm per annum, but there is no evidence of markedly cool or warm temperatures. In fact, the flora suggest a climate similar to that in Hawke's Bay at present. The lignites probably formed during river flooding, which buried and preserved the surrounding vegetation. Only in a lignite in the Trig. N Beds (Lithotype 1) is there evidence of peat formation.

7-5. PALEOENVIRONMENTAL SUCCESSION

The depositional environments of conglomeratic lithotypes in the Kidnappers Group sediments range from proximal fluvial through distal fluvial to nearshore subtidal (Fig. 7-4.). In general, the conglomeratic lithotypes in the coastal section are more distal facies than their equivalents in the inland section (Fig. 7-4.). From the stratigraphic distribution of conglomeratic lithotypes and fossiliferous sandstones and mudstones, it is evident that the Kidnappers paleoshorelines

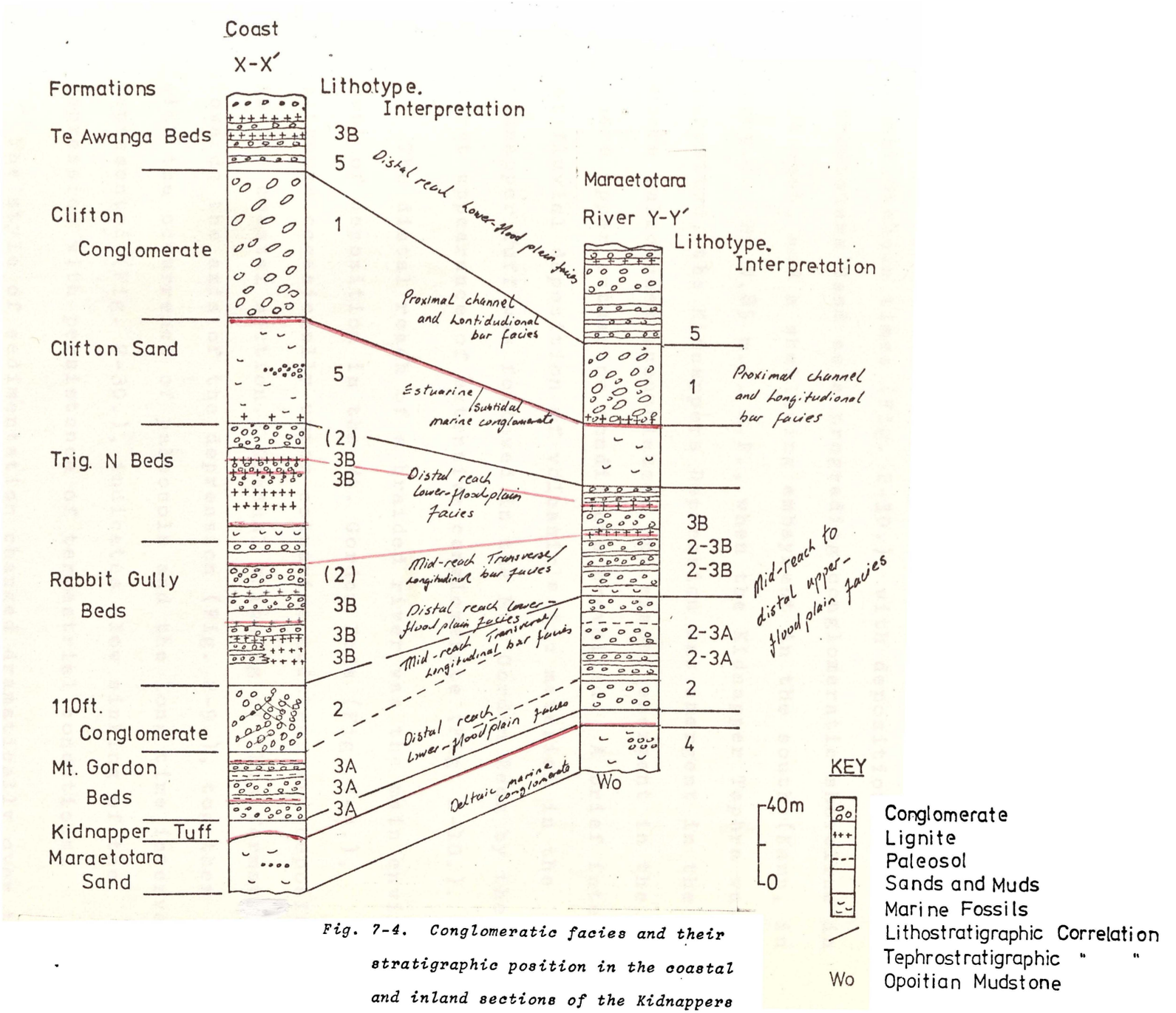

Fig. 7-4. Conglomeratic facies and their stratigraphic position in the coastal and inland sections of the Kidnappers Group.

only rarely migrated inland further than the modern coastline. Hence, from the vertical succession of conglomeratic facies and marine fossiliferous units (Fig. 7-4.), a chronology of submergence and emergence events in the Kidnappers Depression can be derived (Fig. 7-5.).

Sedimentation of the Kidnappers Group commenced during lower Okehuan times (Fig. 2-30.), with deposition of the Maraetotara Sand as a prograding conglomeratic shoreline in the east, and a shallowing embayment in the south (Kamp, in prep.). By 0.85 m.y. B.P., when the Kidnapper Tephra was deposited, the Kidnappers Depression was emergent in the east, where paleodunes accumulated, and almost emergent in the south, where upper estuarine conditions prevailed. A brief interval of fluvial deposition of volcaniclastic material in the Kidnapper Tuff was followed in the Mt. Gordon Beds by the first appearance of extensive conglomerate (Fig. 2-10.).

The distal reach of a braided river was the main environment of deposition in the Mt. Gordon Beds (Fig. 7-4.), although occasionally upper estuarine mudstone was deposited in the coastal section. Gradual thinning of this formation towards the axis of the depression (Fig. 2-9.), together with the occurrence of paleosols and the long time interval represented (Fig. 2-30.), indicates slow sinking of the depression with persistence of terrestrial conditions.

The style of sedimentation changed dramatically over the Okehuan/Putikian boundary with greater subsidence in the axis than on the margins of the depression (Fig. 7-4.). This resulted in rapid lateral thinning to the south-west of succeeding formations, subsidence of this nature persisting

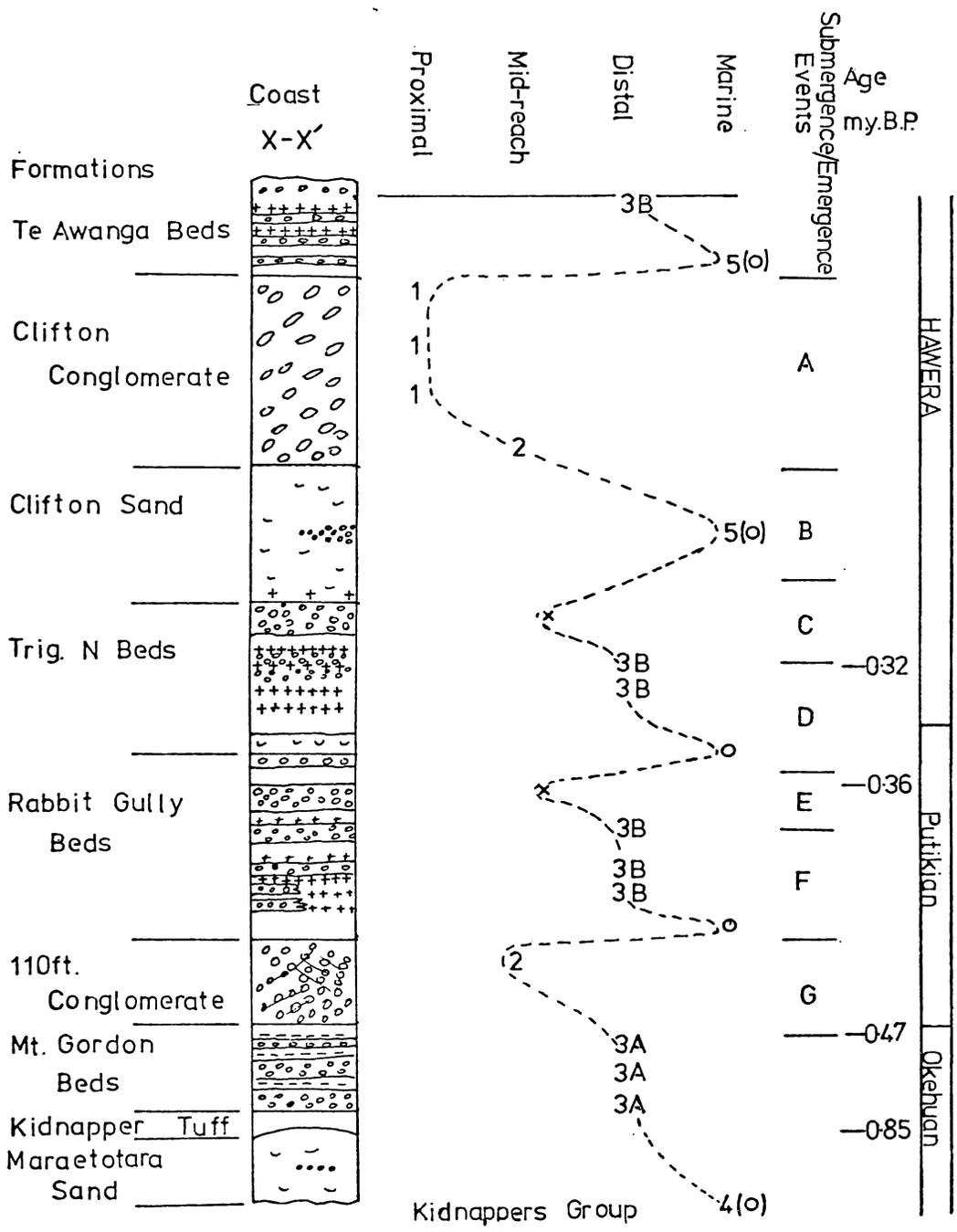

Fig. 7-5. The succession of paleoenvironments recording submergence and emergence events.

to the base of the Te Awanga Beds (Fig. 7-4.).

The 110 ft. Conglomerate (Fig. 2-11.), restricted essentially to the coastal section, represents progradation of mid-reach over distal braided fluvial facies of the Mt. Gordon Beds (Fig. 7-5.).

Rapid submergence of the depression following deposition of the 110 ft. Conglomerate is marked by a thick mudstone unit (Fig. 2-12.) which contains marine fossils in the Maraetotara River section. Marine conditions did not continue in the Rabbit Gully Beds, however, as the basin emerged with deposition of distal flood plain facies (Lithotype 3A). For a time conditions became more terrestrial as a thicker, more cross-bedded conglomerate (Fig. 2-20.), underlying tephric unit E_1 (Fig. 2-9.), was deposited which represents slightly more proximal fluvial facies than does Lithotype 3A (Fig. 7-5.).

The basin rapidly submerged again across the Rabbit Gully/ Trig. N Beds contact (Fig. 7-5.). The submergence event is represented by a fossiliferous siltstone at the base of the Trig. N Beds which overlies a wave planed conglomerate (Fig. 2-13.). The basin became emergent and more proximal towards the upper boundary of the Trig. N Beds (Fig. 7-5.), completing a cycle essentially identical to that recorded in the Rabbit Gully Beds. Rapid subsidence of the depression axis during these cycles is evidenced by marked lateral thinning of the Rabbit Gully and Trig. N Beds towards the south-west (Fig. 7-4.).

Submergence of the basin in the Clifton Sand (Fig. 2-14.) was more gradual and prolonged than it had been in earlier events (Fig. 7-5.). From the base of this formation a sub-

merging sequence is recognised by the change from upper estuarine sand and silt deposition to a thick subtidal mudstone. The sequence is then reversed, and becomes emergent through intertidal sediments to flood plain facies with a thin lignite at the base of the Clifton Conglomerate (Kamp, in prep.).

The same facies succession is recorded inland along the straight line section Z-V-X (Figs. 1-6 and 2-15.), although most of the formational thinning occurs at the expense of the subtidal mudstone unit. A conspicuous feature of the Clifton Sand is the dominance of fine-grained lithologies and the general absence of conglomerate (Fig. 7-4.). The abundance of conglomerate stratigraphically below and above the Clifton Sand suggests that its absence relates to base level control rather than to a lack of supply of conglomerate (Chapter 8). As thickening of the basin axis is of the same order as for most other formations in the group, it appears that basin subsidence is unrelated to lithology.

Sedimentation became most terrestrial in the basin during deposition of the Clifton Conglomerate (Fig. 2-16). A thin lignite, together with thin mudstone lenses and some cross-bedding at the base of the formation, indicates progradation of fluvial mid-reach facies over distal facies. However, the bulk of the formation consists of proximal facies, the deposition of which persisted for a considerable time (Fig. 7-5.).

The rapid lateral thinning of the Clifton Conglomerate along the section Z-V-X (Fig. 2-15.) records progressively greater subsidence of the basin in the north-east. The

paleocurrent directions in the Clifton Conglomerate (Figs. 5-18 and 7-7.) are almost 90° to the cross-section (Fig. 2-16.) which suggests that paleocurrents were funnelled into the axis of the basin from the west.

Deposition of proximal facies in the Clifton Conglomerate ended abruptly with sudden submergence of the basin. As the upper boundary of the Clifton Conglomerate is delineated by a remarkably sharp contact, lacking any undulations (Section 2-5.), the formation is considered to have undergone wave planation prior to deposition of the Te Awanga Beds. The wave planation was followed by an interval of fossiliferous marine conglomerate and sand deposition, before the basin finally became a distal flood plain.

The Te Awanga Beds, in contrast with most underlying formations, thin towards the axis of the depression (Fig. 2-9.). This indicates that the locus of maximum basinal subsidence migrated west after deposition of the Clifton Conglomerate. The Kidnappers Depression ceased to exist as a depositional basin approximately 0.1 m.y. B.P.

7-6. CYCLICITY IN PALEOENVIRONMENTAL SUCCESSION

The single most outstanding feature of Fig. 7-5 is the cyclical alternation of submergence and emergence events recorded by the succession of paleoenvironments. From the base of the 110 ft. Conglomerate four complete cycles are recognised (Fig. 7-5.). It is important to note that these cycles may only be meaningfully compared from the base of the 110 ft. Conglomerate, since when the basin has subsided and accumulated sediment at an essentially constant rate (Fig. 7-6.). Prior to this time the Mt. Gordon Beds accumulated over a

longer time period (Figs. 2-30 and 7-6.) with frequent periods of non-deposition and soil formation.

In considering the cyclical paleoenvironmental succession, two features are especially evident:

(i) there are common facies associations which are repetitive in the sequence;

(ii) the submergence/emergence cycles are asymmetrical, with the submergence event being rapid and the emergence one gradual.

The natural association of facies in each cycle is one of marine sediments followed by a progression in the braided river environment from distal flood plain to mid-reach and, occasionally, to proximal facies.

Submergence of the basin with deposition of a marine fossiliferous unit is consistently a rapid event in the group and is responsible for the asymmetry in each cycle. However, submergence is normally a short-lived event with the basin subsequently becoming a fluvial flood plain. In several of the cycles a number of fining-upward sequences record successions of flood plain progradation in a depression which was constantly subsiding. Eventually the mid-reach facies of the braided river progrades over the flood plain to produce fully terrestrial conditions.

The facies successions and cyclical asymmetry relate primarily to fluctuations in base level. Irrespective of the controls on base level, discussed briefly in Chapter 8, a sudden elevation in base level causes abrupt submergence of the basin. The braided river in its mid-reach becomes

incompetent and the fine-grained sediment which previously by-passed the immediate vicinity of the basin is now deposited, forming a suitable substrate for colonisation by marine organisms. The marine environment, however, remains restricted and never becomes more open than nearshore subtidal (Kingma 1971; Beu & Grant-Taylor 1975).

A sensitive indicator of base level is the ratio of conglomerate to mudstone. Where base level is high and a marine environment prevails, the ratio is nearly always low as exemplified particularily by the Clifton Sand (Fig. 7-4.). Conversely, where the elevation of base level is lowered, progradation through the distal to proximal sequence occurs, with progressively increased amounts of conglomerate. Initially, a slight lowering of base level gives the distal reach of a braided river sufficient competence to deposit thin conglomerate with variable amounts of mudstone. Successive fining-upward sequences within each cycle relate to minor fluctuations in base level. However, a major drop in base level occurs towards the close of each cycle, and facilitates the progradation of more proximal over distal facies.

Although each cycle has similar characteristics, a number of variations occur which are worthy of brief comment.

(1) The submergence event in the Clifton Sand is more gradual and prolonged than equivalent events in other cycles.

(2) The emerging sequence up to the proximal facies of the Clifton Conglomerate is more rapid than normal.

(3) On two occasions, one in the 110 ft. Conglomerate and the other in the Clifton Conglomerate, the basin becomes markedly terrestrial with deposition of a thick sequence of conglomerate (Fig. 7-4.). This is reflected particularly in the Clifton Conglomerate by the greater amplitude of the cycle (Fig. 7-5.).

7-7. *RATE OF SEDIMENTATION AND SEDIMENT SUPPLY*

The rate of sedimentation of the Kidnappers Group appears to have been quite variable, increasing markedly from 150 mm/1000 yrs to 860 mm/1000 yrs across the Okehuan/Putikian boundary (Fig. 7-6A.). Low sedimentation rates during the Okehuan are supported by the presence of three paleosols in the Mt. Gordon Beds, each probably representing up to several thousand years of non-deposition (Fig. 7-6A.). The high sedimentation rate was continuous through the group from the base of the 110 ft. Conglomerate, with no break in sedimentation being apparent at the Okehuan/Putikian boundary (Fig. 7-6A.).

The inland section along the Maraetotara River shows a similar trend, although sedimentation was initially higher during the Okehuan and lower during the Putikian (Fig. 7-6B.).

The abrupt increase in rate of sedimentation over the Okehuan/Putikian boundary reflects increased subsidence of the depression and possibly an increased supply of sediment. From Section 7-6 it is evident that the rate of subsidence of the basin is unrelated to the lithology deposited and therefore subsidence may reasonably be assumed to have been constant. Further it was shown that base level strongly influenced the character of the lithologies.

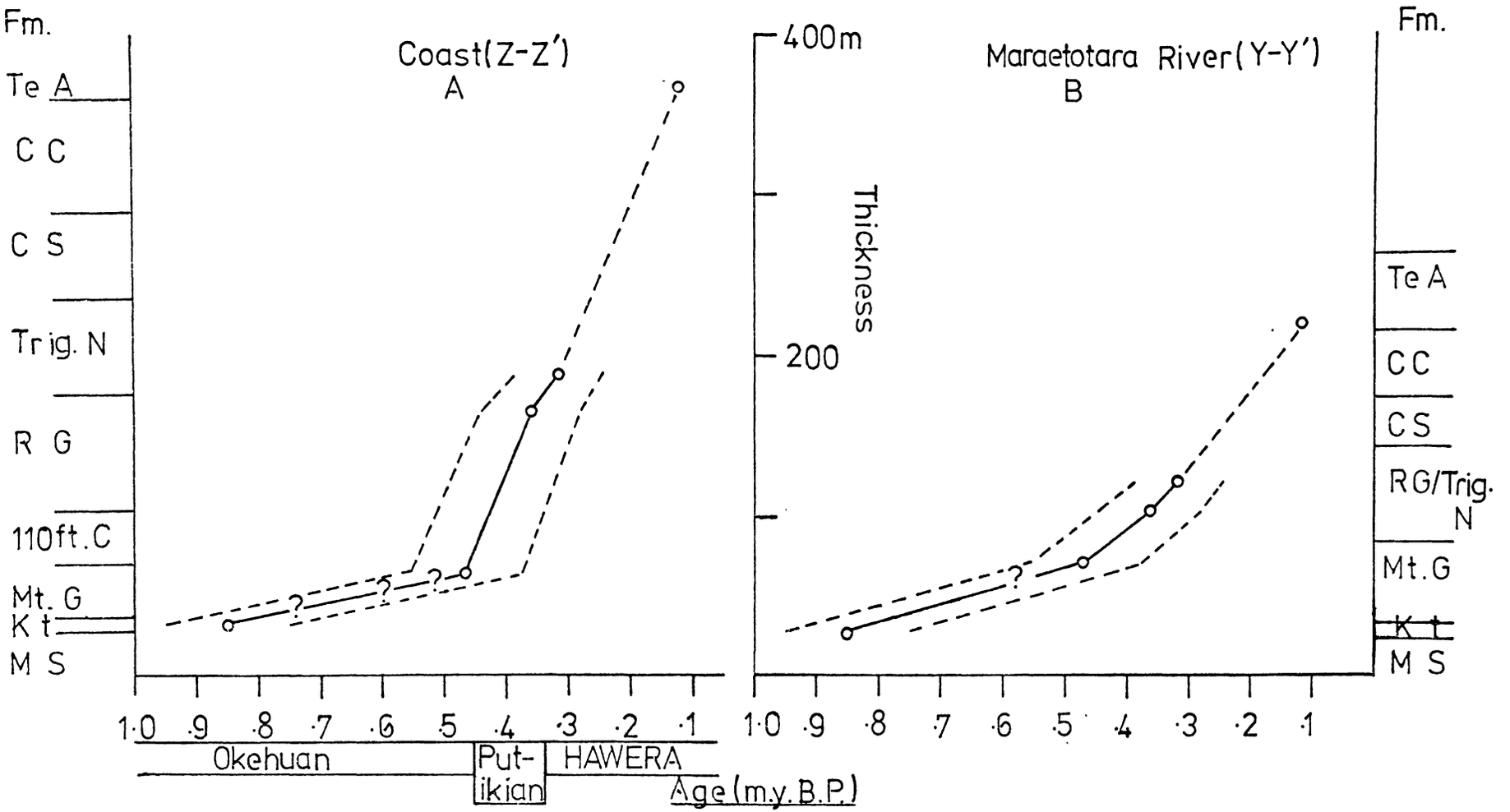

Fig. 7-6. Rate of Sedimentation in the Kidnappers Group as determined from the fission-track ages of various tephras (Seward 1975) and a wave planed last interglacial surface (Lewis 1971, 1973), (Section 2-7). The rate of sedimentation in the Maraetotara River section was established by tephrostratigraphy (Fig. 2-9.). Question marks indicate non-deposition and soil formation, and the dotted lines are the error limits of the fission-track dates.

There is ample sedimentologic evidence (Section 7-3.) to establish that deposition of the Clifton Conglomerate, for example, was rapid. Hence base level must have been depressed for a sufficient length of time for this thick formation to have been deposited. In a depositional setting with rapid subsidence and fluctuations in base level fine grain-sizes do not necessarily indicate slow rates of accumulation. In the Clifton Sand, for example, deposition of fine-grained sediment has occurred because of a rise in base level and because no coarser sediment was being transported into the basin. With sufficient supply of sediment, the rate of accumulation, controlled by the rate of subsidence, is likely to have been comparable to that of conglomerate. Hence, the rate of sedimentation since the Okehuan was most probably linear with respect to thickness (Fig. 7-6.). Therefore the periods represented by the submergence and emergence events in Fig. 7-5 are probably a reasonable estimate of the periods of fluctuations in base level.

The rate of sedimentation may also be related to the supply of sediment which is an important consideration in Hawke's Bay as rivers flowing from the axial ranges have changed direction during Castlecliffian and Hawera times (Kingma 1971).

Beu & Grant-Taylor (1975) considered the quantities of ignimbrite pebbles in the formations overlying the Maraetotara Sand and underlying the Rabbit Gully Beds (Fig. 2-2.) indicated a former course of the Mohaka River south-west into the Kidnappers area (Fig. 7-7.). Further, they considered that the presence of hard, white Whangai Argillite above

the Rabbit Gully Beds indicated a period of major drainage reorganisation, with the Tukituki River flowing north into Hawke Bay about 0.25 m.y. B.P.

Although reversal of a proportion of the dextral transcurrent movement along faults bounding the axial ranges would give a more westerly direction to the Mohaka River (Dr. A.G. Beu, pers. comm.), this is not consistent with the southerly current directions in the Mt. Gordon Beds and the 110 ft. Conglomerate (Figs. 5-9, 7-6 and Appendix III.). Further, as a restricted seaway existed north-west of the Kidnappers Depression, linking the eastern Ruataniwha Basin with Hawke Bay (Kingma 1971), paleocurrent directions from the north-west are thought to be unlikely during Putikian and Lower Hawera times.

Therefore, together with the non-observance by the writer of any ignimbrite pebbles in the 110 ft. Conglomerate, it is likely that the Tukituki River broke through into Hawke's Bay at an earlier date of about 0.5 m.y. B.P. (c.f. 0.25 m.y. of Beu & Grant-Taylor 1975). Hence, an increase in supply of sediment across the Okehuan/Putikian boundary may have coincided with increased subsidence of the basin.

An equally important change in river direction occurred later in Hawera times, immediately prior to deposition of the Clifton Conglomerate. In this formation paleocurrent directions consistently show a west to north-west direction (Fig. 5-18.), in line with the present trend of the Ngauroro River west of Maraekakaho (Fig. 2-3.). During the greater part of Castlecliffian and Hawera times the Ngauroro River supplied gravel to the Ruataniwha Basin and was ponded behind

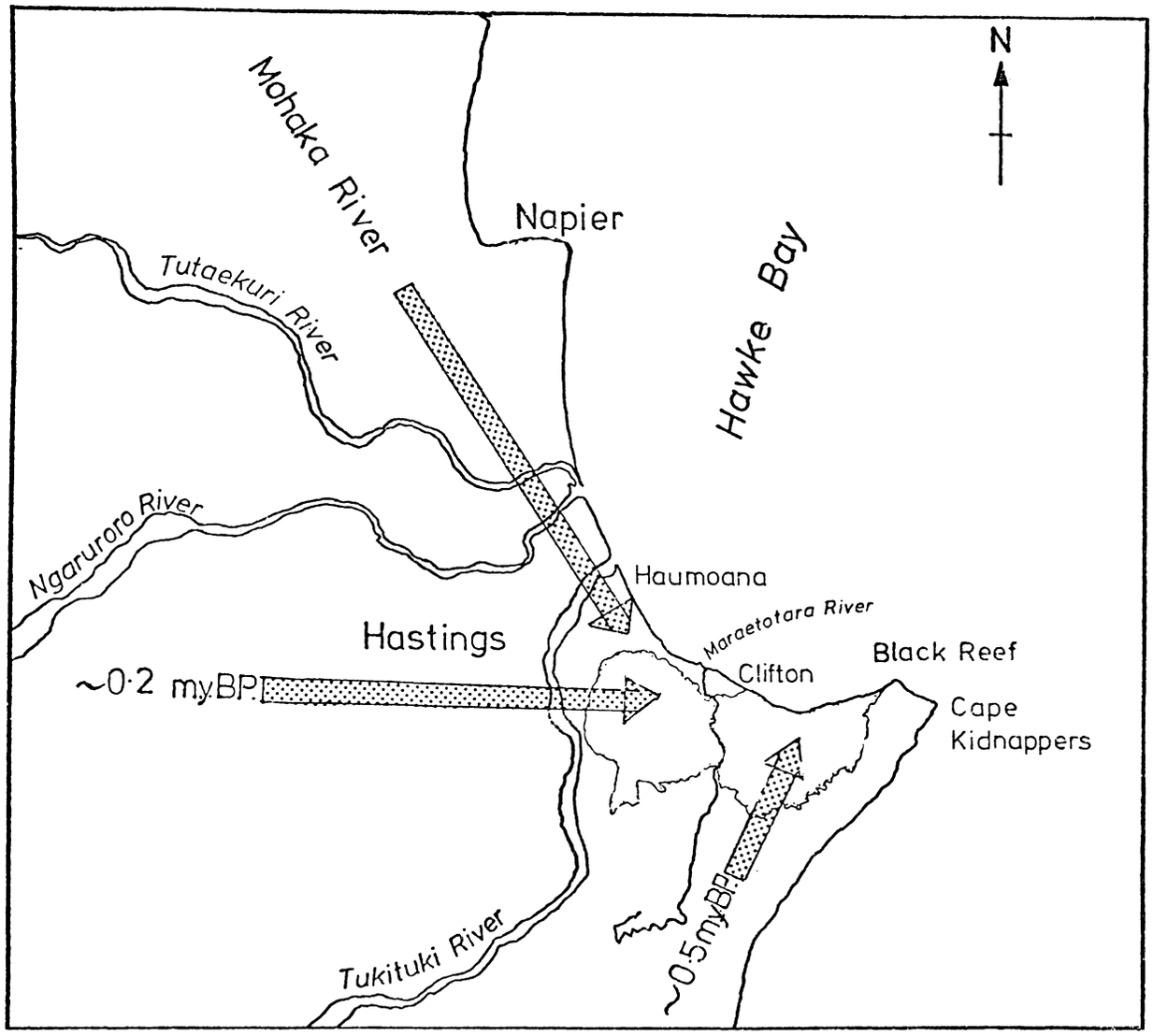

Fig. 7-7. Regional paleocurrent directions important at various times during deposition of the Kidnappers Group.

a resistant barrier at Maraekakaho. At approximately 0.2 m.y. ago the river cut through this barrier and supplied gravel to the Kidnappers Depression (Fig. 7-7.). The correlative of the Clifton Conglomerate and Te Awanga Beds on the north-western flank of Te Mata Peak (Fig. 1-6.) could also only have been deposited by the Ngauroro River.

Pettijohn (1975) found that the mean size of clasts is directly proportional to the diameter of the largest clasts. On this basis it has been shown that measurement of 10 of the largest clasts in outcrop is a reliable way of detecting changes in the mean size of gravel and hence transport directions (e.g. Seward 1974a). In the coastal exposure of the Clifton Conglomerate the mean size of the largest clasts increases upward (Section 2-5.) and therefore, the increase in size relates to the depositional environment becoming more proximal. Moreover, as the distance from source is similar throughout the formational exposure, the increase in size must correspond to a reduced residence time in the braided river. Hence the rate of sediment supply must have increased dramatically with time through the formation, as the mean size of clasts doubles up through the formation.

This relates well to Hein & Walker's (1977) model of bar formation (Fig. 7-3.) in that the proximal facies of Lithotype I formed under the influence of high sediment and fluid discharge. Hence, the dominance of Lithotype I in the upper two-thirds of the Clifton Conglomerate results from an abrupt increase in supply of sediment together with a drop in base level.

CHAPTER 8: SUMMARY AND CONCLUSIONS

Geologic Structure and Stratigraphy

Following a complex history of Mesozoic and Tertiary sedimentation, the Kidnappers Group, located immediately south of Hawke Bay, was deposited in an east-west structural depression lying oblique to the dominant NE/SW and less pronounced NW/SE regional structural trends.

The Kidnappers Depression (Fig. 1-6.) is fault and fold bounded in the south and fault bounded in the north-west. A NE/SW trending anticline (Kidnappers Anticline 1) involving Pliocene - Middle Pleistocene strata 5-10 km east of Cape Kidnappers, formed the eastern boundary of the depression. The Kidnappers Group is presently folded about a growing anticline (Kidnappers Anticline 2) located on the western flank of Kidnappers Anticline 1. A modern westward plunging syncline occurs immediately offshore and intersects Kidnappers Anticline 2. The mildly deformed north and north-westward dipping strata of the group are consistent with the occurrence of an offshore syncline.

The Pleistocene Kidnappers Group rests unconformably on Tertiary lithologies with deposition commencing during the Okehuan and persisting for approximately 0.85 m.y., until 0.1 m.y. B.P.

The group shows wide lithologic diversity, including conglomerates, fossiliferous and unfossiliferous sandstones and mudstones, tephras, paleosols and lignites. The dominant lithology in the majority of formations is greywacke conglomerate.

Ten lithostratigraphic formations were originally established by Kingma (1971): Maraetotara Sand; Kidnapper Tuff; Mt. Gordon Beds; 110 ft. Conglomerate; Rabbit Gully Beds; Trig. N Beds; Clifton Sand; Clifton Conglomerate; Upper Clifton Sand and the Te Awanga Beds. In this study only nine of these formations are recognised, as, on the basis of lithology, the Upper Clifton Sand has no special geologic significance which warrants formational distinction from the Te Awanga Beds and, at best, warrants only member status.

Intrabasinal tephrostratigraphic and lithostratigraphic correlation reveals rapid lateral thickening of some formations towards the axis of the Kidnappers Depression, coinciding in location to the modern coastal section, from which it is evident that subsidence increased abruptly across the Okehuan/ Putikian boundary. From the westwards thickening of the Te Awanga Beds it is deduced that with emergence of Kidnappers Anticline 2 about 0.12 m.y. B.P., the locus of subsidence shifted west into the Heretaunga Plains.

Methods Developed (Chapter 3):

Three computer programmes were developed and a fourth adapted to analyse textural, mineralogic, shape and orientation data of clasts in conglomerates. The texture programme is a rapid method of obtaining a complete graphical, statistical and descriptive summary of the grain-size distribution of earth materials. The mineralogy programme is a rapid, effortless computerised method of mineral identification from X-ray diffraction analysis. The shape programme calculates the shape indices of maximum projection sphericity, oblateness-prolateness, elongation index and bladed index. Further, it calculates the statistics for the distribution of each shape

index and positions the pebble values on a sphericity-form triangle. The fourth programme vectorially and statistically analyses the clast orientation data and is a modification of an existing programme.

Sedimentology and Paleoenvironments

Five conglomeratic lithotypes are recognised to emphasise the distinctive features of different conglomerates in the group:

Lithotype 1 - Imbricated, inverse to normally graded conglomerate;

Lithotype 2 - Planar cross-stratified conglomerate;

Lithotype 3 - Thin, massive to stratified conglomerate;

Lithotype 4 - Planar cross-stratified, shelly, sandy conglomerate;

Lithotype 5 - Thin, massive to low-angle cross-stratified, shelly conglomerate.

The characteristic development of cross-stratification, the shape and orientation fabric of clasts, and the textural and mineralogic analyses, together enable the identification of conglomeratic paleoenvironments.

Shape (Chapter 4):

On the basis of shape indices, pebbles from Lithotypes 1, 2, 3 and 5 have typically fluvial shapes while those from Lithotype 4 have shapes more characteristic of a low energy beach. Compared with the results of Dobkins & Folk (1970), the oblate-prolate index is a more reliable shape discriminatory index, and maximum projection sphericity less so, in establishing the paleoenvironments of pebbles in the Kidnappers Group. The success or otherwise of each shape index to

correctly predict the paleoenvironment, is related to the region on the sphericity-form triangle where most pebble forms occur.

A clast size-dependent and size-independent relationship with shape occurs in conglomerates near the base of the Clifton Conglomerate. Here the concentration of large oblate clasts is considered to be a facies indicator of channel lag deposits.

Orientation Fabric (Chapter 5):

In Lithotype 1 the orientation of clast a-axes transverse to paleocurrent directions and the monoclinic symmetry pattern of ab plane poles are characteristic of fluvial gravels. In comparison in Lithotype 5 the orthorhombic symmetry of the ab plane poles are consistent with deposition in an estuarine/subtidal marine environment. The difference in clast imbrication angles of 15° is comparable with that reported from modern fluvial and marine environments.

A new orientation fabric, namely a(t) ab(i), is defined which identifies the side slope of a channel or channel bar, a feature which may not otherwise be discernable in conglomerates. If a slope exists on the depositional surface then paleocurrent directions derived simply from the direction of dip of the maximum projection of the ab planes of pebbles may be in error. However, if the trend and plunge of the a-axis is also measured the correct paleocurrent direction may be determined by stereographic removal of the plunge on the a-axes.

A model for the origin of clast orientation has been developed (Fig. 5-39.). The orientation fabric of clasts in

Lithotype 1 is indicative of flood and falling stage flows with the development of imbrication being mainly a post-depositional event.

Texture and Mineralogy (Chapter 6):

Clasts in conglomerates in the Kidnappers Group are mainly of pebble size although cobbles occur locally. In the Clifton Conglomerate the mean size of the largest clasts doubles upwards through the formation indicating that the rate of sediment supply increased. The texture and grading in Lithotype 1 imply high concentrations of dispersed clasts, a high shear stress, steep slopes and proximal depostional environments.

Correlation of conglomeratic lithotypes was aided by comparing the heavy mineral assemblages of tephras in the group. The tephras vary markedly in their relative abundance of hypersthene and hornblende (Fig. 6-7.). Despite limited water sorting of some of the tephras, the relative abundance of the major heavy minerals in the volcaniclastic units has not changed significantly from that in the parent tephras.

On the basis of fossil content, clast orientation fabric, clast shape and the stratigraphic context of the conglomerates, Lithotypes 1, 2 and 3 are assigned a braided fluvial origin and Lithotypes 4 and 5 a shallow marine origin. Certain significant differences between Lithotypes 1, 2 and 3 (Fig. 7-1.) identify a proximal-distal sequence within the braided fluvial environment.

Lithotype 1 - channel lag and longitudinal bar facies formed under high fluid and sediment discharge in proximal reaches of a braided river.

Lithotype 2 - transverse and longitudinal/diagonal bar facies formed under lower fluid and sediment discharge, probably on moderately steep slopes in the mid-reaches of a braided river system.

Lithotype 3 - fining upward cycle probably corresponding to a progression in the distal reaches of a braided river environment from channel bar facies through to topstratum overbank deposits.

Lithotype 4 - deposited on the foreset slope of a prograding delta.

Lithotype 5 - lenticular conglomerates deposited in an estuarine/subtidal environment.

In addition to the marine conglomeratic lithotypes, fossiliferous marine sandstones and mudstones occasionally occur in the group and provide evidence of the inland migration of Kidnappers paleoshorelines.

From the vertical succession of conglomeratic facies and marine fossiliferous units (Fig. 7-4.), a chronology of submergence and emergence events in the Kidnappers Group has been derived (Fig. 7-5.). The cyclicity event in paleoenvironmental successions relates primarily to periodic fluctuations in base level. The period of each cycle is considered to be a reasonable estimate of the period of base level fluctuations.

CONTROLS ON SEDIMENTATION IN THE KIDNAPPERS GROUP

(1) Tectonic Control

Tectonism has played an important role during deposition of the Kidnappers Group. Four major influences are recognised:

(i) The group was deposited in a subsiding fault and fold bounded depression;

(ii) Through rapid uplift, the axial greywacke ranges provided a source area for the widespread conglomerates in the group;

(iii) Fault control of river directions has influenced the supply of conglomerate to the depression;

(iv) Uplift of a rising anticline approximately 0.12 m.y. B.P. terminated sedimentation in the depression.

Tectonism may have controlled cyclical changes in base level in at least two ways, one involving irregular rates of subsidence in the basin, and the other involving movements in the hinterland. Irregular rates of basinal subsidence are discounted for several reasons:

(i) There is a complete absence of synsedimentary faulting or slump structures in the group;

(ii) As far as can be determined, all strata are conformable with no detectable disconformities;

(iii) The rate of sedimentation for post-Okehuan sediments, established from fission-track dates, is essentially constant (Fig. 7-6.).

(iv) The nature of lateral thickening of post-Okehuan formations towards the axis of the depression indicates continuous subsidence irrespective of lithology (Fig. 2-9.).

On the other hand a mechanism involving constant subsidence with variable sediment input, a reflection of tectonism outside the basin (Steel 1976, Steel *et al.* 1976), may explain partly the paleoenvironmental succession. With constant subsidence, periods of non-deposition followed by periods of infilling could produce cyclical submergence and emergence events.

However, by itself this mechanism is unlikely to have produced the observed paleoenvironmental successions as there is no evidence in post-Okehuan sediments of disconformities marking breaks in sedimentation. Further, such a mechanism is unlikely to cause the periodicity, asymmetry and magnitude of the paleoenvironmental successions. Nevertheless, the sudden inputs of sediment at approximately 0.5 and 0.2 m.y. B.P. (Fig. 7-7.) have been related to changes in river direction as a consequence of faulting. Thus tectonism may explain, in part, the repetitive paleoenvironmental succession in the group.

(2) Glacio-Eustatic Control

The most reliable sea level curve for the Pleistocene is that derived from the oxygen-isotope record preserved in cores V28-238 and V29-239, from the equatorial western Pacific (Fig. 8-1, Skackleton & Opdyke 1973, 1976). Dating of these cores was done primarily by the geomagnetic scale (Fig. 8-1.). Both cores are complete with sedimentation rates of 1.7 cm/1000 yrs. in core V28-238 and 1 cm/1000 yrs. in core V28-239.

Each core records the same number of events in the last 800,000 years. During this time there have been 10 glacial events at approximately 80,000 to 100,000 year intervals. Typically the glacial periods ended abruptly during times designated by isotope stages 2, 6, 10, 12, 20 and 22 and less

Fig. 8-1. The oxygen-isotope and paleomagnetic record in equatorial Pacific core V28-238 and V28-239 (after Shackleton & Opdyke 1976).

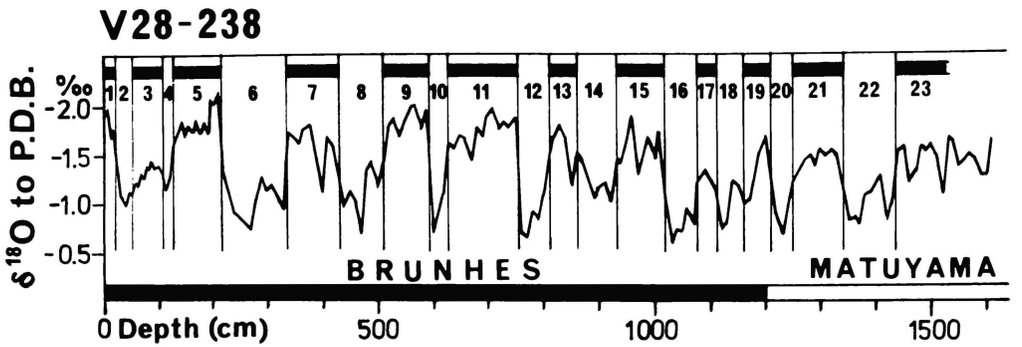
V28-238
δ18O to P.D.B.
‰
-2.0
-1.5
-1.0
-0.5
1 2 3 4 5 6 7 8 9 10 11 12 13 14 15 16 17 18 19 20 21 22 23
BRUNHES
MATUYAMA
0 Depth (cm)
500
1000
1500

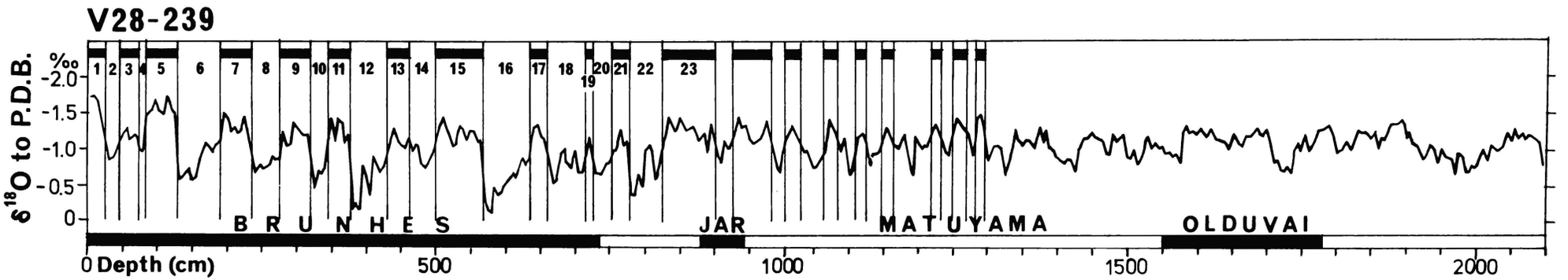
V28-239
δ18O to P.D.B.
‰
-2.0
-1.5
-1.0
-0.5
0
1 2 3 4 5 6 7 8 9 10 11 12 13 14 15 16 17 18 19 20 21 22 23
B R U N H E S
JAR
MATUYAMA
OLDUVAI
0 Depth (cm)
500
1000
1500
2000

clearly in 4, 8 and 14 (Fig. 8-1.).

The sedimentologic record of submergence and emergence events in the Kidnappers Group has been compared using the same time scale with the relevant part of core V28-238 (Fig. 8-2.). Sedimentation of the group is taken as being constant from 0.45 m.y. B.P. (see Section 7-7.). Only slight compression of isotope stage 9 is required to fit core V28-238 between three fission-track dates for the Kidnappers Group. Compression of isotope stage 9 was no further than its reduced duration in core V28-239 (Fig. 8-1.).

The nature of the successive submergence-emergence events derived from the sedimentology of the group resembles closely the sea level curve derived by Shackleton & Opdyke (1973, 1976). This is exemplified by the following points:

(i) Emergence events *A*, *C*, *E* and *G* coincide with, and are of similar duration to, glacial isotope stages 6, 8, 10 and 12.

(ii) The rapid submergence events *G/F*, *E/D* and that following *A* are identical to the abrupt terminations of glacial stages 12, 10 and 6 respectively. The asymmetry in most submergence-emergence cycles is typical of that induced by glacio-eustatic sea level fluctuations (Matthews 1974).

(iii) The more gradual and prolonged submergence event *B* in the Clifton Sand (Section 7-6.), is identical to the prolonged rise in sea level into interglacial event 7 (Fig. 8-2.).

Hence strong evidence exists that the primary control on the succession of paleoenvironments in the Kidnappers Group has

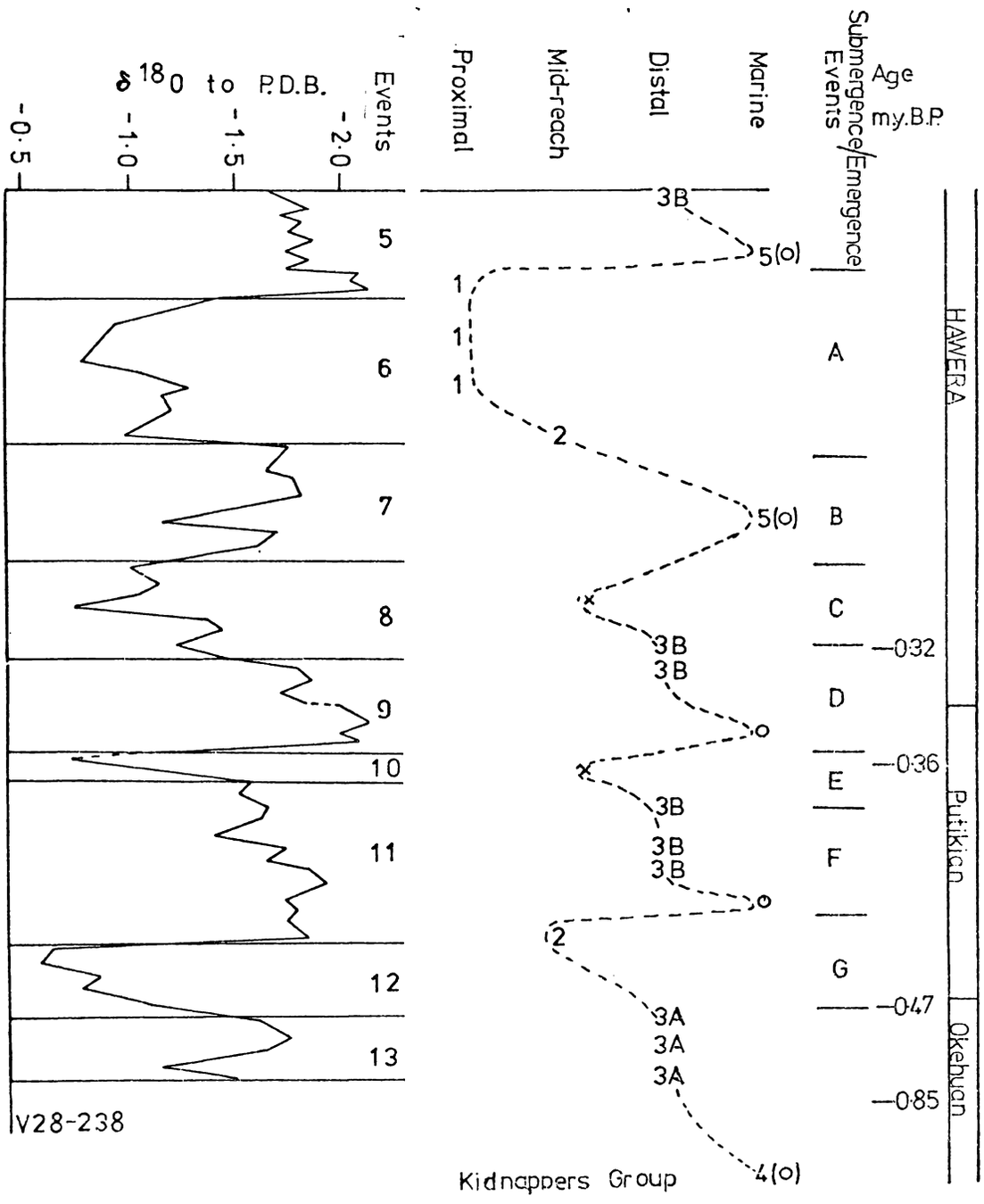

Fig. 8-2. Comparison of submergence and emergence events in the Kidnappers Group with Shackleton & Opdyke's (1976) oxygen isotope record in core V28-238.

been glacio-eustatic sea level fluctuations. The magnitude of facies changes from mid-reach fluvial, and occasionally proximal fluvial, to subtidal marine requires considerable and rapid base level fluctuations which are compatible with glacio-eustatic sea level changes.

Independent support for transgressive event *B* (Fig. 8-2.) is the probable correlation on the basis of its high hypersthene content (Fig. 6-7.) of tephric unit H with the Mt. Curl Tephra (Milne 1973). The Mt. Curl Tephra has an age of 0.23± 0.03 m.y. B.P., which compares with an age for Unit H of 0.28 m.y. estimated on the basis of constant sedimentation from Unit F (0.32 ± 0.07 m.y. B.P., Fig. 2-30.). It has been estimated by Milne (1973) that the Mt. Curl Tephra was deposited within 3000 years of the end of the cold climate episode predating the penultimate interglacial. On this basis the Wanganui marine bench sequence can be correlated satisfactorily with raised coral reef sequences in Barbados and New Guinea. The occurrence of tephric unit H in the upper part of the Trig. N Beds (Fig. 2-9.), and therefore the latter part of glacial stage *C* (Fig. 8-2.), supports correlation of the penultimate interglacial isotope stage 7 with the penultimate interglacial event *B* in the Kidnappers Group.

The interglacial climate indicated by flora in the lignites of Lithotype 3B is consistent with a high interglacial sea level following an interglacial maximum (e.g. event *F*, Fig. 8-2.).

Any record of submergence and emergence in Okehuan sediments of the group is poorly preserved as the rate of subsidence and sediment accumulation was low and discontinuous (Fig. 7-6.).

Nevertheless, three paleosols in the Mt. Gordon Beds, interpreted as forming under climatic conditions similar to that in Hawke's Bay at present, may represent three interglacial stages. If this were so, then they may relate to isotope Stages 13, 15, 17 of Shackleton & Opdyke (1973, 1976).

The New Zealand Late Quaternary glacial/interglacial succession relates well to the regressions and transgressions recorded in the Kidnappers Group.

Stage	Event
Waimean Glacial	*A*
Terangian Interglacial	*B*
Waimaungan Glacial	*C*
Waiwheran Interglacial	*D*
Porikan Glacial	*E*

Hence the earliest recognised Late Quaternary cold phase, the Porikan Glacial Stage, would have occurred in latest Castlecliffian times, at approximately 0.36 m.y. B.P. (Fig. 8-2.). Further, there is evidence of several more glacial/interglacial cycles before the Okehuan/Putikian boundary.

There exists some irregularity in the transgressive-regressive chronology recorded by post-Okehuan sediments, as exemplified by the greater amplitude of event *A*, and to some extent also of event *G* (Fig. 8-2.).

From the sedimentology of conglomeratic facies, particularly Lithotype 1 in the Clifton Conglomerate, it is considered that the greater amplitude reflects the reinforcement of a glacially induced regression with increased sediment discharge. This relates to fault control of river directions and subsequent debouching of the Tukituki River into the depression at about

0.5 m.y. B.P., followed by the Ngauroro River at approximately 0.2 m.y. B.P. (see Section 7-7.).

During Castlecliffian-Hawera times the Ngauroro River was ponded at Maraekakako behind the Puketapu Fault. It is anticipated that the fall in sea level leading into the Waimean Glacial Stage provided the potential for cutting through the resistant barrier of Nukumaruan limestones. With a lower base level, and the large sediment supply behind the barrier, gravel was poured into the Kidnappers Depression forming the proximal fluvial facies in the Clifton Conglomerate. This mechanism, together with renewed uplift of the Puketapu Fault, formed the Waharoa Terraces. A similar mechanism is envisaged for the breaking through of the Tukituki River, although the absence of a large supply of gravel would only have enabled progradation of mid-reach fluvial facies.

IMPLICATIONS

(i) Glacio-eustatic sea level fluctuations recorded in the Kidnappers Group resemble closely those derived from Pacific Ocean cores by Shackleton & Opdyke (1973, 1976).

(ii) The sedimentary record of the Kidnappers Group is essentially continuous with good absolute time control. This potentially enables correlation of Middle to Late Pleistocene successions throughout New Zealand with paleoenvironmental successions in the Kidnappers Group.

It is perhaps appropriate to record Butzer's (1976, p32) comment ....

> *correlation of Shackleton's multiple deep-sea units with existing, continental time-stratigraphic schemes is next to impossible, although cautious comparisons with detailed lithostratigraphic sequences, defined with some measure of radiometric control, appear to be possible eventually.*

BIBLIOGRAPHY

Allen, J.R.L. 1965: A review of the origin and charcteristics of recent alluvial sediments. *Sedimentology 5:* 89-191.

American Society for Testing and Materials 1967: *Powder diffraction file* compiled under the auspices of the joint committee on chemical analysis of powder diffraction methods. Editor: Jospeh V. Smith - Philadelphia.

Andrews, J.T.; King, C.A.M. 1968: Comparative till fabrics and till fabric variability in a till sheet and a drumlin: a small scale study. *Proc. Yorkshire Geol. Soc. 36:* 435-461.

Andrews, J.T.; Shimizu, K. 1966: Three-dimensional vector technique for analysising till fabrics: Discussion and FORTRAN program. *Canada Dept. Mines and Tech. Surveys Geog. Br. Geog. Bull. 8:* 151-165.

Baker, R.A. 1968: Kurtosis and Peakedness. *J. Sedimentary Petrology 38:* 279-681.

Barrett, P.J. 1970: Paleocurrent analysis of the mainly fluviatile Permian and Triassic Beacon rocks, Beardmore Glacier area, Antarctica. *J. Sedimentary Petrology 40:* 395-411.

Beu, A.G.; Grant-Taylor, T.L. 1975: Geology and fossils of the Cape Kidnappers area. *Dept. Lands and Survey, Well. N.Z. Res. Series 1975/2:* 19p.

Blatt, H.: Middleton, G.; Murray, R. 1972: *Origin of Sedimentary Rocks.* Prentice-Hall Inc., New Jersey, 634p.

Bluck, B.J. 1967: Deposition of some Upper Old Red Sandstone conglomerates in the Clyde area: a study in the significance of bedding. *Scottish Journal of Geology 3:* 139-167.

Bluck, B.J. 1974: Structure and directional properties of some valley sandur deposits in southern Iceland. *Sedimentology 21:* 533-554.

Bluck, B.J. 1976: Scottish rivers of low sinuosity. *R. Soc. Edinburgh Trans. 69:* 425-456.

Boellstorff, J.D.; Te Punga, M.T. 1977: Fission-track ages and correlation of Middle and Lower Pleistocene sequences from Nebraska and New Zealand. *N.Z. Journal of Geology and Geophysics 20 (1):* 47-59.

Boothroyd, J.C.; Ashley, G.M. 1975: Process, bar morphology, and sedimentary structures on braided outwash fans, northeastern Gulf of Alaska. *In* Jopling, A.V.; McDonald, B.C. (editors): *Glaciofluvial and glaciolacustrine sedimentation.* Soc. Econ. Paleont. Min., Spec. Publ. 23: 193-222.

Boulton, G.S. 1970a: On the deposition of subglacial and melt-out tills at the margins of certain Svalbard glaciers. *Journal of Glaciology 9:* 231-245.

Boulton, G.S. 1970b: On the origin and transport of englacial debris in Svalbard glaciers. *Journal of Glaciology 9:* 213-229.

Bradley, W.C. 1970: Effect of weathering on abrasion of granitic gravel, Colorado River (Texas). *Geological Society of America Bulletin 81:* 61-80.

Bradley, W.C.; Fahnestock, R.K.; Rowekamp, E.T. 1972: Coarse sediment transport by flood flows on Knik River, Alaska. *Geological Society of America Bulletin 83:* 1261-1284.

Bull, W.B. 1968: Alluvial fans. *Journal of Geological Education 16:* 101-106.

Butzer, K.W. 1976: Pleistocene climates. *Geoscience and man X111:* 27-44.

Buurman, P. 1975: Possibilities of paleopedology. *Sedimentology 22:* 289-298.

Carter, L.; Lewis, K.B. 1976: Subsurface structure and its influence on nearshore sedimentation off southern Hawke's Bay. *N.Z. Oceanographic Institute Records 3 (5):* 33-40.

Carver, R.E. (ed.), 1971: *Procedures in Sedimentary Petrology.* Wiley-Interscience 635p.

Church, M.; Gilbert, R. 1975: Proglacial fluvial and lacustrine environments. *In* Jopling, A.V.; McDonald, B.C. (editors): *Glaciofluvial and glaciolacustrine sedimentation.* Soc. Econ. Paleont. Min., Spec. Publ. 23: 22-100.

Clark, C.L. 1976: *Faunas, environments and structural implications of Nukumaruan mudstone beds of the Ruataniwha Basin, Hawke's Bay.* M.Sc. thesis, University of Auckland.

Collinson, J.D. 1970: Bedforms of the Tana River, Norway. *Geografiska Annalar* 52A: 31-55.

Curray, J.R. 1956: The analysis of two-dimensional orientation data. *Journal of Geology 64:* 117-131.

Davies, I.C.; Walker, R.G. 1974: Transport and deposition of resedimented conglomerates: the Cap Enrage´ formation, Cambro-Ordovician, Gaspe, Quebec. *J. Sedimentary Petrology 44:* 1200-1216.

Denness, B. 1970: A method of contouring polar diagrams using curvilinear contouring cells. *Geological Magazine 107(1):* 61-65.

Denness, B. 1972: A revised method of contouring stereograms using variable curvilinear cells. *Geological Magazine 109(2):* 157-163.

Dobkins, J.E.; Folk, R.L. 1970: Shape development on Tahiti-Nui. *J. Sedimentary Petrology 40(4):* 1167-1203.

Doeglas, D.J. 1962: The structure of sedimentary deposits of braided rivers. *Sedimentology 1:* 167-190.

Drake, L.D. 1974: Till fabric control by clast shape. *Geological Society of America Bulletin 85(2):* 247-250.

Drake, L.D. 1977: Human factor in till-fabric analysis. *Geology 5:* 180-184.

Evans, S.G. 1969: Pebble morphology in a fluvioglacial stream - an example from the Jotunheimen, Norway. *Horizon 18:* 17-22.

Ewart, A. 1966: Review of the mineralogy and chemistry of the acidic volcanic rocks of the Taupo Volcanic Zone. *Volcanologique 29:* 147-172.

Fahnestock, R.K.; Haushild, W.L. 1962: Flume studies of the transport of pebbles and cobbles on a sand bed. *Geological Society of America Bulletin 73(11):* 1431-1436.

Fahnestock, R.K. 1963: Morphology and hydrology of a braided stream. *U.S. Geological Survey, Professional Paper 422A:* 1-70.

Fieldes, M.; Weatherhead, A.V. 1966: Mineralogy of sand fractions of New Zealand soils. *N.Z. Journal of Science 9(4):* 1006-1021.

Fleming, C.A. 1957: The genus Pecten in New Zealand. *N.Z. Geological Survey Palaeontological Bulletin 26:* 69p.

Flinn, D. 1958: On tests of significance of preferred orientation in three-dimensional fabric diagrams. *Journal of Geology 66(5):* 526-539.

Folk, R.L. 1966: A review of grain-size parameters. *Sedimentology 6:* 73-93.

Folk, R.L. 1968: *Petrology of sedimentary rocks.* Hemphill's Austin, Texas. 170p.

Folk, R.L.; Andrews, P.B.; Lewis, D.W. 1970: Detrital sedimentary rock classification and nomenclature for use in New Zealand. *N.Z. Journal of Geology and Geophysics 13(4):* 937-968.

Fraser, H.J. 1935: Experimental study of the porosity and permeability of clastic sediments. *Journal of Geology 43:* 910-1010.

Friedman, G.M. 1961: Distinction between dune, beach, and river sands from their textural characteristics. *J. Sedimentary Petrology 31:* 514-529.

Geode, A. 1975: Downstream changes in shape in the pebble morphometry of the Tambo River, eastern Victoria. *J. Sedimentary Petrology 45(3):* 704-718.

Gibbs, H.S. 1969: Buried soils in Hawke's Bay. *N.Z. Soil News 17:* 92-5.

Gibbs. H.S. 1971. Nature of paleosols in New Zealand. *In* Yaalon, Dan H. (ed.): *Paleopedology, origin, nature, and dating of paleosols.* Israel Universities Press, Jerusalem: 229-44.

Glen, J.W.; Donner, J.J.; West, R.G. 1957: On the mechanism by which stones in till become oriented. *American Journal of Science 255:* 194-205.

Griffiths, J.C.; Smith, C.M. 1964: Relationship between volume and axes of some quartzite pebbles from the Olean Conglomerate, Rock City, N.Y. *American Journal of Science 262:* 497-512.

Griffiths, J.C. 1967: *Scientific method in analysis of sediments.* McGraw-Hill 507p.

Grindley, G.W. 1960: Sheet 8 Taupo. *Geological Map of New Zealand 1: 250 000.* N.Z. Department of Scientific and Industrial Research, Wellington.

Harms, J.C.; Spearing, D.R.; Southland, J.B.; Walker, R.G. 1975: Depositional environments as interpreted from primary sedimentary structures. *Soc. Econ. Paleont. Min., Short Course 2 (Dallas, 1975).* 161p.

Harris, S.A. 1969: The meaning of till fabric. *Canadian Geographer. X111(4):* 317-337.

Harrison, P.W. 1957: A clay-till fabric: its character and origin. *Geology 65(3):* 275-308.

Hayslett, M.S.; Murphy, P. 1967: *Statistics made simple.* W.H. Allen & Company, London. 251p.

Hein, F.J.; Waller, R.G. 1977: Bar evolution and development of stratification in the gravelly, braided, Kicking Horse River, British Columbia. *Canadian Journal of Earth Sciences 14(4):* 562-570.

Hendry, H.F. 1976: The orientation of discoidal clasts in resedimented conglomerates, Cambro-Ordovician, Gaspe´, eastern Quebec. *J. Sedimentary Petrology 46(1):* 48-55.

Henrich, E. Wm. 1965: *Microscope identification of minerals.* McGraw-Hill. 414p.

High, L.R., Jr,; Picard, M.D. 1971: Mathematical treatment of orientation data. *In* Carver, R.E. (ed.): *Procedures in sedimentary petrology*. Wiley, N.Y. 653p.

Hodder, A.P.W.; Wilson, A.T. 1976: Identification and correlation of thinly bedded tephra: the Tirau and Mairoa ashes. *N.Z. Journal of Geology and Geophysics 19(5):* 663-82.

Holmes, C.D. 1941: Till fabric. *Geological Society of America Bulletin 52:* 1299-1354.

Howerth, R.; Rankin, P.C. 1975: Multi-element characterisation of glass shards from stratigraphically correlated rhyolitic tephra units. *Chemical Geology 15:* 239-50.

Hume, T.M. 1978: *Clay petrology of Mesozoic to Recent sediments of central western North Island, New Zealand.* Ph.D. thesis, University of Waikato.

Hume, T.M.; Sherwood, A.M.; Nelson, C.S. 1975: Alluvial sedimentology of the Upper Pleistocene Hinuera Formation, Hamilton Basin, New Zealand. *Journal of the Royal Society of New Zealand 5(4):* 421-462.

Jaquet, J.M.; Vernet, J.P. 1976: Moment and graphic size parameters in the sediments of Lake Geneva (Switzerland). *J. Sedimentary Petrology 46(2):* 305-312.

Jeffery, G.B. 1922: The motion of ellipsoidal particles immersed in a viscous fluid. *Roy. Soc. London Proc. 102A(715):* 161-179.

Jizba, Z.V. 1971: Mathematical analysis of grain orientation. *In* Carver, R.E. (ed.): *Procedures in sedimentary petrology*. Wiley, N.Y. 653p.

Johansson, C.E. 1963: Orientation of pebbles in running water. A laboratory study. *Geografiska Annalar 45:* 85-112.

Jordon, C.F. 1977: Reply size analysis of silt and clay by hydrophotometer. *J. Sedimentary Petrology 47(2):* 931-932.

Jordon, C.F., Fryer, G.E.; Hemmen, E.H. 1971: Size analysis of silt and clay by hydrophotometer. *J. Sedimentary Petrology 41:* 489-496.

Kamb, W.B. 1959: Ice petrofabric observations from Blue Glacier, Washington, in relation to theory and experiment. *J. Geophysical Research 64(11):* 1891-1904.

Kane, W.T.; Hubert, J.F. 1963: FORTRAN program for calculation of grain-size textural parameters on the IBM 1620 computer. *Sedimentology 2:* 87-90.

Katz, H.R. 1973: Pliocene unconformity at Opau Stream, Hawke's Bay, New Zealand. *N.Z. Journal of Geology and Geophysics 16(4):* 917-25.

Kelling, G. 1968: Patterns of sedimentation in Rhondda Beds of South Wales. *Bulletin American Association of Petroleum Geologists 52:* 2369-2386.

Kelling, G.; Williams, P.F. 1968: Flume studies of the reorientation of pebbles and shells. *Journal of Geology 75:* 243-267.

Kerr, P.F. 1959: *Optical mineralogy*. 3rd ed. McGraw-Hill, N.Y. 442p.

Kingma, J.T. 1957a: The North Island Geanticline in the Hawke's Bay Sector. *N.Z. Journal of Science and Technology (Sect. B) 38(6):* 496-499.

Kingma, J.T. 1957b: The Geology of the Kohurau Fault Block, Central Hawke's Bay. *N.Z. Journal of Science and Technology (Sect. B) 38(4):* 342-353.

Kingma, J.T. 1957c: The tectonic setting of the Ruahine-Rimutaka Range. *N.Z. Journal of Science and Technology (Sect. B) 38(8):* 858-861.

Kingma, J.T. 1958: Possible origin of piercement structures, local unconformities, and secondary basins in the Eastern Geosyncline, New Zealand. *N.Z. Journal of Geology and Geophysics 1(2):* 269-274.

Kingma, J.T. 1959: The tectonic history of New Zealand. *N.Z. Journal of Geology and Geophysics 2(1):* 1-55.

Kingma, J.T. 1960a: Outline of the Cretaceo-Tertiery Sedimentation in the eastern Basin of New Zealand. *N.Z. Journal of Geology and Geophysics 3(2):* 222-234.

Kingma, J.T. 1960b: The marine Castlecliffian sedimentation in central Hawke's Bay, New Zealand. *N.Z. Journal of Geology and Geophysics 3(1):* 8-14.

Kingma, J.T. 1962: Sheet 11 Dannevirke (1st Ed.). *Geological Map of New Zealand 1:250 000.* N.Z. Department of Scientific and Industrial Research, Wellington.

Kingma, J.T. 1970a: Sheets N134 Napier and Hastings N135 Kidnappers (1st Ed.). *Geological Map of New Zealand 1:63 360.* N.Z. Department of Scientific and Industrial Research, Wellington.

Kingma, J.T. 1970b: Sheets N141 Waipawa, N142 Waimarama and part N146 Waipukurau (1st Ed.). *Geological Map of New Zealand 1:63 360.* N.Z. Department of Scientific and Industrial Research, Wellington.

Kingma, J.T. 1971: Geology of Te Aute Subdivision. *N.Z. Geological Survey Bulletin 70.* 173p.

Kock, G.S.; Link, R.F. 1971: *Statistical analysis of Geological data, Volume 2.* J. Wiley & Sons, N.Y. 417p.

Krumbein, W.C. 1939: Preferred orientation of pebbles in sedimentary deposits. *Journal of Geology 47:* 673-706.

Krumbein, W.C. 1941: Measurement and geological significance of shape and roundness of sedimentary particles. *J. Sedimentary Petrology 11(1):* 64-72

Krumbein, W.C. 1942: Settling-velocity and flume behaviour of non-spherical particles. *American Geophysical Union Transactions 23:* 621-632.

Laronne, J.B.; Carson, M.A. 1976: Interrelationships between bed morphology and bed-material transport for a small, gravel-bed channel. *Sedimentology 23:* 67-85.

Lewis, K.B. 1971: Growth rate of folds using tilted wave-planed surfaces: coast and continental shelf, Hawke's Bay, New Zealand. *In:* Recent Crustal Movements. *Bulletin of the Royal Society of New Zealand 9:* 225-31.

Lewis, K.B. 1973: Erosion and deposition on a tilting continental shelf during Quaternary oscillations of sea level. *N.Z. Journal of Geology and Geophysics 16:* 281-301.

Lindsay, J.F. 1968: The development of clast fabric in mudflows. *J. Sedimentary Petrology 38(4):* 1242-1253.

Lindsay, J.F.; Summerson, C.H.; Barrett, P.J. 1970a: A long-axis clast fabric comparison of the Squantum Tillite Massachusetts and the Gowganda Formation, Ontario. *J. Sedimentary Petrology 40(2):* 475-479.

Lindsay, J.F. 1970b: Clast fabric of till and its development. *J. Sedimentary Petrology 40(2):* 629-641.

Lindsay, J.F. 1970c: Clast fabric strength of tillite. *Journal of Geology 78:* 597-603.

Lumsden, D.N. 1973: TRI: A FORTRAN subroutine to plot prints on a triangular diagram. *Geological Society of America Bulletin 84(5):* 1765-1767.

Manley, R.St.J.; Arlov, A.P.; Mason, S.G. 1955: Rotations, orientations and collisions of suspended particles in velocity gradients. *Nature 175(4459):* 682-683.

Mark, D.M. 1971: Rotational vector procedures for the analysis of till fabric. *Geological Society of America Bulletin 82:* 2661-2666.

Mark, D.M. 1973: Analysis of axial orientation data, including till fabric. *Geological Society of America Bulletin 84:* 1369-1374.

Mark, D.M. 1974: On the interpretation of till fabrics. *Geology 2(2):* 101-104.

Marks, G.P. 1975: *Sedimentology of Omaro Barrier Spit, Whangapoua harbour, Coromandel Peninsula.* M.Sc. thesis, University of Waikato.

Matthews, R.K. 1974: *Dynamic Stratigraphy.* Prentice-Hall. 370p.

McDonald, B.C.; Banerjee, I. 1971: Sediments and bedforms on a braided outwash plain. *Canadian Journal of Earth Sciences 8:* 1282-1301.

Meyer, R. 1976: Continental sedimentation, soil genesis and marine transgression in the basal beds of the Cretaceous in the east of the Paris Basin. *Sedimentology 23(2):* 235-254.

Miall, A.D. 1977: A review of the braided-river depositional environment. *Earth Science Reviews 13:* 1-62.

Middleton, G.V. 1970: Experimental studies related to problems of flysch sedimentation. *In* Lajoie, J. (ed.): *Flysch sedimentology in North America:* Geol. Assoc. Canada Spec. Publ. 7: 253-272.

Mills, H.H. 1977: Basal till fabrics of modern alpine glaciers. *Geological Society of America Bulletin 88(6):* 824-828.

Milne, L. 1971: Upper Quaternary river terraces in New Zealand: A Selective Bibliography. 27p. *Wellington National Library of N.Z., Library School.*

Milne, J.D.G. 1973: Mount Curl Tephra, a 230,000-year-old marker bed in New Zealand, and its implications for Quaternary chronology. *N.Z. Journal of Geology and Geophysics 16(3):* 519-532.

Milner, H.B. 1962: *Sedimentary petrology* volume 1. *Methods in sedimentary petrology.* 4th ed. George Allen & Urwin. 607p.

Nelson, C.S. 1977: Grain-size parameters of insoluble residues in mixed terrigenous-skeletal carbonate sediments and sedimentary rocks: some New Zealand examples. *Sedimentology, 24(1):* 31-52.

Nelson, C.S.; Cochrane, R.H.A. 1970: A rapid X-ray method for the quantitative determination of selected minerals in fine-grained and altered rocks. *Tane 16:* 151-162.

Ninkovich, D. 1968: Pleistocene volcanic eruptions in New Zealand recorded in deep-sea sediments. *Earth and Planetary Science Letters 4:* 89-102.

Ore, H.T. 1964: Some criteria for recognition of braided stream deposits. *Wyoming University Contributions to Geology 3(1):* 1-14.

Passega, R. 1957: Texture as characteristic of clastic deposition. *American Association of Petroleum Geologists Bulletin 41:* 1952-1984.

Pettijohn, F.J. 1975: *Sedimentary rocks.* 3rd Ed. Harper & Row, N.Y. 628p.

Phillips, F.C. 1971: *The use of stereographic projection in structural geology.* 3rd Ed. Edward Arnold, London.

Pittam, J.C.; Parkinson, P.G. 1971: Till fabric analysis: Practical problems and errors - an example from north Wales. *Horizon 20:* 50-57.

Potter, P.E. Pettijohn, F.J. 1963: *Paleocurrents and basin analysis.* Springer-Verlag. 296p.

Pryor, W.A. 1971: Grain-shape *In* Carver, R.E. (ed.): *Procedures in sedimentary petrology.* Wiley, N.Y. 653p.

Pullar, W.A. 1967: Uses of volcanic ash beds in geomorphology. *Earth Science Journal 1(2):* 154-77.

Pullar, W.A.; Birrell, K.S.; Heine, J.C. 1973: Named tephras and tephra formations occurring in the central North Island, with notes on derived soils and buried paleosols. *N.Z. Journal of Geology and Geophysics 16(3):* 497-518.

Pullar, W.A.; Selby, M.J. 1971: Coastal progradation of Rangitaiki Plains, New Zealand. *N.Z. Journal of Science 14:* 419-434.

Raeside, J.D. 1964: Loess deposits of the South Island, New Zealand, and soils formed on them. *N.Z. Journal of Geology and Geophysics 7:* 811-838.

Ragan, D.M. 1973: *Structural geology.* 2nd Ed. John Wiley & Sons, N.Y. 208p.

Ramsay, J.G. 1961: The effects of folding upon the orientation of sedimentation structures. *Journal of Geology 69:* 84-100.

Reineck, H.-E.; Singh, I.B. 1973: *Depositional sedimentary environments.* Springer-Verlag. 435p.

Rusnak, G.A. 1957: The orientation of sand grains under conditions of "unidirectional" fluid flow 1. Theory and experiment. *Journal of Geology 65:* 384-409.

Russell, R.D. 1939: Effects of transportation on sedimentary particles. *In* Trask, P.D. (ed.): *Recent marine sediments.* Tulsa, American Association of Petroleum Geologists: 32-47.

Rust, B.R. 1972a: Structure and process in a braided river. *Sedimentology 18:* 221-246.

Rust, B.R. 1972: Pebble orientation in fluvial sediments. *J. Sedimentary Petrologists 42:* 384-388.

Rust, B.R. 1975: Fabric and structure in glaciofluvial gravels. *In* Jopling, A.V.; McDonald, B.C. (editors): *Glaciofluvial and glaciolacustrine sedimentation.* Soc. Econ, Paleont. Min., Spec. Publ. 23: 177-192.

Sames, C. 1966: Morphometric data of some recent pebble associations and their application to ancient deposits. *J. Sedimentary Petrology 36:* 126-142.

Sedimentary Petrology Seminar, 1965: Gravel fabric in Wolf Run. *Sedimentology 4:* 273-283.

Seward, D. 1974a: *Some aspects of sedimentology of the Wanganui Basin, North Island, New Zealand.* Ph.D. thesis, Victoria University of Wellington.

Seward, D. 1974b: Age of New Zealand Pleistocene Substages by fission-track dating of glass shards from tephra horizons. *Earth and Planetary Science Letters 24:* 242-8.

Seward, D. 1975: Fission-track ages of some tephras from Cape Kidnappers, Hawke's Bay. *N.Z. Journal of Geology and Geophysics 18(3):* 507-510.

Seward, D. 1976: Tephrostratigraphy of the marine sediments in the Wanganui Basin, New Zealand. *N.Z. Journal of Geology and Geophysics 19(1):* 9-20.

Shackleton, N.J.; Opdyke, N.D. 1976: Oxygen-isotope and paleomagnetic stratigraphy of Pacific core V28-239 Late Pliocene to Latest Pleistocene. *Geological Society of America Memoir 145:* 449-464.

Shackleton, N.J.; Opdyke, N.D. 1973: Oxygen isotope and paleomagnetic stratigraphy of equatorial Pacific core V28-238: Oxygen isotope temperatures and ice volumes on a 10^5 year and 10^6 year scale. *Quaternary Research:* 39-55.

Shaw, J. 1977: Till deposited in arid polar environments. *Canadian Journal of Earth Sciences 14(6):* 1239-1245.

Slatt, R.M.; Press, D.E. 1976: Computer program for presentation of grain-size data by the graphic method. *Sedimentology 23:* 121-131.

Smith, N.D. 1970: The braided stream depositional environment: comparison of the Platte River with some Silurian clastic rocks, north-central Appalachians. *Geological Society of America Bulletin 81:* 2993-3014.

Smith, N.D. 1974: Sedimentology and bar formation in the upper Kicking Horse River, a braided outwash stream. *Journal of Geology 82:* 205-224.

Sneed, E.D.; Folk, R.L. 1958: Pebbles in the lower Colorado River, Texas: A study in particle morphogenesis. *Journal of Geology 66(2):* 114-150.

Spalletti, L.A. 1976: The axial ratio $^{C}/_{B}$ as an indicator of shape selective sorting. *J. Sedimentary Petrology 46(1):* 243-248.

Spörli, K.B.; Barter, T.P. 1973: Geological reconnaissance in the Torlesse Super-group of the Kaimanawa Ranges along the lower reaches of the Waipakihi River, North Island, New Zealand. *N.Z. Journal of Geology and Geophysics 13(3):* 363-380.

Spörli, K.B.; Bell, A.B. 1976: Torlesse Mélange and coherent sequences, eastern Ruahine Range, North Island, New Zealand. *N.Z. Journal of Geology and Geophysics 19(4):* 427-447.

Starkey, J. 1977: The contouring of orientation data represented in spherical projection. *Canadian Journal of Earth Sciences 14(2):* 268-277.

Steel, R.J. 1976: Devonian Basins of western Norway - Sedimentary response to tectonism and varying tectonic context. *Tectonophysics 36:* 207-224.

Steel, R.J.; Moehle, S.; Nilsen, H. 1976: Coarsening-upwards cycles in the alluvium of Hornten Basin (Devonian), Norway: Sedimentary response to tectonic events. *Geological Society of America Bulletin 88(8):* 1124-1134.

Steinmetz, R. 1962: Analysis of vectorial data. *J. Sedimentary Petrology 34(4):* 801-812.

Suggate, R.P. 1965: The tempo of events in New Zealand geological history. *N.Z. Journal of Geology and Geophysics 8(6):* 1139-1149.

Suggate, R.P. 1972: North Island (1st Ed.): *Geological Map of New Zealand 1: 1 000 000.* N.Z. Department of Scientific and Industrial Research, Wellington.

Taylor, G.I. 1923: The motion of ellipsoidal particles in a viscous fluid. *Roy. Soc. London Proc. 103A:* 58-61.

Taylor, N.H.; Pohlen, I.J. 1970: Soil Survey Method. *N.Z. Soil Bur. Bull. 25:* 241p. (2nd ed.). N.Z. Department of Scientific and Industrial Research, Wellington.

Tilly, C.R. 1977: Size analysis of silt and clay by hydrophotometer. *J. Sedimentary Petrology 47(2):* 930-931.

Toots, H. 1962: Random orientation of fossils and its significance. *Wyoming University Contributions to Geology 4(2):* 59-62.

Turner, F.J.; Weiss, L.E. 1963: *Structural analysis of metamorphic tectonites.* International Series in Earth Sciences, Shrock, R.R. consulting editor. McGray-Hill, N.Y.

Turner, J.C. 1970: *Modern applied mathematics.* English Universities Press, London. 502p.

Twenhofel, W.N. 1932: *Treatise on sedimentation.* Williams and Wilkins, Baltimore. 926p.

Unrug, R. 1957: Recent transport and sedimentation of gravels in the Dunager Valley (western Carpathians). *Acta. Geol. Polonica, (English translations) 7:* 217-257.

Visher, G.S. 1965: Fluvial processes as interpreted from ancient and recent fluvial deposits. *In* Middleton, G.V. (ed.): *Primary sedimentary structures and their hydrodynamic interpretation.* Soc. Econ. Paleont. Min., Spec. Publ. 12: 116-132.

Visher, G.S. 1969: Grain size distributions and depositional processes. *J. Sedimentary Petrology 39:* 1074-1106.

Vucetich, C.G.; Pullar, W.A. 1969: Stratigraphy and chronology of Late Pleistocene volcanic ash beds in central North Island. *N.Z. Journal of Geology and Geophysics 12(4):* 786-837.

Walker, J. 1971: Grain size characteristics of pyroclastic deposits. *Journal of Geology 79(6):* 696-714.

Walker, R.G. 1975: Generalized facies models for resedimented conglomerates of turbidite association. *Geological Society of America Bulletin 86:* 737-748.

Watkins, N.D.; Huang, T.C. 1977: Tephras in abyssal sediments east of North Island, New Zealand: chronology, paleowind velocity, and paleoexplosivity. *N.Z. Journal of Geology and Geophysics 20(1):* 179-199.

White, W.S. 1952: Imbrication and initial dip in a Keweenawan conglomerate bed. *J. Sedimentary Petrology 22:* 189-199.

Williams, P.F.; Rust, B.R. 1969: The sedimentology of a braided river. *J. Sedimentary Petrology 39:* 649-679.

Woodcock, N.H. 1977: Specification of fabric shapes using an eigenvalue method. *Geological Society of America Bulletin 88:* 1231-1236.

APPENDIX (I i)

```
C      THIS PROGRAM CALCULATES VARIOUS SHAPE INDICES, DETERMINES
C      THE STATISTICAL NATURE OF THE DISTRIBUTION FOR EACH INDEX AND
C      PLOTS THE SHAPE ON THE SPHERICITY-FORM DIAGRAM OF SNEED AND FOLK
C      THE SHAPE INDICIES CALCULATED ARE : MAXIMUM PROJECTION SPHERICITY
C      (SNEED&FOLK), OBLATENESS-PROLATENESS INDEX (DOBKINS&FOLK),
C      BLADED INDEX (THE BASAL PARAMETER IN THE SPHERICITY-FORM DIAGRAM )
C      AND THE ELONGATION INDEX (FOLK)
C
C      THE SIMPLE STATISTICS CALCULATED ARE : N,MEAN, SUM OF MEAN DEVIATI ONS,
C      VARIANCE, STANDARD DEVIATION, AND 95 PERCENT CONFIDENCE LIMITS.
FILE   5=READIT,UNIT=READER

FILE   6=PRINTDATA,UNIT=PRINTER


       REAL L(1000),M(1000),S(1000),ST(1000),LM(1000),SS(1000),LI(1000),
      1LS(1000),NAMES(6),T(40),LX(1000),LY(1000)
       COMMON IR,IW
       IR = 5
       IW = 6
       READ(IR,1) NRANGE , NO
C      NRANGE SPECIFIES THE RANGE OF THE DATA VALUES. IN THIS CASE 0.0 -  1.0
C      NO SPECIFIES THE NUMBER OF SAMPLES
     1 FORMAT (2I5)
       READ(IR,2)  (T(I),I = 1,35)
     2 FORMAT (20F4.2 / 20F4.2)
       DO 14 NB = 1, NO
       READ (IR,3) NAMES , K
C      K  IS THE NUMBER OF VALUES IN EACH SAMPLE
     3 FORMAT(6A6,I5)
       WRITE (IW,4) NAMES , K
     4 FORMAT ('1',/' ',6A6 ,I5,' PEBBLE MEASUREMENTS')
       II = 1
       JJ = 5
       KK = K/5
       DO 6  J = 1,KK
       READ (IR,5) (L(I),M(I),S(I),I=II,JJ)
C      L = LENGTH LONG AXIS, M = INTERMEDIATE, AND S = SHORT AXIS LENGTH.
     5 FORMAT (5(3F5.2),5X)
       II = II + 5
       JJ = JJ + 5
     6 CONTINUE
       DO 7  I = 1,K
       LY(I) = M(I) / L(I)
       SS(I) = S(I) * S(I)
       LM(I) = L(I) * M(I)
       ST(I) = SS(I)/LM(I)
     7 ST(I) = ST(I) ** 0.333333
       DO 8 I =1,K
       LI(I) = (L(I)-M(I)) / (L(I)-S(I))
       LS(I) = S(I) / L(I)
     8 LX(I) = 10.0*((LI(I) - 0.5)/LS(I))
C      ST = MAXIMUM PROJECTION SPHERICITY
C      LI = RATIO PLATY TO ELONGATED  OR THE BLADED INDEX.
C      LS = RATIO COMPACT TO PLATY
C      LX = OBLATENESS - PROLATENESS INDEX
C      LY = ELONGATION INDEX
```

```
      WRITE (IW,9)
    9 FORMAT(//' ','LONG',2X,'INTERMEDIATE',2X,'SHORT',2X,'SPHERICITY (S
     1NEED&FOLK)',2X,'BLADED INDEX',2X,'RATIO COMPACT : PLATY',5X,'OP IN
     1DEX',8X,'ELONGATION INDEX')
      IC = 0
      DO 13 I = 1,K
      IC = IC + 1
      IF(IC.NE.41)GO TO 11
      WRITE (IW,10)
   10 FORMAT('1',/' ','LONG',2X,'INTERMEDIATE',2X,'SHORT',2X,'SPHERICITY
     1 (SNEED&FOLK)',2X,'BLADED INDEX',2X,'RATIO COMPACT : PLATY',5X,'OP
     1 INDEX',8X,'ELONGATION INDEX')
      IC = 0
   11 WRITE (IW,12) L(I),M(I),S(I),ST(I),LI(I),LS(I),LX(I),LY(I)
   12 FORMAT( ' ',F5.2,5X,F5.2,5X,F5.2,12X,F5.2,11X,F5.2,14X,F5.2,15X,F7
     1.2,10X,F5.2)
   13 CONTINUE
C     SUBROUTINE STAT IS REPEATEDLY CALLED TO CALCULATE STATISTICS ON
C     THE SHAPE INDICIES AND SIZE
      CALL STAT(M,K,T)
      CALL STAT(ST,K,T)
      CALL STAT(LX,K,T)
      CALL STAT(LY,K,T)
      CALL STAT(LI,K,T)
      CALL PLOT(LI,LS,K,NRANGE)
C     SUBROUTINE PLOT IS CALLED TO PLOT THE VALUES.
   14 CONTINUE
      STOP
      END
```

```
      SUBROUTINE STAT(A,K,T)
      DIMENSION A(300),T(40)
      COMMON IR,IW
      SUM = 0.0
      DMEAN = 0.0
      DO 1 I = 1,K
    1 SUM = SUM + A(I)
      AMEAN = SUM / K
      DO 2 I = 1,K
    2 DMEAN = DMEAN + (AMEAN - A(I))** 2
      IF(K-30)3,3,4
    3 VAR = DMEAN / (K-1)
      STDEV = SQRT(VAR)
      GO TO 5
    4 VAR = DMEAN / K
      STDEV = SQRT(VAR)
    5 IF (K - 35) 11,12,6
    6 IF (K - 40) 12,13,7
    7 IF (K - 50) 13,14,8
    8 IF (K - 60) 14,15,9
    9 IF (K - 90) 15,16,10
   10 IF (K - 120) 16,17,18
   11 TE = T(K-1)
      GO TO 19
   12 TE = 2.03
      GO TO 19
```

```
13 TE = 2.02
   GO TO 19
14 TE = 2.01
   GO TO 19
15 TE = 2.00
   GO TO 19
16 TE = 1.99
   GO TO 19
17 TE = 1.98
   GO TO 19
18 TE = 1.96
19 Z = K
   CON = TE * STDEV / SQRT(Z)
   WRITE(IW,20)K,AMEAN,DMEAN,VAR,STDEV,CON
20 FORMAT(' ','N = ',I3,5X,',MEAN = ',F7.2,5X,',DMEAN = ',F9.3,5X,',V
  1ARIANCE =',F7.3,5X,',STDEV = ',F7.3,5X,',CON = ',F7.3)
   RETURN
   END



   SUBROUTINE PLOT(LI,LS,N,NRANGE)
   DIMENSION LI(300),LS(300),POS(51,101),OPOS(300,2),POSPLT(4)
   DATA CLASS/'.'/,BLANK/' '/,POSPLT/'+','2','3','4'/,PERCNT/'*'/
   COMMON IR,IW
   DO 2 J = 1,50
   DO 2 I = 1,101
   POS(J,I) = BLANK
 2 POS(51,I) = CLASS
   DO  3 I = 1,101,10
 3 POS(51,I) = PERCNT
   DO 4 I = 2,50
   K = 52-I
   L = 50+I
   POS (I,K) = CLASS
 4 POS (I,L) = CLASS
   POS (I,51) =PERCNT
   DO 5 I = 6,46,5
   K = 52-I
   L = 50+I
   POS (I,K) = PERCNT
 5 POS (I,L) = PERCNT
   DO 20 I = 1,N
   X = LS(I)
   Y = LI(I)
   IF(Y.EQ.0.0) Y = 0.001
   IF(NRANGE.EQ.100)GO TO 8
   IF(NRANGE.EQ.10)GO TO 7
 6 XPOS = 100.* X/2.
   GO TO 9
 7 XPOS = 10.0 * X/2.
   GO TO 9
 8 XPOS = 1.0 * X/2.
 9 CONTINUE
   LPOS = XPOS + 0.5
   LPOS = 51-LPOS
```

```
      IF(NRANGE.EQ.100)GO TO 13
      IF(NRANGE.EQ.10)GO TO 12
   11 YPOS = (101.-((100. * Y)+ 0.5))
      GO TO 14
   12 YPOS = (101.-((10.0 * Y)+ 0.5))
      GO TO 14
   13 YPOS = (101.-((1.0 * Y)+ 0.5))
   14 CONTINUE
      XPOS = (51.-XPOS)/51.0
      JPOS = (50.-YPOS) * XPOS + 52.0
      IF(JPOS.LE.0)JPOS = 1
      OPOS(I,1) = ℓPOS
      OPOS(I,2) = JPOS
      KOUNT = 0
      DO 15  J = 1,I
      IF(OPOS(J,1).EQ.ℓPOS.AND.OPOS(J,2).EQ.JPOS)KOUNT = KOUNT + 1
   15 CONTINUE
      IF(KOUNT.GT.0)GO TO 16
   16 IF(ℓPOS.GT.0.AND.JPOS.GT.0)GO TO 17
      GO TO 18
   17 IF(ℓPOS.LT.52.AND.JPOS.LT.102)GO TO 19
   18 WRITE(IW,/)I,X,Y,ℓPOS,JPOS
      GO TO 20
   19 CONTINUE
      IF(KOUNT.GT.3)KOUNT = 4
      POS(ℓPOS,JPOS) = POSPLT(KOUNT)
   20 CONTINUE
      WRITE(IW,21)
   21 FORMAT('1')
      WRITE(IW,22) N
   22 FORMAT(' ',63X,'COMPACT',15X,'N =',I4)
      DO 23 M = 1,51
   23 WRITE(IW,24) (POS(M,N),N = 1,101)
   24 FORMAT(' ',16X,101A1)
      WRITE(IW,25)
   25 FORMAT(' ',12X,'PLATY',97X,'ELONGATED')
      WRITE(IW,21)
      RETURN
      END
```

APPENDIX (I ii)

```
C     THIS PROGRAM CALCULATES STATISTICS ABOUT THE DISTRIBUTION OF
C     ORIENTATION DATA.
C     THE PROGRAM IS AN ADAPTION OF AN EXISTING PROGRAM(SEWARD,1974).
C     THE STATISTICS CALCULATED ARE :VECTOR MEAN, VECTOR MAGNITUDE (%)
C     VARIANCE, STANDARD DEVIATION,SUM OF THE MEAN DEVIATIONS ,THE
C     95 AND 99 PERCENT CONFIDENCE LIMITS.
FILE  5=READIT,UNIT=READER

FILE  6=PRINTDATA,UNIT=PRINTER


      REAL LOCET(18),LOCNO
      DIMENSION A(500),M(200),T(40),TT(40)
      IR = 5
      IW = 6
      READ(IR,1) (T(I),I = 1,35)
      READ(IR,1)(TT(I),I = 1,35)
C     T SPECIFIES THE T VALUES IN THE STUDENTS T DISTRIBUTION CORRESPOND
C     -ING TO P=0.05 (2P)
C     TT SPECIFIES THE T VALUES WHERE P=0.01 (2P)
    1 FORMAT(20F4.2/20F4.2)
      WRITE(IW,2)
    2 FORMAT ('1',////' VECTOR MEAN, STANDARD DEVIATION, CONFIDENCE
     1INTERVAL (95%)  AND  (99%) '/10X,'FOR CURRENT DIRECTION DATA')
      GO TO 5
    3 WRITE(IW,4)
    4 FORMAT('1'////)
      P=0
      GO TO 6
    5 P = 1
    6 READ(IR,7)N,LOCET
C     N = THE NUMBER OF VALUES IN EACH SAMPLE
C     LOCET = INFORMATION ABOUT THE SAMPLES : POSITION AND SEDIMENT STR.
    7 FORMAT(I3,1X,18A4)
      IF(N) 49,49,8
    8 CONTINUE
      WRITE(IW,9)LOCET
    9 FORMAT(/' ',20A4)
      P = P+1
      READ(IR,10) (A(I),I = 1,N)
   10 FORMAT(19F4.0)
      L = N
      I = 1
      N = 1
      DO 14 J = 1,L
      IF(A(I))11,11,12
   11 N = N-1
      GO TO 13
   12 A(N) = A(I)
   13 I = I+1
   14 N = N+1
      N = N-1
      IF(N-1)6,15,16
   15 GO TO 47
   16 CONTINUE
      SS = 0.0
      SC = 0.0
```

```
      DO 17 I = 1,N
      SS = SS+SIN(A(I) *0.01745)
   17 SC = SC+COS(A(I) * 0.01745)
      R = SQRT(SS * SS+SC * SC)
      VMEAN = (ATAN(SS/SC) * 180./3.14159)
      IF(SS)21,18,18
   18 IF(SC)20,19,19
   19 VMEAN = VMEAN
      GO TO 23
   20 VMEAN = VMEAN + 180.
      GO TO 23
   21 IF(SC)20,22,22
   22 VMEAN = VMEAN + 360.
   23 CONTINUE
      EL = R * 100.0/N
      SUMV = 0.0
      DO 28 I = 1,N
      DIFF = (VMEAN - A(I))
      IF(DIFF - 180.0)25,24,24
   24 DIFF = A(I) + 360.0 - VMEAN
      GO TO 27
   25 IF(DIFF + 180.0)26,26,27
   26 DIFF = VMEAN + 360.0 - A(I)
   27 CONTINUE
      M(I) = A(I)
   28 SUMV = SUMV + DIFF ** 2
      IF(N-30)29,29,30
   29 VAR = SUMV/N
      STDEV = SQRT(VAR)
      GO TO 31
   30 VAR = SUMV/N
      STDEV = SQRT(VAR)
   31 IF(N-35)37,38,32
   32 IF(N-40)38,39,33
   33 IF(N-50)39,40,34
   34 IF(N-60)40,41,35
   35 IF(N-90)41,42,36
   36 IF(N-120)42,43,44
   37 TE = T(N-1)
      TTE = TT(N-1)
      GO TO 45
   38 TE = 2.03
      TTE = 2.73
      GO TO 45
   39 TE = 2.02
      TTE = 2.70
      GO TO 45
   40 TE = 2.01
      TTE = 2.68
      GO TO 45
   41 TE = 2.00
      TTE = 2.66
      GO TO 45
   42 TE = 1.99
      TTE = 2.64
      GO TO 45
   43 TE = 1.98
      TTE = 2.62
      GO TO 45
   44 TE = 1.96
      TTE = 2.57
   45 Z = N
```

```
      CON = TE * STDEV/SQRT(Z)
      CONN = TTE * STDEV/SQRT(Z)
      VMEAN = VMEAN + 0.5
      SUMV = SUMV + 0.5
      STDEV = STDEV + 0.5
      CON = CON + 0.5
      CONN = CONN + 0.5
      WRITE(6,46)VMEAN,VAR ,STDEV,N,EL
   46 FORMAT(' ','VEC MEAN=',F4.0,1X,'VARIANCE=',F5.0,1X,'STDEV=',F4.0,1
     1X,'READINGS=',I3,1X,'VEC MAG(%)=',F6.2)
      WRITE(IW,60)CON,CONN,SUMV
   60 FORMAT(' ','CON INTVL(95%)=',F4.0,1X,'CON INTVL(99%)=',F4.0,1X,'SU
     1MV=',F9.0)
   47 WRITE(IW,48) (M(I),I = 1,N)
   48 FORMAT(' TRUE AZIMUTH'11I5)
      IF(P-12)6,3,3
   49 STOP
      END
```

APPENDIX (I iii)

```
C     THIS PROGRAM CALCULATES AND PRESENTS THE TEXTURAL DISTRIBUTION OF
C     EARTH MATERIALS
C     IT IS WRITTEN TO COMBINE RAW DATA FROM SIEVES (-6.0 PHI TO 4.0PHI)
C     WITH HYDROPHOTOMETER DATA.
C     THREE TYPES OF INPUT ARE REQUIRED ;THE CUM. WTS.FOR SUCCESSIVE
C     SIEVE INTEVALS, THE TRANSMISSION READINGS FROM THE HYDROPHOTOMETER
C     AND THE WEIGHT OF MUD.
C     THE TEXTURE DISTRIBUTION IS PRESENTED AS PLOTS OR STATISTICS:
C       (1)THREE CURVES  -ACCURACY  0.5%
C          (A)HISTOGRAM
C          (B)% CUM. WT.(ARITHMETIC ORDINATE)
C          (C)% CUM. WT.(PROBABILITY ORDINATE)
C       (2) THE EXACT POSITIONS FOR THE DATA VALUES IN THE CURVES(0.005)
C       (3) PERCENT GRAVEL,SAND,SILT,CLAY, RATIO CLAY/SILT AND SAND/MUD
C       (4) TEXTURAL CLASS FOR GRAVEL FREE /GRAVEL BEARING DETRITAL SEDS
C       (5) FOLK STATISTICS:- MZ,SORTING,SKEWNESS,KURTOSIS
C       (6) MEDIAN  AND  C STATISTIC
C       (7) VERBAL CLASSIFICATION FOR STATISTICAL PARAMETERS(FOLK,ANDREW
C           S,AND LEWIS)
C
FILE  5=READIT,UNIT=READER

FILE  6=PRINTDATA,UNIT=PRINTER


      DIMENSION NAMES(5),RI(10),WI(49),RJ(9),LINE(101),XI(49),
     1RD(9),RP(9),RU(8),WILOG(49)
      DATA RJ/43.08,27.52,17.64,10.80,6.74,4.60,3.10,1.93,0.56/
      DATA IDOT/"."/,IBLANK/" "/,ICROSS/"*"/,IPLUS/"+"/,IEX/"X"/
      COMMON IR,IW
      IR = 5
      IW = 6
  101 S=0
      READ(IR,1,END=102) NAMES
C     NAMES  IS THE SAMPLE NUMBER AND LOCATION.
      READ(IR,2) (RI(I),I=1,9),WM
C     RI SPECIFIES HYDROPHOTOMETER TRANSMISSION READINGS AND WM = WT.MUD
      READ(IR,2) (WI(I),I=1,40)
C     WI SPECIFIES THE CUMULATIVE SIEVE WEIGHTS.
    1 FORMAT(5A6)
    2 FORMAT(10F8.2)
      WRITE(IW,4)NAMES,(RI(I),I=1,9),WM
    4 FORMAT("1",/" ",5A6," RI",9F8.2," WT MUD=",F8.2)
      WRITE(IW,9)
    9 FORMAT(50X,"KEY  : ",5X,"+ = % INTEVAL WT.")
      WRITE(IW,11)
   11 FORMAT(62X,"* = % CUM.WT. (ARITHMETIC ORDINATE)")
      WRITE(IW,12)
   12 FORMAT(62X,"X = % CUM.WT. (PROBABILITY ORDINATE)")
      W=WM+WI(40)
C     CONVERSION OF TRANSMISSION VALUES TO PERCENT OF TOTAL DISTRIBUTION
C     IN HALF PHI INTEVALS BEGINS
      DO 10 I=1,9
   10 RI(I)=100*ALOG(100.0/RI(I))
      RI(10)=0.0
      DO 15 I=1,9
      RI(I)=(RI(I)-RI(I+1))*RJ(I)
   15 S=S+RI(I)
```

```
      DO 21 I=1,9
   21 RD(I)=RI(I)*WM/S
      WMW=WM-RD(9)
      DO 24 I=1,8
   24 RD(I)=RI(I)*WMW/S
      DO 22 I=1,8
      RP(I)=RD(I)
   22 RP(I)=(RP(I)/WMW)*RD(9)
      DO 23 I=1,8
   23 RU(I)=RD(I)+RP(I)
      DO 20 I=1,8
C     COMBINATION OF CUMULATIVE WTS.SIEVE + HYDROPHOTOMETER.
   20 WI(40+I)=WI(39+I)+RU(I)
      WS=WI(40)+WMW
      DO 120 I=1,48
  120 XI(I)=WI(I)
C     SETTING UP OF THE GRAPHS COMMENCES.
      DO 25 I=1,101
   25 LINE(I)=IDOT
      WRITE(IW,5) LINE
    5 FORMAT("0",101A1," PHI %I.WT. C.WT. %C.WT. PROB.")
      R=-6.0
C     START OF A MAJOR LOOP WHICH SUCCESSIVELY CALCULATES AND PLOTS THE
C     APPROXIMATE AND EXACT POSITIONS OF THE DISTRIBUTION IN PHI INTEVAL
      DO 100 I=1,48
      LINE(1)=IDOT
      IF(I.LE.40)GO TO 26
      WRITE(IW,6)LINE(1)
      R=R+0.25
   26 CONTINUE
C     A IS CUM. WEIGHT;WI(I) IS %CUM.WT;B IS % I.WT.
      A=WI(I)
      WI(I)=100*A/WS
      B=WI(I)
      IF(I.NE.1)B=B-WI(I-1)
C     WILOG IS PROB TRANS
      WILOG(I)=PRPLOT(WI(I))
C     K IS ROUNDED WI POS
      K=WI(I)+1.5
C     KK IS ROUNDED B POS
      KK=B+1.5
      IF(KK.GE.101)KK = 101
C     KKK IS ROUNDED WILOG POS
      KKK=WILOG(I)+1.5
      IF (KKK.LE.0) KKK = 1
      IF(KKK.GE.101)KKK= 101
      DO 30 J = 2,101
   30 LINE(J)=IBLANK
      LINE(K)=ICROSS
      LINE(KK)=IPLUS
      LINE(KKK)=IEX
C     R IS PHI
      R=R+0.25
      WRITE(IW,6) LINE,R,B,A,WI(I),WILOG(I)
    6 FORMAT(" ",101A1,F5.2,4F6.2)
  100 CONTINUE
      CALL RVALUE(XI,W)
      CALL STAT(WI)
      GO TO 101
  102 STOP
      END
```

```
      FUNCTION PRPLOT(Z)
C     THE FUNCTION SUBROUTINE TRANSFORMS THE ARITHMETIC VALUE TO THE
C     EQUIVALENT LOG PROBABILITY VALUE AND RETURNS THIS TO THE MAIN
C     PROGRAM WHERE IT IS PLOTTED AS A LOG VALUE ON ARITHMETIC PAPER.
      DATA A1,A2,A3,A4,A5,A6,A7,A8,B1,B2,B3,B4,B5,B6,B7,B8,C1,C2,C3,C4,
     -C5,C6,C7,C8,D1,D2,D3,D4,D5,D6,D7,D8/
     --.44385091430,1.0,.31169251605E-2,-.45542638681,
     -.25349672693,.37769369170,-.84283443971,.25829275637,
     --.25490839451,.92809154567,-1.0,.32994452136,
     ..21073384241,-.31953295769,.63935580804E-1,.46044014867E-1,
     --.18878589624,.79431763639,-1.0,.39466194490,
     -.35955797680,-.88840235361,.70866465260,-.17975642347,
     -.99443262630E-1,-.19325175911,.90713856871E-1,.3100715305E-2,
     -.35318924622,-1.0,.94142741782,-.29461486428/
      Y=Z/100.
      BNEG=1.
      IF(Y.GT.0.5) GO TO 2
      Y=1.-Y
      BNEG=-1.
    2 IF(Y.LT..7661446733) GO TO 4
      IF(Y.LT..9164546629) GO TO 5
      IF(Y.LT..9740244848) GO TO 6
      IF(Y.LT..9918300158) GO TO 7
      IF(Y.LT..9999) GO TO 8
      Y=BNEG*3.7
      GO TO 10
    4 Y=BNEG*(((A4*Y+A3)*Y+A2)*Y+A1)/(((A8*Y+A7)*Y+A6)*Y+A5)
      GO TO 10
    5 Y=(((B4*Y+B3)*Y+B2)*Y+B1)/(((B8*Y+B7)*Y+B6)*Y+B5)*BNEG
      GO TO 10
    6 Y=BNEG*(((C4*Y+C3)*Y+C2)*Y+C1)/(((C8*Y+C7)*Y+C6)*Y+C5)
      GO TO 10
    7 Y=BNEG*(((D4*Y+D3)*Y+D2)*Y+D1)/(((D8*Y+D7)*Y+D6)*Y+D5)
      GO TO 10
    8 Y=172.8395*(Y-0.97791433)*BNEG
   10 PRPLOT=100.*(Y/7.4+0.5)
      RETURN
      END
```

```
      SUBROUTINE RVALUE(XI,W)
C     THE SUBROUTINE CALCULATES THE % GRAVEL,SAND,SILT,CLAY AND FINDS
C     THE CORRECT TEXTURAL CLASS FOR EITHER GRAVEL FREE OR GRAVEL
C     BEARING DETRITAL SEDIMENTS
      DIMENSION XI(49)
      COMMON IR,IW
      DO 110 I=1,48
  110 XI(I)=100*XI(I)/W
      CLAY=100.-XI(48)
      SILT=XI(48)-XI(40)
      SAND=XI(40)-XI(20)
      GRAVEL=XI(20)
      WRITE(IW,7)GRAVEL,SAND,SILT,CLAY
    7 FORMAT(" CUM%WT.GRAVEL=",F7.2,",SAND=",F7.2,",SILT=",F7.2,
     1",CLAY=",F7.2)
      RCS=CLAY/SILT
      RMS=SAND/(SILT+CLAY)
      WRITE(IW,8)RCS,RMS
    8 FORMAT(" ","RATIO CLAY/SILT=",F7.2,",RATIO SAND/MUD=",F7.2)
      IF(GRAVEL.LE.0.0)GO TO 250
      WRITE(IW,200)
  200 FORMAT(" TEXTURAL TERMINOLOGY FOR GRAVEL BEARING DETRITAL SEDIMENT
     1S")
      IF(GRAVEL-80.0)203,201,201
  201 WRITE(IW,202)
  202 FORMAT(5X,'GRAVEL')
      GO TO 300
  203 IF(GRAVEL-30.0)212,204,204
  204 IF(RMS-1.0)205,205,207
  205 WRITE(IW,206)
  206 FORMAT(5X,'MUDDY GRAVEL')
      GO TO 300
  207 IF(RMS - 9.0)208,208,210
  208 WRITE(IW,209)
  209 FORMAT(5X,'MUDDY SANDY GRAVEL')
      GO TO 300
  210 WRITE(IW,211)
  211 FORMAT(5X,'SANDY GRAVEL')
      GO TO 300
  212 IF(GRAVEL-5.0)221,213,213
  213 IF(RMS -1.0)214,214,216
  214 WRITE(IW,215)
  215 FORMAT(5X,'GRAVELLY MUD')
      GO TO 300
  216 IF(RMS-9.0)217,217,219
  217 WRITE(IW,218)
  218 FORMAT(5X,'GRAVELLY MUDDY SAND')
      GO TO 300
  219 WRITE(IW,220)
  220 FORMAT (5X,'GRAVELLY SAND')
      GO TO 300
  221 IF(GRAVEL-0.01)230,222,222
  222 IF(RMS -1.0)223,223,225
  223 WRITE(6,224)
  224 FORMAT(5X,'SLIGHTLY GRAVELLY MUD')
      GO TO 300
  225 IF(RMS-9.0)226,226,228
  226 WRITE(IW,227)
  227 FORMAT(5X,'SLIGHTLY GRAVELLY MUDDY SAND')
```

```
      GO TO 300
  228 WRITE(IW,229)
  229 FORMAT(5X,'SLIGHTLY GRAVELLY SAND')
      GO TO 300
  230 IF(RMS -0.1111) 231,231,233
  231 WRITE (IW,232)
  232 FORMAT (5X,'MUD')
      GO TO 300
  233 IF(RMS- 1.0) 234,234,236
  234 WRITE (IW,235)
  235 FORMAT (5X,'SANDY MUD')
      GO TO  300
  236 IF(RMS - 9.0) 237,237,239
  237 WRITE(IW,238)
  238 FORMAT(5X,'MUDDY SAND')
      GO TO 300
  239 WRITE (IW,240)
  240 FORMAT (5X,'SAND')
  250 WRITE( IW,251)
  251 FORMAT (' TEXTURAL TERMINOLOGY  FOR  GRAVEL FREE DETRITAL SEDIMENT
     1S')
      IF(SAND - 90.0)254,252,252
  252 WRITE(IW,253)
  253 FORMAT (5X,'SAND')
      GO TO  300
  254 IF(SAND- 50.0)263,255,255
  255 IF(RCS - 2.0) 258,256,256
  256 WRITE (IW,257)
  257 FORMAT (5X,'CLAYEY SAND')
      GO TO  300
  258 IF(RCS-0.5) 261,259,259
  259 WRITE (Iw,260)
  260 FORMAT (5X,'MUDDY SAND')
      GO TO 300
  261 WRITE( IW,262)
  262 FORMAT (5X,'SILTY SAND ')
      GO TO 300
  263 IF(SAND -10.0)272,264,264
  264 IF(RCS - 2.0)267,265,265
  266 FORMAT(5X,'SANDY CLAY')
  265 WRITE(IW,266)
      GO TO 300
  267 IF(RCS - 0.5) 270,268,268
  268 WRITE (IW,269)
  269 FORMAT (5X,'SANDY MUD')
      GO TO 300
  270 WRITE (IW,271)
  271 FORMAT (5X,'SANDY SILT')
      GO TO  300
  272 IF (RCS-2.0)275,273,273
  273 WRITE (IW,274)
  274 FORMAT (5X,'CLAY')
      GO TO 300
  275 IF (RCS - 0.5) 278,276,276
  276 WRITE(IW,277)
  277 FORMAT(5X,'MUD')
      GO TO 300
  278 WRITE (IW,279)
  279 FORMAT (5X,'SILT')
  300 RETURN
      END
```

```
      SUBROUTINE STAT(WI)
C     THE SUBROUTINE CALCULATES THE FOLK&WARD STATISTICS AND
C     DETERMINES THE VERBAL CLASSIFICATION FOR THE PARAMETERS AFTER
C     THE SCHEME OF FOLK,ANDREWS AND LEWIS.
      DIMENSION WI(49)
      COMMON IR,IW
      DO 318 I=1,48
      IF(WI(I).GE.95)GO TO 319
  318 CONTINUE
      WRITE(IW,320)
  320 FORMAT(' 95 PERCENTILE NOT PRESENT ; CALCULATION OF FOLK PARAMETER
     1S NOT POSSIBLE ')
      GO TO 101
  319 IF(I-42)801,801,802
  801 PL95 = -5.75 +(I-2)*0.25
      IF(I.GE.41)PL95 =PL95 +0.25
      GO TO 827
  802 PL95 = 4.50+(I-42)*0.5
  827 PU95 =PL95+0.25
      IF(I.GE.40)PU95 =PU95 + 0.25
      PHI95 =PL95 +(95.-WI(I-1))*(PU95-PL95)/(WI(I)-WI(I-1))
  300 DO 301 I=1,48
      IF(WI(I).GE.1.0)GOTO 302
  301 CONTINUE
  302 PL1=-5.75+(I-2)*0.25
      IF(I.GE.41)PL1=PL1+0.25
      PU1 =PL1+0.25
      IF(I.GE.40)PU1=PU1+0.25
      PHI1 = PL1+(1.0-WI(I-1))*(PU1 - PL1)/(WI(I)-WI(I-1))
      DO 304 I =1,48
      IF(WI(I).GE.5)GO TO 305
  304 CONTINUE
  305 IF(I-42)817,817,818
  817 PL5 =-5.75+(I-2)*0.25
      IF(I.GE.41)PL5 = PL5 + 0.25
      GO TO 820
  818 PL5 = 4.50 +(I-42) * 0.5
  820 PU5 = PL5+0.25
      IF(I.GE.40)PU5 = PU5 +0.25
      PHI5 =PL5+ (5.-WI(I-1))*(PU5-PL5)/(WI(I)-WI(I-1))
      DO 308 I =1,48
      IF(WI(I).GE.16)GO TO 309
  308 CONTINUE
  309 IF(I-42)813,813,814
  813 PL16 = -5.75+(I-2)*0.25
      IF(I.GE.41)PL16 = PL16+0.25
      GO TO 822
  814 PL16 = 4.50 + (I-42)*0.5
  822 PU16 = PL16 +0.25
      IF(I.GE.40)PU16=PU16 +0.25
      PHI16 = PL16 +(16.-WI(I-1))*(PU16 - PL16)/(WI(I)-WI(I-1))
      DO 310 I =1,48
      IF(WI(I).GE.25)GO TO 311
  310 CONTINUE
  311 IF(I-42)810,810,811
  810 PL25 = -5.75 +(I-2)*0.25
      IF(I.GE.41)PL25 = PL25+0.25
      GO TO 823
  811 PL25 = 4.50+(I-42)*0.5
  823 PU25 =PL25 +0.25
      IF(I.GE.40)PU25 =PU25+0.25
      PHI25 =PL25 +(25.-WI(I-1))*(PU25-PL25)/(WI(I)-WI(I-1))
```

```
      DO 312 I=1,48
      IF(WI(I).GE.50)GOTO 313
  312 CONTINUE
  313 IF(I-42)808,808,809
  808 PL50 = -5.75 +(I-2)*0.25
      IF(I.GE.41)PL50 =PL50 +0.25
      GO TO 824
  809 PL50 = 4.50 +(I-42)*0.5
  824 PU50 =PL50+0.25
      IF(I.GE.40)PU50 =PU50+0.25
      PHI50 =PL50 +(50.-WI(I-1))*(PU50-PL50)/(WI(I)-WI(I-1))
      DO 314 I= 1,48
      IF(WI(I).GE.75)GO TO 315
  314 CONTINUE
  315 IF(I-42)806,806,807
  806 PL75 = -5.75 +(I-2)*0.25
      IF(I.GE.41)PL75 = PL75+0.25
      GO TO 825
  807 PL75 = 4.50 + (I-42)*0.5
  825 PU75=PL75+0.25
      IF(I.GE.40)PU75 = PU75+0.25
      PHI75 = PL75 +(75.-WI(I-1))*(PU75-PL75)/(WI(I)-WI(I-1))
      DO 316  I= 1,48
      IF(WI(I).GE.84)GO TO 317
  316 CONTINUE
  317 IF(I-42)804,804,805
  804 PL84= -5.75+(I-2)*0.25
      IF(I.GE.41)PL84 =PL84+0.25
      GO TO 826
  805 PL84 = 4.50 +(I-42)*0.5
  826 PU84 = PL84 +0.25
      IF(I.GE.40)PU84=PU84+0.25
      PHI84 =PL84+(84.-WI(I-1))*(PU84-PL84)/(WI(I)-WI(I-1))
C     CALCULATION OF FOLK STATISTICS
      FMZ = .3333*(PHI16 + PHI50 + PHI84)
      FSI = .25*(PHI84-PHI16)+.1515*(PHI95-PHI5)
      FSKEW = .5*(((PHI16+PHI84-2.*PHI50)/(PHI84-PHI16))+((PHI5+PHI95-2.
     1*PHI50)/(PHI95-PHI5)))
      FKG = .4098*((PHI95-PHI5)/(PHI75-PHI25))
      WRITE(IW,321)FMZ,FSI,FSKEW,FKG
  321 FORMAT(' FOLK STATISTICS : MZ =',F7.2,',SORTING =',F7.3,',SKEWNESS
     1 =',F7.3,',KURTOSIS =',F7.3)
      WRITE(IW,322)PHI50,PHI1
  322 FORMAT(' MEDIAN =',F7.2,5X,'C STATISTIC = ',F7.2)
      WRITE(IW,401)
  401 FORMAT(" VERBAL CLASSIFICATION FOR STATISTICAL PARAMETERS (FOLK,AN
     1DREWS,AND LEWIS)")
C     DETERMINATION FOR VERBAL CLASS FOR SORTING
      IF (FSI -4.0) 404,404,402
  402 WRITE (IW,403)
  403 FORMAT (5X,'EXTREMELY POORLY SORTED')
      GO TO 425
  404 IF(FSI -2.0) 407,407,405
  405 WRITE (IW,406)
  406 FORMAT (5X,'VERY POORLY SORTED')
      GO TO  425
  407 IF(FSI -1.0 )410,410,408
  408 WRITE(IW,409)
  409 FORMAT(5X,'POORLY SORTED')
      GO TO 425
  410 IF(FSI -0.71)413,413,411
  411 WRITE (IW,412)
  412 FORMAT (5X,'MODERATELY SORTED')
      GO TO  425
```

```
  413 IF (FSI -0.5)416,416,414
  414 WRITE(IW,415)
  415 FORMAT(5X,'MODERATELY WELL SORTED')
      GO TO  425
  416 IF(FSI - 3.5)419,417,417
  417 WRITE(IW,418)
  418 FORMAT (5X,'WELL SORTED')
      GO TO  425
  419 WRITE (IW,420)
  420 FORMAT (5X,'VERY WELL SORTED')
  425 IF((FSKEW +1.0)-1.30) 428,426,426
  426 WRITE (IW,427)
  427 FORMAT (5X,'STRONGLY FINE SKEWED')
      GO TO  450
C     DETERMINATION OF VERBAL CLASS FOR SKEWNESS
  428 IF((SKEW +1.0)-1.1)431,429,429
  429 WRITE(IW,430)
  430 FORMAT (5X,' FINE -SKEWED')
      GO TO 450
  431 IF ((FSKEW +1.0) -.9 )434,432,432
  432 WRITE (IW,433)
  433 FORMAT (5X,'NEAR-SYMMETRICAL')
      GO TO  450
  434 IF((FSKEW  +1.0) -.7)437, 435,435
  435 WRITE (IW,436)
  436 FORMAT (5X,'COARSE SKEWED')
      GO TO 450
  437 WRITE (IW,438)
  438 FORMAT (5X,'STRONGLY COARSE SKEWED')
C     DETERMINATION OF VERBAL CLASS FOR KURTOSIS
  450 IF (FKG -3.0) 453,453,451
  451 WRITE (IW,452)
  452 FORMAT (5X,'EXTREMELY LEPTOKURTIC')
      GO TO 101
  453 IF(FKG -1.5) 456,456,454
  454 WRITE (IW,455)
  455 FORMAT(5X,'VERY LEPTOKURTIC')
      GO TO 101
  456 IF(FKG -1.11)459,459,457
  457 WRITE (IW,458)
  458 FORMAT (5X,'LEPTOKURTIC')
      GO TO  101
  459 IF (FKG-0.9) 462,462,460
  460 WRITE(IW,461)
  461 FORMAT (5X,'MESOKURTIC')
      GO TO 101
  462 IF (FKG -0.67)465,463,463
  463 WRITE (IW,464)
  464 FORMAT (5X,'PLATYKURTIC')
      GO TO 101
  465 WRITE (IW,466)
  466 FORMAT (5X,'VERY PLATYKURTIC')
  101 RETURN
      END
```

KIDNAPPERS TEST SAMPLE 1 RI 8.80 9.30 10.10 11.20 13.60 15.80 19.50 23.50 30.30 WT MUD= 4.84

KEY : + = % INTEVAL WT.
* = % CUM.WT. (ARITHMETIC ORDINATE)
X = % CUM.WT. (PROBABILITY ORDINATE)

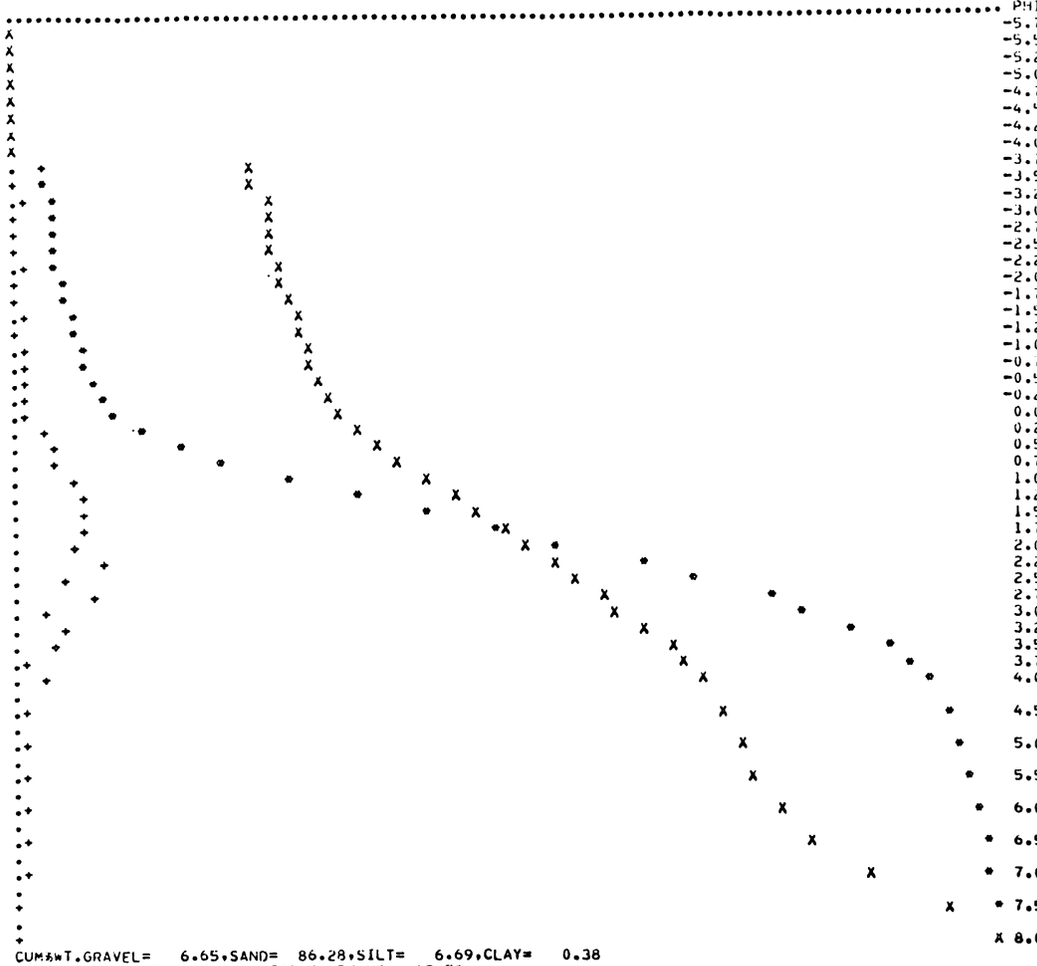

PHI	%I.WT.	C.WT.	%C.WT.	PROB.
-5.75	0.00	0.00	0.00	0.00
-5.50	0.00	0.00	0.00	0.00
-5.25	0.00	0.00	0.00	0.00
-5.00	0.00	0.00	0.00	0.00
-4.75	0.00	0.00	0.00	0.00
-4.50	0.00	0.00	0.00	0.00
-4.25	0.00	0.00	0.00	0.00
-4.00	0.00	0.00	0.00	0.00
-3.75	2.68	1.83	2.68	23.93
-3.50	0.00	1.83	2.68	23.93
-3.25	0.89	2.44	3.58	25.65
-3.00	0.00	2.44	3.58	25.65
-2.75	0.00	2.44	3.58	25.65
-2.50	0.28	2.63	3.86	26.11
-2.25	0.56	3.01	4.41	26.97
-2.00	0.32	3.23	4.74	27.42
-1.75	0.31	3.44	5.04	27.83
-1.50	0.62	3.86	5.66	28.60
-1.25	0.50	4.20	6.16	29.17
-1.00	0.51	4.55	6.67	29.72
-0.75	0.60	4.96	7.27	30.33
-0.50	0.89	5.57	8.17	31.16
-0.25	0.91	6.19	9.08	31.95
0.00	1.39	7.14	10.47	33.04
0.25	2.65	8.95	13.13	34.86
0.50	4.30	11.88	17.42	37.33
0.75	3.95	14.57	21.37	39.27
1.00	6.50	19.00	27.86	42.07
1.25	6.66	23.54	34.52	44.62
1.50	7.49	28.65	42.02	47.28
1.75	7.16	33.53	49.17	49.72
2.00	5.87	37.53	55.04	51.71
2.25	8.76	43.50	63.80	54.77
2.50	5.21	47.05	69.00	56.70
2.75	7.63	52.25	76.63	59.82
3.00	3.39	54.56	80.02	61.38
3.25	5.04	58.00	85.06	64.04
3.50	4.27	60.91	89.33	66.81
3.75	1.45	61.90	90.78	67.94
4.00	2.51	63.61	93.29	70.24
4.50	1.38	64.55	94.66	71.80
5.00	1.31	65.44	95.98	73.62
5.50	1.05	66.16	97.03	75.47
6.00	1.21	66.99	98.24	78.46
6.50	0.58	67.38	98.82	80.60
7.00	0.56	67.77	99.38	87.16
7.50	0.33	67.99	99.72	94.97
8.00	0.28	68.19	100.00	100.00

CUM%WT.GRAVEL= 6.65,SAND= 86.28,SILT= 6.69,CLAY= 0.38
RATIO CLAY/SILT= 0.06,RATIO SAND/MUD= 12.20
TEXTURAL TERMINOLOGY FOR GRAVEL BEARING DETRITAL SEDIMENTS
GRAVELLY SAND
FOLK STATISTICS : MZ = 1.80,SORTING = 1.667,SKEWNESS = -0.049,KURTOSIS = 1.455
MEDIAN = 1.79 C STATISTIC = -3.91
VERBAL CLASSIFICATION FOR STATISTICAL PARAMETERS (FOLK,ANDREWS,AND LEWIS)
POORLY SORTED
NEAR-SYMMETRICAL
LEPTOKURTIC

APPENDIX (I iv)

```
C      THIS PROGRAM IDENTIFIES THE MINERALOGY OF A SAMPLE ANALYS  ED BY
C      X-RAY DIFFRACTION.
C      THE VALUES INPUT ARE THE DEGREES 2-THETA AT WHICH PEAKS OCCUR IN
C      THE XRD TRACE
C      THE PROGRAM CONVERTS THESE VALUES TO ANGSTROMS AND COMPARES THE
C      VALUES TO A STANDARD VALUE LIST FOR MINERALS.
C      THE OUTPUT CONSISTS OF THE ORIGINAL VALUES INPUT,THE CONVERTED
C      VALUES, AND THE MINERALS IDENTIFIED.
FILE   5=READIT,UNIT=READER

FILE   6=PRINTDATA,UNIT=PRINTER


       DIMENSION XMINRL (6,30),ARRAY (25),PTR(30), NAMES (6)
       COMMON IR,IW
       IR = 5
       IW = 6
       N=1
C      TAB FOR ERROR OR DISCREPENCY TO BE ALLOWED IN COMPARING A STANDARD
C     1VALUE WITH AN OBSERVED VALUE
       ERROR = 0.02
C      READING IN MINERAL NAMES AND THEIR ASSOCIATED PEAKS. LAST CARD HAS
C      "XXXXXX" PUNCHED IN THE IST SIX SPACES. THIS GIVES A DATA ERROR WH
C       EN
C      AN ATTEMPT IS  MADE TO READ IN USING F6.4 FORMAT.
     1 READ(IR,2 ,DATA =7)(XMINRL(I,N),I=1,6)
     2 FORMAT(3F6.4,3A6)
C      WRITE OUT THIS LIST OF MINERALS AND THEIR STANDARD VALUES.
       WRITE(IW,3 )(XMINRL(I,N),I=1,6)
     3 FORMAT(3(2X,F7.4),10X,3A6)
       N=N+1
       IF(N.LE.30)GO TO 1
C      ERROR MESSAGE IF ATTEMPT TO READ MORE THAN ALLOWED 30 MINERALS.
       WRITE(IW,4)
     4 FORMAT(" ONLY THE IST 30 MINERALS AND INFO HAVE BEEN STORED.")
C      SKIP OVER REMAINING MINERALS.(UNTIL CARD = "XXXXXX")
     5 READ(IR,6,DATA=7)PTR(1)
     6 FORMAT(12F6.4,8X)
       GO TO 5
C      SET "MINRL" COUNTER BACK TO TRUE VALUE.
     7 N=N-1
C      COUNTER FOR ARRAY THAT STORES OBSERVED PEAKS.
     8 ICOUNT=1
C      READ IN OBSERVED PEAKS.
       READ(IR,9,END=23)NAMES
     9 FORMAT(F6.4,6A6)
       WRITE(IW,10)NAMES
    10 FORMAT("1",/" ",6A6,)
       JJ=12
       DO 11 J=1,2
       READ(IR,6,DATA=12)(ARRAY(I),I=ICOUNT,JJ)
       ICOUNT=ICOUNT+12
       JJ=JJ+12
    11 CONTINUE
```

```
C       SET "PEAK COUNTER" BACK TO TRUE VALUE
   12   ICOUNT=ICOUNT-1
C       WRITE THE VALUES OF THESE PEAKS
        WRITE(IW,13 ) (ARRAY(I),I=1,ICOUNT)
   13   FORMAT(//" VALUES INPUT ARE :"/(T20,F9.4))
C       CALL CONVERSION ROUTINE TO CONVERT DEGREES TO ANGSTROM UNITS.
        CALL CONVRT(ARRAY,ICOUNT)
C       START CHECKING STANDARD MINERAL VALUE  AGAINST THOSE OBSERVED VALU
C       ES
C       ONLY CHECK UP TO THE LAST OBSERVED VALUE ON THE IST PASS BECAUSE
C       AT LEAST ONE MORE VALUE IS NEEDED TO "CROSSCHECK" A 2ND OR 3RD VAL
C       UE IN THE STANDARD VALUE LIST.
        DO 21 I=1,ICOUNT-1
C       COUNTER FOR NO OF MINERALS THAT CHECK WITH "I"TH OBSERVED VALUE.
        KOUNT=0
C       ALLOWING FOR A     DISCREPENCY, TEST WHICH OF THE STANDARD PEAKS
C       CHECKS WITH THE "I"TH OBSERVED PEAK.
        DO 14 J=1,N
        IF (ABS(ARRAY(I)-XMINRL(1,J)).GE.ERROR)GO TO 14
        KOUNT=KOUNT+1
C       STORE THE ARRAY NO OF THAT MINERAL
C       THIS ARRAY BEHAVES AS A POINTER LATER ON TO INDICATE WHICH MINERAL
C       S CHECK WITH THE OBSERVED VALUE
        PTR(KOUNT)=J
   14   CONTINUE
C       IF NO MINERALS CHECK, GO TO NEXT OBSERVED PECK
        IF (KOUNT.EQ.0)GO TO 21
C       FOR EACH OF THOSE MINERALS THAT CHECK WITH THE "I"TH OBSERVED PEAK ,
C       CHECK IF THE SECOND STANDARD PEAK MATCHES WITH ANY OF THE SUBSEQUE
C       NT OBSERVED PEAKS
        DO 20 J=1,KOUNT
        NMINS=1
C       CHECK 2ND STANDARD PEAK.
        DO 16 K=I+1,ICOUNT
        IF(ABS(ARRAY(K)-XMINRL(2,PTR(J))).GE.ERROR)GO TO 16
        NMINS=NMINS+1
C       IF A SECOND PEAK IS FOUND CHECK FIRST IF THERE ARE ONLY 2 STANDARD
C       PEAKS
        IF(XMINRL(3,PTR(J)).EQ.0.)GOTO 17
C       IF THERE ARE 3 STANDARD PEAKS ,CHECK FOR THIS THIRD ONE IN THE SUB
C       SEQUENT OBSERVED PEAK VALUES
        DO 15 L=K,ICOUNT
        IF (ABS(ARRAY(L)-XMINRL(3,PTR(J))).GE.ERROR)GOTO 15
        NMINS=NMINS+1
        GOTO 17
   15   CONTINUE
C       THREE STANDARD PEAKS CANNOT BE FOUND. GO ON TO NEXT MINERAL.
        GOTO 20
   16   CONTINUE
C       TEST FOR NO OF PEAKS. IF ONLY ONE GO TO THE NEXT MINERAL.
   17   IF(NMINS-2)20,18,18
   18   WRITE(IW,19)NMINS,(XMINRL(L,PTR(J)),L=4,6)
   19   FORMAT("   ",I1," PEAKS FOUND. MINERAL IS ",3A6)
   20   CONTINUE
   21   CONTINUE
        WRITE(IW,22)
   22   FORMAT (/" ALL OBSERVED PEAKS TESTED.")
        GOTO 8
   23   STOP
        END
```

```
      SUBROUTINE CONVRT  (ARRAY,ICOUNT)
C     THE SUBROUTINE CONVERTS THE DEGREES 2-THETA TO ANGSTROMS.
      DIMENSION ARRAY (1)
      COMMON IR,IW
      DO 1 I=1,ICOUNT
      NCOUNT = I
      IF(ARRAY(I).EQ.0.0)GO TO 2
    1 ARRAY(I)=1.5418/(2.*SIN(ARRAY(I)*3.1415926/180./2.))
      GO TO 3
    2 ICOUNT = (NCOUNT-1)
    3 WRITE(IW,4 )(ARRAY(I),I=1,ICOUNT)
    4 FORMAT(" CONVERTED VALUES ARE :"/(T20,F9.4))
      WRITE(IW,5)
    5 FORMAT(//" PEAK PAIRING STARTED.")
      RETURN
      END
```

4.2600	3.3400	0.0000	QUARTZ
8.4200	3.1100	2.7100	ACTINOLITE
5.5400	4.5300	2.7700	ANDALUCITE
3.4000	2.7700	2.6900	APATITE ,CARB
3.4000	3.2700	1.9800	ARAGONITE
10.1000	3.3700	2.6600	BIOTITE
9.9500	3.3200	0.0000	MUSCOVITE
3.3500	2.6400	1.7700	CASSIDERITE
3.0400	2.2900	0.0000	CALCITE
4.0500	2.8400	2.4900	CRISTOBALITE ALPHA
8.3800	3.0700	2.7500	CUMMINGTONITE
2.9900	2.8900	2.5300	DIOPSIDE
2.8900	2.1900	1.7900	DOLOMITE
2.9000	2.4000	1.6400	EPIDOTE
2.8300	2.5700	2.5000	FAYALITE
2.7700	2.5100	2.4600	FOSTERITE
2.7100	3.1200	2.5000	GLAUCOPHANE
2.9700	2.5600	2.5300	HEDENBERGITE
8.9000	3.9700	2.9700	HEULANDITE
3.1700	3.0100	2.8300	LARSENITE
12.3000	8.7100	2.9900	ZEOLITE A,SODIUM
6.3900	3.7800	3.2000	ALBITE *
4.2100	3.2400	0.0000	MICROCLINE
4.0200	3.8000	3.1800	ORTHOCLASE
4.8300	2.5300	0.0000	MAGNETITE
3.3500	3.0300	0.0000	HORNBLENDE
3.3100	2.9900	0.0000	AUGITE
3.2000	2.8900	0.0000	HYPERSPHENE
10.0000	4.4800	0.0000	ILLITE

```
??????              TEST SAMPLE


VALUES INPUT ARE :
                      8.7600
                      9.9400
                     10.5500
                     20.8700
                     22.4000
                     26.2000
                     26.4000
                     26.7000
                     29.0000
                     30.1000
                     32.3000
                     32.5500
                     33.3000
                     33.6000
                      0.0000
                      0.0000
                      0.0000
                      0.0000
                      0.0000
                      0.0000
                      0.0000
                      0.0000
                      0.0000
                      0.0000
CONVERTED VALUES ARE :
                     10.0941
                      8.8983
                      8.3852
                      4.2563
                      3.9689
                      3.4013
                      3.3759
                      3.3387
                      3.0789
                      2.9689
                      2.7715
                      2.7508
                      2.6905
                      2.6672


PEAK PAIRING STARTED.
  3 PEAKS FOUND. MINERAL IS BIOTITE
  3 PEAKS FOUND. MINERAL IS HEULANDITE
  3 PEAKS FOUND. MINERAL IS CUMMINGTONITE
  2 PEAKS FOUND. MINERAL IS QUARTZ
  3 PEAKS FOUND. MINERAL IS APATITE ,CARB

ALL OBSERVED PEAKS TESTED.
```

APPENDIX (II i) SITE 1.

Note: *(i) The values are recorded in degrees.*
(ii) ab direction refers to the direction of dip.

	Field Measurements				Corrected for Tectonic Tilt			
	a		*ab*		*a*		*ab*	
	Plunge	Trend	Dip	Direction	Plunge	Trend	Dip	Direction
1.	37 W	319	40 W	329	30 W	320	32 W	327
2.	5 E	38	54 W	311	11 N	360	47 W	308
3.	26 W	330	29 W	340	18 W	330	21 W	341
4.	19 E	4	20 W	257	12 E	3	20.5 W	236.5
5.	20 E	73	40 E	73	21 E	70	42 E	81.5
6.	25 E	17	50 W	343	19 E	15	42 W	344
7.	30 W	315	35 W	305	22 W	316	29 W	297
8.	15 W	348	37 E	29	7 W	348	33 E	39
9.	17 E	2	50 W	264	9.5 E	1	48 W	257
10.	18 E	8	31 W	344	11 E	7	23 W	346.5
11.	15 W	299	48 E	22	8 W	298	43 E	27.5
12.	25 W	329	40 W	324	17 W	329	32 W	321
13.	19 W	306	19 W	306	12 W	307	12.5 W	286
14.	12 E	60	20 N	360	11 E	58	13 E	14
15.	10 E	48	18 E	10	7.5 E	47	12 E	32
16.	24 W	290	30 W	303	18 W	292	24 W	292
17.	10 E	43	26 W	326	7 E	42	17.5 W	322
18.	5 E	44	38 W	274	1 E	43	35 W	264
19.	25 W	336	54 W	286	17 W	336	49.5 W	281
20.	5 E	46	54 W	326	2 E	45	46 W	325
21.	4 W	201	42 W	283	10 W	202	38 W	275
22.	5 W	314	50 W	308	3 W	134	43 W	304
23.	40 W	345	28 W	282	32 W	344	24 W	267
24.	10 E	56	65 W	332	8 E	55	57 W	331.5
25.	6 W	245	68 W	324	6 W	245	60.5 W	323
26.	25 W	333	40 W	284	17 W	333	35.5 W	275
27.	0 E	23	47 W	296	6 W	203	41 W	290
28.	36 W	340	36 W	340	28 W	340	28 W	341
29.	53 W	350	53 W	350	45 W	348	45 W	351.5
30.	0 E	29	36 W	347	5 W	210	28 W	349
31.	10 E	65	20 E	101	9.5 E	64	26 E	114
32.	14 E	27	24 W	357	9 E	26	17 E	5
33.	26 W	345	30 W	357	18 W	345	23 E	3
34.	5 E	48	19 W	270	2 E	47	11 W	270
35.	20 E	35	50 W	321	16 E	33	42 W	319
36.	11 W	329	23 W	263	3 W	329	22 W	242
37.	36 E	2	37 W	328	29 N	360	29 W	325
38.	0	81	68 W	350	2 W	261	60.5 W	351
39.	31 N	360	33 W	310	23 W	358	26 W	303
40.	20 E	39	51 W	350	16 E	36	44 W	351
41.	20 W	350	20 W	350	12 W	349	12.5 W	357
42.	0	336	20 W	271	8 E	156	18.5 W	246
43.	18 W	350	58 E	33	10 W	349.5	54 E	37.5
44.	0 E	46	52 W	313	3 W	226	45 W	310
45.	6 W	236	59 W	334	8 W	237	51 W	333
46.	28 W	316	28 W	316	20 W	317	21 W	308
47.	7 W	303	7 W	303	0	303	5 W	220

	Field Measurements				Corrected for Tectonic Tilt			
	a		*ab*		*a*		*ab*	
	Plunge	Trend	Dip	Direction	Plunge	Trend	Dip	Direction
48.	0	13	44 W	280	7 W	194	40 W	272
49.	8 E	82	38 W	350	10 E	81	30 W	353
50.	18 W	321	18 W	321	10 W	322	10.5 W	308
51.	0 E	62	29 W	277	1 W	242	25.5 W	264
52.	20 W	343	30 W	279	12 W	343	26 W	266.5
53.	20 W	342	32 W	264	12 W	342	31 W	250
54.	0	20	14 E	96	6 W	200	19.5 E	118
55.	12 E	59	83 W	340	11 E	57	75 W	340
56.	20 E	56	55 W	352	18 E	53	48 W	354
57.	26 W	324	28 W	277	18 W	325	25 W	264
58.	15 W	342	23 W	278	7 W	342	19 W	265
59.	22 W	306	31 W	352	15 W	307	24 W	357
60.	28 W	340	34 W	355	20 W	340	26.5 W	359.5
61.	15 W	282	40 E	10	10 W	284	34 E	16
62.	15 N	360	25 W	335	8 W	359	17 W	335
63.	48 E	20	48 E	20	42 E	14	42.5 E	26
64.	11 E	96	25 E	20	15 E	94	20 E	35
65.	14 W	290	30 N	360	8 W	291	23 E	6
66.	25 E	16	38 W	323	19 E	13	30 W	320
67.	17 E	52	39 N	360	15 E	50	32 W	5
68.	13 E	30	36 W	303	8 E	28	29.5 W	295
69.	0	77	18 W	308	2 W	257	12 W	285
70.	22 E	2	28 W	331	14 E	0.5	20 W	328
71.	25 E	15	43 W	338	19 E	13	35 W	338
72.	19 E	20	45 W	350	13 E	18	37 W	352
73.	15 E	17	30 W	334	10 E	17	22 W	346
74.	0	8	32 W	286	7 W	188.5	27.5 W	275
75.	0	10	28 W	299	7 W	191	22.5 W	286
76.	21 E	23	42 E	75	15 E	21	44 E	83
77.	19 E	10	32 W	292	12 E	9	27 W	281
78.	23 N	360	41 E	18	16 W	359	35 E	25
79.	0	5	31 W	279	7.5 W	185	27.5 W	268
80.	29 N	349	32 W	308	21 W	347	25 W	300
81.	15 E	79	56 W	358	17 E	77	49 N	360
82.	17 E	2	23 E	103	10 E	1	29 E	115
83.	30 W	300	37 W	310	23 W	302	30 W	303.5
84.	16 E	15	24 W	335	10 E	13.5	16 W	330
85.	0 E	37	10 W	323	4 W	218	2.5 W	280
86.	11 E	85	23 N	360	13 E	83	16 E	10
87.	15 W	212	47 W	295	20 W	214	41 W	289
88.	32 E	65	83 W	350	32 E	60	75 W	350.5
89.	59 N	345	59 W	345	51 W	345	51 W	345.5
90.	9 W	242	52 W	334	10 W	242	44 W	333
91.	8 E	17	20 E	64	2 E	17	21 E	85
92.	5 E	60	27 W	348	6 W	241	19 W	353
93.	4 W	237	14 W	307	5 W	238	8 W	280
94.	5 W	249	14 W	275	5 W	250	12.5 W	242
95.	12 W	308	35 N	360	6 W	307	28 E	5
96.	8 E	31	38 W	297	3 E	30	32 W	289
97.	0	38	58 W	310	4 W	218.5	51 W	307
98.	0	50	2 W	343	2.5 W	230	6 E	150
99.	4 W	219	22 W	293	8 W	220	17 W	275
100.	10 E	78	14 E	14	11.5 E	76	9 E	47

	Field Measurements				Corrected for Tectonic Tilt			
	a		*ab*		*a*		*ab*	
	Plunge	Trend	Dip	Direction	Plunge	Trend	Dip	Direction
101.	0	30	50 W	303	5 W	210	43 W	298
102.	10 E	96	40 N	360	15 E	94	33 E	5
103.	8 E	60	33 N	360	7 E	59	26 E	6
104.	35 W	352	30.5 W	315	27 W	351	25 W	310
105.	10 E	90	40 N	360	7 W	271	33 E	4
106.	15 E	13	28 W	320	9 E	12	20 W	314
107.	22 W	333	30 W	270	14 W	333	27.5 W	255
108.	23 E	60	52 N	360	22 E	57	59 E	178
109.	22 E	42	38 E	45	19 E	39	31 W	310
110.	15 W	301	24 W	269	8 W	300	16 W	268
111.	30 E	16	47 W	347	23 E	13	39 W	349
112.	4 W	239	60 W	338	5 W	240	52 W	338.5
113.	0	18	20 W	260	6 W	199	19 W	237
114.	0	18	38 W	327	6 W	199	30 W	324
115.	60 W	348	60 W	348	52 W	345	52 W	349
116.	12 E	34	74 W	307	7 E	33	77 W	306
117.	10 W	212	50 W	298	15 W	214	44 W	293
118.	12 E	37	41 W	314	8 E	36	34 W	309
119.	44 W	333	44 W	333	36 W	333	37.5 W	297
120.	28 E	58	90 W	320	26 E	54	82.5 W	320

APPENDIX (IIii) SITE 1.

Note: *(i) L, I and S refer to the lengths of the Long, Intermediate and Short axes of a clast recorded in cm.*
(ii) I/L is the elongation index.
(iii) Sphericity is the maximum projection sphericity.

	L	I	S	I/L	Sphericity
1.	13.2	12.7	3.8	.96	.44
2.	11.4	5.2	3.2	.46	.55
3.	12.6	11.5	4.1	.91	.49
4.	13.0	12.2	3.0	.93	.38
5.	6.3	6.0	2.7	.95	.57
6.	6.7	3.8	1.9	.57	.52
7.	9.6	8.8	4.6	.92	.63
8.	10.9	5.9	2.7	.54	.48
9.	15.2	11.0	6.0	.73	.60
10.	9.9	5.7	4.3	.57	.69
11.	10.7	8.2	3.1	.77	.48
12.	9.3	7.0	1.5	.76	.32
13.	10.6	8.3	2.8	.78	.45
14.	6.6	4.5	2.8	.68	.63
15.	6.4	4.7	2.5	.74	.55
16.	15.0	12.0	6.0	.80	.58
17.	8.7	7.2	3.1	.83	.53
18.	8.5	4.4	3.2	.52	.65
19.	7.2	7.1	3.4	.98	.60
20.	7.0	4.8	1.8	.68	.45
21.	7.6	4.7	1.9	.62	.47
22.	9.6	5.8	2.9	.60	.53
23.	9.0	7.3	4.5	.82	.68
24.	23.2	14.4	10.6	.62	.69
25.	11.8	8.8	5.8	.75	.68
26.	6.8	3.6	1.2	.53	.39
27.	5.6	4.5	1.5	.79	.44
28.	17.4	8.7	4.6	.50	.52
29.	9.1	6.8	2.5	.75	.47
30.	7.7	6.3	3.0	.82	.57
31.	6.8	5.6	4.2	.82	.77
32.	7.1	6.4	3.0	.89	.58
33.	11.3	11.1	3.8	.99	.22
34.	6.4	3.1	2.2	.48	.62
35.	13.1	7.7	4.1	.59	.55
36.	11.9	8.6	4.0	.72	.54
37.	12.2	11.3	5.7	.93	.61
38.	23.8	12.2	11.3	.51	.75
39.	9.7	7.1	4.0	.73	.61
40.	4.8	4.5	1.8	.94	.53
41.	8.3	7.0	4.0	.85	.64
42.	13.0	6.8	3.1	.52	.64
43.	9.1	5.4	2.9	.59	156
44.	13.7	9.6	5.1	.70	.58
45.	13.6	8.7	5.5	.64	.63
46.	9.0	8.1	5.1	.90	.71

	L	I	S	I/L	Sphericity
47.	13.3	9.7	5.8	.73	.63
48.	7.2	5.5	3.2	.76	.64
49.	11.2	7.4	4.2	.66	.59
50.	13.1	12.1	6.0	.92	.61
51.	12.4	9.7	2.8	.78	.40
52.	9.6	6.9	2.8	.72	.49
53.	13.4	10.6	4.3	.79	.50
54.	12.1	4.6	2.6	.38	.49
55.	13.3	8.0	5.0	.60	.61
56.	5.9	4.6	3.0	.79	.69
57.	8.9	6.4	3.1	.72	.55
58.	11.4	7.5	4.6	.66	.62
59.	7.1	4.9	1.9	.69	.47
60.	10.9	8.9	3.9	.81	.54
61.	7.4	4.0	3.0	.54	.67
62.	12.5	5.9	5.2	.47	.71
63.	10.1	7.7	5.2	.76	.70
64.	7.9	6.3	3.2	.79	.59
65.	11.4	5.6	4.3	.49	.65
66.	9.3	6.5	3.1	.70	.54
67.	7.4	4.2	3.3	.56	.69
68.	8.9	6.5	2.3	.72	.44
69.	9.1	5.3	4.1	.58	.70
70.	12.0	9.5	5.7	.80	.65
71.	9.0	6.8	4.4	.76	.68
72.	9.9	5.7	4.2	.58	.68
73.	8.3	6.6	4.3	.80	.70
74.	10.9	7.9	3.6	.73	.53
75.	16.8	11.6	4.9	.69	.50
76.	9.2	6.7	3.4	.69	.56
77.	14.0	9.7	4.4	.69	.52
78.	7.8	4.9	3.5	.63	.68
79.	9.2	7.1	4.0	.77	.63
80.	6.4	6.3	2.6	.98	.55
81.	7.5	6.3	2.5	.84	.51
82.	5.8	4.9	2.2	.84	.55
83.	10.5	9.4	3.6	.89	.51
84.	9.6	9.6	4.0	1.00	.56
85.	12.5	8.7	4.2	.69	.54
86.	5.8	5.2	3.4	.89	.73
87.	8.2	4.9	2.7	.60	.56
88.	4.4	3.3	1.3	.76	.49
89.	6.5	5.4	3.5	.83	.70
90.	6.1	3.7	1.8	.61	.52
91.	5.5	3.4	2.5	.70	.70
92.	8.1	7.5	3.6	.59	.59
93.	6.3	5.0	2.4	.57	.57
94.	7.4	5.3	3.2	.64	.64
95.	12.8	9.0	4.2	.53	.53
96.	7.4	3.9	2.7	.42	.42
97.	15.6	9.7	5.5	.62	.58
98.	6.5	4.0	1.4	.62	.41
99.	5.7	4.6	2.0	.81	.54
100	8.4	6.8	3.4	.81	.58
101	5.2	5.1	2.5	.97	.62
102.	12.0	9.6	6.0	.80	.68

	L	I	S	I/L	Sphericity
103.	5.4	3.7	2.2	.69	.62
104.	8.5	7.5	2.1	.88	.40
105.	8.2	5.6	2.7	.68	.54
106.	9.3	6.2	3.4	.66	.58
107.	7.6	4.5	2.3	.59	.54
108.	5.5	3.7	1.9	.67	.55
109.	14.5	7.4	3.0	.51	.44
110.	7.3	4.7	2.3	.64	.53
111.	10.4	6.1	3.7	.59	.60
112.	10.5	8.1	3.2	.77	.49
113.	5.6	4.8	2.9	.86	.68
114.	5.6	4.1	1.9	.72	.54
115.	4.5	4.3	1.1	.96	.38
116.	11.3	6.8	3.0	.60	.48
117.	9.2	4.7	2.3	.51	.50
118.	8.1	6.4	3.4	.78	.60
119.	7.2	6.3	2.9	.87	.57
120.	10.0	7.1	2.4	.71	.43

APPENDIX (II iii) SITE 6.

Note: *(i) The values are recorded in degrees.*
(ii) ab direction refers to the direction of dip.

	Field Measurements				Corrected for Tectonic Tilt			
	a		*ab*		*a*		*ab*	
	Plunge	Trend	Dip	Direction	Plunge	Trend	Dip	Direction
1.	0 E	30	12 W	312	4 W	210	5 W	288
2.	29 E	53	60 E	102	27 E	46	66 E	105
3.	12 E	123	12 E	123	20 E	122	20 E	133
4.	20 E	15	23 E	67	14 E	13	25 E	83
5.	16 E	27	16 W	322	11 E	25	9 W	318
6.	6 W	304	6 W	304	2 E	125	4 W	200
7.	15 W	355	17 W	334	7 W	355	9 W	340
8.	19 W	344	28 E	12	11 W	343	23 E	25
9.	9 W	312	9 W	312	1 W	312	3 W	262
10.	17 E	38	22 E	45	14 E	36	21 E	66
11.	10 E	90	22 E	53	14 E	88	22 E	72
12.	15 E	22	26 E	59	10 E	20	27 E	74
13.	0	53	4 E	132	1 W	233	12 E	143
14.	0	353	52 E	54	7 E	173	52 E	60
15.	2 W	344	2 W	344	6 E	164	6 E	145
16.	4 E	39	8 E	90	1 E	38	14 E	119
17.	0	23	10 E	70	5 W	224	14 E	102
18.	3 E	4	19 W	340	4 E	165	12 W	347
19.	5 E	64	8 E	127	5 E	63	16 E	138
20.	0	52	10 W	347	1 W	232	4 W	28
21.	2 E	4	15 E	57	5 E	164	16 E	83
22.	10 W	310	10 W	310	2 W	310	4 W	267
23.	15 E	10	25 W	330	9 E	9	17 W	331
24.	14 W	350	27 E	68	7 W	349	29 E	83
25.	14 E	22	32 E	70	9 E	21	32 E	82
26.	0	35	14 W	298	3 W	215	9 W	271
27.	16 E	52	16 E	52	14 E	50	17 E	79
28.	10 E	20	35 E	82	4 E	19	39 E	91
29.	2 E	21	15 W	287	4 E	167	10 W	257
30.	15 W	357	29 W	328	8 W	356	20 W	327
31.	5 W	315	18 E	66	4 E	136	20 E	86
32.	16 E	30	48 E	2	12 E	28	41 E	6
33.	3 E	5	11 N	284	4 E	165	8 W	242
34.	12 E	70	12 E	70	13 E	68	16 E	98
35.	6 E	47	6 E	47	4 E	46	9 E	106
36.	13 E	100	21 E	29	18 E	98	18 E	49
37.	0 E	30	17 W	311	4 W	210	10 W	300
38.	0 E	25	41 W	294	5 W	205	35 W	288
39.	6 E	8	7 E	50	1 W	188	9 E	101
40.	8 E	44	13 E	72	6 E	43	16 E	100
41.	25 E	44	32 N	360	22 E	40	25 E	8
42.	2 W	290	10 E	7	5 E	112	6 E	53
43.	2 E	10	2 E	10	5 W	191	6 E	133
44.	0 E	75	18 W	351	2 E	75	10 E	8
45.	8 E	77	19 E	14	10 E	76	14 E	35
46.	0 E	33	17 W	300	4 W	213	10 W	303
47.	0 E	33	13 W	317	4 W	211	5 W	301

	Field Measurements				Corrected for Tectonic Tilt			
	a		*ab*		*a*		*ab*	
	Plunge	Trend	Dip	Direction	Plunge	Trend	Dip	Direction
48.	18 E	31	28 E	76	14 E	29	32 E	89
49.	5 E	20	5 E	20	1 W	199	6 E	108
50.	16 E	20	16 E	20	11 E	18	12 E	48
51.	10 E	69	16 E	90	11 E	67	21 E	108
52.	14 E	65	14 E	65	14 E	63	16 E	91
53.	20 W	316	40 W	360	12 W	316	33 E	5
54.	10 N	360	12 E	64	3 W	359	19 E	95
55.	10 W	316	10 W	316	2 W	316	3 W	280
56.	8 W	349	17 W	265	0 W	348	7 W	239
57.	0 E	20	39 W	319	5 W	200	31 W	316
58.	7 E	34	7 E	34	3 E	34	8 E	89
59.	15 W	293	27 W	340	9 W	294	18 W	345
60.	0 E	54	17 W	323	1 W	234	10 W	323
61.	8 E	70	18 E	20	9 E	69	24 E	44
62.	10 E	23	10 E	23	22 E	5	8 E	72
63.	10 E	14	10 E	14	4 E	13	7 E	59
64.	5 E	34	5 E	34	1 E	33	7 E	107
65.	18 E	43	21 W	353	15 E	41	24 E	5
66.	4 E	54	29 E	20	3 E	53	25 E	32
67.	21 E	25	21 E	25	16 E	22	22 E	16
68.	17 W	353	36 W	296	9 W	352	30 W	289
69.	0	9	16 E	90	7 W	189	21 E	109
70.	14 E	30	90 W	307	10 E	29	82 W	307
71.	10 E	63	33 W	341	11 E	61	25 W	345
72.	14 E	53	14 E	53	13 E	51	15 E	82
73.	0	360	12 E	72	7 S	180	15 E	100
74.	6 E	53	25 E	141	5 E	52	32 E	143
75.	6 W	313	14 E	54	3 E	134	15 E	83
76.	22 E	43	25 W	356	19 E	40	18 E	7
77.	3 W	306	9 W	260	5 E	126	10 W	210
78.	18 W	356	18 W	356	11 W	355	21 E	15
79.	20 E	53	21 E	159	19 E	50	22 W	220
80.	23 E	44	23 E	44	20 E	41	22 E	63
81.	3 E	27	3 E	27	2 W	207	7 E	121
82.	18 W	303	18 W	303	11 W	304	11 W	284
83.	0	56	22 W	327	1 W	237	15 W	327
84.	4 E	64	12 W	303	5 E	63	6 W	270
85.	0	33	33 M	297	4 W	213	26 W	289
86.	18 E	30	18 E	30	14 E	28	16 E	54
87.	20 E	70	25 E	41	21 E	67	24 E	57
88.	3 W	297	3 W	297	5 E	118	5 E	172
89.	8 E	38	20 W	343	5 E	37	22 W	352
90.	8 E	33	46 W	300	4 E	32	39 W	295
91.	15 E	12	46 W	300	9 E	11	39 W	295
92.	0 N	355	14 W	228	8 E	175	17 W	203
93.	8 W	354	20 W	255	15 E	173	20 W	234
94.	4 E	26	23 E	126	1 W	205	16 E	115
95.	0	352	13 E	136	8 E	173	15 E	130
96.	14 E	85	20 E	108	17 E	83	15 E	90
97.	13 E	30	15 W	335	9 E	29	6 W	341
98.	9 E	11	24 W	318	3 E	10	16 W	313
99.	20 E	10	31 W	292	13 E	9	25 W	282
100.	0	50	0	50	2 W	230	8 E	146
101.	0 W	354	286 W	19	8 E	174	15 W	264

APPENDIX (IIiv) SITE 6.

Note: *(i) L, I and S refer to the lengths of the Long, Intermediate and Short axes recorded in cm.*
(ii) I/L is the elongation index.
(iii) Sphericity is the maximum projection.

	L	I	S	I/L	Sphericity
1.	11.4	5.5	5.3	.48	.76
2.	5.8	4.2	2.2	.73	.58
3.	5.3	3.9	2.3	.77	.64
4.	5.3	4.1	2.7	.77	.69
5.	9.7	6.8	6.8	.70	.88
6.	4.3	3.8	2.2	.87	.67
7.	5.3	4.1	3.2	.77	.78
8.	3.8	2.7	1.7	.70	.65
9.	4.2	3.0	1.3	.71	.51
10.	6.7	5.3	4.0	.78	.77
11.	4.6	3.4	2.6	.74	.75
12.	7.6	5.5	3.5	.72	.67
13.	5.3	3.5	3.1	.67	.80
14.	5.1	4.3	1.8	.84	.52
15.	6.5	4.2	2.1	.64	.55
16.	6.8	5.4	3.6	.80	.72
17.	4.4	3.9	1.9	.90	.59
18.	8.6	5.3	4.7	.62	.79
19.	5.3	4.0	2.1	.75	.59
20.	6.0	3.4	1.6	.56	.49
21.	4.8	2.6	1.5	.54	.55
22.	4.8	2.5	2.3	.52	.75
23.	6.9	5.8	3.8	.84	.71
24.	7.5	4.6	2.9	.61	.63
25.	6.9	3.8	1.6	.55	.22
26.	7.4	5.4	3.6	.73	.68
27.	3.7	2.9	2.2	.78	.76
28.	5.6	4.1	1.8	.73	.52
29.	4.8	3.5	1.6	.73	.53
30.	7.4	5.3	3.2	.72	.63
31.	7.2	4.7	1.8	.65	.22
32.	4.0	3.4	1.3	.85	.49
33.	5.7	4.7	2.7	.82	.66
34.	8.2	3.2	2.3	.39	.58
35.	5.0	3.6	2.4	.73	.68
36.	7.8	5.3	3.0	.68	.59
37.	4.0	2.6	1.8	.65	.66
38.	5.4	2.4	1.8	.44	.64
39.	4.6	3.2	0.9	.70	.22
40.	3.7	2.8	0.9	.77	.22
41.	5.1	5.1	3.4	.99	.76
42.	7.7	4.3	2.7	.56	.59
43.	4.7	3.2	1.1	.67	.22
44.	4.5	2.9	1.6	.63	.59
45.	4.1	3.8	2.0	.93	.64
46.	7.1	2.6	2.3	.37	.66
47.	5.2	3.1	2.8	.60	.79

	L	I	S	I/L	Sphericity
48.	3.9	2.9	2.3	.73	.77
49.	4.4	2.4	1.5	.54	.60
50.	5.5	4.0	3.2	.72	.78
51.	3.7	3.0	2.7	.82	.88
52.	4.2	3.5	2.3	.83	.71
53.	8.0	5.0	3.8	.63	.71
54.	5.4	4.7	1.6	.87	.47
55.	7.6	4.9	3.5	.64	.69
56.	6.9	4.3	2.6	.62	.61
57.	5.1	3.4	2.3	.67	.67
58.	6.6	4.2	3.2	.64	.71
59.	7.0	5.2	2.8	.74	.59
60.	6.2	4.9	3.2	.79	.69
61.	6.7	3.8	3.0	.57	.71
62.	6.2	5.1	3.0	.81	.66
63.	6.0	3.0	2.6	.50	.71
64.	6.7	3.6	3.2	.54	.74
65.	5.3	4.1	2.1	.78	.59
66.	5.1	4.3	2.8	.84	.71
67.	3.6	2.5	2.4	.68	.87
68.	5.5	4.4	2.0	.80	.54
69.	6.0	3.9	2.0	.65	.89
70.	4.3	3.2	1.4	.74	.63
71.	5.4	2.7	2.2	.50	.76
72.	5.1	4.5	2.2	.87	.59
73.	3.8	2.9	0.7	.76	.22
74.	-	-	-	-	-
75.	6.4	4.5	2.6	.71	.62
76.	7.1	4.9	4.3	.68	.81
77.	5.2	3.1	2.2	.60	.67
78.	8.9	6.0	4.0	.67	.67
79.	4.5	3.9	2.5	.87	.71
80.	7.6	5.0	3.0	.65	.61
81.	5.2	3.3	1.5	.63	.51
82.	-	-	-	-	-
83.	5.6	2.7	1.4	.48	.49
84.	5.4	3.7	3.0	.68	.76
85.	6.8	4.1	2.9	.60	.67
86.	4.2	2.8	1.5	.66	.56
87.	7.4	5.9	3.6	.80	.67
88.	5.1	3.3	2.1	.63	.63
89.	6.1	5.7	2.3	.94	.54
90.	6.8	4.6	2.6	.67	.59
91.	4.9	3.4	1.9	.70	.60
92.	7.7	4.3	3.6	.56	.72
93.	5.2	2.3	1.0	.43	.22
94.	4.7	3.9	1.2	.83	.22
95.	4.4	3.2	1.5	.73	.53
96.	4.9	3.8	2.1	.78	.48
97.	6.9	5.2	2.2	.75	.51
98.	5.1	2.3	1.6	.45	.59
99.	10.2	4.5	3.2	.44	.60
100.	5.2	3.3	1.1	.63	.22
101.	6.1	2.8	1.4	.45	.48

APPENDIX (II v) SITE 2.

	Field		Corrected Tectonic Tilt			Field		Corrected Tectonic Tilt	
	ab Dip	Direction	ab Dip	Direction		ab Dip	Direction	ab Dip	Direction
1.	24W	274	21W	256	28.	14W	260	14W	226
2.	20W	314	13W	301	29.	18W	317	11W	306
3.	15W	265	14W	234	30.	26W	299	20W	287
4.	38W	309	31W	304	31.	22W	218	27W	203
5.	56W	309	49W	308	32.	30W	314	22W	308
6.	47W	303	40W	299.5	33.	0	311	8E	157
7.	38W	305	31W	299	34.	9W	268	9W	217
8.	12W	307	6W	273	35.	4W	258	8E	187
9.	35W	299	29W	290	36.	26E	4	19E	15
10.	53W	358	46E	1	37.	24W	283	20W	266
11.	10E	158	18E	156	38.	28E	21	23E	35
12.	22W	270	20W	250	39.	55W	260	54W	254
13.	28W	316	20W	309	40.	16W	248	17W	223
14.	18E	126	15E	134	41.	38W	254	38W	243
15.	27W	271	15W	256	42.	24W	260	23W	241
16.	23W	322	15W	316	43.	37W	255	37W	244
17.	25W	315	18W	307	44.	31W	325	23W	323
18.	11W	311	5W	273	45.	30W	306	23W	297
19.	18W	322	10W	312	46.	21W	303	15W	286
20.	16W	319	9W	306	47.	27W	315	19W	308
21.	10W	334	2W	334	48.	44W	346	36W	348
22.	42E	110	48E	115	49.	28E	120	34W	307
23.	25W	257	25W	240	50.	16E	172	23.5W	347
24.	14W	297	19W	264	51.	39W	338	30W	339
25.	30W	276	27W	262	52.	37W	318	30W	315
26.	23W	272	20W	253	53.	22W	298	16.5W	282
27.	22W	309	16W	295	54.	11W	293	8W	253

APPENDIX (IIvi) SITE 3.

	Field Measurements ab		Corrected Tectonic Tilt ab			Field Measurements ab		Corrected Tectonic Tilt ab	
	Dip	Direction	Dip	Direction		Dip	Direction	Dip	Direction
1.	90	296	83W	296	51.	16W	323	18W	319
2.	53W	326	45W	321	52.	38E	15	32E	23
3.	35W	273	32W	261	53.	35W	320	27W	316
4.	34W	314	27W	309	54.	43W	350	35W	352
5.	16E	11	10E	36	55.	41W	261	40W	254
6.	64W	355	56W	356	56.	48W	359	41E	2
7.	48W	311	41W	221	57.	31W	301	24W	292
8.	52W	260	50W	253	58.	29W	265	27W	250
9.	46W	342	38W	343	59.	50W	272	47W	266
10.	36W	273	33W	262	60.	29W	358	21E	6
11.	23W	309	16W	297	61.	32E	10	8E	81
12.	53W	270	50W	264	62.	38W	324	30W	321
13.	37W	335	28W	335	63.	30W	258	29W	244
14.	30W	267	28W	253	64.	44W	289	39W	282
15.	37W	315	30W	311	65.	50W	350	42W	352
16.	23W	277	20W	259	66.	56W	333	47W	333
17.	31W	300	25W	290	67.	44W	295	38W	289
18.	64W	289	58W	286	68.	57W	351	49W	353
19.	25W	283	21W	267	69.	45N	360	38E	4
20.	10W	297	6.5W	247	70.	52W	336	44W	336
21.	22W	310	15W	297	71.	20W	353	12E	1
22.	15W	341	7W	348	72.	21W	270	19W	248
23.	24W	315	16W	305	73.	39W	310	32W	305
24.	20W	274	18W	252	74.	36W	304	30W	297
25.	36N	360	28E	6	75.	53W	305	46W	302
26.	29W	281	25W	266	76.	31W	260	30W	246
27.	33N	315	26W	309	77.	26E	5	19E	17
28.	29W	293	23W	281	78.	40W	343	32W	345
29.	26W	318	18W	311	79.	35W	282	31W	271
30.	21W	322	13W	315	80.	48W	349	40W	351
31.	15E	13	10E	43	81.	28W	318	20W	312
32.	24W	322	17W	316	82.	18W	309	11W	290
33.	26W	286	21W	270	83.	40W	326	32W	373
34.	15W	345	7W	355	84.	19W	341	11W	345
35.	20W	317	12W	306	85.	49W	323	41W	321
36.	41E	15	35E	22	86.	49E	16	42E	21
37.	55W	336	37W	336	87.	27W	252	27W	237
38.	21W	266	20W	244	88.	50W	358	42W	1
39.	41W	263	40W	253	89.	32W	355	24N	360
40.	76E	14	30E	21	90.	22W	284	18W	265
41.	41W	270	38W	261	91.	27W	344	18W	347
42.	15W	270	14W	238	92.	37W	280	33W	270
43.	38W	290	33W	281	93.	29W	305	22W	295
44.	57E	7	50E	10	94.	57W	353	49W	355
45.	33W	275	30W	263	95.	56E	10	49E	13
46.	38W	295	32W	287	96.	54W	320	46W	318
47.	60N	360	52E	2	97.	26W	309	19W	298
48.	71N	360	64E	2	98.	31W	307	24W	299
49.	29W	337	21W	336	99.	15W	319	8W	302
50.	53E	30	48E	35	100.	43W	281	39W	273

APPENDIX (II vii) SITE 4.

	Field		Corrected Tectonic Tilt			Field		Corrected Tectonic Tilt	
	ab Dip	Direction	ab Dip	Direction		ab Dip	Direction	ab Dip	Direction
1.	38W	318	30W	315	29.	34W	310	27W	304
2.	27W	330	19W	328	30.	47W	305	40.5W	301
3.	32W	294	26W	284	31.	36W	252	36W	241
4.	20W	310	13W	296	32.	18W	336	10.5W	334
5.	33W	272	30W	260	33.	28W	261	27W	246
6.	37W	257	36W	246	34.	40W	263	38W	254
7.	39W	258	38W	248	35.	50W	255	49W	248
8.	26W	263	25W	247	36.	38W	243	39W	233
9.	25W	297	20W	284	37.	30W	292	25W	280
10.	27W	273	24W	257	38.	36W	271	33W	260
11.	37W	273	34W	262	39.	54W	295	48W	291
12.	6W	265	8W	206	40.	24W	246	25W	229
13.	18W	264	17W	239	41.	51W	246	51W	240
14.	72W	336	64W	336	42.	33W	280	30W	269
15.	34W	340	26W	341	43.	40W	303	33W	297
16.	24W	327	16W	323	44.	28W	292	23W	279
17.	23W	325	15W	320	45.	52W	340	44W	341
18.	34W	357	26E	3	46.	37W	307	30W	301
19.	14W	260	14W	227	47.	19W	306	13W	289
20.	1W	309	7E	156	48.	60W	342	52W	343
21.	11W	324	3W	302	49.	30E	9	23E	20
22.	6N	360	4E	99	50.	20W	316	23W	304
23.	71W	304	64W	303	51.	22W	296	16W	279
24.	84W	304	77W	303	52.	26W	298	20W	285
25.	70W	304	63W	302	53.	88W	300	84W	300
26.	47W	256	46W	249	54.	47W	321	39W	319
27.	14E	85	18E	108	55.	90W	305	83W	305
28.	33W	287	28W	276	56.	68W	290	63W	288

APPENDIX (II viii) SITE 5.

	Field		Corrected Tectonic Tilt			Field		Corrected Tectonic Tilt	
	ab Dip	Direction	ab Dip	Direction		ab Dip	Direction	ab Dip	Direction
1.	38W	353	30W	356	26.	39W	306	32W	300
2.	40E	18	34E	25	27.	63W	349	55W	350
3.	42W	338	34W	338	28.	63W	349	55W	350
4.	18W	330	10W	325	29.	53W	327	45W	326
5.	32W	330	24W	328	30.	61W	349	53W	350
6.	33W	324	25W	320	31.	]3W	331	5W	325
7.	44W	328	36W	327	32.	56E	2	49E	5
8.	34W	284	29W	273	33.	47W	258	46W	250
9.	71W	317	63W	316	34.	17W	246	19W	269
10.	8W	302	5W	228	35.	61E	14	54E	17
11.	40E	12	34E	19	36.	35W	312	28W	307
12.	50E	33	46E	40	37.	47W	311	40W	307.5
13.	33W	306	26W	299	38.	33W	330	25W	328
14.	31W	301	25W	281	39.	56W	324	48W	323
15.	65W	285	60W	282	40.	51W	259	44E	2
16.	48E	4	41E	8	41.	19E	7	17E	25
17.	41E	4	34E	9	42.	72W	315	64W	314
18.	29W	352	21W	356	43.	72W	315	64W	314
19.	58W	354	50W	356	44.	59W	303	52W	301
20.	30W	312	23W	305	45.	28W	309	20W	299
21.	10W	301	6W	246	46.	14W	320	9W	308
22.	29W	306	22W	297	47.	40W	290	35W	282
23.	28N	360	21W	8	48.	32W	340	24W	340
24.	54W	293	48W	289	49.	30W	290	25W	278
25.	20W	318	12W	310	50.	35W	319	27W	315
					51.	39W	348	31W	251

APPENDIX (III)

CLIFTON CONG. SITE 2 AB PLANE(POLES)
VEC MEAN=103. VARIANCE=3836. STDEV= 62. READINGS= 53 VEC MAG(%)= 59.68
CON INTVL(95%)= 18. CON INTVL(99%)= 23. SUMV= 203300.

TRUE AZIMUTH	167	76	121	54	124	128	120	93	110	181	336
TRUE AZIMUTH	270	129	314	76	136	127	93	73	102	132	126
TRUE AZIMUTH	154	295	60	84	82	73	115	46	126	107	23
TRUE AZIMUTH	128	337	37	7	135	159	195	86	215	74	43
TRUE AZIMUTH	63	61	64	143	117	106	128	168	127		

CLIFTON CONG. SITE 3 AB PLANE(POLES)
VEC MEAN=132. VARIANCE=2085. STDEV= 46. READINGS=100 VEC MAG(%)= 71.88
CON INTVL(95%)= 10. CON INTVL(99%)= 13. SUMV= 208498.

TRUE AZIMUTH	233	175	126	202	156	64	73	201	81	58	101
TRUE AZIMUTH	190	83	107	182	182	156	215	139	203	136	172
TRUE AZIMUTH	74	182	112	70	86	186	261	141	64	102	172
TRUE AZIMUTH	153	109	173	184	156	181	68	125	117	122	66
TRUE AZIMUTH	197	165	91	171	132	110	143	165	141	201	57
TRUE AZIMUTH	181	180	85	167	90	115	175	193	138	118	119
TRUE AZIMUTH	122	93	116	145	81	129	216	176	127	90	73
TRUE AZIMUTH	163	82	117	84	155	73	131	79	110	106	87
TRUE AZIMUTH	67	117	168	125	72	186	136	86	129	101	131
TRUE AZIMUTH	135										

CLIFTON CONG. SITE 4 AB PLANE(POLES)
VEC MEAN=105. VARIANCE=2713. STDEV= 53. READINGS= 56 VEC MAG(%)= 71.66
CON INTVL(95%)= 14. CON INTVL(99%)= 19. SUMV= 151910.

TRUE AZIMUTH	108	135	148	104	116	80	66	68	67	104	77
TRUE AZIMUTH	82	26	59	156	161	143	140	183	47	336	122
TRUE AZIMUTH	279	123	123	122	69	288	96	124	121	61	154
TRUE AZIMUTH	66	74	68	53	100	80	111	49	60	89	117
TRUE AZIMUTH	99	161	121	109	163	200	124	99	105	120	139
TRUE AZIMUTH	125										

CLIFTON CONG. SITE 5 AB PLANE(POLES)
VEC MEAN=144. VARIANCE=1443. STDEV= 38. READINGS= 51 VEC MAG(%)= 80.05
CON INTVL(95%)= 11. CON INTVL(99%)= 15. SUMV= 73587.

TRUE AZIMUTH	171	176	205	158	145	148	140	147	93	136	48
TRUE AZIMUTH	199	220	119	111	102	188	189	176	176	125	66
TRUE AZIMUTH	117	188	109	130	120	170	170	146	170	145	185
TRUE AZIMUTH	70	89	197	127	127	148	143	182	205	134	134
TRUE AZIMUTH	121	119	128	102	160	98	135				

110FT CONGLOMERATE FORMATION 8 M CROSS-BEDDING
VEC MEAN=344. VARIANCE= 7. STDEV= 3. READINGS= 3 VEC MAG(%)= 99.90
CON INTVL(95%)= 7. CON INTVL(99%)= 16. SUMV= 21.
TRUE AZIMUTH 340 345 346

110FT CONGLOMERATE FORMATION 8 M CROSS-BEDDING
VEC MEAN= 18. VARIANCE=1459. STDEV= 39. READINGS= 6 VEC MAG(%)= 80.57
CON INTVL(95%)= 41. CON INTVL(99%)= 63. SUMV= 8756.
TRUE AZIMUTH 355 360 10 36 100 350

110FT CONGLOMERATE FORMATION 12 M CROSS-BEDDING
VEC MEAN=323. VARIANCE=1271. STDEV= 36. READINGS= 8 VEC MAG(%)= 81.87
CON INTVL(95%)= 30. CON INTVL(99%)= 45. SUMV= 10171.
TRUE AZIMUTH 356 354 344 305 270 260 340 340

110FT CONGLOMERATE FORMATION 12 M CROSS-BEDDING
VEC MEAN= 23. VARIANCE= 156. STDEV= 13. READINGS= 4 VEC MAG(%)= 97.64
CON INTVL(95%)= 20. CON INTVL(99%)= 37. SUMV= 626.
TRUE AZIMUTH 5 25 40 20

110FT CONGLOMERATE FORMATION 15 M CROSS-BEDDING
VEC MEAN=336. VARIANCE= 26. STDEV= 6. READINGS= 4 VEC MAG(%)= 99.61
CON INTVL(95%)= 9. CON INTVL(99%)= 15. SUMV= 103.
TRUE AZIMUTH 340 333 328 340

110FT CONGLOMERATE FORMATION 15 M CROSS-BEDDING
VEC MEAN= 16. VARIANCE= 136. STDEV= 12. READINGS= 3 VEC MAG(%)= 97.94
CON INTVL(95%)= 29. CON INTVL(99%)= 67. SUMV= 409.
TRUE AZIMUTH 31 3 12

110FT CONGLOMERATE FORMATION 18 M CROSS-BEDDING
VEC MEAN= 29. VARIANCE= 61. STDEV= 8. READINGS= 4 VEC MAG(%)= 99.08
CON INTVL(95%)= 13. CON INTVL(99%)= 23. SUMV= 243.
TRUE AZIMUTH 41 30 22 22

110FT CONGLOMERATE FORMATION 18 M CROSS-BEDDING
VEC MEAN=254. VARIANCE= 9. STDEV= 3. READINGS= 3 VEC MAG(%)= 99.87
CON INTVL(95%)= 8. CON INTVL(99%)= 17. SUMV= 27.
TRUE AZIMUTH 250 255 257

110FT CONGLOMERATE FORMATION 22 M CROSS-BEDDING
VEC MEAN=292. VARIANCE=1862. STDEV= 44. READINGS= 4 VEC MAG(%)= 73.00
CON INTVL(95%)= 69. CON INTVL(99%)=127. SUMV= 7449.
TRUE AZIMUTH 335 253 243 333

110FT CONGLOMERATE FORMATION 22 M CROSS-BEDDING
VEC MEAN= 43. VARIANCE= 114. STDEV= 11. READINGS= 6 VEC MAG(%)= 98.28
CON INTVL(95%)= 12. CON INTVL(99%)= 18. SUMV= 685.
TRUE AZIMUTH 35 53 22 43 50 49

110FT CONGLOMERATE FORMATION 25 M CROSS-BEDDING
VEC MEAN=265. VARIANCE= 17. STDEV= 5. READINGS= 3 VEC MAG(%)= 99.75
CON INTVL(95%)= 11. CON INTVL(99%)= 24. SUMV= 51.
TRUE AZIMUTH 260 270 265

110FT CONGLOMERATE FORMATION 25 M CROSS-BEDDING
VEC MEAN=354. VARIANCE= 3. STDEV= 2. READINGS= 3 VEC MAG(%)= 99.96
CON INTVL(95%)= 5. CON INTVL(99%)= 10. SUMV= 9.
TRUE AZIMUTH 353 356 352

110FT CONGLOMERATE FORMATION 27 M CROSS-BEDDING
VEC MEAN=263. VARIANCE= 185. STDEV= 14. READINGS= 4 VEC MAG(%)= 97.20
CON INTVL(95%)= 22. CON INTVL(99%)= 40. SUMV= 741.
TRUE AZIMUTH 254 245 270 280

110FT CONGLOMERATE FORMATION 27 M CROSS-BEDDING
VEC MEAN=346. VARIANCE= 168. STDEV= 13. READINGS= 3 VEC MAG(%)= 97.45
CON INTVL(95%)= 33. CON INTVL(99%)= 75. SUMV= 505.
TRUE AZIMUTH 334 340 4

110FT CONGLOMERATE FORMATION 30 M CROSS-BEDDING
VEC MEAN= 58. VARIANCE= 776. STDEV= 28. READINGS= 3 VEC MAG(%)= 88.53
CON INTVL(95%)= 70. CON INTVL(99%)=160. SUMV= 2330.
TRUE AZIMUTH 96 30 48

110FT CONGLOMERATE FORMATION 31 M CROSS-BEDDING
VEC MEAN= 7. VARIANCE= 441. STDEV= 22. READINGS= 2 VEC MAG(%)= 93.34
CON INTVL(95%)=189. CON INTVL(99%)=946. SUMV= 883.
TRUE AZIMUTH 28 346

110FT CONGLOMERATE FORMATION 32 M CROSS-BEDDING
VEC MEAN=291. VARIANCE= 54. STDEV= 8. READINGS= 3 VEC MAG(%)= 99.18
CON INTVL(95%)= 19. CON INTVL(99%)= 43. SUMV= 163.
TRUE AZIMUTH 282 300 290

110FT CONGLOMERATE FORMATION 32 M CROSS-BEDDING
VEC MEAN=339. VARIANCE=1511. STDEV= 39. READINGS= 3 VEC MAG(%)= 78.40
CON INTVL(95%)= 97. CON INTVL(99%)=223. SUMV= 4534.
TRUE AZIMUTH 36 318 310

MT GORDON FORMATION MIDDLE CROSS-BEDDING
VEC MEAN=324. VARIANCE=1942. STDEV= 45. READINGS= 12 VEC MAG(%)= 73.50
CON INTVL(95%)= 28. CON INTVL(99%)= 40. SUMV= 23301.
TRUE AZIMUTH 50 350 266 330 8 13 264 311 321 310 330
TRUE AZIMUTH 265

MT GORDON FORMATION TOP CROSS-BEDDING
VEC MEAN= 30. VARIANCE= 313. STDEV= 18. READINGS= 5 VEC MAG(%)= 95.30
CON INTVL(95%)= 22. CON INTVL(99%)= 37. SUMV= 1564.
TRUE AZIMUTH 40 38 360 20 50

RABBIT GULLY BEDS MIDDLE CONGLOMERATE CROSS-BEDDING
VEC MEAN= 24. VARIANCE= 401. STDEV= 21. READINGS= 5 VEC MAG(%)= 93.98
CON INTVL(95%)= 25. CON INTVL(99%)= 42. SUMV= 2006.
TRUE AZIMUTH 356 40 50 25 7

RABBIT GULLY BEDS UPPER CONGLOMERATE UNIT CROSS-BEDDING
VEC MEAN= 71. VARIANCE=3163. STDEV= 57. READINGS= 7 VEC MAG(%)= 66.56
CON INTVL(95%)= 53. CON INTVL(99%)= 79. SUMV= 22139.
TRUE AZIMUTH 37 298 98 60 80 120 76

TRIG N UPPER CONGLOMERATE UNIT CROSS-BEDDING
VEC MEAN= 42. VARIANCE= 465. STDEV= 22. READINGS= 3 VEC MAG(%)= 93.05
CON INTVL(95%)= 54. CON INTVL(99%)=124. SUMV= 1395.
TRUE AZIMUTH 18 70 36

APPENDIX (IV i) SITE 1.

Values for selected ab plane pole positions rotated about the normal to the trend of the a-axes maxima to remove the effect of a-axes plunge.

(A) ab plane pole rotation about the normal to the a-axes maxima trending north-east.

a-axis		ab plane pole position		New ab plane pole position	
Plunge	Trend	Dip	Dip Direction	Dip	Dip Direction
10°E	45°	18°N	360°	13°W	329°
15°E	54°	18°N	360°	15°W	306°
10°E	54°	18°N	360°	14.5°W	327°
10°E	45°	32°N	360°	25.5°W	346°
15°E	54°	32°N	360°	26°W	335°
10°E	54°	32°N	360°	27°W	344°
10°E	45°	20°W	353°	15.5°W	324°
15°E	54°	20°W	353°	18°W	308°
10°E	54°	20°W	353°	17.5°W	325°
10°E	45°	30°W	353°	25°W	336°
15°E	54°	30°W	353°	26°W	326°
10°E	54°	30°W	353°	26.5°W	335°

(B) ab plane pole rotation about the normal to the a-axes maxima trending south-west.

10°W	196°	32°W	260°	29°W	276°
6°W	200°	32°W	260°	29.5°W	269°
4°W	206°	32°W	260°	30°W	265°
10°W	196°	30°W	270°	29°W	287°
6°W	200°	30°W	270°	29°W	280°
4°W	206°	30°W	270°	28°W	279°

APPENDIX (IVii) SITE 1.

ab Plane pole positions rotated about the normal to the trend of a-axes.

	Dip	Direction		Dip	Direction
1.	4 E	20	49.	31 W	336
2.	41 W	299	50.	3 W	244
3.	5 E	24	51.	24 W	265
4.	31 W	220	52.	26 W	243
5.	22 E	91	53.	34 W	232
6.	30 W	332	54.	20 E	101
7.	11 W	261	55.	73 W	337
8.	29 E	49	56.	41 W	337
9.	51 W	250	57.	21 W	224
10.	13 W	331	58.	19 W	245
11.	43 E	34	59.	18 E	33
12.	15 W	313	60.	9 E	41
13.	5 W	218	61.	35 E	30
14.	9 W	322	62.	10 W	316
15.	5 E	10	63.	8 E	99
16.	6 W	292	64.	18 W	351
17.	18 W	300	65.	22 E	25
18.	37 W	262	66.	23 W	284
19.	42 W	267	67.	24 W	340
20.	46 W	323	68.	30 W	283
21.	36 W	287	69.	20 W	289
22.	46 W	304	70.	11 W	288
23.	35 W	209	71.	22 W	312
24.	56 W	326	72.	26 W	340
25.	60 W	326	73.	14 W	325
26.	30 W	250	74.	28 W	288
27.	42 W	297	75.	24 W	301
28.	0	0	76.	39 E	99
29.	1 E	64	77.	29 W	260
30.	32 W	354	78.	22 E	42
31.	21 E	137	79.	27 W	282
32.	19 W	344	80.	18 E	67
33.	8 E	43	81.	47 W	344
34.	22 W	265	82.	34 E	129
35.	40 W	301	83.	7 W	305
36.	21 W	235	84.	11 W	294
37.	18 W	256	85.	4 W	352
38.	61 W	350	86.	17 W	327
39.	22 W	252	87.	40 W	312
40.	34 W	336	88.	66 W	340
41.	0	0	89.	6 W	345
42.	20 W	268	90.	45 W	343
43.	48 E	44	91.	21 E	89
44.	45 W	313	92.	22 E	7
45.	52 W	340	93.	5 W	316
46.	4 W	249	94.	7 W	233
47.	5 W	220	95.	25 E	15
48.	39 W	280	96.	32 W	284

	Dip	Direction		Dip	Direction
97.	51 W	311	109.	36 W	282
98.	6 E	128	110.	11 W	245
99.	14 W	301	111.	20 W	326
100.	5 W	308	112.	53 W	342
101.	43 W	303	113.	14 W	250
102.	36 W	344	114.	34 W	332
103.	22 W	352	115.	7 E	9
104.	18 W	239	116.	77 W	304
105.	34 E	14	117.	43 W	309
106.	17 W	290	118.	34 W	207
107.	28 W	228	119.	21 W	235
108.	72 W	189	120.	84 W	317

APPENDIX (V)

VECTOR MEAN, STANDARD DEVIATION, CONFIDENCE INTERVAL (95%) AND (99%)
FOR CURRENT DIRECTION DATA

CLIFTON CONGLOMERATE FM. SITE 1 AB POLES
VEC MEAN=140. VARIANCE=3139. STDEV= 57. READINGS=120 VEC MAG(%)= 64.27
CON INTVL(95%)= 11. CON INTVL(99%)= 14. SUMV= 376677.

TRUE AZIMUTH	140	147	128	161	56	261	164	117	219	77	166
TRUE AZIMUTH	207	141	106	194	212	112	142	84	101	145	95
TRUE AZIMUTH	124	87	151	143	95	110	161	171	169	294	185
TRUE AZIMUTH	183	90	139	62	145	171	123	171	177	66	217
TRUE AZIMUTH	130	153	128	40	92	173	128	84	86	70	298
TRUE AZIMUTH	160	174	84	85	117	179	196	155	206	215	186
TRUE AZIMUTH	30	185	115	105	148	158	172	166	95	106	263
TRUE AZIMUTH	101	205	88	120	180	295	123	150	100	190	109
TRUE AZIMUTH	170	165	153	265	173	100	62	185	109	127	303
TRUE AZIMUTH	95	227	118	185	186	130	184	134	75	358	130
TRUE AZIMUTH	88	169	158	57	144	169	126	113	129	117	

CLIFTON CONG. FM. SITE 1 AB POLES (EFFECT OF A AXIS TILT REMOVED)
VEC MEAN=133. VARIANCE=4515. STDEV= 68. READINGS=120 VEC MAG(%)= 52.03
CON INTVL(95%)= 13. CON INTVL(99%)= 17. SUMV= 541766.

TRUE AZIMUTH	200	119	204	40	271	162	81	229	70	161	214
TRUE AZIMUTH	133	38	142	190	112	120	82	87	143	107	124
TRUE AZIMUTH	29	146	146	70	117	180	244	174	317	164	223
TRUE AZIMUTH	85	121	55	76	170	72	156	180	88	224	133
TRUE AZIMUTH	160	69	40	100	156	64	85	63	52	281	157
TRUE AZIMUTH	157	44	65	213	221	210	136	279	171	205	104
TRUE AZIMUTH	160	103	109	108	132	160	145	108	121	279	80
TRUE AZIMUTH	222	102	247	164	309	125	114	162	147	132	160
TRUE AZIMUTH	165	163	269	187	136	53	195	104	131	308	121
TRUE AZIMUTH	128	123	164	172	59	194	110	48	6	102	665
TRUE AZIMUTH	146	162	70	152	189	124	129	27	55	137	

CLIFTON CONG. SITE 1 A AXIS TOTAL
VEC MEAN=349. VARIANCE=5892. STDEV= 77. READINGS=120 VEC MAG(%)= 39.24
CON INTVL(95%)= 14. CON INTVL(99%)= 19. SUMV= 707076.

TRUE AZIMUTH	199	320	360	330	3	70	15	316	348	1	7
TRUE AZIMUTH	298	329	307	58	47	292	42	54	43	336	45
TRUE AZIMUTH	202	134	334	55	245	333	203	340	348	210	64
TRUE AZIMUTH	26	345	47	33	333	329	360	261	358	36	349
TRUE AZIMUTH	156	349	226	237	317	303	194	81	322	242	343
TRUE AZIMUTH	342	36	200	57	53	325	343	307	340	284	359
TRUE AZIMUTH	14	94	291	13	50	28	257	1	13	214	18
TRUE AZIMUTH	17	188	191	21	9	359	185	347	77	1	302
TRUE AZIMUTH	13	218	83	214	60	345	33	242	17	241	238
TRUE AZIMUTH	250	307	30	218	230	220	76	210	94	59	351
TRUE AZIMUTH	271	12	333	345	57	39	300	13	240	199	

CLIFTON CONG. SITE 1 'A'AXIS ORIENTATION, SIZE.GE.8.0CMS
VEC MEAN=315. VARIANCE=3708. STDEV= 61. READINGS= 34 VEC MAG(%)= 55.75
CON INTVL(95%)= 21. CON INTVL(99%)= 28. SUMV= 126064.

TRUE AZIMUTH	320	330	3	316	1	298	307	292	245	55	340
TRUE AZIMUTH	345	329	360	261	226	237	317	303	322	242	342
TRUE AZIMUTH	57	340	1	191	9	302	14	218	307	219	94
TRUE AZIMUTH	240										

SITE 1'A'AXIS SIZE.LT.8.0CMS.AND.GT.6.0CMS
VEC MEAN= 15. VARIANCE=4464. STDEV= 67. READINGS= 36 VEC MAG(%)= 59.55
CON INTVL(95%)= 23. CON INTVL(99%)= 31. SUMV= 160715.

TRUE AZIMUTH	329	42	336	344	348	210	26	33	358	349	156
TRUE AZIMUTH	81	343	325	342	14	94	13	28	13	17	189
TRUE AZIMUTH	21	185	347	77	241	76	351	12	39	13	33
TRUE AZIMUTH	36	333	54								

SITE 1'A'AXIS SIZE.LE.6.0CMS.AND.GT.3.0CMS
VEC MEAN=353. VARIANCE=7553. STDEV= 87. READINGS= 50 VEC MAG(%)= 24.46
CON INTVL(95%)= 25. CON INTVL(99%)= 33. SUMV= 377661.

TRUE AZIMUTH	360	70	15	348	7	58	47	43	45	202	134
TRUE AZIMUTH	333	203	64	47	36	350	194	200	53	307	284
TRUE AZIMUTH	359	291	50	257	18	359	1	83	214	60	345
TRUE AZIMUTH	242	17	238	250	30	230	220	210	59	271	333
TRUE AZIMUTH	57	300	199	199	345	214					

SITE 1 'A'AXIS SPHERICITY .GE.0.6
VEC MEAN=359. VARIANCE=5816. STDEV= 77. READINGS= 44 VEC MAG(%)= 42.48
CON INTVL(95%)= 24. CON INTVL(99%)= 32. SUMV= 255912.

TRUE AZIMUTH	316	7	58	43	336	344	55	245	64	47	360
TRUE AZIMUTH	261	358	349	156	237	317	303	194	322	57	53
TRUE AZIMUTH	342	284	359	14	291	50	257	1	13	18	17
TRUE AZIMUTH	359	185	83	345	17	250	210	94	59	199	36

SITE 1 'A'AXIS SPHERICITY.LT.0.6.AND.GE.0.5
VEC MEAN=351. VARIANCE=6204. STDEV= 79. READINGS= 47 VEC MAG(%)= 35.45
CON INTVL(95%)= 24. CON INTVL(99%)= 32. SUMV= 291590.

TRUE AZIMUTH	38	70	15	1	47	292	42	134	340	210	26
TRUE AZIMUTH	33	329	36	350	226	81	342	325	340	94	13
TRUE AZIMUTH	189	21	9	347	77	1	302	14	218	214	242
TRUE AZIMUTH	241	238	307	219	220	76	271	12	333	57	300
TRUE AZIMUTH	13	199	333								

SITE 1 'A'AXIS SPHERICITY.LT.0.5
VEC MEAN=332. VARIANCE=5208. STDEV= 73. READINGS= 29 VEC MAG(%)= 42.31
CON INTVL(95%)= 28. CON INTVL(99%)= 37. SUMV= 151026.

TRUE AZIMUTH	320	330	3	348	298	329	307	45	202	333	203
TRUE AZIMUTH	348	345	242	343	200	307	28	191	60	30	230
TRUE AZIMUTH	351	39	240	345	33	214	54				

SITE 1 A AXIS ELONGATION GE. 0.8
VEC MEAN=353. VARIANCE=4253. STDEV= 66. READINGS= 37 VEC MAG(%)= 54.64
CON INTVL(95%)= 22. CON INTVL(99%)= 30. SUMV= 157369.
TRUE AZIMUTH 320 330 3 70 316 292 42 336 344 210 64
TRUE AZIMUTH 26 345 360 36 349 317 322 340 1 17 347
TRUE AZIMUTH 77 1 302 14 83 345 241 220 76 210 94
TRUE AZIMUTH 351 199 345 333

SITE 1 A AXIS ELONGATION GE. 0.8
VEC MEAN=333. VARIANCE=6166. STDEV= 79. READINGS= 55 VEC MAG(%)= 30.86
CON INTVL(95%)= 22. CON INTVL(99%)= 29. SUMV= 339103.
TRUE AZIMUTH 1 298 329 307 58 47 45 202 55 245 203
TRUE AZIMUTH 348 329 358 226 237 303 194 81 242 343 342
TRUE AZIMUTH 53 325 342 307 14 94 13 28 13 189 191
TRUE AZIMUTH 21 9 359 185 218 60 242 17 238 250 307
TRUE AZIMUTH 219 230 59 271 12 57 300 240 299 36 54

SITE 1 A AXIS ELONGATION GE. 0.6
VEC MEAN= 5. VARIANCE=5795. STDEV= 77. READINGS= 28 VEC MAG(%)= 44.00
CON INTVL(95%)= 30. CON INTVL(99%)= 40. SUMV= 162251.
TRUE AZIMUTH 38 15 348 7 43 134 333 340 47 33 261
TRUE AZIMUTH 156 350 200 57 284 359 291 50 257 18 214
TRUE AZIMUTH 30 333 39 13 33 214

SITE 1 'A'AXIS CROSS CORRELATION SIZE.GE. 8CMS,RATIO.GE.0.8 LL
VEC MEAN=343. VARIANCE=1675. STDEV= 41. READINGS= 14 VEC MAG(%)= 78.74
CON INTVL(95%)= 24. CON INTVL(99%)= 33. SUMV= 23447.
TRUE AZIMUTH 320 330 3 316 292 345 360 317 322 31 1
TRUE AZIMUTH 302 13 94

'A'AXIS SIZE.GE. 8CMS,RATIO.LT.0.8.AND.GT. 0.6 LM
VEC MEAN=280. VARIANCE=3881. STDEV= 63. READINGS= 17 VEC MAG(%)= 52.41
CON INTVL(95%)= 33. CON INTVL(99%)= 45. SUMV= 65969.
TRUE AZIMUTH 1 298 307 55 245 329 226 237 303 242 342
TRUE AZIMUTH 191 9 218 307 219 240

'A'AXIS SIZE.GE. 8CMS,RATIO .LE. 0.6 LS
VEC MEAN=340. VARIANCE=4056. STDEV= 64. READINGS= 3 VEC MAG(%)= 47.17
CON INTVL(95%)=159. CON INTVL(99%)=366. SUMV= 12169.
TRUE AZIMUTH 340 261 57

'A'AXIS SIZE.LT.8CMS.AND.GE.6CMS, RATIO GE 0.8 ML
VEC MEAN= 2. VARIANCE=4123. STDEV= 65. READINGS= 13 VEC MAG(%)= 57.12
CON INTVL(95%)= 39. CON INTVL(99%)= 55. SUMV= 53595.
TRUE AZIMUTH 42 336 344 210 26 349 17 347 77 241 76
TRUE AZIMUTH 351 333

'A'AXIS SIZE.LT.8CMS.AND.GE.6CMS, RATIO LT 0.8.AND.GT. 0.6 MM
VEC MEAN= 15. VARIANCE=2914. STDEV= 54. READINGS= 17 VEC MAG(%)= 71.52
CON INTVL(95%)= 28. CON INTVL(99%)= 39. SUMV= 49543.
TRUE AZIMUTH 329 348 358 81 343 325 342 14 94 13 28
TRUE AZIMUTH 13 21 185 12 36 54

'A'AXIS SIZE.LT.8CMS.AND.GE.6CMS, RATIO.LE.0.6 MS
VEC MEAN= 44. VARIANCE=2776. STDEV= 53. READINGS= 5 VEC MAG(%)= 68.86
CON INTVL(95%)= 66. CON INTVL(99%)=109. SUMV= 13879.
TRUE AZIMUTH 33 156 39 13 33

'A'AXIS SIZE.LE.6CMS ,RATIO.GE.0.8 SL
VEC MEAN= 22. VARIANCE=***** STDEV=104. READINGS= 11 VEC MAG(%)= 14.98
CON INTVL(95%)= 70. CON INTVL(99%)=100. SUMV= 118796.
TRUE AZIMUTH 70 64 36 1 83 345 238 220 210 199 345

'A'AXIS SIZE.LE.6CMS ,RATIO.LT.0.8.AND.GT. 0.6 SM
VEC MEAN=313. VARIANCE=7656. STDEV= 88. READINGS= 20 VEC MAG(%)= 10.31
CON INTVL(95%)= 41. CON INTVL(99%)= 56. SUMV= 153113.
TRUE AZIMUTH 58 47 45 202 203 194 53 307 359 60 242
TRUE AZIMUTH 17 238 250 230 59 271 57 300 199

'A'AXIS SIZE.LE.6CMS ,RATIO.LE.0.6 SS
VEC MEAN=350. VARIANCE=4825. STDEV= 70. READINGS= 19 VEC MAG(%)= 48.88
CON INTVL(95%)= 34. CON INTVL(99%)= 46. SUMV= 91680.
TRUE AZIMUTH 38 15 348 7 43 333 47 350 200 284 359
TRUE AZIMUTH 291 50 257 18 214 30 333 214

'A'AXIS GROUPED CORRELATION LL,LM,ML,SL
VEC MEAN=330. VARIANCE=4889. STDEV= 70. READINGS= 55 VEC MAG(%)= 44.03
CON INTVL(95%)= 19. CON INTVL(99%)= 26. SUMV= 268889.
TRUE AZIMUTH 320 330 3 316 292 345 360 317 322 340 1
TRUE AZIMUTH 302 13 94 1 298 307 55 245 329 226 237
TRUE AZIMUTH 303 242 342 191 9 218 307 219 240 42 336
TRUE AZIMUTH 344 210 26 349 17 347 77 241 76 351 333
TRUE AZIMUTH 70 64 36 1 83 345 238 220 210 199 345

'A'AXIS GROUPED CORRELATION LS,MS,SM,SS
VEC MEAN=355. VARIANCE=6952. STDEV= 84. READINGS= 47 VEC MAG(%)= 30.73
CON INTVL(95%)= 25. CON INTVL(99%)= 33. SUMV= 326729.
TRUE AZIMUTH 340 261 57 33 156 39 13 33 58 47 45
TRUE AZIMUTH 202 203 194 53 307 359 60 242 17 238 250
TRUE AZIMUTH 230 59 271 57 300 199 38 15 348 7 43
TRUE AZIMUTH 333 47 350 200 284 359 291 50 257 18 214
TRUE AZIMUTH 30 333 214

CLIFTON CONSLOMERATE SITE 1 ABPLANE (POLES) SIZE.GE.8.0CMS
VEC MEAN=133. VARIANCE=1625. STDEV= 41. READINGS= 34 VEC MAG(%)= 77.72
CON INTVL(95%)= 14. CON INTVL(99%)= 19. SUMV= 55248.
TRUE AZIMUTH 147 161 57 117 77 208 106 112 152 143 161
TRUE AZIMUTH 183 62 145 171 130 153 128 40 128 84 70
TRUE AZIMUTH 160 180 148 106 101 124 150 100 185 127 185
TRUE AZIMUTH 159

SITE 1 ABPLANE (POLES) SIZE.LT.8CMS AND .GT.6CMS
VEC MEAN=143. VARIANCE=1953. STDEV= 45. READINGS= 36 VEC MAG(%)= 74.30
CON INTVL(95%)= 15. CON INTVL(99%)= 21. SUMV= 70307.
TRUE AZIMUTH 141 142 101 87 172 169 185 139 123 177 66
TRUE AZIMUTH 173 87 84 85 206 215 176 115 158 166 95
TRUE AZIMUTH 263 88 120 180 173 227 130 134 130 169 126
TRUE AZIMUTH 129 117 140

SITE 1 AB PLANE (POLES) SIZE.LE.6CMS
VEC MEAN=150. VARIANCE=4701. STDEV= 69. READINGS= 50 VEC MAG(%)= 50.91
CON INTVL(95%)= 20. CON INTVL(99%)= 26. SUMV= 235050.
TRUE AZIMUTH 128 262 164 219 167 194 212 84 145 95 124
TRUE AZIMUTH 95 110 294 90 171 218 92 298 174 177 196
TRUE AZIMUTH 155 186 185 105 172 205 295 190 109 171 166
TRUE AZIMUTH 153 265 100 62 109 330 95 118 186 184 75
TRUE AZIMUTH 358 88 57 144 169 113

SITE 1 AB PLANE (POLES) SPHERICITY .LE.0.6
VEC MEAN=144. VARIANCE=2748. STDEV= 53. READINGS= 44 VEC MAG(%)= 66.52
CON INTVL(95%)= 16. CON INTVL(99%)= 22. SUMV= 120907.
TRUE AZIMUTH 117 167 194 84 101 87 152 143 294 90 145
TRUE AZIMUTH 171 123 177 66 153 128 40 92 128 160 174
TRUE AZIMUTH 85 196 155 206 186 185 105 148 158 172 166
TRUE AZIMUTH 205 88 190 166 265 62 118 185 186 57 129

SITE 1 AB PLANE (POLES) SPHERICITY .LT.0.6.AND.GE. 0.5
VEC MEAN=142. VARIANCE=3206. STDEV= 57. READINGS= 47 VEC MAG(%)= 63.00
CON INTVL(95%)= 17. CON INTVL(99%)= 23. SUMV= 150662.
TRUE AZIMUTH 128 262 164 77 212 112 142 124 161 169 185
TRUE AZIMUTH 139 62 171 218 130 173 70 84 180 215 140
TRUE AZIMUTH 95 263 101 120 180 295 124 150 100 109 153
TRUE AZIMUTH 173 100 185 127 95 227 184 134 75 358 88
TRUE AZIMUTH 169 144 117

SITE 1 AB PLANE (POLES) SPHERICITY.LT. 0.5
VEC MEAN=135. VARIANCE=3235. STDEV= 57. READINGS= 29 VEC MAG(%)= 67.35
CON INTVL(95%)= 22. CON INTVL(99%)= 30. SUMV= 93820.
TRUE AZIMUTH 147 161 57 219 208 141 106 145 95 95 110
TRUE AZIMUTH 172 183 84 87 298 177 115 106 171 109 330
TRUE AZIMUTH 130 130 159 169 126 113 140

SITE 1 AB PLANE (POLES) ELONGATION GE. 0.8
VEC MEAN=150. VARIANCE=2829. STDEV= 54. READINGS= 37 VEC MAG(%)= 68.04
CON INTVL(95%)= 18. CON INTVL(99%)= 24. SUMV= 104667.
TRUE AZIMUTH 147 161 57 262 117 112 142 101 87 169 294
TRUE AZIMUTH 185 183 145 171 177 128 128 180 148 166 120
TRUE AZIMUTH 180 295 124 150 190 166 173 95 227 118 185
TRUE AZIMUTH 130 57 169 117

SITE 1 AB PLANE (POLES) ELONGATION LT. 0.8 AND GT. 0.6
VEC MEAN=133. VARIANCE=3302. STDEV= 58. READINGS= 55 VEC MAG(%)= 62.35
CON INTVL(95%)= 16. CON INTVL(99%)= 21. SUMV= 181620.
TRUE AZIMUTH 77 208 141 106 194 212 145 95 152 143 110
TRUE AZIMUTH 172 62 123 130 153 40 92 173 84 87 70
TRUE AZIMUTH 174 84 85 117 206 215 140 115 158 95 106
TRUE AZIMUTH 263 101 205 88 100 171 153 265 100 62 185
TRUE AZIMUTH 127 303 186 185 134 358 88 159 144 129 140

SITE 1 AB PLANE (POLES) ELONGATION LE. 0.6
VEC MEAN=143. VARIANCE=2534. STDEV= 51. READINGS= 28 VEC MAG(%)= 70.00
CON INTVL(95%)= 20. CON INTVL(99%)= 27. SUMV= 70954.
TRUE AZIMUTH 128 164 219 167 84 124 95 161 90 139 171
TRUE AZIMUTH 66 218 298 160 196 155 186 185 105 172 109
TRUE AZIMUTH 109 75 130 169 126 113

AB PLANE (POLES)CROSS CORRELATION SIZE.GE.8CMS,RATIO.GE.0.8 LL
VEC MEAN=135. VARIANCE=1120. STDEV= 34. READINGS= 14 VEC MAG(%)= 84.39
CON INTVL(95%)= 20. CON INTVL(99%)= 27. SUMV= 15674.
TRUE AZIMUTH 147 161 57 117 112 83 145 128 128 180 148
TRUE AZIMUTH 124 150 185

AB PLANE (POLES)SIZE.GE.8CMS,RATIO.LE.0.6 LS
VEC MEAN=164. VARIANCE= 25. STDEV= 5. READINGS= 3 VEC MAG(%)= 99.62
CON INTVL(95%)= 13. CON INTVL(99%)= 29. SUMV= 75.
TRUE AZIMUTH 161 171 160

AB PLANE (POLES)SIZE.GE.8CMS,RATIO.LT.0.8.AND.GT.0.6 LM
VEC MEAN=117. VARIANCE=1929. STDEV= 44. READINGS= 17 VEC MAG(%)= 73.85
CON INTVL(95%)= 23. CON INTVL(99%)= 32. SUMV= 32786.
TRUE AZIMUTH 77 208 106 152 143 62 130 153 40 84 70
TRUE AZIMUTH 106 101 100 185 127 159

AB PLANE (POLES)SIZE.LT.8CMS.AND.GE.6CMS,RATIO GE 0.8 ML
VEC MEAN=152. VARIANCE=1439. STDEV= 38. READINGS= 13 VEC MAG(%)= 79.84
CON INTVL(95%)= 23. CON INTVL(99%)= 33. SUMV= 18708.
TRUE AZIMUTH 142 101 87 169 185 177 166 120 180 173 227
TRUE AZIMUTH 130 117

AB PLANE (POLES) SIZE.LT.8CMS.AND.GE.6CMS,RATIO.LT.0.8.AND.GT.0.6 MM
VEC MEAN=140. VARIANCE=2376. STDEV= 49. READINGS= 17 VEC MAG(%)= 70.29
CON INTVL(95%)= 26. CON INTVL(99%)= 35. SUMV= 40392.
TRUE AZIMUTH 141 172 123 173 87 84 85 206 215 140 115
TRUE AZIMUTH 158 263 88 134 129 140

ABPLANE (POLES) SIZE.LT.8CMS.AND.GE.6CMS,RATIO.LE.0.6 MS
VEC MEAN=128. VARIANCE=1129. STDEV= 34. READINGS= 5 VEC MAG(%)= 84.10
CON INTVL(95%)= 42. CON INTVL(99%)= 70. SUMV= 5646.
TRUE AZIMUTH 139 66 130 169 126

AB PLANE (POLES)SIZE .LE.6CMS,RATIO.GE.0.8 SL
VEC MEAN=160. VARIANCE=6203. STDEV= 79. READINGS= 11 VEC MAG(%)= 33.30
CON INTVL(95%)= 53. CON INTVL(99%)= 76. SUMV= 68229.
TRUE AZIMUTH 262 294 171 295 190 166 100 95 118 57 169

AB PLANE (POLES) SIZE.LE.6CMS,RATIO.LT.0.8.AND.GT.0.6 SM
VEC MEAN=148. VARIANCE=4772. STDEV= 70. READINGS= 20 VEC MAG(%)= 49.48
CON INTVL(95%)= 33. CON INTVL(99%)= 45. SUMV= 95438.
TRUE AZIMUTH 194 212 145 95 110 92 174 117 205 171 153
TRUE AZIMUTH 265 100 62 303 186 185 358 88 144

AB PLANE (POLES) SIZE.LE.6CMS,RATIO.LE.0.6 SS
VEC MEAN=144. VARIANCE=3250. STDEV= 58. READINGS= 19 VEC MAG(%)= 62.17
CON INTVL(95%)= 28. CON INTVL(99%)= 38. SUMV= 61750.
TRUE AZIMUTH 128 164 219 167 84 95 90 218 298 196 155
TRUE AZIMUTH 186 185 105 172 109 109 75 113

AB PLANE (POLES) GROUPED CORRELATION LL,ML
VEC MEAN=143. VARIANCE=1359. STDEV= 37. READINGS= 27 VEC MAG(%)= 81.26
CON INTVL(95%)= 15. CON INTVL(99%)= 20. SUMV= 36705.
TRUE AZIMUTH 147 161 57 117 112 83 145 128 128 180 148
TRUE AZIMUTH 124 150 185 142 101 87 169 185 177 166 120
TRUE AZIMUTH 180 173 227 130 117

AB PLANE (POLES) GROUPED CORRELATION LS,MS,SM,SS
VEC MEAN=139. VARIANCE=3593. STDEV= 60. READINGS= 92 VEC MAG(%)= 60.21
CON INTVL(95%)= 13. CON INTVL(99%)= 17. SUMV= 330542.
TRUE AZIMUTH 161 171 160 139 66 130 169 126 194 212 145
TRUE AZIMUTH 95 110 92 174 117 205 171 153 265 100 62
TRUE AZIMUTH 303 186 185 358 88 144 128 164 219 167 84
TRUE AZIMUTH 95 90 218 298 196 155 186 185 105 172 109
TRUE AZIMUTH 109 75 113 141 172 123 173 87 84 85 206
TRUE AZIMUTH 215 140 115 158 263 88 134 129 140 262 294
TRUE AZIMUTH 171 295 190 166 100 95 118 57 169 77 208
TRUE AZIMUTH 106 152 143 62 130 153 40 84 70 106 101
TRUE AZIMUTH 100 185 127 159

CLIFTON SANDSTONE SITE 6 AB PLANE(POLES)
VEC MEAN=225. VARIANCE=7191. STDEV= 85. READINGS=101 VEC MAG(%)= 25.73
CON INTVL(95%)= 17. CON INTVL(99%)= 23. SUMV= 726272.
TRUE AZIMUTH 84 108 285 313 263 138 20 160 205 82 246
TRUE AZIMUTH 252 254 323 240 325 299 282 167 318 208 263
TRUE AZIMUTH 87 151 263 262 91 259 271 77 147 266 186
TRUE AZIMUTH 62 278 286 229 120 108 281 280 188 233 313
TRUE AZIMUTH 188 215 123 121 269 288 228 288 271 165 275
TRUE AZIMUTH 100 59 136 269 165 143 224 252 239 287 185
TRUE AZIMUTH 212 196 109 289 127 165 262 280 323 263 187
TRUE AZIMUTH 30 195 40 243 301 104 147 90 109 234 237
TRUE AZIMUTH 352 172 115 115 23 54 295 310 270 161 133
TRUE AZIMUTH 102 326

APPENDIX (VI i)

Heavy mineralogy versus grain-size. Relative abundance expressed as a percentage.

Sample	Biotite	Zircon	Opaques	Augite	Epidote	Calcic-Hb	Hornblende	Hypersthene	Wt. % Heavies
039									
2.0 - 2.25ϕ	1.6	0.0	4.0	7.0	0.6	6.2	39.1	41.5	6.0
2.25 - 2.5ϕ	1.0	0.0	4.0	6.6	1.2	2.3	42.5	42.4	9.0
2.5 - 3.0ϕ	0.6	0.3	7.3	6.4	1.2	1.2	44.4	38.6	13.2
3.0 - 3.5ϕ	0.4	1.9	25.2	6.7	1.9	1.0	30.6	32.3	21.4
3.5 - 4.0ϕ	0.2	2.5	40.2	6.6	1.6	1.0	32.0	15.9	17.6
Total/average	0.8	0.9	16.1	6.7	1.3	2.3	37.7	34.2	13.4
Total excluding opaques	0.9	1.0		8.0	1.6	2.7	44.9	40.9	
040									
2.0 - 2.25ϕ	1.2	0.0	6.2	8.8	2.8	4.0	34.5	42.5	3.6
2.25 - 2.5ϕ	0.9	0.0	6.3	7.4	1.9	3.7	39.1	40.7	5.1
2.5 - 3.0ϕ	0.4	0.6	8.5	7.7	2.4	2.4	33.9	44.1	8.0
3.0 - 3.5ϕ	1.0	1.9	23.0	9.9	1.4	1.4	29.1	32.3	11.0
3.5 - 4.0ϕ	0.1	4.0	38.1	9.5	1.0	0.9	27.5	18.9	10.3
Total/average	0.7	1.3	16.4	8.7	1.9	2.5	32.8	35.7	7.6
Total excluding opaques	0.8	1.6		10.4	2.3	3.0	39.2	42.7	

APPENDIX (VI ii)

Percent ferromagnesian minerals in tephric units A to I_2.

Sample/Unit		Biotite	Zircon	Augite	Calcic-Hb	Hornblende	Hypersthene	% Opaques	Wt.% Heavies
041	A_1	2.3	5.3	2.9	2.3	41.1	46.1	0.7	26.4
042	A_2	7.5	2.8	5.1	2.2	39.6	42.8	1.6	27.9
043	B	0.6	2.7	10.5	0.3	5.1	80.8	1.0	33.5
044	C	1.3	4.1	13.9	0.0	14.4	66.3	0.5	30.0
045	D	0.5	0.5	4.7	0.2	35.7	57.9	1.3	17.0
046	E_1	0.0	0.0	18.6	0.0	41.4	40.0	13.3	19.4
049	E_2	0.0	1.2	7.0	1.6	53.7	35.1	18.9	2.0
047	F	0.0	1.1	11.7	0.4	16.3	70.5	34.5	1.0
048	G	0.9	0.9	12.8	0.9	30.7	53.5	31.5	1.1
050	H_1	0.3	0.0	21.8	0.0	6.9	69.3	10.3	2.8
051	H_2	0.5	0.0	11.3	0.5	4.2	82.8	11.3	9.6
052	H_3	0.2	0.0	16.1	1.8	8.2	73.5	17.3	13.1
053	I_1	0.0	0.0	1.6	0.0	92.6	2.7	28.2	8.0
054	I_2	0.3	0.0	0.6	2.6	91.9	2.8	14.5	1.7

Coastal Section

X-X′

Formations

Te Awanga Beds

Tephric Units

Clifton Conglomer-ate

Clifton Sand

Trig. N Beds

Rabbit Gully Beds

110ft. Conglomerate

Mt. Gordon Beds

Kidnapper Tuff

Maraetotara Sand

Ma

I_1

H_1

G

F

E_1

D

C

B

A_1

Maraetotara River Section

Y-Y′

Te Awanga Beds

Clifton Conglomerate

Clifton Sand

Trig. N / Rabbit Gully Beds

Mt Gordon Beds

Kidnapper Tuff

Maraetotara Sand

Wo

I_2

H_2

E_2

A_2

40m

0

Key

- Conglomerate
- Lignite
- Paleosol
- Marine Fossils
- Bioturbated sands + muds
- Sands + Muds
- Lithostratigraphic Correlation
- Tephrostratigraphic " "

Wo: Opoitian Mudstone

Ma: Mangapanian Black Reef Calcareous Sand

Stratigraphic columns through the Pleistocene Kidnappers Group, Hawke's Bay.